Therapeutic potential of aptamer-mediated targeting of the voltage-gated Na^+ channel β1 subunit in human breast cancer cells

Faheemmuddeen Patel

PhD

University of York

Biology

June 2019

Abstract

Voltage-gated sodium channels (VGSCs), classically responsible for action potential firing in excitable cells, also play an important role in non-excitable cells and in particular, cancer cells. VGSCs contain a pore-forming α subunit and one or more auxiliary β subunits, which contain immunoglobulin (Ig) loops and function as cell adhesion molecules (CAMs). The VGSC α subunit, $Na_V1.5$, and its auxiliary $\beta1$ subunit have been shown to increase invasion of breast cancer cells and metastasis in a xenograft mouse model of breast cancer. In addition, $\beta1$ expression is increased in breast cancer specimens relative to control samples. Thus, $\beta1$ may serve as a valuable therapeutic target to inhibit metastasis. The hypothesis of this project was that the Ig domain of $\beta1$ is critical for regulating its function as an auxiliary channel subunit and a cell adhesion molecule (CAM) in breast cancer cells such that aptamers targeting the Ig domain would abrogate its function. This project used various approaches to block the function of the Ig loop, including truncations, amino acid substitutions, antibodies and aptamers, and evaluated these perturbations in adhesion assays and whole cell patch clamp recordings of the I_{Na}. The data presented in this Thesis demonstrate: (1) the ability of the $\beta1$ subunit to act as a CAM in breast cancer cells through homophilic interactions between the extracellularly located Ig loop of β1; (2) a mechanism by which $\beta1$ may increase the Na^+ current in breast cancer cells via regulation of $Na_v1.7$ expression, through cleavage of the intracellular domain; (3) the importance of the $\beta1$ Ig loop to support its function as both a CAM and modulator of Na^+ current; (4) the potential interplay between $\beta1$ and L1CAM, another CAM whose expression is increased in breast cancer, in regulating adhesion and invasion; and (5) that aptamers raised using the cell-SELEX approach to target the Ig domain of $\beta1$ can inhibit its adhesion-dependent activity. The data thus underscore the potential utility of inhibiting $\beta1$ function in breast cancer cells using Ig domain-directed aptamers and highlight a potential mechanism through which increased expression of β1 and Na^+ current may potentiate invasion and/or migration.

Table of Contents

List of Figures

List of Tables

Acknowledgments

The research presented in this thesis which was carried out over the past few years would not have been possible without the help of many people. Far too many to be named.

I would like to thank Dr William Brackenbury for all of his support, advice, understanding and his continued persistence. None of this would be possible without him.

I would like to thank all the members of the Brackenbury lab over the years. Dr Ming Yang for being a great wealth of knowledge, Michaela Nelson for a lot of things, but in particular for always making me laugh, Amy Thurber for teaching me electrophysiology, Alex Haworth for being a dependable and reliable colleague and Theresa Leslie for improving my bouldering ability.

I would also like to thank all the members of the Whittington group for making the office a lively place to work in and especially Iain Hartnell for being the best buddy a guy could ask for.

The advice given to me by the members of my thesis advisory panel, Professor Norman Maitland, Dr Dani Ungar, Dr Peter O'Toole and Dr David Bunka, was pivotal in shaping the direction of this PhD project. Support in many forms came from many labs but the continued support from the lab of Dr Gareth Evans, the imaging facility and Aptamer Solutions made a lot of this work possible.

Thanks to Jenny for the chilli cheese toasties and free cookies.

And finally, I'd like to thank my friends in Blackburn for keeping me sane when I was going insane and of course the continued and unwavering support of all my family and in particular my mum. She made sure I was functional throughout my PhD and without her I would have collapsed at the first hurdle.

Declaration

I, Faheemmuddeen Patel, declare that this thesis is a presentation of original work and I am the sole author. This work has not previously been presented for an award at this, or any other, University. All sources are acknowledged as References. All experiments were performed by the author. Parts of Chapter 1 have been published in the International Journal of Developmental Biology. The publication of Faheemmuddeen Patel is given below:

PATEL, F. & BRACKENBURY, W. J. 2015. Dual roles of voltage-gated sodium channels in development and cancer. Int J Dev Biol. 2015;59(7-9):357-66.

1. Introduction

1.1. Overview

The overarching focus of the research described in this Thesis is to understand the functional role of the auxiliary β1 subunit of the voltage-gated Na^+ channel (VGSC) in metastatic breast cancer cells. The literature review in this Introduction, therefore, brings together key aspects of both ion channel physiology and breast cancer biology. The Introduction is thus subdivided into four main sections. The first section summarises the structure and function of VGSCs. The second section describes the role of VGSCs in normal physiological and cellular function during development. The third section provides a basic overview of breast cancer and briefly introduces the involvement of ion channels in cancer cell biology. The last section covers the specific involvement of VGSC α and β subunits in cancer progression and how these subunits may be targeted therapeutically using existing drugs and/or novel approaches, including aptamers.

1.2. Structure and function of Voltage-gated Na^+ channels

Parts of the following text have been published in a recent review article (Patel & Brackenbury, 2015). VGSCs are heteromeric transmembrane protein complexes containing pore-forming α subunits in association with non-pore-forming β subunits (Figure 1.1A) (Catterall, 2000). The β subunits regulate channel gating. All β subunits contain an extracellular immunoglobulin (Ig) domain and are thus also cell adhesion molecules (CAMs) (Brackenbury & Isom, 2011). The classical role of VGSCs is the initiation and conduction of action potentials in electrically excitable cells, e.g. neurons (Hille, 1992). However, VGSCs are also expressed in a number of "non-excitable" cells, including fibroblasts, glia, immune cells, and cancer cells, where their role is less well understood (Brackenbury *et al.*, 2008b). Clearly, in both excitable and non-excitable cells, VGSCs regulate a number of key cellular processes, through a combination of conducting (i.e. *via* Na^+ current) and non-conducting mechanisms.

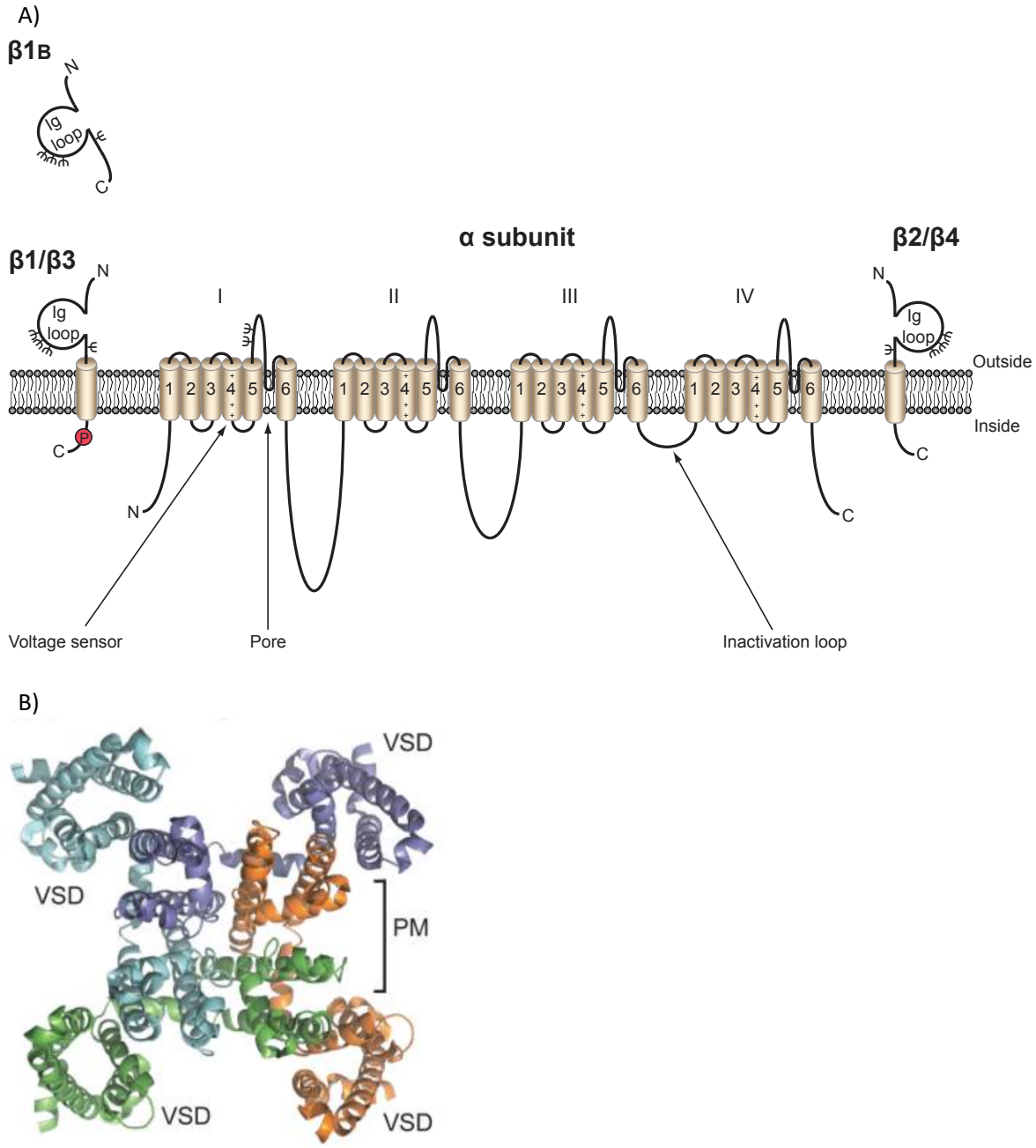

Figure 1.1 Topology of VGSCs

(A) VGSCs contain a pore-forming α subunit that has four homologous domains, each containing six transmembrane segments. The voltage sensor is in segment 4 (Catterall, 2000). The β subunits contain an extracellular immunoglobulin (Ig) loop, transmembrane domain, and an intracellular C-terminal domain, with the exception of β1B, which lacks a transmembrane domain, and is thus a soluble protein (Patino *et al.*, 2011). Red P, tyrosine phosphorylation site in β1 C-terminus (Malhotra *et al.*, 2004); ψ, glycosylation sites. (B) Crystal structure of bacterial Na_VAb channel as seen from the extracellular side. The voltage-sensing domain (VSD) is formed of S1-S4 and the pore module (PM) is formed of S5-S6. The four repeating domains (coloured blue, purple, orange and green) collectively form the pore and the opening of the pore is mediated through all the VSDs. Figure 1.1A as originally published in Brackenbury WJ and Isom LL (2011). Figure 1.1B adapted from Catterall WA and Zheng N (2015).

1.2.1. VGSC α subunits

The pore-forming α subunit consists of four homologous domains, each with six transmembrane segments. The pore is formed from the membrane dipping loop between the 5th and 6th transmembrane segments of each domain (Figure 1.1A, B) (Catterall, 2000). There are nine α subunits, $Na_v1.1$-$Na_v1.9$, encoded by *SCN1A*-*SCN11A* (Catterall, 2000). The different α subunits have unique, but often overlapping, tissue-specific expression patterns (Table 1.1) (Goldin *et al.*, 2000). There is considerable electrophysiological and pharmacological diversity between α subunits, which may, in part explain their tissue specificity (Catterall, 2000). Alternative splicing of α subunits provides additional functional, developmental, and tissue-specific variability (Diss *et al.*, 2004). The α subunits can be broadly subdivided into two categories based on their sensitivity to blockage by the potent and specific neurotoxin tetrodotoxin (TTX; Table 1.1), with TTX-sensitive VGSCs being blocked in the nanomolar range and TTX-resistant VGSCs being blocked in the micromolar range. Typically, the TTX-sensitive α subunits display faster kinetics of activation and inactivation compared to their TTX-resistant counterparts (Elliott & Elliott, 1993). However, it is important to note that many factors, such as the presence of auxiliary subunits and glycosylation patterns, all alter channel kinetics.

VGSC α subunits exist in three confirmations: closed, open and inactivated. At negative resting membrane voltages below ~-60 mV, VGSCs are in the closed state and are impermeable to the conductance of Na^+ (Ahern, 2013). Following depolarisation of the membrane, VGSCs change their conformation to the 'open' state and allow the flow of Na^+ down its electrochemical gradient as calculated by the Nernst equation (Section 2.15.6). The electrochemical gradient takes into account the both the concentration gradient of the ions and the relative difference in charge across the membrane which is generated as a result of unequal distribution of ions (Kaback, 1974). A short period (~1 ms) following activation and opening, VGSCs enter the inactivated state in which they are again impermeable to the conductance of Na^+. VGSCs are unlikely to open in response to further

membrane depolarisations until the membrane potential returns to a more negative value and the channels enter the closed state again (Ahern, 2013). The time required for the conformational changes needed to enter each stage, and the time spent in each stage, are collectively referred to as the channel kinetics and determines the biophysical properties of each α subunit subtype and therefore the shape of the action potential waveform.

Table 1.1 Tissue and cancer expression of VGSC α subunits.

Protein	Gene	Tissue location[1]	Cancer type[1]	TTX sensitivity[2]
$Na_v1.1$	*SCN1A*	CNS, PNS, heart	Ovarian	Sensitive
$Na_v1.2$	*SCN2A*	CNS, PNS	Cervical, mesothelioma, ovarian, prostate	Sensitive
$Na_v1.3$	*SCN3A*	CNS, PNS	Ovarian, prostate, small cell lung cancer	Sensitive
$Na_v1.4$	*SCN4A*	Skeletal muscle	Cervical, ovarian, prostate	Sensitive
$Na_v1.5$	*SCN5A*	Uninnervated skeletal muscle, heart, brain	Breast, colon, lymphoma, neuroblastoma, non-small cell lung cancer, ovarian, small cell lung cancer	Resistant
$Na_v1.6$	*SCN8A*	CNS, PNS, heart	Breast, cervical, lymphoma, melanoma, mesothelioma, non-small cell lung cancer, prostate, small cell lung cancer	Sensitive
$Na_v1.7$	*SCN9A*	PNS, neuroendocrine cells, sensory neurons	Breast, cervical, lymphoma, mesothelioma, non-small cell lung cancer, ovarian, prostate	Sensitive
$Na_v1.8$	*SCN10A*	sensory neurons	Prostate	Resistant
$Na_v1.9$	*SCN11A*	sensory neurons	Lymphoma, small-cell lung cancer	Resistant

[1](Goldin *et al.*, 2000; Brackenbury, 2012).

[2](Bagal *et al.*, 2015)

Through resolving the crystal structure of the three bacterial VGSCs and by comparing the homology of these channels to their mammalian counterparts, the 3D structure of the mammalian VGSC has been estimated (Payandeh *et al.*, 2011; McCusker *et al.*, 2012; Catterall & Zheng, 2015). The centrally located S5-S6 segments and membrane-dipping linker form the pore (McCusker *et al.*, 2012). The voltage-sensing domain (VSD), which is made up of S1-S4 in each domain, is located externally to the pore (Payandeh *et al.*, 2011). The pore itself contains a large externally-facing funnel followed by the ion selectivity filter which relies on charged residues to determine selectivity, a water-filled central cavity which is lined by the S6 segments, and an internally-facing inactivation gate where the S6 segments overlap (Figure 1.1B) (Catterall & Zheng, 2015).

In the VSD, S4, which is responsible for voltage dependent activation, contains repeating motifs of a positively charged residue followed by two hydrophobic residues. There are four such repeating motifs in the mammalian VGSC, termed gating charges (R1-R4), with a hydrophobic constriction site (HCS) (in either S1 or S3) present between R3 and R4 (Payandeh *et al.*, 2011). In the closed state, R1-R3 interact with an externally located negatively charged cluster of amino acids in S1-S3 whilst R4 interacts with an internally located negatively charged cluster of residues again in S1-S3 (Payandeh *et al.*, 2011). The HCS is proposed to 'seal' the VSD and prevent transmembrane movement of ions or water. Upon membrane depolarisation, S4 moves through the HCS transferring the gating charges of R4 from the intracellular negatively-charged cluster (INC) to the extracellular negatively-charged cluster ENC (Payandeh *et al.*, 2011). The linker between S3 and S4 lacks rigidity allowing for the large dynamic movements of S4 which ultimately allow for activation of the channel (Payandeh *et al.*, 2011).

Unlike VGSCs in prokaryotes, mammalian VGSCs can undergo fast inactivation. During fast inactivation, the domain-linking loop between DIII:DIV folds into the intracellularly-facing mouth of the pore, resulting in its block (Catterall & Zheng, 2015). Fast inactivation is required for the fast

spiking seen in neuronal action potentials and allows for the repetitive firing of action potentials typical of neural circuits (Catterall, 2012). Slow inactivation is seen in both prokaryotic and eukaryotic VGSCs and in cardiac tissue is proposed to regulate excitability through sustained depolarisation (Richmond *et al.*, 1998). Slow inactivation occurs through a 'collapse' of the pore wherein two of the S6 segments lining the pore move towards the centre of the pore and the other two S6 segments move away (Zhao *et al.*, 2004).

1.2.2. Pharmacology of VGSC α subunits

In addition to TTX, VGSCs are targets for a number of channel-modulating toxins, including other pore blockers, e.g. saxitoxin, μ-conotoxins, persistent activators, e.g. aconitine, veratridine, and voltage sensor-trapping toxins, e.g. scorpion toxins (Catterall *et al.*, 2005; Munasinghe & Christie, 2015; Ghovanloo *et al.*, 2016; Israel *et al.*, 2017). Given the widespread expression of α subunits in excitable cells and their key role in action potential initiation and conduction, aberrant VGSC expression and/or function, e.g. through conductance-altering channel mutations, is responsible for a number of excitability-related pathologies, including epilepsy, cardiac arrhythmia, affective disorders, and chronic pain (An *et al.*, 1998; Escayg & Goldin, 2010; Estacion *et al.*, 2010). Therefore, there is a number of therapeutically-relevant pharmacological agents in widespread clinical use which block VGSC α subunits (Catterall, 2012). An important set of VGSC blockers is the Class Ib antiarrhythmic agents, e.g. carbamazepine, lidocaine, and phenytoin, which preferentially bind to the inner pore surface at DIV:S6 of VGSCs in the inactivated state, thus providing specificity for hyperexcitable neurons, and ameliorating seizure activity in epilepsy patients (Kowey, 1998). These inhibitors commonly enhance fast inactivation and are referred to as use-dependent inhibitors (Brodie, 2017).

1.2.3. Functional recording of VGSC activity using the whole-cell patch clamp technique

Whole-cell patch clamp recording in voltage clamp mode is a frequently used method to record VGSC currents in mammalian cells (Brackenbury *et al.*, 2007; Aman *et al.*, 2009; Chioni *et al.*, 2009; Lin *et al.*, 2015). A glass pipette is used to form a tight seal with the cell membrane by applying a small amount of suction forming a tight seal which prevents the flow of ions between the solution in the pipette and the extracellular solution. By further applying a small amount of suction, the membrane present within the mouth of the tip is ruptured allowing the intracellular pipette solution and the cytoplasmic solution to dialyse. The intracellular pipette solution is usually designed such that the concentrations of the various ions replicate as closely as possible those of the cytoplasm. The voltage can then be clamped by injecting current and changing the voltage as required. In the voltage clamp mode, the current injected to maintain the set voltage is measured by the amplifier and is equal and opposite to the current flowing through ion channels across the plasma membrane. When the membrane voltage is depolarised, the probability of VGSCs opening will increase, permitting the flow of Na^+ down its electrochemical gradient, thus increasing transmembrane current (Perkins, 2006). A typical voltage-clamp protocol, such as the protocol used to measure the current voltage relationship of VGSCs in this Thesis, depolarises the voltage clamp in a stepwise manner. The resultant current is recorded at each voltage, and a current-voltage (IV) curve can be compiled (Figure 1.2A). The availability of VGSCs present in the membrane, calculated using a steady state inactivation protocol, allows the researcher to determine the fraction of VGSCs available to open at a given voltage (Figure 1.2B). By calculating the conductance and availability at each voltage and fitting Boltzmann curves to both parameters and overlapping these curves, the window current can be visualised (Figure 1.2B). This is the window, or range of voltages, within which both a proportion of the VGSCs are available for opening and not fully inactivated. If the resting membrane potential lies within this voltage window a steady-state persistent Na^+ current will occur.

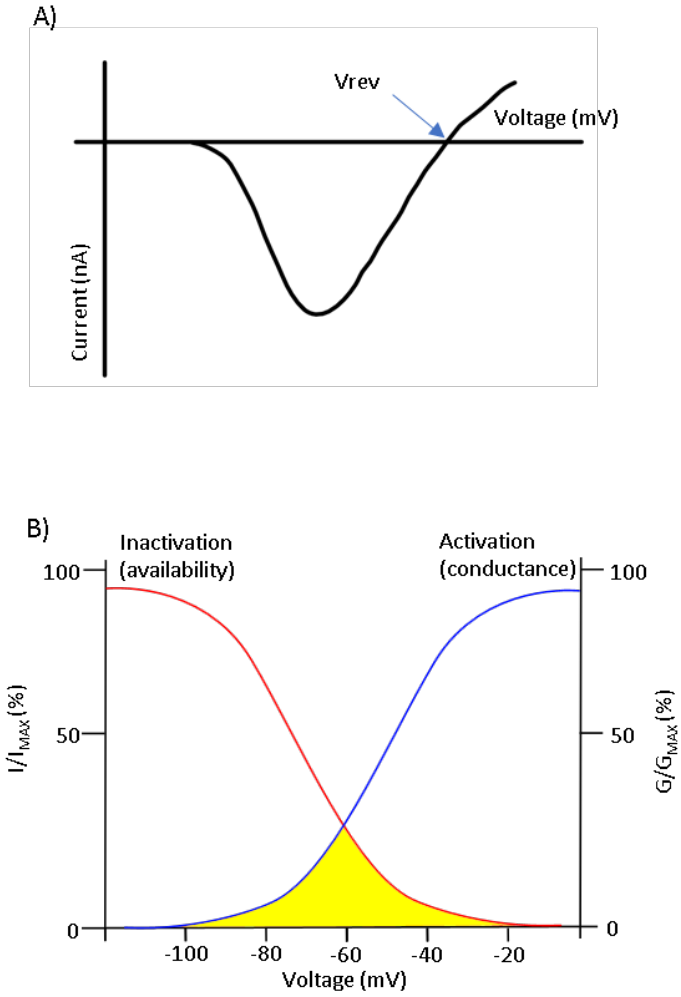

Figure 1.2 VGSC current, conductance and availability curves.

(A) Current-voltage (IV) curve which would occur from VGSCs recorded in a whole-cell patch clamp. Depolarisation activates the channels generating in an inward current. As the voltage is further depolarised the magnitude of the current decreases approaching the reversal potential (Vrev) of Na^+. (B) The proportion of channels available for opening (red line) and the percentage of maximal conductance (blue line) plotted as a function of voltage. The window current occurs where the membrane voltage is above the activation threshold and the VGSCs are incompletely inactivated (yellow area).

1.2.4. VGSC β subunits

Four genes (*SCN1B-SCN4B*) encode five different β subunits, β1, and its splice variant β1B, and β2-4 (Table 1.2) (Brackenbury & Isom, 2011). With the exception of β1B, the β subunits are type 1 topology transmembrane proteins, with a small intracellular C-terminus, and an extracellular N-

Table 1.2 β subunits.

Protein	Gene	Tissue location[1]	Cancer type[1]
β1	*SCN1B*	Heart, skeletal muscle, adrenal gland, CNS, glia, PNS	Breast, cervical, non-small cell lung cancer, prostate
β2	*SCN2B*	CNS, PNS, heart, glia	Breast, cervical, non-small cell lung cancer, prostate
β3	*SCN3B*	CNS, adrenal gland, kidney, PNS	Non-small cell lung cancer, prostate
β4	*SCN4B*	Heart, skeletal muscle, CNS, PNS	Breast, cervical, non-small cell lung cancer, prostate

[1](Brackenbury & Isom, 2011; Brackenbury, 2012).

terminus containing an Ig loop (Figure 1.3) (Isom *et al.*, 1992; Gilchrist *et al.*, 2013; Namadurai *et al.*, 2014). β1B is a splice variant of β1, which, through the retention of exon 3A, transcribes an early stop codon and does not contain the transmembrane region of β1 (Kazen-Gillespie *et al.*, 2000; Qin *et al.*, 2003). β1 and β3 are non-covalently linked to α subunits, whereas β2 and β4 are covalently linked (Isom *et al.*, 1992; Isom *et al.*, 1995; Morgan *et al.*, 2000; Yu *et al.*, 2003). Charged residues in the extracellular domain of β1 have been shown using mutagenesis studies to be responsible for regulating α subunit gating. Thus, the Ig loop is proposed to function as a platform from which these charged residues are able to interact with the α subunit (McCormick *et al.*, 1998).

Classically, the β subunits modulate the biophysical properties and trafficking of the α subunit. For example, in cardiomyocytes, colocalization of β1 with $Na_v1.5$ in the endoplasmic reticulum is proposed to enhance trafficking to the cell membrane resulting in an increase in Na^+ current density (Zimmer *et al.*, 2002). β1 and β2 increase current density, accelerate inactivation, and hyperpolarize

the voltage-dependence of inactivation in heterologous *Xenopus laevis* oocytes (Isom *et al.*, 1992; Isom *et al.*, 1995). In contrast, β3 depolarizes the voltage dependence of activation and inactivation of $Na_v1.3$ in HEK-293 cells (Cusdin *et al.*, 2010), and increases Na^+ current density by enhancing trafficking of $Na_v1.5$ to the plasma membrane in cardiomyocytes (Ishikawa *et al.*, 2013). The V110I mutation inhibits the ability of β3 to traffic $Na_V1.5$ to the plasma membrane, reducing channel conductance and resulting in Brugada syndrome, highlighting the importance of β3 for cardiac function (Ishikawa *et al.*, 2013). β4 hyperpolarizes the voltage-dependence of activation of $Na_v1.2$ in tsA-201 cells and is able to override the modulatory effects of both β1 and β3 (Qu *et al.*, 2001; Yu *et al.*, 2003). In addition, the intracellular domain of β4 has been proposed to act as an open-channel blocker in cerebellar Purkinje neurones preventing resurgent Na^+ current (Grieco *et al.*, 2005).

Importantly, however, there have been inconsistent reports on the type and magnitude of alteration of the Na^+ current by individual β subunits, which may be dependent on the cell line/type used and/or the specific combination of the α and β subunit examined (Moran *et al.*, 2003; Meadows & Isom, 2005). This variability may also be due to differences in the endogenous levels of α subunits and β subunits as well as different glycosylation states. For example, β1 and β3 have recently been shown to alter the expression and glycosylation of $Na_v1.7$ in HEK293 cells. β1 increases the expression and glycosylation of $Na_V1.7$ whilst β3 increases expression of core glycosylated $Na_V1.7$ (Laedermann *et al.*, 2013). The β1-mediated increase in glycosylation was hypothesized to increase retention of $Na_V1.7$ at the cell membrane by reducing proteasomal degradation, although this was not shown (Laedermann *et al.*, 2013).

The β subunits are also substrates for proteolytic processing by α, β and γ-secretases (Figure 1.3) (Kim *et al.*, 2005; Wong *et al.*, 2005). Sequential cleavage by β-secretase (BACE1) and γ-secretase first releases the Ig domain, leaving a short membrane-bound C-terminal fragment, and then releases a soluble intracellular domain (Kim *et al.*, 2005; Kim *et al.*, 2007).

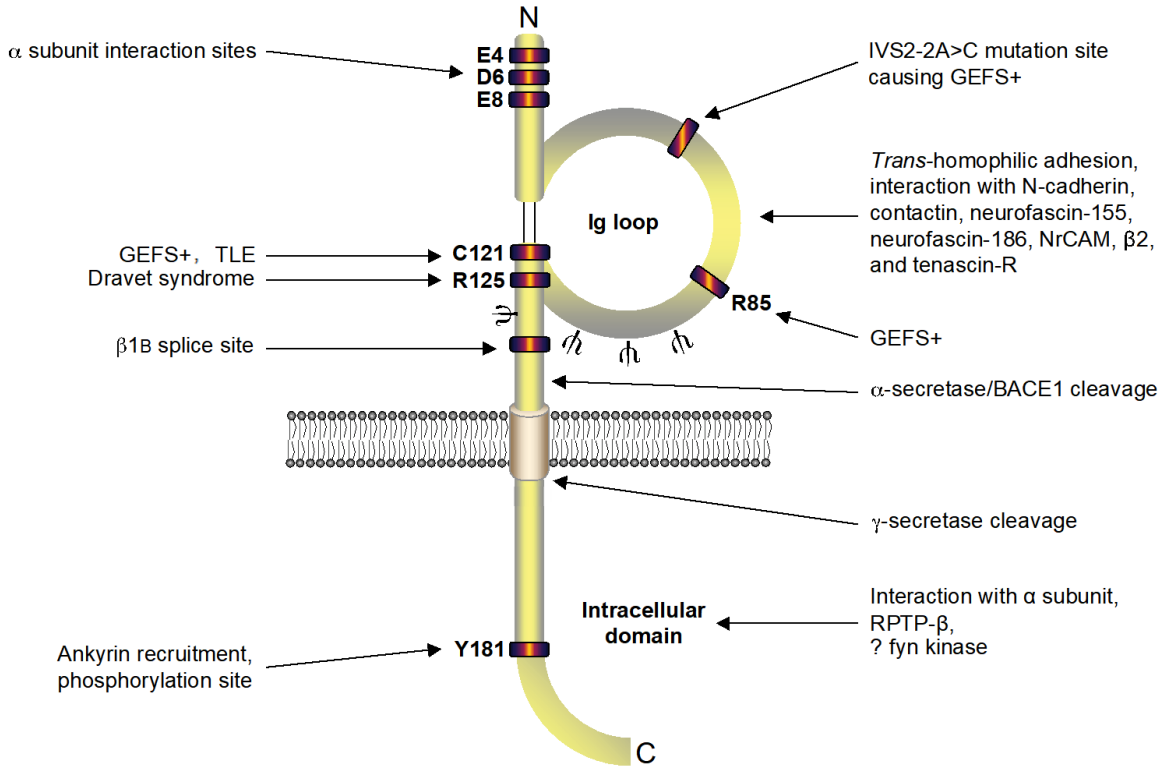

Figure 1.3 Functional map of β1.

The extracellular immunoglobulin loop interacts with other cell adhesion molecules and extracellular matrix proteins (Xiao *et al.*, 1999; Malhotra *et al.*, 2000; Kazarinova-Noyes *et al.*, 2001; Ratcliffe *et al.*, 2001; McEwen & Isom, 2004). A number of mutations at the indicated sites in and adjacent to the immunoglobulin loop have been identified as responsible for causing temporal lobe epilepsy (TLE) and genetic epilepsy with febrile seizures plus (GEFS+) (Patino & Isom, 2010). Other sites indicated: alternative splice site, putative palmitoylation site, secretase cleavage sites, glycosylation sites (ψ), sites for interaction with ankyrin, receptor tyrosine phosphatase β (RPTPβ), and fyn kinase (Malhotra *et al.*, 2002; Malhotra *et al.*, 2004; Wong *et al.*, 2005; Brackenbury *et al.*, 2008a; Patino *et al.*, 2011). Figure as originally published in Brackenbury WJ and Isom LL (2011).

Interestingly, the β subunits may also regulate other classes of ion channels. For example, β1 has been shown to regulate A-type K^+ currents in isolated cortical neurons by increasing channel retention at the membrane resulting in an increased K^+ current (Marionneau *et al.*, 2012). β1 also speeds up $K_V4.3$ inactivation whilst slowing down recovery from inactivation in cardiomyocytes (Deschenes & Tomaselli, 2002; Deschenes *et al.*, 2008). β1 has also been demonstrated to accelerate activation of $K_V1.2$, depolarise voltage dependence of activation and speed up the fast component of deactivation. Additionally, β1 hyperpolarised voltage dependence of activation and slowed deactivation of $K_V1.1$ (Nguyen *et al.*, 2012).

In addition to regulating Na^+/K^+ current, the presence of the Ig loop means that the β subunits are also CAMs. Cell-based adhesion assays have shown that β1 can interact both homophilically and heterophilically with a number of extracellular proteins and other CAMs, including β2, contactin, neurofascin-186, NrCAM and N-cadherin (Figure 1.3) (Xiao *et al.*, 1999; Malhotra *et al.*, 2000; Kazarinova-Noyes *et al.*, 2001; Ratcliffe *et al.*, 2001; McEwen & Isom, 2004). It has been proposed that such heterophilic adhesion interactions may regulate intracellular signalling downstream of β1. In *Drosophila* S2 cells, trans-homophilic interactions through β1 enhances interaction with ankyrin and recruits the actin cytoskeleton to points of cell-cell contact (Figure 1.3) (Malhotra *et al.*, 2000). In Chinese hamster lung cells, phosphorylation of Y181 on β1 abolishes recruitment of $ankyrin_G$ and $ankyrin_B$ (Malhotra *et al.*, 2002). Further, phosphorylation of Y181 regulates subcellular localization of β1 to the intercalated disk in cardiomyocytes (Malhotra *et al.*, 2004). β2 interacts with the extracellular matrix proteins tenascin-C and tenascin-R (Srinivasan *et al.*, 1998). Although β1 has been shown to interact with tenascin-R only, it has been proposed that β subunits initially recognise and interact with tenascins, but are then repelled, which may serve an important function in neuronal pathfinding (Srinivasan *et al.*, 1998; Xiao *et al.*, 1999).

β3 shows significant homology to β1, however, when expressed in *Drosophila* S2 cells, β3 does not participate in *trans*-homophilic adhesion, nor does it interact with β1 or contactin in Chinese hamster lung cells, although it does interact with neurofascin-186 (McEwen & Isom, 2004; McEwen *et al.*, 2009). In contrast, another study has shown that in HEK-293 cells, the Ig domain of β3 can indeed participate in trans-homophilic binding and can interact heterophilically with β1 (Yereddi *et al.*, 2013). Clearly, further work is required to resolve these conflicting observations. It is possible that β3-mediated adhesive interactions may be dependent on species/cell type, although the physiological implications of this were not considered in these studies. Heterophilic binding of β1 and β3 may serve unique functions in the tissues where co-expression of both subunits is seen, such

as the hippocampus (Yereddi *et al.*, 2013). The ability β4 to interact heterophilically with possible binding partners also remains untested.

1.3. Role of VGSCs in central nervous system development and function

1.3.1. Developmental expression and function of VGSC α subunits

Electrical activity is required for axonal and dendritic development and synaptogenesis in the retinogeniculate pathway, visual cortex and development of the lateral geniculate nucleus is significantly slowed in mice injected with TTX (Riccio & Matthews, 1985; Casagrande & Condo, 1988). Similarly, deletion of $Na_v1.1$, $Na_v1.2$, or $Na_v1.6$ in mice results in central nervous system (CNS) defects and premature lethality (Harris & Pollard, 1986; Planells-Cases *et al.*, 2000; Yu *et al.*, 2006). Thus, α subunit expression and activity appear to be critical for normal CNS development. Fine-tuning of electrical activity *via* VGSC α subunit expression is tightly regulated during development. For example, $Na_v1.3$ is expressed during foetal development and is replaced by $Na_v1.1$, $Na_v1.2$, and $Na_v1.6$ in the CNS from postnatal day 7 in the mouse (Beckh *et al.*, 1989; Schaller & Caldwell, 2000).

Later in postnatal development, $Na_v1.6$ replaces $Na_v1.2$ at the axon initial segment, and nodes of Ranvier following myelination (Boiko *et al.*, 2001; Kaplan *et al.*, 2001; Boiko *et al.*, 2003). Interestingly however, α subunits may also play a non-conducting role (independent of Na^+ current) in regulating tissue development. For example, although $Na_v1.5$ expression is required for normal heart development in zebrafish, TTX did not perturb early cardiomyocyte development, however, $Na_V1.5$ knockout did, suggesting involvement of a non-conducting mechanism (Chopra *et al.*, 2010).

Further developmental regulation of VGSCs is achieved by alternative splicing. Alternative splicing in domain I segment 3 (DI:S3) occurs in a number of the α subunits, and is developmentally regulated for $Na_v1.2$, $Na_v1.3$ and $Na_v1.5$ (Diss *et al.*, 2004). $Na_V1.7$ has four splice variants, all of which show different β1-mediated alterations to their kinetic properties (Farmer *et al.*, 2012). Finally, the

developmentally regulated expression profile of VGSCs is disrupted in CNS diseases. For example, in multiple sclerosis (MS), $Na_v1.2$, $Na_v1.6$ and $Na_v1.8$ are up-regulated in CNS neurons in response to demyelination (Black *et al.*, 2000; Craner *et al.*, 2004).

1.3.2. Developmental expression and function of VGSC β subunits

β subunit expression is also developmentally regulated. During CNS development, the *SCN1B* splice variant β1B is predominantly expressed embryonically (Kazen-Gillespie *et al.*, 2000; Patino *et al.*, 2011). In contrast, β1 expression increases from birth, peaking at postnatal day 14 in mice (Kazen-Gillespie *et al.*, 2000). The β1 subunit plays a critical role in CNS development. *Scn1b* null mice are ataxic and display spontaneous generalized seizures (Klugbauer *et al.*, 2003). In the CNS of β1 null mice, expression of $Na_V1.1$ is reduced and $Na_V1.3$ is increased. Postnatal $Na_V1.3$ expression is predicted to give rise to an epileptic phenotype, although the β1 subunit itself may also play a critical role (Chen *et al.*, 2004).

Mutations in *SCN1B* result in genetic epilepsy with febrile seizures plus (GEFS+) or temporal lobe epilepsy (Patino & Isom, 2010) (Figure 1.3). The first, and best characterised heritable mutation in the β1 subunit is C121W, which results in a mutation of the second cysteine required to form the disulphide bond of the Ig loop. This mutation, which causes epileptic seizures in humans and mice, results in a loss of channel modulating and adhesive function compared to wild type β1 (Meadows *et al.*, 2002; Wimmer *et al.*, 2010; Kruger *et al.*, 2016). Interestingly, the C121W mutant displays a lower molecular weight compared to wild type β1, possibly as a result of incomplete glycosylation (Kruger *et al.*, 2016). The C121W mutant is expressed at the plasma membrane although it does not associate with α subunits, and its localisation to the axon initial segment is disrupted (Wimmer *et al.*, 2015; Kruger *et al.*, 2016).

Two additional heritable mutations, R85C and R85H, were subsequently identified as associated with epilepsy (Scheffer *et al.*, 2007; Thomas *et al.*, 2007). Mutation of R85 to either cysteine or histidine results in a loss of β1 membrane expression (Xu *et al.*, 2007). The R85C mutation results in a loss of the ability of β1 to modulate the kinetics of the Na^+ current, whereas the R85H mutant maintains the ability to modulate the voltage-dependence of steady-state slow inactivation similar to wild type β1 (Xu *et al.*, 2007). More recently, a recessive mutation, R125C, has been shown to cause Dravet Syndrome, a severe form of paediatric epilepsy, in humans, (Patino *et al.*, 2009). The mutant β1 is not expressed at the plasma membrane, thus disrupting β1 function (Patino *et al.*, 2009). The epilepsy-related mutation G257R, unique to the β1B splice variant, also results in loss of secretion and expression at the plasma membrane, generating a loss of β1B function (Patino *et al.*, 2011). Thus, different mutations in residues in the Ig loop of β1/β1B appear to have slightly different effects on functionality, however, in general, the mutations do result in at least a partial loss of function, thus explaining the epileptogenic phenotype.

In cerebellar granule neurons (CGNs), β1 promotes neurite outgrowth *via trans*-homophilic adhesion (Davis *et al.*, 2004). β1B can also promote neurite outgrowth (Patino *et al.*, 2011). β1-mediated neurite outgrowth also requires fyn kinase and contactin and although β1 deletion does not affect fyn kinase expression it does reduce contactin levels (Brackenbury *et al.*, 2008a). β1 is required for neuronal pathfinding and fasciculation in the postnatally developing CNS (Brackenbury *et al.*, 2008a; Brackenbury *et al.*, 2013). β1 is also required for normal localization of $Na_v1.6$ to the axon initial segment in CGNs and the resultant inward Na^+ current is required for β1 mediated neurite outgrowth, suggesting a specific reciprocal relationship between these two subunits (Figure 1.4A) (Brackenbury *et al.*, 2010).

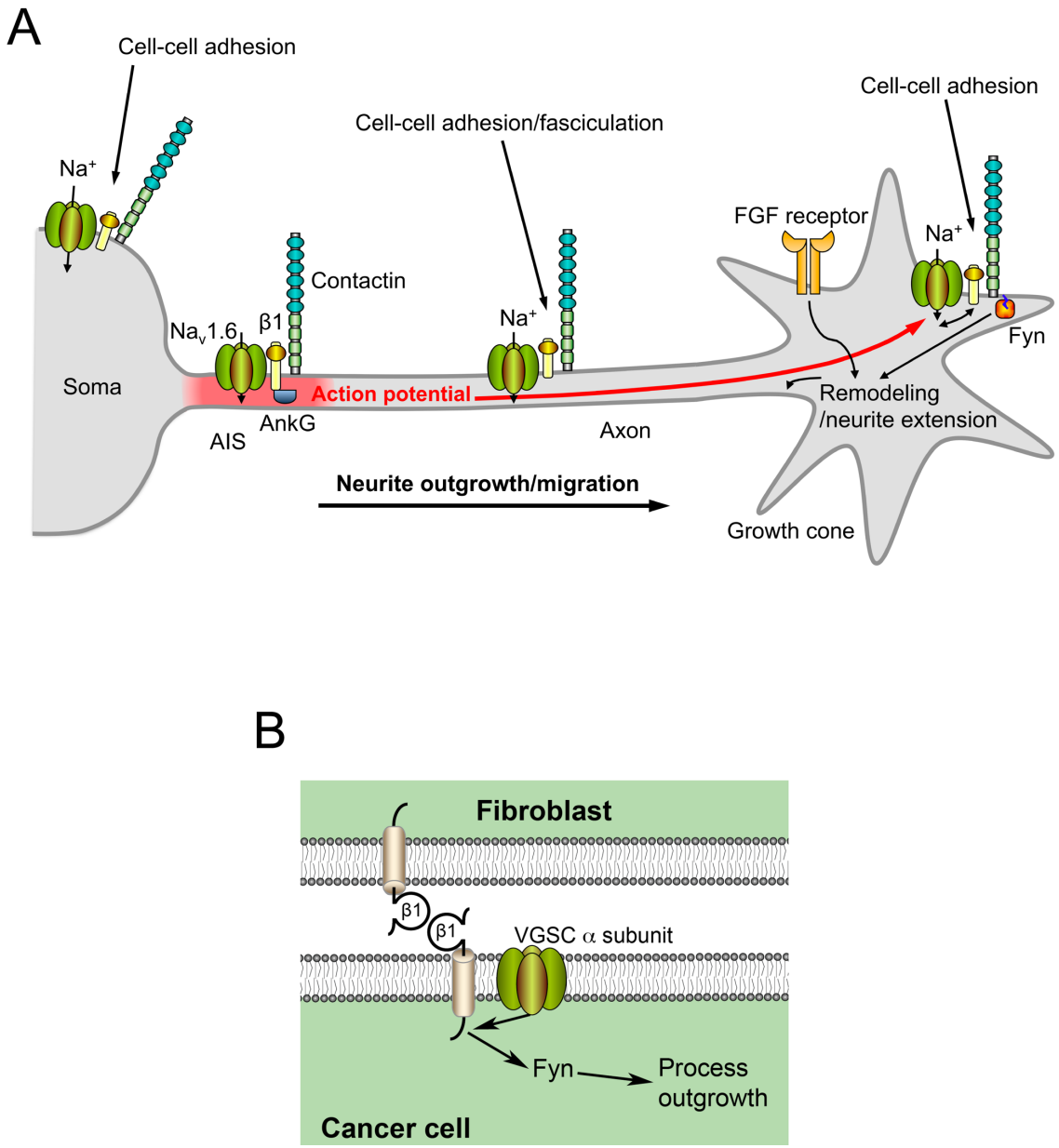

Figure 1.4 Functional reciprocity between α and β subunits regulating neurite outgrowth and migration during CNS development and metastasis.

(A) β1 is required for localization of $Na_v1.6$ to the axon initial segment and high frequency action potential firing. The electrical activity and resultant membrane depolarisation promotes β1-mediated neurite outgrowth towards the growth cone. (B) A similar mechanism is proposed for β1-mediated process outgrowth in breast cancer cells. β1 from an adjacent fibroblast or cancer cell interacts with β1 on the cancer cell, initiating a signalling cascade that requires Na^+ current and fyn kinase. Figure panels as originally published (Brackenbury *et al.*, 2010; Nelson *et al.*, 2014).

Scn2b null mice appear normal in neurological tests, although they display increased seizure susceptibility, and altered sensitivity to pain stimuli (Chen *et al.*, 2002; Lopez-Santiago *et al.*, 2006).

Physiologically, β2 increases $Na_v1.7$ expression and β2 null mice display a more sensitive response to noxious thermal stimuli (Chen *et al.*, 2002; Lopez-Santiago *et al.*, 2006). Electrical activity is reduced in the optic nerve of *Scn2b* null mice, and Na^+ current is reduced in hippocampal and dorsal root ganglion neurons, compared to wildtype animals (Chen *et al.*, 2002; Lopez-Santiago *et al.*, 2006). Interestingly, *Scn2b* deletion is neuroprotective in the experimental allergic encephalomyelitis MS model in mice, possibly by reducing α subunit up-regulation (O'Malley *et al.*, 2009).

In cardiac electrocardiograms, *Scn3b* null mice display longer P waves and prolonged QR intervals, which ultimately resulted in a slower heart rate, but show no abnormalities in the CNS (Hakim *et al.*, 2008). It is possible that β1 may compensate for the lack of β3 allowing for an apparently normal neurological phenotype, although this has not been investigated. Overexpression of β4 in Neuro2a cells increases neurite outgrowth, dendrite formation, and filopodia-like protrusions (Oyama *et al.*, 2006), suggesting that, like β1, β4 may regulate migration and pathfinding *in vivo*. β4 is downregulated in the striatum of Huntington's Disease patients and knockout of *Scn4b* in mice leads to abnormal VGSC expression, reduced resurgent current and repetitive action potential firing in striatal neurons, suggesting a possible pathological role for β4 down-regulation in neurodegeneration (Oyama *et al.*, 2006; Tamura *et al.*, 2014).

Finally, the β subunits may play a role in downstream signalling pathways and gene transcription following proteolytic processing by secretases (Kim *et al.*, 2005; Wong *et al.*, 2005). The soluble cleaved β2 intracellular domain is proposed to translocate to the nucleus and regulate expression of $Na_v1.1$ although the means of translocation is currently unknown (Kim *et al.*, 2005; Kim *et al.*, 2007). Secretase-mediated cleavage of β1 regulates neurite outgrowth, suggesting that proteolytic processing of β subunits may be an essential step in transducing the adhesion signal to promote migration (Brackenbury & Isom, 2011).

In summary, VGSC α and β subunit expression is temporally regulated during CNS development. Regulated expression of specific subtypes is critical for maintaining electrical excitability and activity-dependent synaptic connections on the one hand, and adhesive interactions, neurite outgrowth, fasciculation and migration on the other. Several studies point towards a potential causal relationship between altered VGSC expression, developmental aberrations, and CNS pathophysiologies, which requires further investigation.

1.4. Ion transport and cancer

1.4.1. Breast cancer

Cancer is a disease of uncontrolled proliferation and survival. Hanahan and Weinberg (2011) laid out eight hallmarks healthy cells must attain to become cancerous (sustaining proliferative signalling, evading growth suppressors, resisting cell death, enabling replicative immortality, inducing angiogenesis, and activating invasion and metastasis) and two further emerging hallmarks (reprogramming of energy metabolism and evading immune destruction) (Hanahan & Weinberg, 2011). Breast adenocarcinoma has its origin in glandular epithelial cells (Cetin & Topcul, 2014) and is the leading cause of cancer related death in women worldwide (Jemal *et al.*, 2011). Importantly, most breast cancer deaths are the result of metastasis, where the primary tumour invades and spreads to distant sites (Figure 1.5). The metastatic cascade is a complex multistep process in which cancerous cells within a tumour become detached from the initial tumour, invade the surrounding tissues, intravasate into the lymphatic or blood circulatory system, extravasate at a different location in the body and form a new tumour at the distant location (Figure 1.5). An important distinction to be made here is between the processes of migration and invasion. Migration denotes the movement of cells across a substrate (e.g. dish in cell culture, or adjacent stroma in a tumour), whereas invasion describes the process by which tumour cells proteolytically digest the extracellular matrix (ECM) via protease activity (e.g. through secretion of cathepsins or matrix metalloproteinases). By digesting

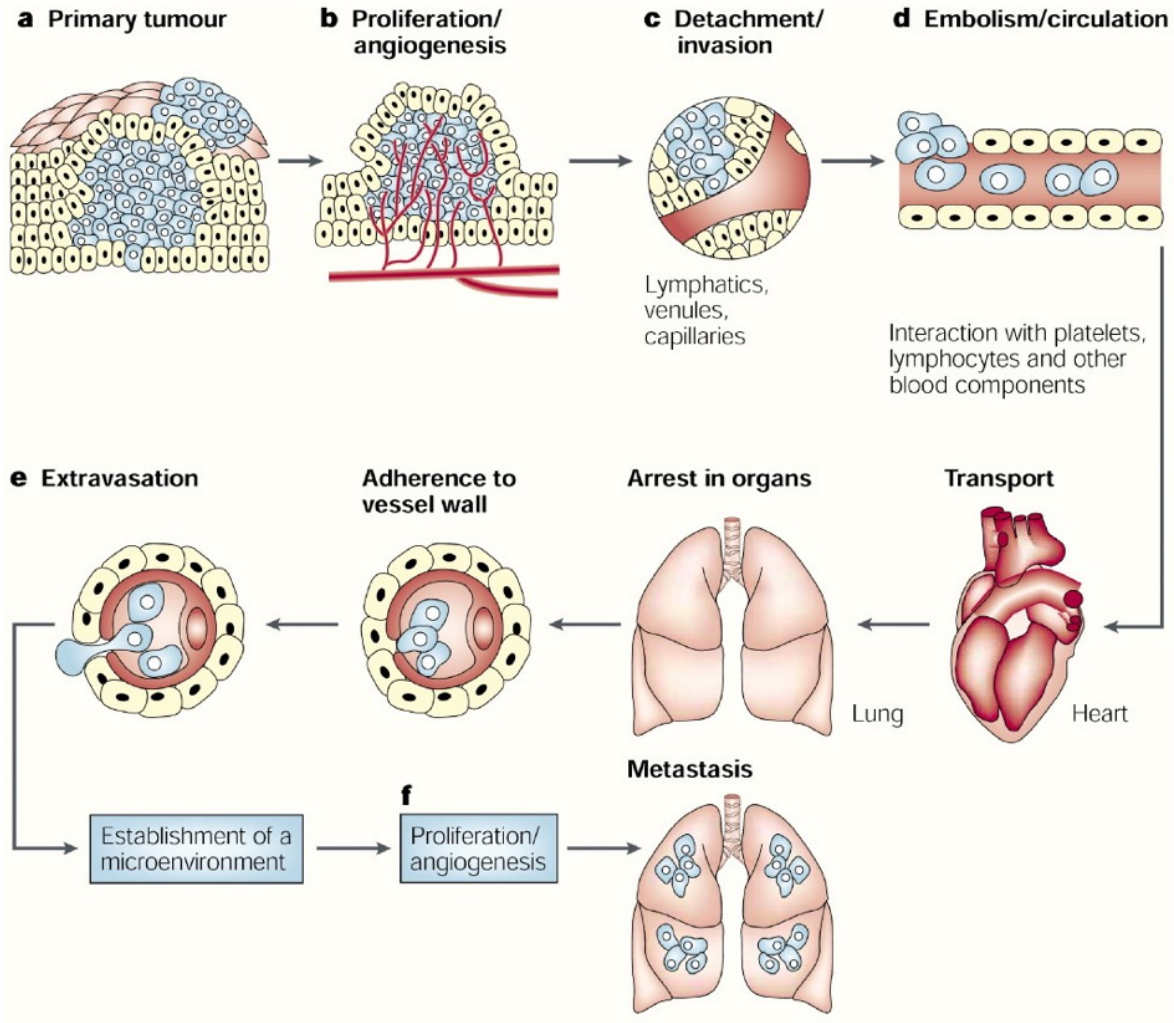

Figure 1.5 The metastatic cascade.

Metastasis is a complex, multi-step process involving proliferation, angiogenesis, detachment, migration, invasion, intravasation, transport in the circulation, extravasation, adhesion, and establishment of a secondary tumour. Figure reproduced from (Fidler, 2003).

the ECM, the invading cancer cells can 'break free' from the tumour and facilitate migration to distant sites (van Zijl *et al.*, 2011; Yang & Lin, 2017).

Breast cancer can be classified into distinct subtypes based on the expression profile of the estrogen receptor (ER), progesterone receptor (PR) and human epidermal growth factor receptor type 2 (HER2) (Cetin & Topcul, 2014). Classification of breast cancer into these subtypes allows for better

patient management and prediction of outcome (Zubeda *et al.*, 2013). Triple negative breast cancer (TNBC), in which expression of ER, PR and HER2 is absent, is an aggressive, often lethal, subtype for which there are no curative therapies and so treatment is often limited to palliative care (Cetin & Topcul, 2014). Through the use of whole-genome sequencing studies, breast cancers have been further subclassified based on their genetic and molecular profiles. This could potentially lead to better personalised medicine for individual patients. However, accessing repeated tumour samples over time is difficult although this may be somewhat remediated through analysis of circulating tumour DNA analysis in blood samples (Baird & Caldas, 2013). Another major challenge in understanding and treating breast cancer, is the origin of the cancer itself. Currently it is not possible to detect dormant cancer stem cells (CSCs) and there are no clear markers for all breast CSCs, suggesting the possibility that breast CSCs adapt to the specific niche and do not represent a fixed population (Eccles *et al.*, 2013). Arguably the biggest challenge faced when treating breast cancer is that of metastasis. If we could better understand the role of the environment at the secondary tumour sites, especially the similarities between permissive metastatic microenvironments such as the bone, liver and brain, we may be able to tailor treatment to patients and at the same time reduce the risk of overtreating patients who do not develop metastases (Eccles *et al.*, 2013).

1.4.2. Ion channels and cancer

Over the past two decades it has become apparent that ion channels play a diverse range of functions in cancer cells. Thus, specific ion channels have been shown to play roles in the deregulation of the 'normal' mechanics of cells allowing for the development of a cancerous phenotype (Prevarskaya *et al.*, 2010). Importantly, ion channels, including VGSCs, have been shown to play key roles in all the cancer hallmarks (Prevarskaya *et al.*, 2010). For example, aberrant expression of voltage-gated calcium channels alters cell cycle progression, promoting proliferation (Lu *et al.*, 2008; Buchanan & McCloskey, 2016). A similar role has been shown for certain classes of transient receptor potential (TRP) channels (Bodding, 2007). Abnormal K^+ channel expression or

function in cancer cells also results in altered cell cycle progression although this may be a consequence of indirect effects of altered membrane potential on Ca^{2+} influx (Gentile, 2016). K^+ channel activity, in conjunction with Cl^- transport, allows for increased invasion through regulation of cytosolic osmolarity, movement of water and altered cell shape. Such a mechanism has been proposed to promote glioma invasion into surrounding brain parenchyma (Turner & Sontheimer, 2014).

Ion channels play key roles in facilitating invasion, migration and metastasis (Figure 1.6). Ion channel-dependent mechanisms promote the formation of invadopodia, filopodia and lamellipodia, as well as facilitating secretion of ECM-degrading proteins, commonly associated with an increase in the metastatic potential of a cancer cell (Klemke, 2012; Hoshino *et al.*, 2013). Given the diversity of channels expressed, across a range of tumour types, a potentially unique ion channel expression profile of each cancer may permit a tailored therapeutic approach. However, a challenge will be to accurately delineate these profiles within tumours. The next section of the Introduction will focus on VGSC α and β subunits in cancer.

1.5. VGSCs and cancer

1.5.1. α subunit expression in cancer

VGSC α subunits are widely expressed in a range of different types of cancer, including breast cancer, cervical cancer, colon cancer, glioma, leukaemia, lung cancer, lymphoma, melanoma, mesothelioma, neuroblastoma, ovarian cancer and prostate cancer (Table 1.1) (Brackenbury, 2012). Although the majority of evidence is based on studies using cell lines cultured *in vitro*, a number of reports have now confirmed that α subunit expression occurs in tumours *in vivo*, e.g. (Fraser *et al.*, 2005; Gao *et al.*, 2010; House *et al.*, 2010; Hernandez-Plata *et al.*, 2012). In several cancers where multiple α subunits have been detected, one α subunit has been identified as most highly expressed, e.g. $Na_v1.5$ is predominant in breast cancer (Fraser *et al.*, 2005), whereas $Na_v1.7$ is predominant in

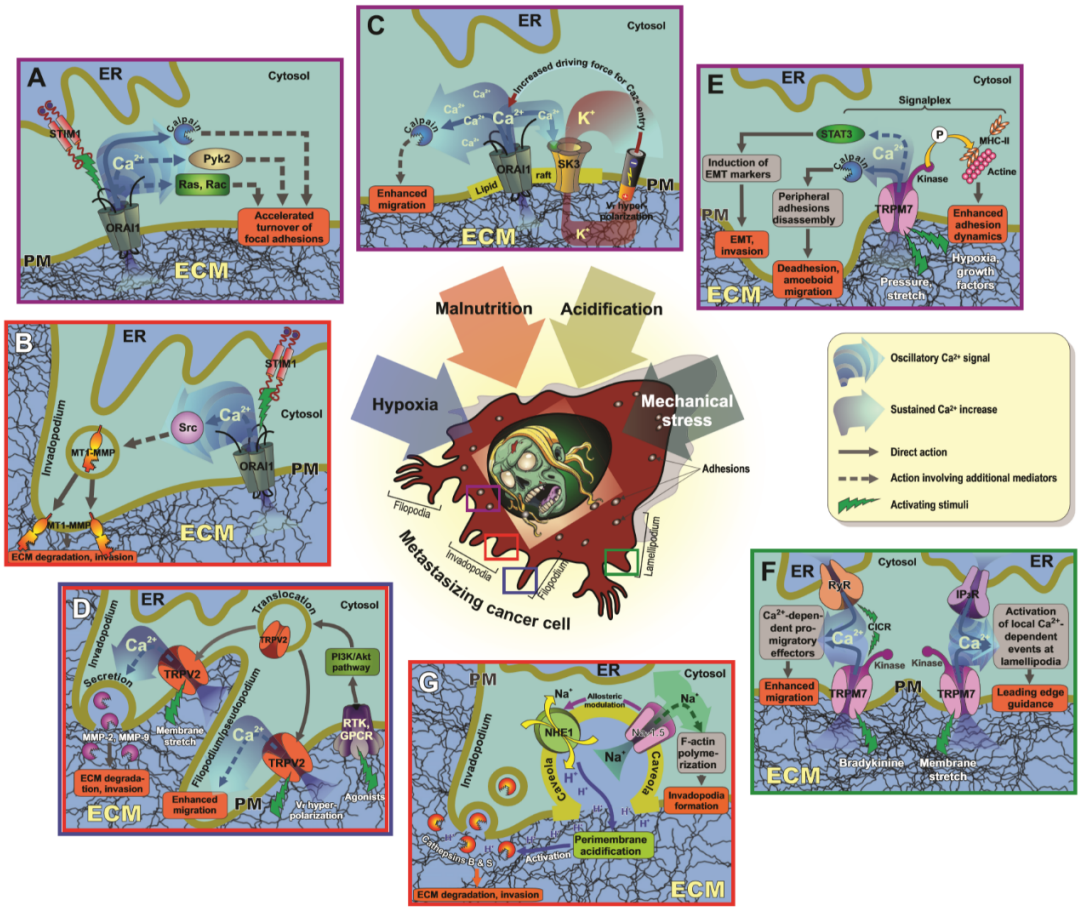

Figure 1.6 Involvement of ion channels in migration, invasion and metastasis of cancer cells.

Centre: metastatic cancer cell with morphological changes common to invasive, metastatic and migratory phenotypes. Boxes A-G depict ion channel-dependent processes which promote metastatic behaviours in the tumour areas outlined by the same colour box. Gradients of blue indicate a change in Ca^{2+} concentration. ECM, extracellular matrix; ER, endoplasmic reticulum; PM, plasma membrane. Figure reproduced from (Prevarskaya *et al.*, 2018).

prostate and non-small cell lung cancer (Diss *et al.*, 2004; Campbell *et al.*, 2013). Interestingly, $Na_v1.5$ and $Na_v1.7$ have been shown to be mainly expressed in their neonatal DI:S3 splice forms in several cancers (Brackenbury, 2012). However, this splicing pattern is not conserved across all the tumour types studied, e.g., the neonatal DI:S3 splice form is absent in colon cancer cells, and the adult variant is expressed instead (House *et al.*, 2010). There also appears to be a cancer type-specific relationship between α subunit expression and metastatic propensity. For example, $Na_v1.5$ is more highly expressed in strongly metastatic MDA-MB-231 breast cancer cells than weakly metastatic

MCF-7 cells, and elevated $Na_v1.5$ expression in tumours correlates with increased risk of recurrence, metastasis and reduced overall survival (Fraser *et al.*, 2005; Yang *et al.*, 2012; Nelson *et al.*, 2014). A similar pattern has been shown for α subunit expression in colon, prostate, ovarian and non-small cell lung cancers (Brackenbury & Djamgoz, 2006; Gao *et al.*, 2010; House *et al.*, 2010; Campbell *et al.*, 2013). However, there is an inverse correlation between α subunit expression and clinical grade in glioma (Brackenbury, 2012).

The mechanisms by which VGSCs are up-regulated in cancer cells are not well understood. Several studies suggest that growth factors may play a role (Fraser *et al.*, 2014). Epidermal growth factor (EGF) and nerve growth factor (NGF) both increase Na^+ current in rat Mat-LyLu prostate cancer cells, the latter *via* activation of protein kinase A (PKA) (Brackenbury & Djamgoz, 2007; Ding *et al.*, 2008). Similarly, EGF signalling *via* the extracellular signal-regulated kinase (ERK)1/2 pathway increases expression of $Na_v1.7$ and Na^+ current in H460 non-small cell lung cancer cells (Campbell *et al.*, 2013). In MDA-MB-231 breast cancer cells, external application of β-Estradiol (E2) activates the G-protein coupled estrogen receptor GPR30, increasing VGSC expression. Application of the PKA inhibitor, PKI abrogates the effect of E2 on VGSC expression whereas the adenylate cyclase activator, forskolin, increases VGSC expression, suggesting the E2/GPR30-mediated upregulation of VGSC expression is PKA-dependent (Fraser *et al.*, 2010). E2 also increases adhesion in MDA-MB-231 cells, suggesting a possible role in upregulating CAM expression/activity (Fraser *et al.*, 2010). Further fine-tuning of VGSC expression in cancer cells is achieved through positive feedback auto-regulation. In both metastatic human MDA-MB-231 breast and rat Mat-LyLu prostate cancer cells, Na^+ current activates PKA, which in turn, promotes functional expression of $Na_v1.5$ and $Na_v1.7$, respectively, possibly through promoting trafficking of the channels to the plasma membrane (Brackenbury & Djamgoz, 2006; Chioni *et al.*, 2010).

1.5.2. Function of α subunits in cancer cells

In vitro, pharmacological blockage of VGSC α subunits with TTX has been shown to inhibit various cellular behaviours associated with metastasis, including endocytosis (Mycielska *et al.*, 2003), galvanotaxis (Djamgoz *et al.*, 2001), gene expression (Mycielska *et al.*, 2005), invasion (Grimes *et al.*, 1995), migration (Fraser *et al.*, 2003), and process outgrowth (Fraser *et al.*, 1999). These results suggest that functional activity of VGSCs is necessary to promote metastatic cell behaviour. The functional consequences of VGSC activity in cancer cells are intriguing given that these cells are non-excitable. Thus, how is a VGSC functional in non-excitable cells with relatively depolarised membrane potentials? A clue to this comes from the electrophysiological properties of VGSCs discussed above. In strongly metastatic cells, the resting membrane potential is relatively depolarised compared to weakly metastatic cells, and thus, the Na_V channels are partially activated, carrying a small inward Na^+ current. The window current of $Na_v1.5$ channels in MDA-MB-231 cells implies that there is a persistent inward Na^+ current at the resting membrane potential (~-15 mV) (Roger *et al.*, 2003). This persistent inward current, whilst a fraction of the transient current observed in excitable cells, or under voltage clamp conditions, is likely to be functionally significant. Indeed, it has been shown that VGSC activity elevates the intracellular Na^+ level in H460 non-small cell lung cancer cells, as the persistent Na^+ current maintains a depolarised resting membrane potential, keeping the Na^+ channels open, and thus allowing Na^+ to come in, creating a positive feedback loop (Campbell *et al.*, 2013).

Conflicting reports suggest that α subunits may, or may not, also regulate proliferation. In the Mat-LyLu prostate cancer cell line, TTX application has no effect on proliferation but the VGSC opener veratridine increases proliferation (Fraser *et al.*, 2000). In addition, the VGSC blockers flunarizine and riluzole have been shown to inhibit proliferation of PC3, DU145, LNCaP and MDA-PCA-2B prostate cancer cell lines (Abdul & Hoosein, 2001). On the other hand, TTX does not inhibit proliferation of MDA-MB-231 cells in 2D culture (Roger *et al.*, 2003). These discrepancies may be due to the differing

specificity of the various pharmacological approaches used in different studies and further work is required to resolve these discrepancies.

Several studies have indicated that specific α subunits contribute to the invasive capacity of different cancer cell types. For example, the neonatal DI:S3 splice variant of $Na_v1.5$ enhances migration and invasion of metastatic MDA-MB-231 breast cancer cells (Brackenbury *et al.*, 2007). In contrast, $Na_v1.6$ enhances invasion of primary cervical cancer cells (Hernandez-Plata *et al.*, 2012), and $Na_v1.6$ and $Na_v1.7$ enhance invasion and endocytosis in PC-3 and Mat-LyLu prostate cancer cells (Nakajima *et al.*, 2009). Nonetheless, expression of any subtype may be sufficient to promote invasion. For example, overexpression of $Na_v1.4$ increases the invasiveness of LNCaP prostate cancer cells (Bennett *et al.*, 2004) suggesting that the Na^+ current itself is more important for promoting an invasive phenotype than the specific α subunit expressed.

Several theories have been proposed to explain how Na^+ flux through VGSCs contributes to invasion and metastasis. In MDA-MB-231 breast cancer cells, $Na_v1.5$-mediated Na^+ influx has been shown to increase H^+ efflux through modification of activity of the Na^+/H^+ exchanger (NHE1), causing intracellular alkalinisation and extracellular perimembrane acidification, thus enhancing the activity of pH-dependent cathepsin proteases and invadopodia formation (Gillet *et al.*, 2009; Brisson *et al.*, 2013). Several questions remain unresolved surrounding this mechanism, however. For example, how does $Na_v1.5$ activity regulate NHE1? Could Na^+ influx via other mechanisms also play a role? NHE1 activation is mediated by the RhoA signalling pathway which is itself modulated by PKA mediated phosphorylation (Cardone *et al.*, 2005). RhoA phosphorylation by PKA results in its inhibition which ultimately results in a remodelling of the cytoskeleton leading to altered expression of plasma membrane proteins (Brisson *et al.*, 2011). Thus, one possibility is that VGSCs may impact on NHE1 activity at the plasma membrane via PKA activation.

VGSCs may also regulate gene expression in cancer cells (Brackenbury & Djamgoz, 2006). In SW620, SW480 and HT29 colon cancer cells, $Na_v1.5$ has been proposed to be a key regulator of a network of invasion-promoting genes (House *et al.*, 2010). However, the intermediate steps between Na^+ current and gene transcription remain to be elucidated. A third possibility is that VGSCs may regulate intracellular Ca^{2+} levels. For example, activation of VGSCs present on intracellular membranes in macrophages and melanoma cells causes Na^+ release from cationic stores, followed by Na^+ uptake by mitochondria, and Ca^{2+} release, which then increases podosome and invadopodia formation, and enhanced invasiveness and this can be prevented by EGTA-mediated chelation of Ca^{2+} (Carrithers *et al.*, 2009). An additional, untested possibility is that Na^+ influx via $Na_v1.5$ could lead to reverse mode operation of the Na^+/Ca^{2+} exchanger NCX, thus resulting in Ca^{2+} influx. Such VGSC-mediated Ca^{2+}-dependent mechanisms have been largely ignored and need to be tested in cancer cells. Finally, a significant number of somatic mutations have been identified in *SCN5A* in tumours (Figure 1.7A). These mutations span all functional domains of the channel, including the pore module, the VSD and the inactivation gate (Figure 1.1A). Such mutations may impact on channel activity, regulation, and/or interaction with intracellular signalling partners. Further work is required to establish whether and how these mutations may confer a functional advantage on the VGSC to promote invasive behaviour.

1.5.3. Therapeutic value of α subunits

The fact that α subunits appear to be up-regulated in cancer cells and promote metastasis-like behaviour suggests that they may be useful therapeutic targets. Indeed, the VGSC-inhibiting drugs ranolazine, which blocks the persistent Na^+ current, and phenytoin, a therapeutic used to treat epilepsy, have both recently been shown to inhibit metastasis in xenograft mouse models of breast cancer (Driffort *et al.*, 2014; Nelson *et al.*, 2015). In support of this, several other VGSC-targeting antiepileptic drugs, including phenytoin, carbamazepine and riluzole, have been shown to inhibit secretory activity, cellular migration, proliferation and invasion in cell lines from several different

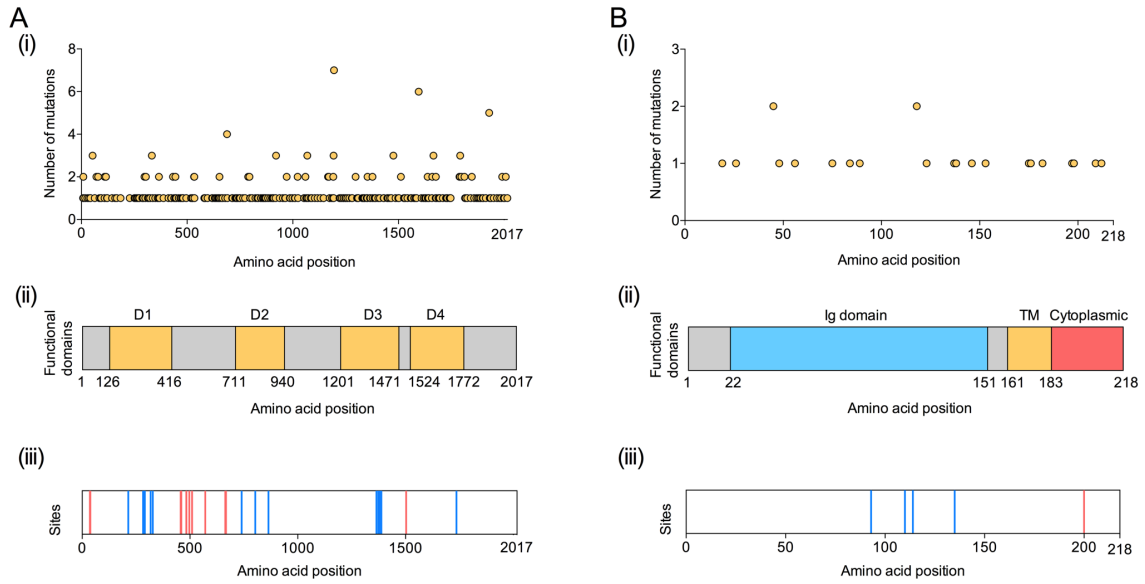

Figure 1.7 $Na_v1.5$ and β1 mutations in cancer.

(A) $Na_v1.5$: (i) Number of mutations reported in the COSMIC database (http://cancer.sanger.ac.uk/cancergenome/projects/cosmic/) for each amino acid position on x-axis. (ii) Location of Domains 1-4 (yellow) (Catterall, 2000). (iii) Putative phosphorylation (red) and glycosylation sites (blue). (B) β1: (i) Number of mutations reported in the COSMIC database for each amino acid position. (ii) Location of immunoglobulin (Ig) domain (blue), transmembrane (TM) domain (yellow) and cytoplasmic domain (red) (Brackenbury & Isom, 2011). (iii) Phosphorylation (red) and glycosylation sites (blue).

cancers, including prostate and breast cancer (Abdul & Hoosein, 2001, 2002; Fraser *et al.*, 2003; Yang *et al.*, 2012). Given that the membrane potential (V_m) of cancer cells is relatively depolarised (~-10 to -50 mV) compared with terminally differentiated cells (less than -50 mV) (Yang & Brackenbury, 2013), the persistent Na^+ current is likely to be predominant and may prove to be an important therapeutic target (Yang *et al.*, 2012).

Together, these data suggest that repurposing approved antiarrhythmic and antiepileptic drugs to breast cancer may have therapeutic value. However, in a recent retrospective cohort analysis of breast, bowel and prostate cancer patients, it was shown that those prescribed antiarrhythmic and antiepileptic drugs did not live as long as those not exposed to such medications (Fairhurst *et al.*, 2015). Nonetheless, confounding factors such as missing information on the cancer stage, co-morbidities and the cause of death from these patients made it difficult to a draw a conclusion from

this observation. A better way to test the hypothesis would be in a properly controlled prospective clinical trial.

An alternative approach would be to target VGSCs in breast cancer cells using new drugs. A potential advantage is that in MDA-MB-231 breast cancer cells, the culprit VGSC, $Na_v1.5$, is expressed predominantly in its neonatal splice form (Fraser *et al.*, 2005). Given the lack of physiological expression of the neonatal $Na_v1.5$ splice variant elsewhere in adult tissues, including the heart (Fraser *et al.*, 2005), the neonatal $Na_v1.5$ splice variant provides a unique target for development of new compounds without unwanted side effects on the $Na_v1.5$ in non-cancer tissues.

1.5.4. β subunit expression in cancer

VGSC β subunits have been detected in prostate, breast, lung, and cervical cancers (Table 1.2) (Brackenbury, 2012). Subtype-specific expression varies across cancer types: β3 is present in prostate and lung cancer cells but is absent in breast and cervical cancer cells. In contrast, β1 is predominant in breast, prostate, and cervical cancer cells (Diss *et al.*, 2008; Chioni *et al.*, 2009; Hernandez-Plata *et al.*, 2012). β1 and β2 expression levels correlate with metastatic potential in prostate cancer (Diss *et al.*, 2008; Jansson *et al.*, 2012). However, this pattern is not reflected in breast cancer. β1 is upregulated in breast cancer specimens compared to normal breast tissue samples, but without any relationship to subtype or grade (Nelson *et al.*, 2014). β1 is variably expressed in breast cancer cell lines (Chioni *et al.*, 2009; Nelson *et al.*, 2014). β1 expression is significantly higher in the weakly metastatic MCF-7 cells compared to strongly metastatic MDA-MB-231 cells. Thus, β subunit expression may vary across cancer type and grade, dependent on specific functional specialisations and heterotypic interactions.

Similar to *SCN5A*, a number of somatic mutations have been identified in *SCN1B* in tumours (Figure 1.7B), in both the Ig and cytoplasmic domains (Figure 1.3). Given that β1 is expressed in breast

cancer cells and plays a role in regulating VGSC activity and cancer cell behaviour (detailed in next Section), cancer-associated somatic mutations in β1 which affect its function may therefore impact on tumour progression. Further work is required to characterise the functional consequences of these mutations on adhesion, Na^+ current and β1-mediated cancer cell behaviour.

1.5.5. Function of β subunits in breast cancer cells

In MCF-7 and MDA-MB-231 breast cancer cells cultured *in vitro*, β1 enhances cell-cell and cell-substrate adhesion (Chioni *et al.*, 2009; Nelson *et al.*, 2014). In an orthotopic xenograft model of breast cancer, β1 over-expression increases tumour growth and metastasis (Nelson *et al.*, 2014). Interestingly, β1 promotes neurite-like process outgrowth from MDA-MB-231 breast cancer cells via *trans*-homophilic adhesion. This process outgrowth contributes to the generation of a more metastatic mesenchymal-like phenotype and increases the cells' invasive capacity (Nelson *et al.*, 2014). β1-mediated process outgrowth in breast cancer cells requires fyn kinase activity and Na^+ current, thus recapitulating the mechanism by which β1 promotes neurite outgrowth in cerebellar granule neurons (Figure 1.4B) (Brackenbury *et al.*, 2008a; Brackenbury *et al.*, 2010). Thus, it appears that β1 plays parallel roles in regulating neuronal migration during CNS development, on the one hand, and cancer cell invasion during metastasis, on the other. However, the specific role of the Ig domain in this tumour progression-promoting behaviour has not been delineated. Nonetheless, targeting the adhesive function of β1 may provide a novel approach to anti-cancer therapy (Brackenbury & Isom, 2008).

In LNCaP prostate cancer cells, over-expression of β2 induces a bipolar morphology and increases overall length with a concurrent reduction in volume (Jansson *et al.*, 2012). These changes could allow for greater invasion and motility. In agreement with this, β2 over-expressing cells have increased migratory capability compared to control cells in a wound healing assay (Jansson *et al.*,

2012). β2 over-expressing cells plated on various substrates preferentially adhere to vitronectin and Matrigel over fibronectin, suggesting that β2 may selectively increase adhesion dependent on the surrounding tissue/substrate (Jansson *et al.*, 2012). In contrast, β2 over-expression reduces tumour size and growth following subcutaneous implantation of LNCaP cells into nude mice (Jansson *et al.*, 2012). Thus, β2 may enhance invasion and metastasis whilst also reducing the ability of tumours to form localized masses. In support of this notion, β2 over-expression increases invasion and growth on laminin, and enhances association between prostate cancer cells and nerve axons in organotypic cultures (Jansson *et al.*, 2014). Therefore, β2 may permit association between prostate cancer cells and neural matrices, enhancing perineural invasion, thus enabling glandular egress and subsequent metastatic dissemination. However, the relevance of these observations to other cancer types where β2 may be expressed are not clear. Further work is required to evaluate the functional consequences of β2 expression across other tumour types.

In contrast to β1 and β2, β3 may function as a tumour suppressor. *SCN3B* (encoding β3) contains two functional p53 response elements, suggesting that it may be directly regulated by the tumour suppressor p53 (Adachi *et al.*, 2004). In addition, *Scn3b* is up-regulated in wildtype mouse embryo fibroblasts (MEFs), but not *p53* null MEFs following treatment with Adriamycin, which induces apoptosis and p53 activation (Adachi *et al.*, 2004). Furthermore, β3 suppresses colony formation, and promotes apoptosis in a p53-dependent manner in response to anticancer agents (Adachi *et al.*, 2004). This mechanism may explain why β3 is not expressed in MDA-MB-231 cells.

Less is known about the expression/function of β4 in cancers. Interestingly, a strong down-regulation of β4 has been reported in primary cultures of cervical cancer cells relative to cells from noncancerous cervix (Hernandez-Plata *et al.*, 2012). A similar pattern of expression has also been reported in prostate cancer cell lines and breast tumours (Diss *et al.*, 2008; Bon *et al.*, 2016). However, β4 expression is increased in cervical cancer biopsies compared to noncancerous cervix

(Hernandez-Plata *et al.*, 2012). On the other hand, β4 overexpression MDA-MB-231 cells reduces invasion and tumour progression, suggesting that β4 may represent a novel metastasis suppressor gene (Bon *et al.*, 2016). The difference in relative expression levels between biopsies and primary cell cultures is unresolved. This discrepancy may be due to the adhesive function differing *in vivo* as opposed to *in vitro* and further work is required to investigate this possibility. In summary, VGSCs are up-regulated in a number of different types of cancer. Increasing evidence suggests that α and β subunits both play an important role in promoting various aspects of cancer progression and metastasis (Figure 1.8). The role(s) played by specific subtypes appears to be complex and may be dependent on tumour type. A common theme is that α subunits regulate invasion *via* Na^+ current, whereas β subunits also regulate adhesion interactions. The next step is to establish the extent and distribution of expression of VGSCs across tumour types, and the precise involvement of different α and β subunits, with the goal of harnessing their therapeutic potential.

1.5.6. L1CAM and its similarity to β1

Changes in the expression profile of CAMs have been directly linked to the progress of breast cancer from the more manageable epithelial phenotype to the invasive and metastatic mesenchymal phenotype (Cavallaro & Christofori, 2004; Kiefel *et al.*, 2012b). In addition, interactions between abnormally expressed CAMs on cancer cells and CAMs expressed on cancer associated fibroblasts (CAFs) may enable invasion of cancer cells into the surrounding tissues and ultimately intravasation into either the lymphatic or circulatory system (McCarthy *et al.*, 2018). Therefore, targeting and inhibiting the function of various CAMs has been suggested as a means of preventing metastasis (Wolterink *et al.*, 2010; Doberstein *et al.*, 2015).

L1CAM is a member of the L1 family of the immunoglobulin super family of proteins. Similar to β1, L1CAM plays a significant role in neuronal pathfinding during development, facilitating neurite outgrowth through trans heterophilic interactions (Peng *et al.*, 2016). L1CAM is also expressed in

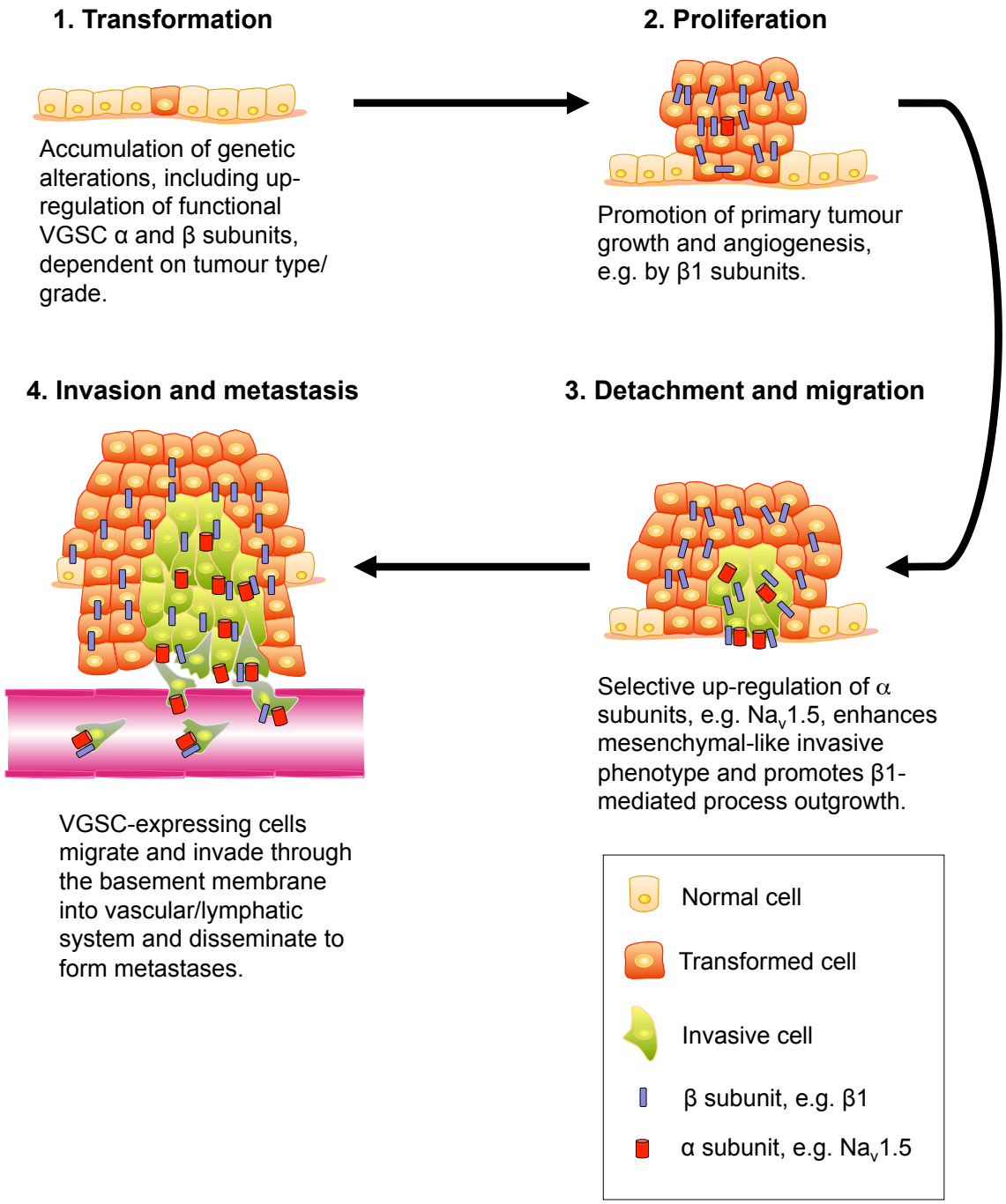

Figure 1.8 A model for VGSC involvement in cancer progression.

β subunits are expressed in proliferating primary tumours, contributing to adhesion (Chioni *et al.*, 2009), and in the case of β1, promoting angiogenesis and resistance to apoptosis (Nelson *et al.*, 2014). Up-regulation of α subunits, e.g. $Na_v1.5$, promotes a mesenchymal-like phenotype (Brisson *et al.*, 2013; Nelson *et al.*, 2014), activation of proteases (Gillet *et al.*, 2009) and local invasion from the primary tumour (Roger *et al.*, 2003; Fraser *et al.*, 2005; Brackenbury *et al.*, 2007). VGSC-expressing cells subsequently intravasate and metastasise to distant sites (Fraser *et al.*, 2005; Jansson *et al.*, 2012; Nelson *et al.*, 2014). Figure adapted from (Brackenbury *et al.*, 2008b).

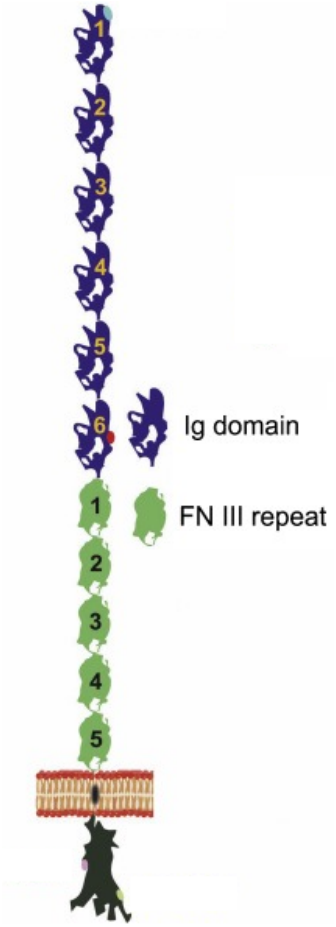

Figure 1.9 Structure of L1CAM

Topological map of the L1 cell adhesion molecule. Blue motifs depict the immunoglobulin domains and the green motifs depict the fibronectin III repeats. These are followed by a transmembrane domain and a conserved intracellular tail. Figure adapted from (Samatov *et al.*, 2016).

non-neuronal cells including cells of the lymphatic and renal system (Debiec *et al.*, 1998). L1CAM consists of six Ig-like loops and five fibronectin type III domains which are located extracellularly and a conserved intracellular tail domain and is thus a significantly larger CAM than β1 (Figure 1.9) (Samatov *et al.*, 2016). The interactions of the Ig-loops in L1CAM are cooperative such that if one is disrupted, the rest would also be disrupted. Alcohol binding to two residues inhibits adhesion of the whole protein by disrupting the adhesion between Ig-loop 1 and 4 (Dou *et al.*, 2011). L1CAM interacts homophilically in *trans* through interactions between Ig-loops 1-4 (Gouveia *et al.*, 2008). A conserved arginine-glycine-aspartic acid domain in the sixth Ig-loop is responsible for heterophilic *cis* interactions of L1CAM with $\alpha_v\beta_3$ integrin (Yip *et al.*, 1998) and these *cis* interactions are proposed to

take place between the ectodomain of L1CAM and $\alpha_v\beta_3$ integrin (Friedli *et al.*, 2009). Like β1, L1CAM is a glycosylated protein. Ig-loops 1-4 have 4 glycosylation sites, Ig-loops 5-6 have 5 glycosylation sites and the fibronectin domains have 12 (Wei & Ryu, 2012). The sites of glycosylation in Ig-loops 1-4 are highly conserved across species and modifications of these sites disrupt adhesion (Wei & Ryu, 2012). Similar to β1, L1CAM binds heterophilically to other cell adhesion molecules, including NCAM and contactin. In addition, L1CAM also interacts with the epidermal growth factor receptor (EGFR) and the fibroblast growth factor receptor 1 (FGFR1) (Kulahin *et al.*, 2008; Donier *et al.*, 2012; Mualla *et al.*, 2013).

L1CAM can exist as two splice variants. In neurons and MCF-7 breast cancer cells, the full-length neurooncological ventral antigen 2 (NOVA-2) variant is expressed (Shtutman *et al.*, 2006; Mikulak *et al.*, 2012). In other cells, such as cells in the renal system, two exons are removed, one each from the N and C terminals of L1CAM (Samatov *et al.*, 2016). The N-terminal exon, which is removed, is responsible for binding homophilically and heterophilically to other neural CAMs whereas the C-terminal exon may be involved in clathrin-mediated endocytosis (Samatov *et al.*, 2016). In hippocampal excitatory neurons, siRNA-mediated knockdown of L1CAM decreases single cell spiking frequency and reduces Na^+ current density (Valente *et al.*, 2016). The latter was attributed to the reduced expression of VGSCs in the absence of L1CAM (Valente *et al.*, 2016). Thus, like β1, L1CAM may modulate VGSC expression.

L1CAM is expressed in various cancers, including ovarian cancer, prostate cancer, neuroblastoma, colorectal cancer and breast cancer (Samatov *et al.*, 2016). In the Oncomine database, L1CAM ranks in the top 2 % of genes that are overexpressed and advanced cancers have higher L1CAM expression (Li & Galileo, 2010). L1CAM is a substrate for a disintegrase and metalloproteinase 10 (ADAM10) - mediated cleavage and the soluble extracellular region has been found in serum from patients with ovarian cancer (Gutwein *et al.*, 2000; Fogel *et al.*, 2003; Finas *et al.*, 2008). Cells which are further

advanced along the epithelial to mesenchymal transition (EMT) have a higher level of expression of L1CAM compared to more epithelial-like cells (Kiefel *et al.*, 2012b). L1CAM also disrupts E-cadherin interactions at adherens junctions, thus promoting a more mesenchymal-like phenotype (Gavert *et al.*, 2005; Weidle *et al.*, 2009). L1CAM expression also increases β-catenin levels in MCF-7 cells, increasing motility (Shtutman *et al.*, 2006). On the other hand, silencing of L1CAM in MDA-MB-231 cells results in a reversion to an epithelial phenotype (Shtutman *et al.*, 2006). In migrating monolayers of uterine and ovarian carcinoma cells, L1CAM expression is found at increased levels in the leading cells, consistent with other findings showing elevated L1CAM expression in cells at the invasive perimeter of tumours (Fogel *et al.*, 2003; Gavert *et al.*, 2005). Overexpressing L1CAM in MDA-MB-468 breast cancer cells increases adhesion and migration but interestingly does not affect invasion (Li & Galileo, 2010). On the other hand, silencing of L1CAM expression in MDA-MB-231 cells decreases adhesion and migration (Li & Galileo, 2010).

Given that L1CAM can interact with EGFR, this may play a role in EGF-mediated up-regulation of VGSC α-subunit expression in cancer cells (Fraser *et al.*, 2014). L1CAM and β1 both share a number of the same adhesion partners and so an intriguing possibility is that interaction of β1 with L1CAM may enhance cell-cell adhesion. Furthermore, such an interaction may localise the VGSC complex to membranes where other regulatory partners, e.g. EGFR, may be expressed.

In summary, there are clear parallels between β1 and L1CAM function. Both promote cell-cell adhesion and are both neuronally expressed. Similarly, both have shown to modulate VGSC currents, although the evidence showing L1CAM-mediated channel modulation is very limited compared to β1. Finally, expression of both proteins is increased in breast cancer and promotes invasion, and both CAMs are substrates for cleavage by secretases. However, although the role of L1CAM in regulating adhesion and motility in neurons and breast cancer cells is well established, and a link has been previously made between L1CAM and VGSCs, no work has been done to investigate the impact

of L1CAM on Na^+ current in breast cancer cells. Similarly, although the heterophilic interaction between β1 and a number of other CAMs and ECM proteins has been delineated, including for N-cadherin, contactin, neurofascin-155, neurofascin-186, NrCAM, β2, tenascin-C and tenascin-R (Srinivasan *et al.*, 1998; Kazarinova-Noyes *et al.*, 2001; Malhotra *et al.*, 2004; McEwen & Isom, 2004; McEwen *et al.*, 2004), possible interaction between β1 and L1CAM has not been previously investigated.

1.5.7. Therapeutic targeting of β1 subunits in breast cancer – possible use of aptamers

Given the functional contribution of β1 subunits to enhancing Na^+ current, invasion and metastasis in breast cancer cells (Chioni *et al.*, 2009; Nelson *et al.*, 2014; Nelson *et al.*, 2015), an intriguing possibility is that β1 subunits may be novel targets for breast cancer treatment. No drugs have been developed to target β1. However, other CAMs have been targeted in a cancer context using antibodies or peptides. For example, monoclonal antibodies to the L1CAM extracellular domain reduced tumour burden and prolonged survival in a mouse model of ovarian cancer (Wolterink *et al.*, 2010; Fischer *et al.*, 2012).

An alternative approach would be to use aptamers. Aptamers are uniquely folded short oligonucleotide or peptide sequences which are selected to recognise a specific protein. Oligonucleotide aptamers have the advantage over peptide aptamers in that they are considerably more stable (Song *et al.*, 2012; Zhu *et al.*, 2012). Conceptually, aptamers function in a similar manner to antibodies but with some advantages, most notably the much greater specificity of recognition, such that aptamers may even distinguish between the same protein between cancerous and healthy cells (Kim *et al.*, 2017). In addition, oligonucleotide aptamers are less immunogenic compared to non-humanized antibodies (Zhu *et al.*, 2012; Radom *et al.*, 2013).

The two general methods for aptamer selection against a protein are systematic evolution of ligands by exponential enrichment (SELEX) (Blackwell & Weintraub, 1990; Tuerk *et al.*, 1992) and cell-SELEX (Cooper, 1999; Hicke *et al.*, 2001; Darmostuk *et al.*, 2015). Aptamers are allowed to bind to the target and bound aptamers are then amplified (Sections 2.24, 2.25). Through iterative rounds with stricter binding conditions, the specificity of aptamers is increased. SELEX is usually carried out on purified proteins, so aptamers are selected against a protein which is not in its native environment. Cell-SELEX aims to alleviate this problem, at least for transmembrane proteins, by selecting aptamers against a protein expressed on live cells, thus proteins would be expected to be in their native state with relevant post-translational modifications (Cooper, 1999). A further problem is that post-translational modifications may differ between cell types, especially if the cell line is of a different species to that in which the aptamers will ultimately be used (Croset *et al.*, 2012; Kannicht *et al.*, 2013). Therefore, it is desirable to select against a protein in a cell line which closely resembles the environment in which the aptamers will be used. Another problem with cell-SELEX is that aptamers may bind to any protein expressed on the cell. Thus, a cell line negative for the target protein is often used to remove aptamers which are not binding to the protein of interest (Shangguan *et al.*, 2006). It is possible to combine both SELEX and cell-SELEX, such that initially aptamers are selected against purified protein and then against a cell line expressing the protein of interest.

Aptamers can be used in a variety of ways, including as emerging therapeutic or diagnostic tools. For example, aptamers targeting vascular endothelial growth factor (VEGF) have been used as a novel therapy in mice for the treatment of macular degeneration in diabetic retinopathy (Eyetech Study, 2002). In this study, 80% of treated patients showed stable or improved eyesight after three years. Aptamers have also been developed to act as delivery agents for both imaging probes or drug substances to cancer cells (Cerchia & de Franciscis, 2010). Using breast cancer cell lines, aptamers have been selected which bind HER2, using the HER2-expressing SKBR3 cell line for positive selection and the HER2-negative MDA-MB-231 cell line for negative selection (Kang *et al.*, 2009). Another

study used a similar approach, although MDA-MB-468 cells were used for negative selection (Dastjerdi *et al.*, 2011). Aptamers have also been raised against CAMs, including the epithelial CAM (EpCAM), which is expressed on cancer cells (Shigdar *et al.*, 2011). The same group propose that the development of aptamers targeting proteins which are upregulated in cancer stem cells may allow delivery of targeted therapeutics to tumours (Shigdar *et al.*, 2013). Aptamers have been raised to target the IgV-like N-domain of the carcinoembryonic antigen (CEA) (Orava *et al.*, 2013). Like β1, CEA functions as a CAM possibly through its Ig-like region. By using aptamers to block the adhesive functions of CEA, it was possible to inhibit peritoneal tumour nodule formation *in vivo* (Orava *et al.*, 2013).

A recent advancement in aptamer selection technology is the incorporation of fluorescence-activated cell sorting (FACS) into the selection process. FACS is used in conjunction with fluorescently-modified aptamers for cell-SELEX. Use of FACS can reduce the number of rounds required for selection as it results in a much greater partitioning efficiency of cells binding aptamers from cells that are not binding aptamers (Zhang *et al.*, 2010). One possible drawback with the use of FACS is the increased possibility of losing sequences which could potentially bind with a greater affinity. In the first round of selection there will only be one copy of each sequence. Thus, a cell with only a few fluorescently-labelled aptamers bound may not be retained as it may not be sufficiently fluorescent to be detected by the cell sorter. This is not a problem in later rounds where there are multiple copies of each sequence. A further issue complicating cell-SELEX is dead cells, which must be removed prior to FACS, as these would otherwise non-specifically internalise aptamers, resulting in false positives (Mayer *et al.*, 2010; Li *et al.*, 2018). Finally, one issue, which has not been considered in the field, is the possibility of apoptotic cells taking up aptamers and acting as additional non-specific sinks.

1.6. Hypothesis and aims

It is generally accepted that VGSCs function as macromolecular signalling complexes in which Na^+ current through the α subunit pore is coupled with non-conducting signalling *via* the β subunits. Thus, complexes of $Na_v1.5$ and $\beta1$ may occur in breast cancer cells, regulating morphological changes and metastasis. The overall hypothesis under test in this Thesis is that, through the Ig domain, $\beta1$ functions as both a CAM and a modulator of VGSC α subunits in cancer cells. This hypothesis was tested in this Thesis through three main approaches, described in the three results Chapters.

The aim of Chapter 3 was to test the hypothesis that deletion of the Ig loop of the $\beta1$ subunit would reduce Na^+ current and adhesion in MDA-MB-231 breast cancer cells. This was tested using whole-cell patch clamp recording, pharmacology, adhesion and morphology assays.

The aims of Chapter 4 were twofold: (1) to test the hypothesis that the cancer-associated somatic R89C mutation in the $\beta1$ Ig domain reduced Na^+ current and adhesion, and (2) given, the parallels between $\beta1$ and L1CAM expression and function, to test the hypothesis that L1CAM over-expression would increase adhesive properties and Na^+ current. These hypotheses were again tested by expressing wildtype vs. mutant $\beta1$ or L1CAM in MDA-MB-231 cells and using whole-cell patch clamp recording, pharmacology and adhesion and morphology assays.

The aim of Chapter 5 was to test the hypothesis that aptamers targeting the extracellular Ig domain of $\beta1$ could be used to inhibit adhesion. This was tested by raising aptamers to the Ig domain of $\beta1$ using cell-SELEX with MCF-7 breast cancer cells, which express high endogenous levels of $\beta1$. The approach was refined using FACS and the functional effect of the aptamers was tested using adhesion assays.

2. Materials and Methods

An overview of the experimental approaches used summarised in relation to the specific research questions addressed in this Thesis is shown in Figure 2.1.

2.1. Cell culture

HEK293T cells (a variant of HEK293 cells stably expressing the SV40 large T antigen to increase protein production from expression vectors containing SV40 enhancers) were a gift from J. Cartwright (University of York). Chinese hamster lung (CHL) and CHL-β1 cells were a gift from L. Isom (University of Michigan). MDA-MB-231 and MCF-7 human breast cancer cells were a gift from M. B. A. Djamgoz (Imperial College London) (Fraser *et al.*, 2005). Variants of MDA-MB-231 cells stably expressing enhanced green fluorescent protein (MDA-MB-231-GFP), overexpressing β1 (MDA-MB-231-β1-GFP), and overexpressing a truncated β1 mutant lacking the Ig loop (MDA-MB-231-β1ΔIg$_{40-124}$-GFP) were generated previously (Chioni *et al.*, 2009; Nelson *et al.*, 2014). All cell lines were grown in Dulbecco's modified eagle medium (DMEM) supplemented with 5% FBS and L-glutamine at 37 °C and 5 % CO_2 (Yang *et al.*, 2012). Cells were discarded after they had been passaged 10 times. Antibiotics were used in the maintenance of MDA-MB-231-GFP cells (G418, 0.2 mg/ml), MDA-MB-231-β1-GFP cells (hygromycin, 0.1 mg/ml) and MDA-MB-231-β1ΔIg$_{40–124}$-GFP cells (G418, 0.2 mg/ml). Table 2.1 shows the properties of each cell line used in this Thesis and the use cases.

2.2. Plasmids

pcDNA3.1-Hygro containing β1B with a V5-peptide tag and a 6x His-tag was a gift from L. Isom (University of Michigan) (Patino *et al.*, 2011). The plasmid pcDNA3.1-Hygro containing L1CAM was a gift from Dr G. Evans (University of York) (Figure 2.2). The pOPINTTGNeo vectors contained either a 6X His-tag, an F_C-tag or a CD4-tag both followed by a 6X His-tag and were created with the help of the MRC Oxford Protein Production Facility (OPPF) (Figure 2.3).

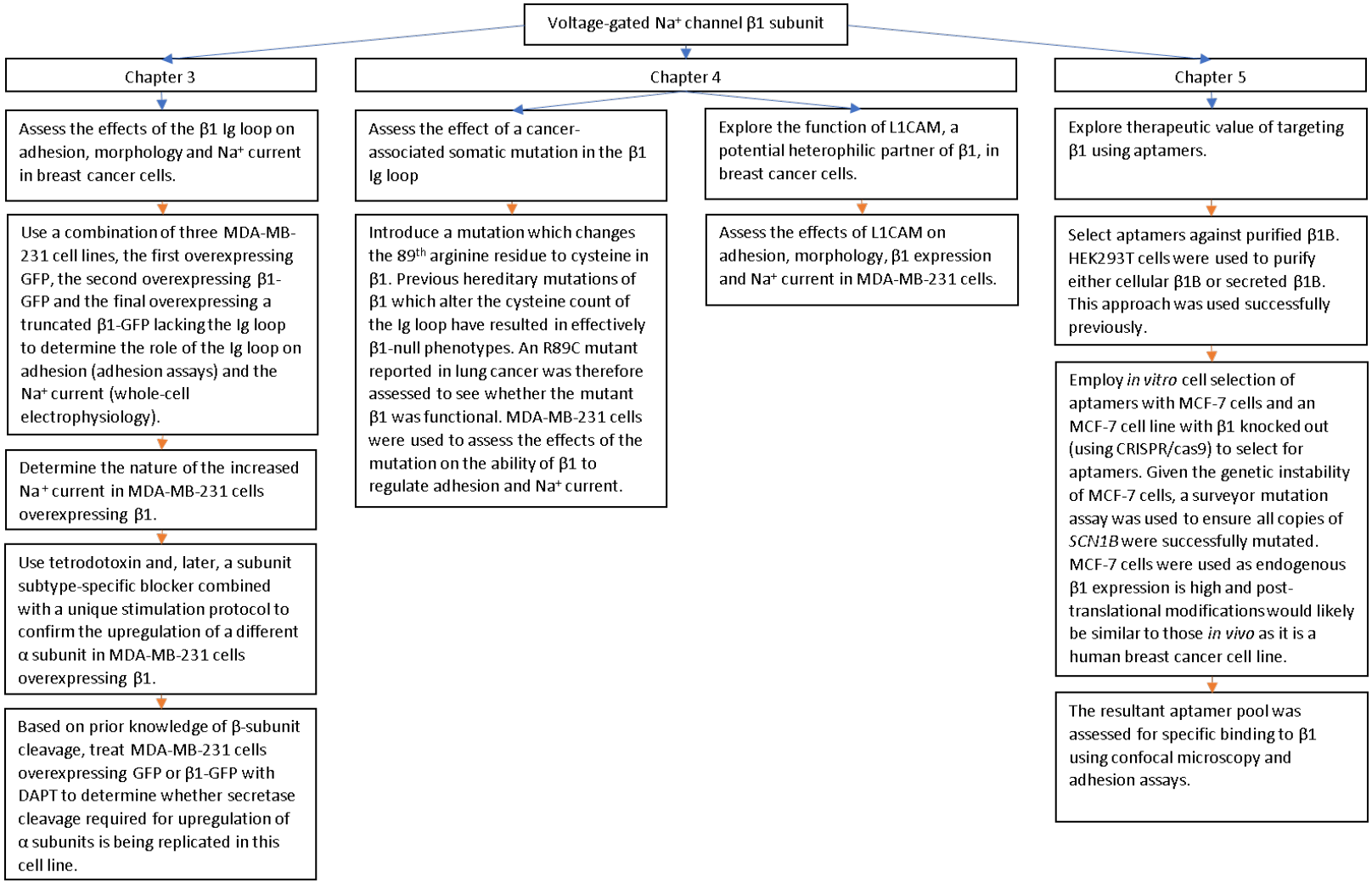

Figure 2.1 Flowchart of the experimental goals of the thesis.

The flowchart shows the main experimental goals of this thesis and is further broken down into core aims and experimental approaches used.

Table 2.1 Cell lines used in this Thesis

Cell line	Properties	Antibiotic	Use case
CHL	Adherent fibroblast cell line - Previously used as a monolayer upon which process outgrowth of breast cancer cells is measured. Lacks β1 expression (Davis *et al.*, 2004).	-	As a monolayer upon which to assess the role of β1 mediated interactions on process outgrowth
CHL-β1	CHL cells stably expressing β1 (Davis *et al.*, 2004).	G418	As a monolayer upon which to assess the role of β1 mediated interactions on process outgrowth
HEK293T	A Variant of HEK293 cells stably overexpressing the SV40 antigen. When transfected with plasmids containing SV40 origin of replication, this cell line will greatly increase the expression of the recombinant protein.	-	For transient transfection for purification of recombinant proteins.
MDA-MB-231	Strongly metastatic triple negative breast cancer cell line which displays a high invasive capacity both *in vitro* and *in vivo.* Endogenously, the expression of β1 is very low (Nelson *et al.*, 2014).		The parental cell line from which the various stably overexpressing lines (below) were produced.
MDA-MB-231-GFP	Stably overexpressing the GFP protein.	G418	As a negative control to assess the role of the Ig loop of β1 in breast cancer cells.
MDA-MB-231-β1-GFP	Stably overexpressing β1-GFP.	Hygromycin	As a positive control to assess the role of the Ig loop of β1 in breast cancer cells.
MDA-MB-231-β1-ΔIg-GFP	Stably overexpressing truncated variant of β1 lacking the Ig loop, in which residues 40-124 have been deleted (Nelson *et al.*, 2014).	G418	To assess the role of the Ig loop of β1 in breast cancer cells.
MDA-MB-231-β1R89C	Stably overexpressing the β1R89C mutant.	Hygromycin	To assess the effects of the R89C mutation in breast cancer cells.
MDA-MB-231-pcDNA3.1	Stably overexpressing empty pcDNA3.1 vector	Hygromycin	As a negative control for L1CAM overexpressing cells (below)
MDA-MB-231-L1CAM	Stably overexpressing L1CAM	Hygromycin	To assess the role of L1CAM in breast cancer cells.
MCF-7	A weakly metastatic breast cancer cell line with high level of endogenous β1 expression.	-	Used as a positive cell line for aptamer selection for β1.
MCF-7-Δβ1	MCF-7 cells in which β1 was deleted using CRISPR.	-	Used as a negative counter cell line for aptamer selection for β1.

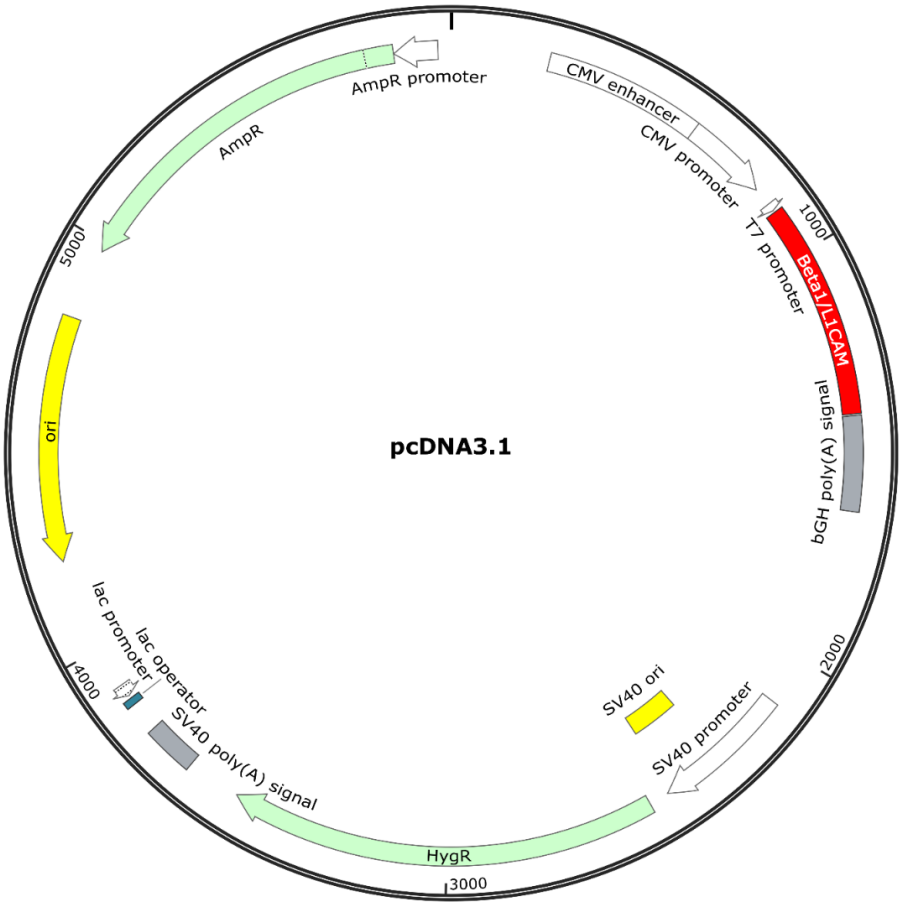

Figure 2.2 Plasmid map of pcDNA3.1-Hygro.

The plasmid has had either (i) the human β1B gene followed by a V5-tag and a 6x His-tag, or (ii) the human L1CAM gene with no tags, inserted into it between the T7 promoter and the bGH poly(A) signal. The CMV enhancer/promoter allows for expression in mammalian systems. The plasmid confers ampicillin resistance (AmpR) in bacterial expression systems and hygromycin resistance (HygR) in mammalian expression systems. Simian virus 40 origin of replication (SV40 ori) allows for expression of the hygromycin resistance gene in mammalian expression systems expressing T-antigen. Map was created using SnapGene software.

Vectors of the pOPIN suite containing either control proteins 6218, 9816 or eGFP were obtained from OPPF. The identities of 6218 and 9816 were not disclosed by the OPPF for confidentiality reasons. The pOPIN suite of vectors developed by the OPPF allows for single step cloning with no extra amino acids between the inserted gene and tag, a cleavable His-tag and easy transfection into HEK293T cells with high amounts of protein expressed. For the CRSIPR/*cas9* experiment the guide RNAs (gRNAs) were present in pSpCas9 BB-2A-GFP vectors (GenScript). This commercially available

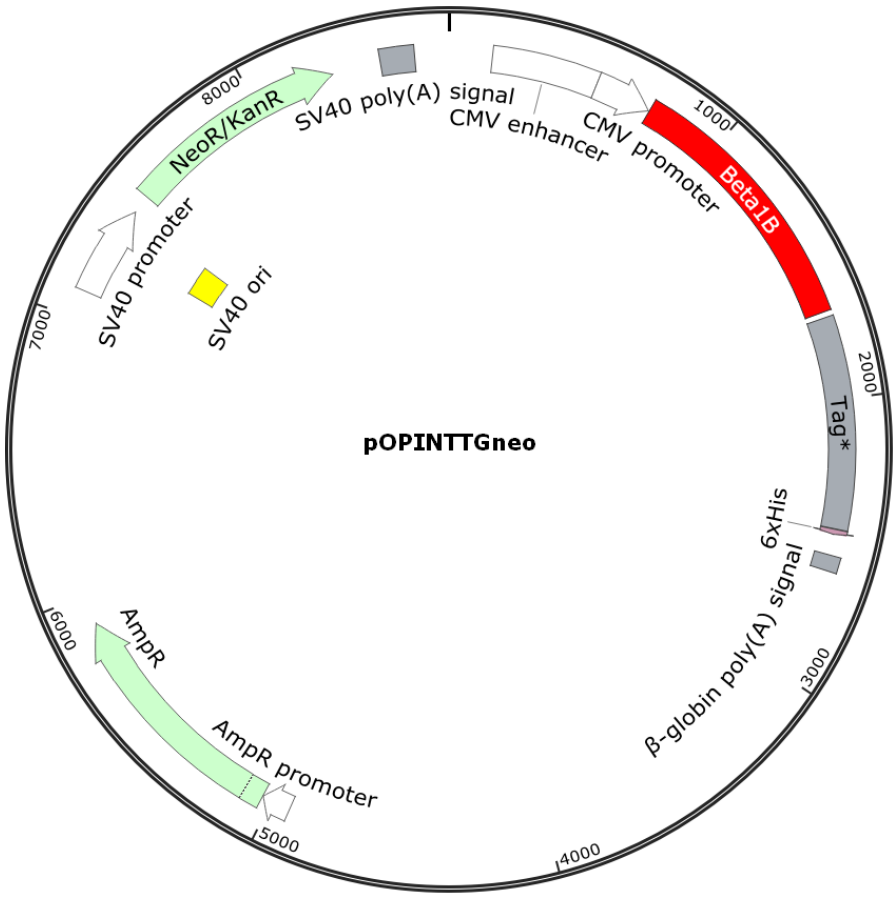

Figure 2.3 Schematic map of pOPINTTGneo vectors used for expression of β1B.

The plasmids contain one of two tags (* CD4 or F_C) followed by a 6xHis tag. The CMV enhancer/promoter allows for expression in mammalian systems. The plasmid confers ampicillin resistance (AmpR) in bacterial expression systems and neomycin resistance (NeoR) in mammalian expression systems. SV40 allows for expression of the hygromycin resistance gene in mammalian expression systems expressing T-antigen. Map was created using SnapGene software.

vector has the advantage that the gRNAs and the *cas9* gene are present within the same plasmid. In addition, the presence of eGFP allowed for selection of successfully transfected cells by FACS (Figure 2.4).

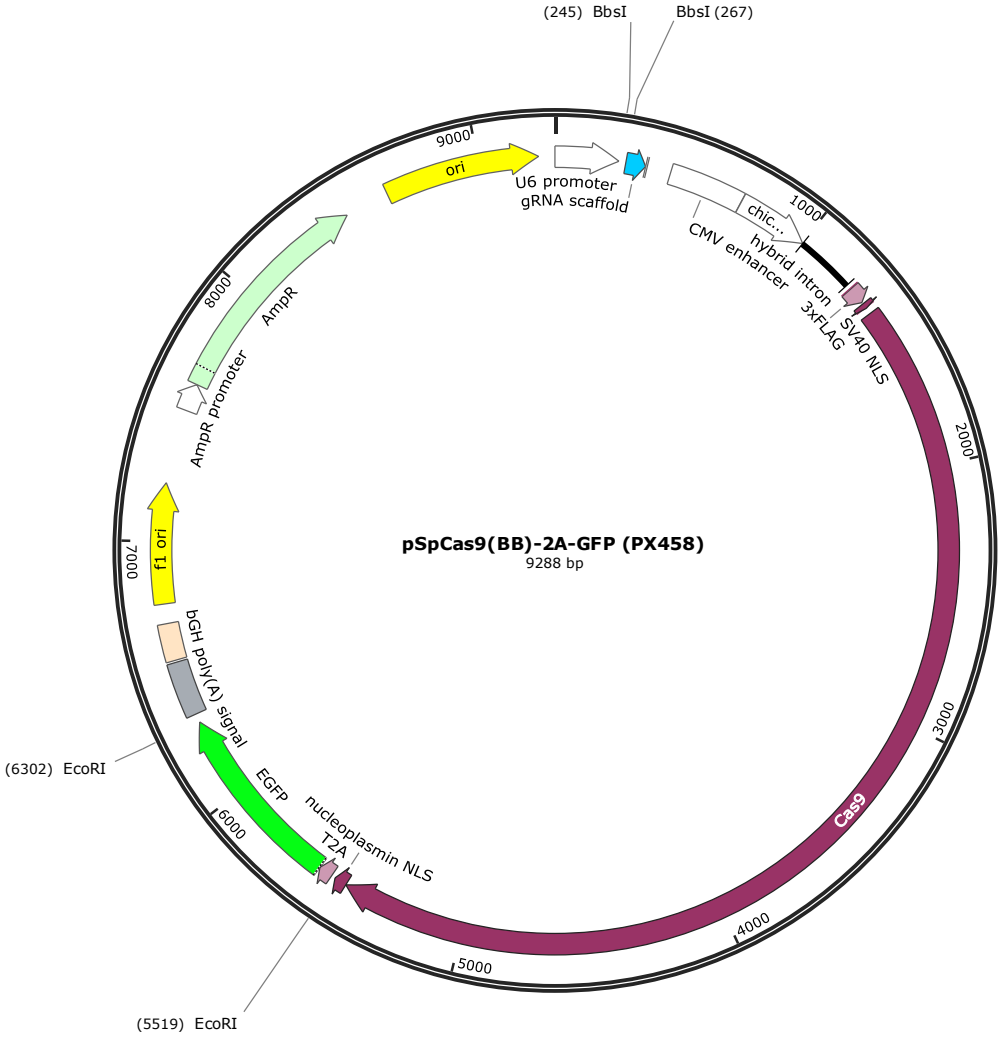

Figure 2.4 Schematic map of pSpCas9 BB-2A-GFP vectors used for CRSIPR/*cas9*-mediated knockdown of β1.

The plasmid contains the two gRNAs used present after the U6 promoter, the *cas9* gene with a nuclear localisation signal (NLS) and eGFP which is used for selection of successfully transfected cells. The plasmid also enables ampicillin resistance in transformed bacteria.

2.3. PCR

RNA was extracted from cell samples using RNA extraction kits (Qiagen) according to the manufacturer's instructions. cDNA synthesis was performed as described previously (Nelson *et al.*, 2014).PCR was performed as described (Nelson *et al.*, 2014) with the following modifications. Different PCR protocols were used to amplify β1B, $Na_V1.7$ and GAPDH. For β1B, the PCR was carried out according to the OPPF protocol (25 units (u) Recombinant *Thermococcus kodakaraensis* (KOD)

Hot Start Buffer (Novagen), 10 µM dNTP mix, 1 u KOD Hot Start Taq (Novagen), 10 µM primers, 10 ng template and made to 50 µl with sterile water). For $Na_V1.7$ and GAPDH, the PCR contained 5 u 5x *Taq* hot start buffer (Promega), 1.25 mM $MgCl_2$ (Promega), 10 µM dNTP mix, 1.25 u *Taq* DNA polymerase (Promega), 10 µM primers and 20 ng template and made to 50 µl with sterile water. Primers, annealing temperature, and expected product size are in Table 2.2. Amplification conditions for the β1B primers were: 94 °C for 2 minutes followed by 30 cycles of 98 °C for 10 s, 60 °C for 30 s and 68 °C for 1 minute, followed by 68 °C for 2 minutes. Amplification conditions for $Na_V1.7$ and GAPDH were: 98 °C for 2 minutes followed by 35 cycles of 98°C for 30 s, 55 °C (GAPDH) or 59 °C ($Na_V1.7$) for 30 s followed by 72 °C for 30 s with a final extension step at 72 °C for 10 minutes. The β1B PCR products were then run on a 1.25 % agarose gel at 100 V for 30 minutes. The $Na_V1.7$ and GAPDH PCR products were run on a 1.5 % agarose gel at 80 V for 45 minutes.

2.4. Quantitative PCR

Quantitative PCR (QPCR) was performed as described previously (Nelson *et al.*, 2014). QPCR was carried out using a Bio-Rad thermal cycler. Triplicate 12 µl reactions containing 20 ng cDNA were amplified by 35 cycles of 95 ˚C for 5 seconds and 60 ˚C for 10 seconds. Primer sequences expected product lengths and annealing temperatures are given in Table 2.2. Relative gene expression was quantified using the $^{\Delta\Delta}C_T$ method with GAPDH as a control (Livak & Schmittgen, 2001).

2.5. Creation of a His, F_c or CD4 tagged β1B construct and a truncated β1B construct lacking the C-terminal tail region

Three new β1B vectors were created by cloning the *SCN1B* gene from the pcDNA3.1 plasmid (Figure 2.2) into three pOPINTGneo vectors (Figure 2.3). Three of the pOPINTGneo vectors contained the full

Table 2.2 PCR Primers

Target	Sense primer (5' - 3')	Anti-sense primer (5' - 3')	T_a[a] (°C)	Product Size (bp)
β1B F_c	gcgtagctgaaaccggcgcctgcgggggctgcgtgg	cagaacttccagtttaaccacaccccgagaaacacatcgg	60	447
β1B CD4	gcgtagctgaaaccggcgcctgcgggggctgcgtgg	gtgatggtgatgtttaaccacaccccgagaaacacatcgg	60	447
β1B His	gcgtagctgaaaccggcgcctgcgggggctgcgtgg	gtgatggtgatgtttaaccacaccccgagaaacacatcgg	60	447
$Na_v1.7$	tatgaccatgaataacccac	tcaggtttcccatgaacagc	59	389
β1 (QPCR)	gtcgtcaagaagatccacattgaggt	ttcggccacctggacgcccgtgcag	60	243
GAPDH	aaggtgaaggtcggagtcaac	ccagagttaaaagcagccctg	55	71

[a] **Abbreviations:** T_a, annealing temperature.

length β1B gene. In each case, β1B was inserted into a vector containing either a 6xHis-tag, a C-terminal F_c tag followed by a 6xHis-tag or a CD4 tag followed by a 6xHis-tag (pOPINTTGneo-3C-His, pOPINTTGneo-3C-FC and pOPINTTGneo-3C-CD4 respectively). Primer sequences expected product lengths and annealing temperatures are given in Table 2.2.

The β1B PCR products were treated with DpnI to digest any methylated DNA without digesting the PCR products. Products were purified using AMPure XP magnetic beads (Beckman Coulter). Beads were washed with 70 % ethanol and allowed to air dry. Bound DNA was eluted using 10 mM Tris pH 8.0. The purified products were infused into the pOPINTGneo vectors (100 ng of the vector and 100 ng of the PCR product) by reaction with the infusion enzyme (Clontech) for 30 minutes at 42 °C. Infusion products were diluted with Tris-EDTA and 5 µl of the diluted product was added to 50 µl of OmniMaxII competent *E. coli* according to manufacturer's instructions (Invitrogen). The *E. coli* were plated on LB Agar plates supplemented with Ampicillin, X-Gal and IPTG and allowed to incubate at 37 °C overnight. Successfully transformed colonies (white colonies) were picked and grown in LB Broth overnight at 37 °C with shaking (225 rpm). The following day the DNA was extracted from the *E. coli* using a Qiagen miniprep kit following the manufacturer's instructions.

2.6. Transfections

Cells were transfected as described in (Tom *et al.*, 2008). HEK293T, MCF-7, cells or MDA-MB-231 cells were passaged 24 hours before transfection to a density such that they would achieve 60 % confluency the next day. Cells were transfected with PEI (gift from J. Cartwright, University of York) or Fugene (Promega) according to the protocol described in (Tom *et al.*, 2008). A 1:3 DNA:transfection reagent ratio was used (unless otherwise stated). Medium was changed after 24 hours and cells were harvested after 96 hours when transfected with the pcDNA3.1-β1BV5/His vector (unless otherwise stated), after 72 hours when transfected with pcDNA3.1-L1CAM or the

pOPINTTGneo vectors or 24 hours when transfected with the pSpCas9 BB-2A-GFP vectors. In some experiments, stable clones were selected by growing cells in the presence of selection antibiotic at low density to allow colonies to form, which were then picked using the ring approach. In this approach, the larger end of a cut 1 ml pipette tip was dipped in vacuum grease then placed around an individual colony of cells after removing the medium. Trypsin was added into the tip and then dissociated cells were removed after differing periods of time dependent on the cell line (a few seconds for HEK239T cells and one minute for MCF-7 and MDA-MB-231 cells).

2.7. Protein extraction

Proteins were extracted as described by (Nelson *et al.*, 2014) with the following modifications. HEK293T cells were harvested in PBS using a cell scraper. Harvested cells were spun at 5000X g for 10 minutes at 4 ^{o}C and the supernatant discarded. Cells were resuspended in PBS supplemented with EDTA-free Complete Protease Inhibitors (Roche) and homogenized. Samples were spun at 2500X g for 10 minutes at 4 ^{o}C to pellet out the nuclei. For crude separation of the soluble and insoluble fractions, cells were harvested in Tris-EGTA supplemented with Protease Inhibitors and after removal of the nuclei, further spun at 18000X g for 20 minutes at 4 ^{o}C. The supernatant (soluble fraction) was collected and the pellet (insoluble fraction) was resuspended in an equivalent volume of Tris-EGTA. Protein concentration was measured using the Bradford assay. Absorbance was measured at 590 nm and compared against a standard curve created from known concentrations of BSA (Figure 2.5).

2.8. Small-scale protein purification

GE Healthcare Ni Sepharose^{TM} 6 Fast Flow (Ni^{2+} bead) suspension (100 µl) containing 15 µl of packed bead slurry was washed twice with PBS. The supernatant was carefully removed from the Ni^{2+} beads

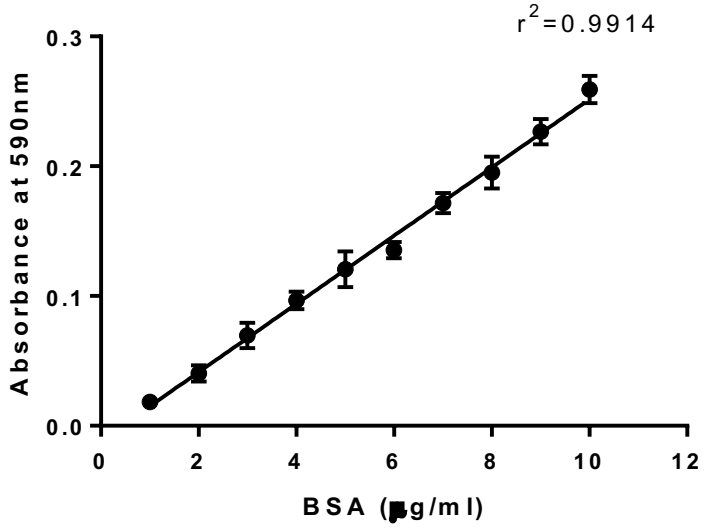

Figure 2.5 Standard curve for Bradford Assay.

Absorbance at 590 nm was measured for BSA concentrations in the range 1-10 µg/ml measured by the Bradford assay. Data are mean ± S.E.M., n=3.

and the clarified cell lysate (soluble fraction), harvested in 20 mM imidazole elution buffer (20 mM phosphate buffer, 20 mM imidazole, 0.3 M NaCl, pH 7.4) was added. The sample was allowed to bind for 20 minutes, inverting the tube every 5 minutes. The solution was transferred to a 750 µl spin column (Sigma) and spun briefly until a speed of 2000X g was reached. Flow-through was collected Each wash was collected and stored at -80 ^{o}C. Beads were resuspended in PBS and transferred to an Eppendorf tube and spun down. PBS was removed, and the beads were resuspended in elution buffer (five minutes each) of increasing imidazole concentrations (50 mM, 100 mM, 200 mM, 300 mM, 500 mM and 1 M) to further decouple His-rich proteins. After the elution stages, beads were resuspended in 80 µl PBS. Sample buffer (1:4) was added to each wash, elution stage and the resuspended beads. Samples were run on a 12 % SDS-PAGE gel and either transferred onto a nitrocellulose membrane for western blotting using the anti-V5 antibody or the gel was stained using Fairbanks Coomassie solutions.

2.9. Large scale purification of secreted protein at OPPF

Two 5 L roller bottles of HEK293T cells at 50 % confluency grown in 0.25 L of medium were transfected with PEI and the pcDNA3.1-β1BV5/His plasmid in Figure 2.2, as described above. Cells were left for four days, after which the medium was collected, filtered and degassed. Medium was purified by automated Ni^{2+} affinity purification using an AKTApurifier (GE Healthcare). The His-Trap column (Invitrogen) was washed and equilibrated using a Ni^{2+} wash buffer: 50 mM Tris pH 7.5, 500 mM NaCl and 30 mM imidazole. Medium was fed through the His-Trap column. The column was washed again with the Ni^{2+} wash buffer to remove unbound proteins. The contents of the His-Trap column were eluted using a Ni^{2+} elution buffer: 20 mM Tris pH 7.5, 200 mM NaCl and 500 mM imidazole.

2.10. SDS-PAGE

SDS-PAGE and western blotting were performed as described (Nelson *et al.*, 2014) with the following modifications. One-part sample buffer (0.25 M Tris HCl pH 8.8, 0.5 M glycerol, 167.8 mM SDS, 2.87 mM bromophenol blue, 97.25 mM dithiothreitol, 3.6 M β-mercaptoethanol) was added to four parts of protein sample of interest. The samples were heated at 80 ^{o}C for 10 minutes and 50 µg protein loaded per lane on a stacking gel (0.25 M Tris pH 6.8, 12.9 % (v/v) Protogel (National Diagnostics), 8.79 mM ammonium persulfate, 1 % (v/v) TEMED). A 12 % SDS-PAGE gel (0.25 M Tris pH 8.8, 42.5 % (v/v) Protogel (National Diagnostics), 43.9 mM ammonium persulfate, 0.13% (v/v) TEMED (Sigma)) was used to resolve the proteins and was run at 120 V until the 10 kDa marker in the ladder (PageRuler Plus, Thermoscientific) had run off the bottom.

2.11. Western blotting

Wet transfer was used to transfer proteins onto a nitrocellulose membrane (GE Healthcare Life Sciences). After transfer, the membrane was placed in blocking solution (0.1 M Tris-buffered saline with 1 % Tween-20 (TBST), 1 % (w/v) bovine serum albumin, 2.5 % (w/v) non-fat dry milk). For the L1CAM antibody, a different blocking solution was used (3 % (w/v) non-fat dry milk). Blocking was for 10 minutes at room temperature on a shaker. Primary antibody, diluted in blocking solution, was then added, and left shaking overnight at 4 ^{o}C. The primary antibodies were: mouse anti-V5 antibody (1:1000, AbD Serotec), mouse anti-GAPDH (1:5000, Sigma), mouse anti-CD71 (1:5000, Sigma), mouse anti-α-tubulin (1:10,000, Sigma), mouse anti-His (1:1000, GE Healthcare), mouse anti-L1CAM (1:1000, Abcam), mouse anti-GFP (1:1000, NeuroMab) or rabbit anti-β1 (1:500, Abgent).

Following incubation with the primary antibody, the membrane was washed three times with TBST for 10 minutes. The membrane was placed in blocking solution with diluted secondary goat anti-mouse antibody (1:800; Thermo Scientific) for one hour at room temperature. West-Dura (Pierce) was used for chemiluminescence detection and the blot was exposed to Fujifilm Fuji Medical X-Ray Film. In typical experiments, membranes were stripped in stripping solution (69.4 mM SDS, 62.5 mM Tris, 100 mM 2-mercaptoethanol), and probed with mouse anti-α-tubulin as a loading control. For the large-scale purification experiments conducted at the OPPF, some alterations to the protocol were used, following OPPF guidelines, and these are indicated in the applicable Figure legends.

2.12. Fairbanks Coomassie staining

Following SDS-PAGE, the gel was washed three times with distilled water, 10 minutes each, to remove any residual SDS. Enough Fairbanks solution A (0.05 % (w/v) Coomassie Brilliant Blue G-250 (Serva), 10 % (v/v) acetic acid and 25 % (v/v) isopropanol made to a final volume of 500 ml with

water) was added to cover the gel and microwaved for 1 minute. The gel was placed on a rocker for 10 minutes. Solution A was removed, the gel was washed briefly with distilled water and placed in Fairbanks solution B (0.005 % (w/v) Coomassie, 10 % acetic acid and 10 % (v/v) isopropanol) and microwaved for 1 minute. Solution B was removed, the gel was washed and microwaved in Fairbanks solution C (0.002 % (w/v) Coomassie, and 10 % (v/v) acetic acid) for 1 minute. Solution C was removed and a larger volume of Fairbanks solution D (10 % (v/v) acetic acid) was added and microwaved for 1 minute. The gel was left in solution D overnight at room temperature with shaking to de-stain, after which the gel was imaged using a G:Box Chemi Imager (Syngene) (Fairbanks *et al.*, 1971).

2.13. Sodium azide viability assay

The viability assay was performed as described (Yang *et al.*, 2012). MDA-MB-231-β1 cells were incubated in medium ± sodium azide (11.7 μM) for two hours. After incubation, the medium was removed and replaced with trypan blue medium (20 % v/v trypan blue: DMEM) for 10 minutes. The trypan blue medium was removed and replaced with medium and the number of live and dead cells in 10 fields of view was counted at 10X zoom using an inverted cell culture microscope.

2.14. Cell-cell adhesion assays

Adhesion assays were performed as described (Chioni *et al.*, 2009). MDA-MB-231-GFP, MDA-MB-231-β1-GFP or MDA-MB-231-β1ΔIg$_{40–124}$-GFP cells were trypsinised and gently dissociated using cell culture medium. Cells were counted using a haemocytometer and 1 x 10^6 cells were placed in a 15 ml falcon tube. Medium was then added to the tube to a final volume of 2 ml. Where an N-terminal β1 antibody was used (Abgent) to functionally block β1 mediated adhesion, or rabbit anti-IgG antibody (control antibody), antibody was added to a final concentration of 10 μg/ml to the 2 ml of

cell medium mix and equivalent concentration (11.7 µM) Na^+ azide in PBS was added to the comparison cells. Where aptamers were used, 15 pmol of the FITC tagged aptamers in PBS was added at time 0 and an equivalent volume of PBS with no aptamers was added to the control cells. Cells were shaken at 25 rpm at 37 ^oC for 2 hours. A 50 µl sample was taken every 30 minutes including a sample before shaking, using a cut tip to prevent shearing of cell clumps. Samples were placed on a microscope slide and a glass coverslip placed on top. The number of particles (of size one cell or more) in 10 fields of view at 10X were counted and images (4272 x 2848 pixels) acquired using a Canon EOS Rebel T3 attached to a Zeiss Axiovert 135 microscope. A minimum of three technical repeats per condition were carried out.

2.15. Electrophysiology

2.15.1. Cell preparation

Two days prior to recording, 6 x 10^4 cells were plated on two coverslips in a 35 mm culture dish in 2 ml of medium. The medium was changed on the morning of the recording and cells left to incubate for at least two hours prior to recording.

2.15.2. Solutions

The extracellular physiological saline solution (PSS) contained 144 mM NaCl, 5.4 mM KCl, 1 mM $MgCl_2$, 5 mM HEPES, 2.5 mM $CaCl_2$ and 5.6 mM D-glucose and the pH was adjusted to 7.2 with NaOH with an osmolarity of 312 milliosmol/L. The intracellular pipette solution (IPS) contained 5 mM NaCl, 145 mM CsCl, 2 mM $MgCl_2$, 1 mM $CaCl_2$, 10 mM HEPES and 11 mM EGTA at pH 7.4 adjusted with CsOH with an osmolarity of 330 milliosmol/L. In some experiments, cells were perfused with either 1 µM tetrodotoxin (TTX) or 1 µM PF-04856042 in PSS.

2.15.3. Equipment and software

Data were acquired using an Axopatch 200B amplifier and an Axon Digidata 1550 digitizer with a low-pass filter at 10 KHz, compensating for series resistance (typically ~5-10 MΩ; the sum of all the resistances between the amplifier circuitry and the cytosol) by 40 %. Clampex 10.5 software (Molecular Devices) was used to programme the voltage clamp protocols and record the currents, and the data were analysed using Clampfit 10.5 (Molecular Devices). Pipette tips were pulled using a Sutter Instrument Co. Model P-97 Micropipette puller and the tips were fire-polished using a Narashige MF-830 micro-forge to a resistance of 4.0 – 5.0 MΩ. Where cells were perfused with drugs, a switchable 4-channel gravity perfusion system (ValveLink 8.2, Automate Scientific) was used.

2.15.4. Whole cell voltage clamp Na^+ current recording

Whole cell patch clamp was used to record VGSC currents in voltage clamp mode (Yang *et al.*, 2012). Pipettes containing IPS solution were lowered under positive pressure onto target cells visualised using brightfield microscopy at 40x magnification. The pipette was progressively moved closer to the target single cell, first by moving the pipette closer to the coverslip at 10X magnification and then further moved closer to the top of the cell at 40X magnification. When the pipette was sufficiently close to the membrane of the target cell, a dimple became visible, at which point, the positive pressure was released, and a small amount of negative pressure applied to facilitate gigaseal formation. To achieve a whole-cell configuration, further negative pressure was applied to rupture the patch of membrane in the pipette tip. The whole-cell capacitance and the fast and slow pipette capacitance were manually adjusted for using Axopatch 200B amplifier. For each condition, recordings were made from ≥3, but typically 18-19 cells, dependent on experiment.

2.15.5. Whole-cell voltage-clamp recording protocols

A 250 ms prepulse at -120 mV was applied prior to the start of each protocol to remove inactivation.

(1) Current-Voltage protocol: Depolarising voltages in +5 mV increments for 50 ms from -80 mV to +30 mV.

(2) Steady-state inactivation: Depolarising prepulse voltages in +10 mV increments from -120 mV to -10 mV for 250 ms followed by a test pulse to -10 mV for 60 ms.

(3) Simple stimulation protocol (SSP): 10 repeat depolarising steps to +10 mV for 50 ms from a holding potential of -120 mV.

(4) Ramp protocol: Ramp depolarisation at a rate of 1 mV/ms from -100 mV to -50 mV.

(5) Extended ramp protocol: Ramp depolarisation at a rate of 1 mV/ms from -100 mV to +30 mV.

2.15.6. Curve fitting

Membrane current was converted to conductance, and activation-inactivation curves were fitted to Boltzmann functions, as described previously (Chioni *et al.*, 2009). Curve fitting was carried out in GraphPad Prism. The conductance-voltage relationship was calculated using the following equation:

$$G = \frac{I}{V - V_{rev}}$$

where G is the conductance, I is the current, V is the membrane voltage and V_{rev} is the reversal potential calculated using the Nernst equation:

$$V_{rev} = \frac{RT}{zF} \ln \frac{[\text{Cation}] \text{ outside the cell}}{[\text{Cation}] \text{ inside the cell}}$$

where R is the gas constant (8.31 $J \cdot mol^{-1} \cdot K^{-1}$), T the temperature in Kelvin, z the valence of the ion (in the case of Na^+ always +1) and F the Faraday constant (96485.3 C mol^{-1}).

A Boltzmann equation was used to fit the availability and conductance-voltage relationships:

$$X = \frac{1}{1 + e^{\frac{(V_{\frac{1}{2}} - V)}{k}}}$$

where X is the fitted parameter, $V_{1/2}$ the voltage for half-maximal conductance or availability, k the slope factor and V the membrane voltage.

2.15.7. Predicting V_{rev}

V_{rev} for each IV curve was predicted by plotting each value after the peak current and fitting a linear regression with these points. The equation for the line of best fit was calculated using Microsoft Excel 2019. Using Y=0, the equation was rearranged to calculated x which was used as the measured V_{rev} for that individual IV curve.

2.16. Inhibition of γ-secretase cleavage

To inhibit γ-secretase mediated cleavage of β1, MDA-MB-231-GFP and MDA-MB-231-β1-GFP cells were treated with 0.5 μM N-[N-(3,5-Difluorophenacetyl)-L-alanyl]-S-phenylglycine t-butyl ester (DAPT) (Sigma-Aldrich) (Kim *et al.*, 2005) and an equivalent amount of DMSO (0.1 % v/v) was added to control cells, 24 hours before recording. The current-voltage relationship and steady-state inactivation of VGSC currents were recorded as described above.

2.17. Creation of β1R89C by site-directed mutagenesis

Site-directed mutagenesis was carried out using a Phusion site directed mutagenesis kit (Thermoscientific) according to the manufacturer's instructions (Nelson *et al.*, 2014). pcDNA3.1

containing β1-V5/His was used at the template for site-directed mutagenesis. Primers were designed to mutate the 89th arginine residue of β1 to cysteine. PCR products were run on a 0.1 % agarose gel. Ligation of the plasmid was carried out using the Phusion site directed mutagenesis kit according to manufacturer's instructions. Ligated products were transformed into Xl-1 ultracompetent cells (Agilent) according to the manufacturer's instructions and resultant bacteria were grown in ampicillin. DNA was minipreppred using a Machery-Nagel DNA purification kit according to the manufacturer's instructions. Samples were sequenced using the Sanger sequencing service (Source Bioscience).

2.18. Deletion of β1 using CRISPR/CAS9 technology

β1 was deleted from MCF-7 cells using CRISPR-CAS9 (Ran *et al.*, 2013). Two commercially-available guide RNAs (gRNA) targeting β1 in pSpCas9 BB-2A-GFP vectors (Genscript) were transfected in to MCF-7 cells using Fugene 6 reagent according to the protocol described in (Tom *et al.*, 2008). A 1:3 DNA:transfection reagent ratio was used. Medium was changed after 24 hours and cells were harvested after 72 hours for collection of GFP-positive cells containing the gRNA vectors by fluorescence-activated cell sorting (FACS). As controls, MCF-7 cells were either not transfected or mock transfected (no plasmid).

2.19. Fluorescence activated cell sorting

MCF-7 cells were trypsinized and resuspended in DMEM. A Beckman Coulter MoFlo Astrios fluorescence activated cell sorter was used to separate transiently transfected, dead and apoptotic cells based on fluorescence in APC-Cy7, PE Texas Red and FITC channels. As a negative control, mock transfected and non-transfected MCF-7 cells were used to determine the window of live non-GFP expressing cells in the PE and FITC channels. Positively sorted cells were considered as MCF-7 cells

successfully transfected with the pSpCas9 BB-2A-GFP due to the GFP transcript in the vector. Mock transfected cells which had been sorted were considered the negatively sorted cells and were used as the negative control for all subsequent experiments.

For selection of aptamer-bound cells, live, non-apoptotic cells and cells fluorescing in the 488 nm range were sorted and collected in DMEM using the Beckman-Coulter MoFlo Astrios. Live cells were selected using 3 µM DRAQ-7 which stains dead cells and is detected at 660 nm (PE Texas Red). Non-apoptotic cells were sorted using 1 µM Tetramethylrhodamine, ethyl ester (TMRE) which stains non-apoptotic cells and is detected at 561 nm (APC-Cy7). TMRE was added to the resuspended cells for the final 30 minutes during the aptamer binding period after which both unbound aptamers and TMRE were removed. Gates for live and non-apoptotic cells were set using a series of control samples: cells only, cells with DRAQ-7, cells with TMRE and cells with DRAQ-7 + TMRE. Cells with bound FITC-tagged aptamers were detected in the 488 nm range (FITC) and only the strongest fluorescing 40 % of the live 'green' cells were collected.

2.20. Surveyor mutation assay

The surveyor mutation assay is used to detect single or multiple nucleotide mutations in the gDNA of a cell line. The assay was performed as described (Ran *et al.*, 2013). Briefly, DNA was extracted from cells using Qiagen DNA extraction kits and diluted to a final concentration of 100 ng/µl. A PCR was then set up using this DNA template and surveyor primers, followed by purification of PCR products using QIAQuick PCR purification kits. DNA homoduplex and heteroduplex formation using reactions containing 20 ng/µl PCR product was then achieved using a reaction series starting at 95 ˚C in ramps of 10 ˚C at a rate of -0.3 ˚C/s, finishing at 4 ˚C. The formed heteroduplexes were then subjected to Surveyor Nuclease S digestion at 42 ˚C for 30 min. Surveyor nuclease digestion products were then visualised on a 2 % (v/v) agarose gel.

2.21. Modelling the structure of β1

The structures of both the wildtype β1 and β1R89C were modelled using the Phyre2 Protein Fold Recognition Server (http://www.sbg.bio.ic.ac.uk/) based of the resolved structure of myelin p0 (Patino *et al.*, 2009; Patino & Isom, 2010; Patino *et al.*, 2011).

2.22. Cell morphology assay

The cell morphology assay was performed as described (Chioni *et al.*, 2009). Cells (1 x 10^5) were grown on glass coverslips for 24 hours. Cells were then fixed in 4 % paraformaldehyde for 10 minutes followed by three 5-minute washes with PBS. Coverslips were then mounted onto slides using Prolong Gold mounting medium (Invitrogen). Bright field images were taken of the cell lines at 40X magnification using a Nikon Eclipse TE200 microscope equipped with a RoleraXR Fast1394 charge-coupled device (CCD) camera (QImaging) and SimplePCI 6.0 image control software. Images were exported to ImageJ (NIH) for downstream analysis. The process length on individual cells was calculated by manually drawing a segmented line along the middle of the longest process extension on each cell. The area and circularity of cells were calculated using ImageJ after manually drawing around the perimeter of the cell using the freehand tool (Brisson *et al.*, 2013). Circularity was calculated using the following equation:

$$\text{Circularity} = 4\pi \frac{\text{Area}}{\text{Perimeter}^2}$$

and is used as a measure of roundness (Brisson *et al.*, 2013). For each condition, 20 cells were analysed across at least 3 technical repeats.

2.23. Immunocytochemistry and confocal microscopy

Immunocytochemistry and confocal microscopy were performed as described (Nelson *et al.*, 2014). Cells (1.6 x 10^5) were grown on glass coverslips for 24-48 hours. Cells were then fixed in 4 % paraformaldehyde for 10 minutes followed by three 5-minute washes with 0.1M phosphate buffer (PB). Cells were blocked in PB containing 10 % normal goat serum and 0.1 % Tween-20 for 1 hour. Blocking solution containing diluted primary antibody was then added to the cells for 24 hours at room temperature. The following primary antibodies were used: mouse anti-V5 antibody (1:500, AbD Serotec) mouse anti-GFP antibody (1:1000, NeuroMab) or mouse anti-CD44 antibody (1:500, AbD Serotec). The cells were then washed 3X in PB for 10 minutes, followed by incubation in Alexa Fluor-conjugated secondary antibodies (1:500; Invitrogen), for 2 hours at room temperature in the dark. Where aptamers were used, 15 pmol of the FITC tagged aptamers in PBS was added for 30 minutes and an equivalent volume of PBS with no aptamers was added to the control cells. In some experiments, cells were counter-stained using Alexa-488-conjugated wheat-germ agglutinin (Invitrogen) according to the manufacturer's protocol. Cells were then washed 3X in PB for 5 minutes and then mounted on slides using Prolong Gold mounting medium with DAPI (Invitrogen). Labelled cells were visualised using a Zeiss LSM 880 laser scanning confocal microscope with a 40X oil immersion objective. Acquired images (1024 x 1024 pixels) were exported to ImageJ for downstream analysis.

2.24. Aptamer folding and binding

An N40B DNA aptamer library tagged with FITC was obtained from Aptamer Solutions Ltd and was used for the first round of aptamer selection. Aptamer concentration was determined using a Nanodrop-1000 and 166 pM was added to a 2x PBS solution. Aptamers were heated at 95 ^{o}C for 10

minutes then cooled for 2 minutes to allow optimal folding. MCF-7 cells were dissociated using cell dissociation buffer (Sigma) and lifted in DMEM. Cells were then spun down at 500 xg and medium replaced with diluted aptamers. Folded aptamers were added to the resuspended cells and allowed to bind at 37 ^{o}C and 5% CO_2 with constant rocking for 30 minutes – 2 hours dependent on round: 2 hours for the first two rounds, 1 hour for the third and fourth rounds and 30 minutes for the fifth and sixth rounds.

2.25. Elution of aptamers and initial amplification

Following aptamer binding, cells were spun down at 10,000 xg for 20 minutes and the medium was replaced with 2.4 ml of distilled water. However, this volume was halved in the third round and halved again in the fifth round. Cells were then heated at 95 ^{o}C for 10 minutes to elute aptamers. The eluate containing removed aptamers was added to an equal volume of PCR solution containing a 1x Solis BioDyne HOT FIREPol DNA Polymerase, 50 µM each of both forward and reverse primers (N40B primers) and made to a final volume equivalent to the volume of the eluted sample with DNA and RNA free water. Aliquots of 10 µl were amplified, semi-quantitatively, in cycles of 2 from 10-22 cycles. The optimal number of cycles for specific aptamer amplification was determined by running the aliquots on a 10 % (w/v) denaturing polyacrylamide gel. Once the optimum number of cycles had been determined, the remaining mixture of eluted aptamers and PCR solution was amplified to this optimum number of cycles and pooled for subsequent purification.

2.26. Purification of aptamers

Aptamers were purified from the PCR reaction using magnetic beads. A 400 µl sample of aptamers was stored at -20 ^{o}C and the remaining volume of amplified aptamers added to magnetic beads and 70 % (v/v) isopropanol (isopropanol added last). The aptamers were allowed to bind for 5 minutes,

after which, the tubes were placed on a magnetic rack to separate out the magnetic beads. The beads were washed 3x with 80 % ethanol and allowed to dry for 1 minute. Bound aptamers were eluted in 50 µl Ambion nuclease-free water for 5 minutes and the beads were removed using the magnetic rack. Eluted aptamers in water were collected and used for asymmetric amplification by PCR.

2.27. Statistical analyses

All data are presented as the mean ± SEM. Statistical analysis and curve fitting were performed using GraphPad Prism 6. A Kolmogorov Smirnov test was used to test for normal distribution. For analysis of the adhesion assays, the data were normalized against the starting 'particle' count and plotted against time. For each time point, a t-test was used to test for significance against the control in each condition. Multiple comparisons were made using one-way ANOVA with a post-hoc Tukey tests for normally distributed data, or Kruskal-Wallis with a post-hoc Dunn's test for nonparametric data. Repeated measures one-way ANOVA, assuming sphericity, with a post-hoc Tukey's test or a paired t-test were used to test for significance for the drug perfusion electrophysiological recordings.

3. Assessing the effect of the Ig domain on β1 function

3.1. Introduction

VGSC β subunits, with one exception, are type I transmembrane proteins and are also members of the Ig superfamily (Patel & Brackenbury, 2015). The extracellular Ig loop in the β1 subunit allows it to function as a CAM (Isom, 2001), interact with heterophilic adhesion partners, and regulate neuronal migration via trans-homophilic adhesion interactions (Xiao *et al.*, 1999; Malhotra *et al.*, 2000; Davis *et al.*, 2004; McEwen & Isom, 2004; Brackenbury *et al.*, 2008a; Brackenbury *et al.*, 2010). In addition, mutagenesis studies have indicated that the extracellular Ig domain of β1 is critical for regulating gating of the pore-forming α subunit (McCormick *et al.*, 1998). Thus, the Ig domain of β1 appears to play dual roles: regulating adhesion on the one hand, and channel activity on the other.

In addition to its dual roles in excitable cells, β1 is also present in metastatic breast cancer cells (Chioni *et al.*, 2009). In breast cancer specimens, β1 expression is elevated compared to control tissue (Nelson *et al.*, 2014). In a xenograft mouse model of breast cancer, implanting β1-overexpressing MDA-MB-231 cells significantly increased both tumour size and metastasis, suggesting that β1 plays a key role in promoting tumour progression (Nelson *et al.*, 2014). Weakly metastatic MCF-7 cells express significantly higher levels of endogenous β1 compared to strongly metastatic MDA-MB-231 cells (Nelson *et al.*, 2014). On the other hand, MDA-MB-231 cells express significantly higher levels of $Na_v1.5$ compared to MCF-7 cells, suggesting that there may be an inverse relationship between β1 and $Na_v1.5$ in these breast cancer cell lines (Fraser *et al.*, 2005; Brackenbury *et al.*, 2007). Silencing β1 in MCF-7 cells with siRNA reduces adhesion, increases migration and increases the plasma membrane expression of $Na_v1.5$ without affecting the mRNA levels of *SCN5A* (Chioni *et al.*, 2009). Overexpressing β1 in MDA-MB-231 cells increases Na^+ current density and adhesion (Chioni *et al.*, 2009). However, the identity of the increased Na^+ current is not known. Similarly, the functional significance of the Ig domain in regulating adhesion and Na^+ current in breast cancer cells has not been studied.

The β subunits are substrates for cleavage by α, β and γ secretase. For β2, BACE1-mediated cleavage has been shown to result in the release of the intracellular domain, which then translocates to the nucleus and transcriptionally upregulates expression of $Na_V1.1$ in SH-SY5Y neuroblastoma cells (Kim *et al.*, 2005; Wong *et al.*, 2005). If such a mechanism also operates for β1 cleavage, this may explain the increase in the Na^+ current density caused by β1 overexpression in MDA-MB-231 cells (Chioni *et al.*, 2009). However, the possible involvement of secretase activity in regulation of β1-mediated changes in Na^+ current in MDA-MB-231 cells has not been explored.

Given the ability of β1 to increase tumour growth and invasion (Nelson *et al.*, 2014), and the presumed role of the Ig loop in both adhesion and channel modulation, the Ig loop of β1 may present a valuable therapeutic target. To explore this possibility, it is first necessary to determine, what role, if any, the Ig loop plays in altering the adhesion and Na^+ current properties of MDA-MB-231 cells. To achieve this, three modified MDA-MB-231 cell lines were studied in this Chapter. MDA-MB-231-GFP cells were used as a negative control lacking significant β1 expression. The electrophysiological properties of these cells were indistinguishable from parental MDA-MB-231 cells (Fraser *et al.*, 2005; Chioni *et al.*, 2009). MDA-MB-231-β1-GFP cells stably overexpressing β1-GFP and were used as a positive control. Previously these cells were shown to have a significantly larger Na^+ current density and adhesion compared to parental MDA-MB-231 cells (Chioni *et al.*, 2009; Nelson *et al.*, 2014). MDA-MB-231-β1-ΔIg-GFP cells were the experimental group. MDA-MB-231-β1-ΔIg-GFP cells overexpress a truncated variant of β1 which completely lacks the Ig loop (Nelson *et al.*, 2014).

3.2. Hypothesis and Aims

The purpose of the set of experiments in this Chapter was to determine the role of the Ig loop of the β1 subunit in modulating the Na^+ current and adhesion in breast cancer cells and to design and undertake a set of experiments which could later be used to test the potential use of aptamers specifically targeting the β1 Ig domain. The hypothesis of this Chapter is that the Ig loop of β1 is critical for regulating both adhesion and the Na^+ current in MDA-MB-231 cells.

The specific aims were as follows:

1. Determine the role of the Ig loop in modulating the Na^+ current.
2. Establish the role of the Ig loop in regulating adhesion.
3. Identify the mechanistic basis for any alteration in Na^+ current caused by β1.
4. Determine the α subunit responsible for the increased Na^+ in β1 overexpressing cells.

3.3. Results

3.3.1. The β1 Ig loop increases adhesion in breast cancer cells *in vitro*

As β1 can function as a CAM, and the ultimate goal of the project was to select aptamers to inhibit this adhesive function, it was necessary to establish assays which could be used to assess the functional viability of the aptamers. A simple adhesion assay adapted from (Malhotra *et al.*, 2000) was used to evaluate the involvement of the Ig loop in cell-cell adhesion. In this assay, an increase adhesion is seen as a decrease in particle count. Representative images of the different conditions at varying time points are shown in Figure 3.1A. MDA-MB-231-β1-GFP cells were significantly more adherent than control cells after 30 minutes (Figure 3.1B; n = 4, 10 fields of view per n; $P < 0.001$). However, the adhesion of MDA-MB-231-β1$\Delta Ig_{40–124}$-GFP cells overexpressing β1 lacking the Ig loop did not significantly differ from that of control cells (Figure 3.1B; n = 3, 10 fields of view per n; $P < 0.05$). Thus, β1 increases cell-cell adhesion and this requires the Ig loop.

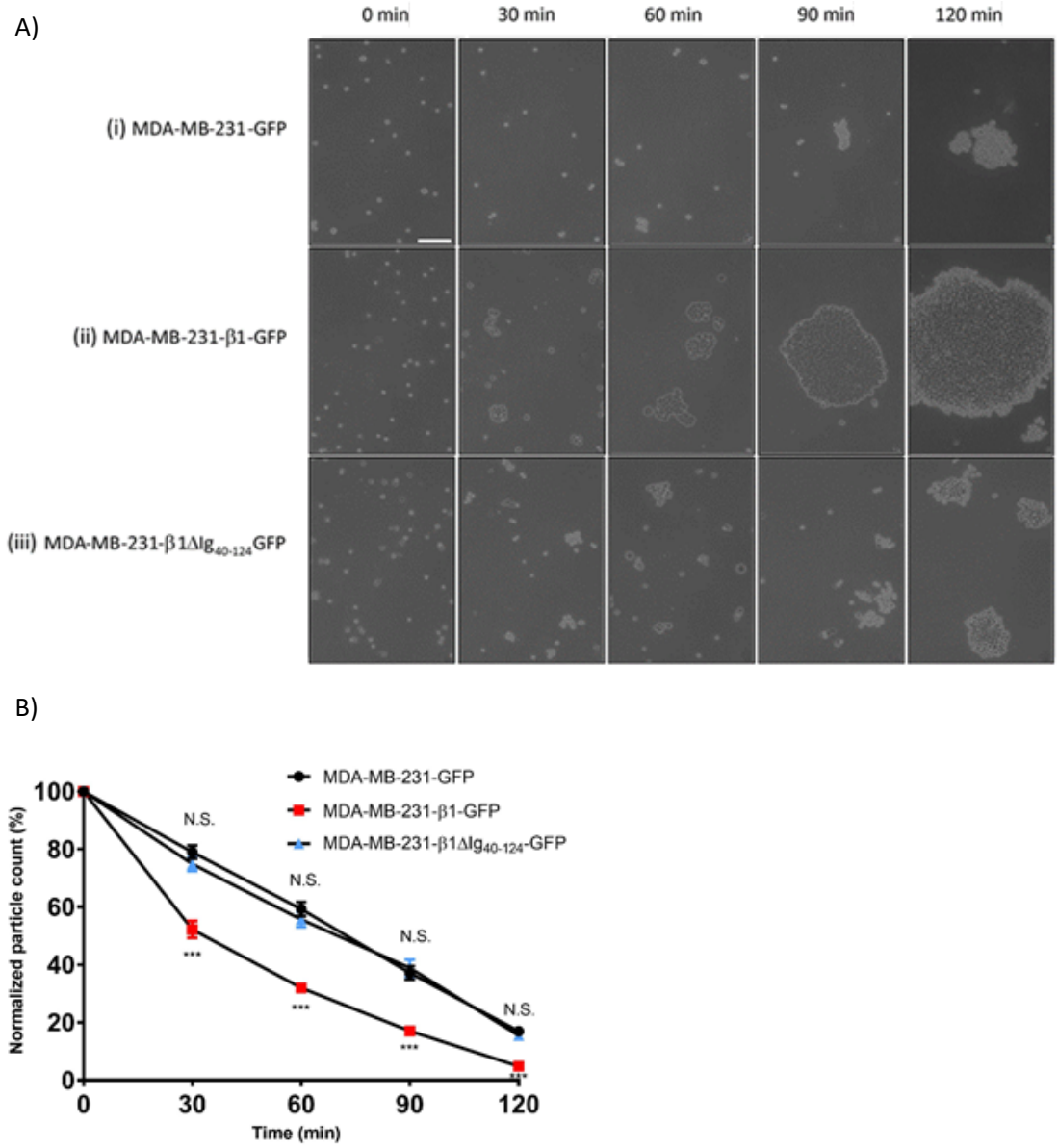

Figure 3.1 Adhesion assay determining the role of the β1 Ig loop on adhesiveness of MDA-MB-231 cells.

(A) Images of cells in adhesion assay, taken at 30-minute intervals. (i) Negative control MDA-MB-231-GFP, (ii) positive control MDA-MB-231-β1-GFP, (iii) experimental MDA-MB-231-β1ΔIg_{40-124}-GFP. Note that as adhesion increased over time, the size of the cell clumps increased but the number of clumps (particles) decreased. Scale bar = 100 μm. (B) Normalized particle counts from MDA-MB-231-GFP cells, MDA-MB-231-β1-GFP cells and MDA-MB-231-β1Δ$Ig_{40–124}$-GFP cells. Increase in adhesion is seen as a reduction in the particle count. Particles were counted on an Axiovert 135 microscope at 10X zoom, n = 4-7, 10 fields of view per n. Data are presented as mean and SEM. One-way ANOVA with Tukey test was used to test for significance at each timepoint. ***P < 0.001, N.S., not significant.

3.3.2. An antibody targeting β1 inhibits cell adhesion

An anti-β1 antibody, targeting the Ig loop of β1, was added to the MDA-MB-231-β1-GFP cell suspension during the assay to functionally block β1-dependent adhesion. Representative images of the different conditions at varying time points are shown in Figure 3.2A. Addition of the anti-β1 antibody very slightly reduced cell-cell adhesion after 90 minutes compared to cells not treated with antibody and this was statistically significant (n = 6, 10 fields of view per n; $P < 0.05$; Figure 3.2B). This result implies that the Ig loop of β1 is required for increasing cell-cell adhesion in MDA-MB-231 cells, and this may be partially inhibited using a function-blocking antibody, although the inhibitory effect of the antibody is marginal. The addition of a control non-targeting IgG antibody had no significant effect on adhesion, confirming the specific effect of the anti-β1 N-terminal antibody (Figure 3.2B). Importantly, the NaN_3 preservative present in the antibody treatments (11.7 μM) had no effect on cell viability (Figure 3.3A, B). Thus, the effect of the anti-β1 antibody on β1-mediated cell adhesion appears not to be a non-specific cytotoxic effect of the preservative.

3.3.3. β1 expression increases peak current density, and this requires the Ig loop

Whole cell patch clamp recording in voltage clamp mode was used to assess whether the Ig loop was required for the β1-mediated increase in Na^+ current reported previously in MDA-MB-231 cells (Chioni *et al.*, 2009). The peak Na^+ current density (I_P) was significantly larger in MDA-MB-231-β1-GFP cells compared to control MDA-MB-231-GFP cells, consistent with previous report (Figure 3.4A, B; $P < 0.001$) (Chioni *et al.*, 2009). However, the Ig loop-deficient mutant MDA-MB-231-β1Δ$Ig_{40–124}$-GFP cells did not display increased Na^+ current compared to control cells (Figure 3.4B; $P > 0.05$). Overexpression of β1-GFP hyperpolarised the voltage at activation compared to control cells ($P < 0.05$), although there was no significant difference in the activation $V_{1/2}$ between the three cell lines, suggesting that the activation may not differ between the cell lines ($P<0.05$; Figure 3.4C, D; Table 3.1). This was also the case for the β1Δ$Ig_{40–124}$-GFP mutant ($P < 0.05$; Figure 3.4C, D; Table 3.1). However, expression of β1-GFP also caused a significant hyperpolarising shift in the steady state

inactivation curve, indicating increased channel availability, compared with control cells and this was not recapitulated in the MDA-MB-231-β1Δ$Ig_{40–124}$-GFP mutant ($P < 0.05$; Figure 3.4E; Table 3.1).

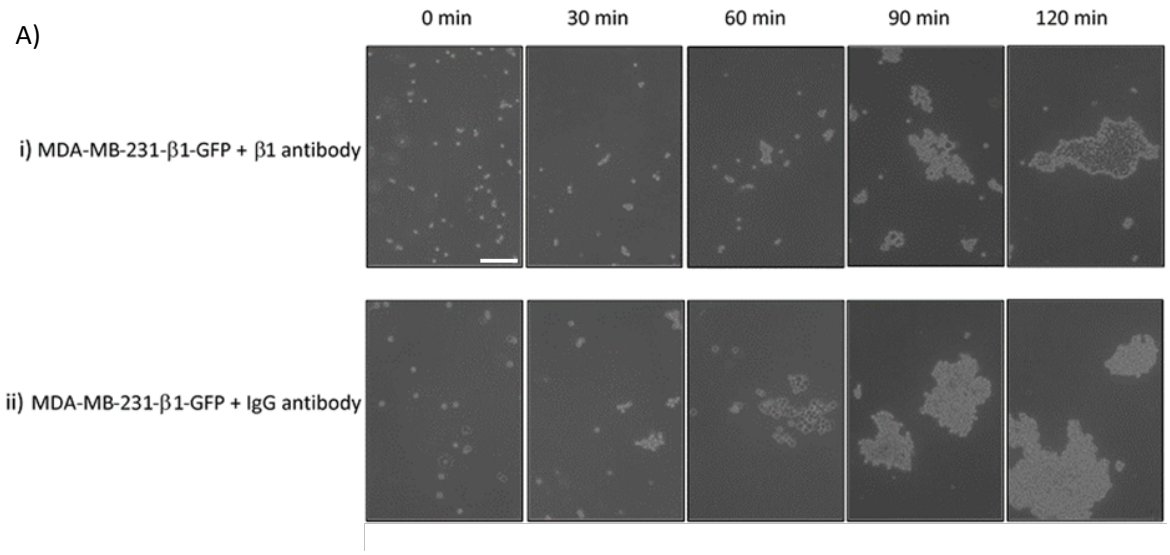

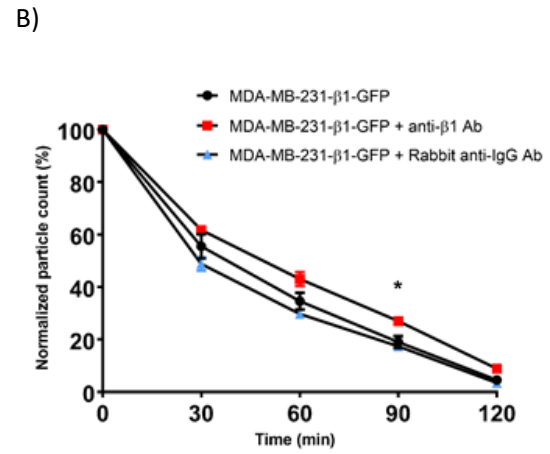

Figure 3.2 Adhesion assay showing the effect of anti-β1 antibody on adhesiveness of MDA-MB-231-β1-GFP cells

(A) Images of cells in adhesion assay, taken at 30-minute intervals. (i) MDA-MB-231-β1-GFP cells in the presence of anti β1-N-ternimus antibody (10 µg/ml). (ii) MDA-MB-231-β1-GFP cells in the presence of rabbit anti-IgG antibody (10 µg/ml). Scale bar = 100 µm. B) Normalized particle counts from control MDA-MB-231-β1-GFP cells and MDA-MB-231-β1-GFP cells with a β1 N-terminus or rabbit anti-IgG antibody added to a final concentration of 10 µg/ml. An equal concentration of Na^+ azide (11.7 µM) in PBS was added to the control cells. Particles were counted on an Axiovert 135 microscope at 10X zoom, n = 4-7, 10 fields of view per n. Data are presented as mean and SEM. One-way ANOVA with Tukey test was used to test for significance at each timepoint. *$P < 0.05$.

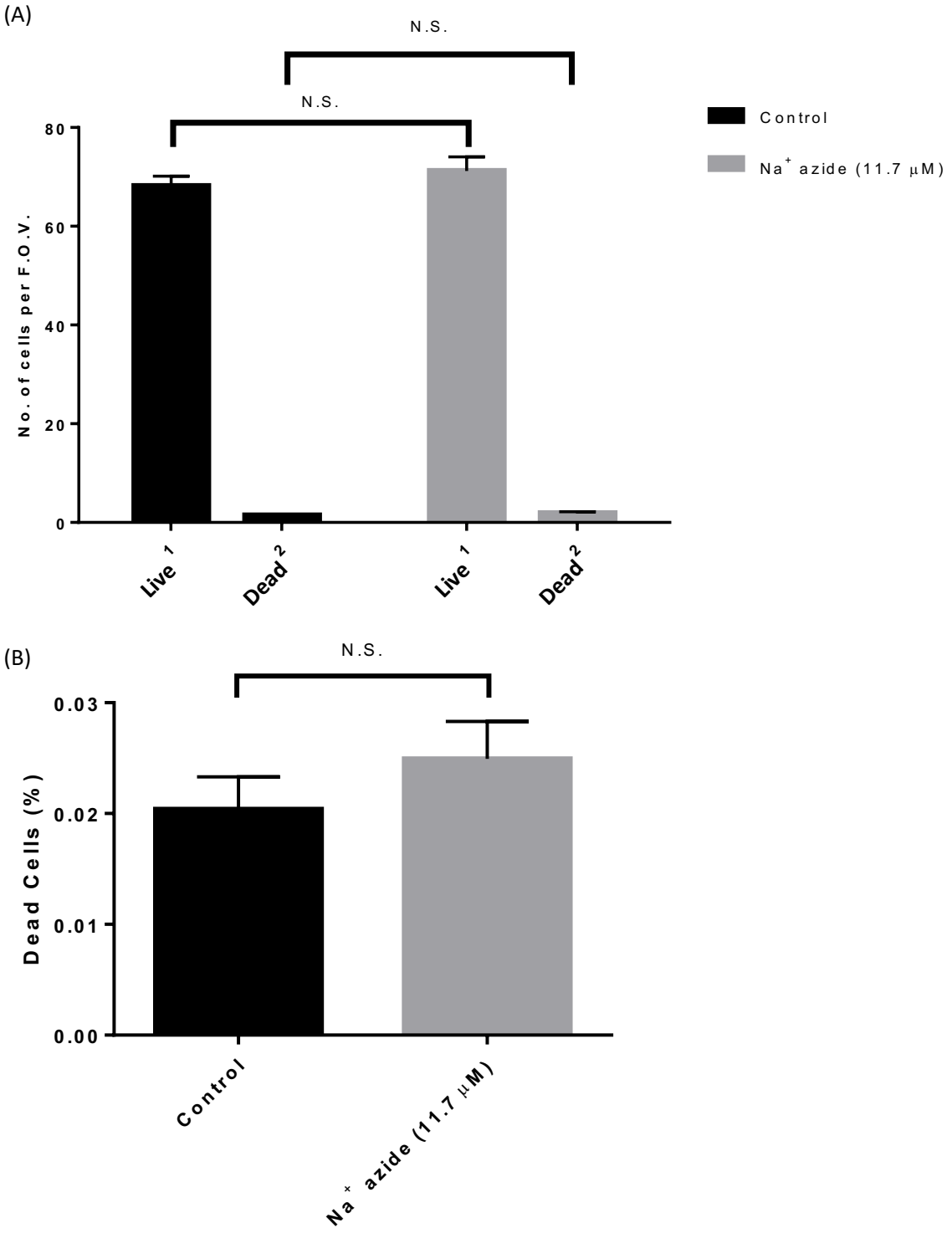

Figure 3.3 Effect of Na^+ azide on cell viability.

(A) The mean number of live and dead cells after a 2h treatment with either PBS or PBS + Na^+ azide (11.7 µM) determined by trypan blue assay (n = 3, 10 fields of view per n). A one-way ANOVA showed there was no significant difference in the number of live cells across treatments or dead cells across treatments respectively ($P > 0.05$). (B) Dead cells, expressed as a % of total cell count, following treatment for 2h with PBS or PBS + Na^+ azide (11.7 µM). An unpaired t-test showed there was no significant difference (N.S.).

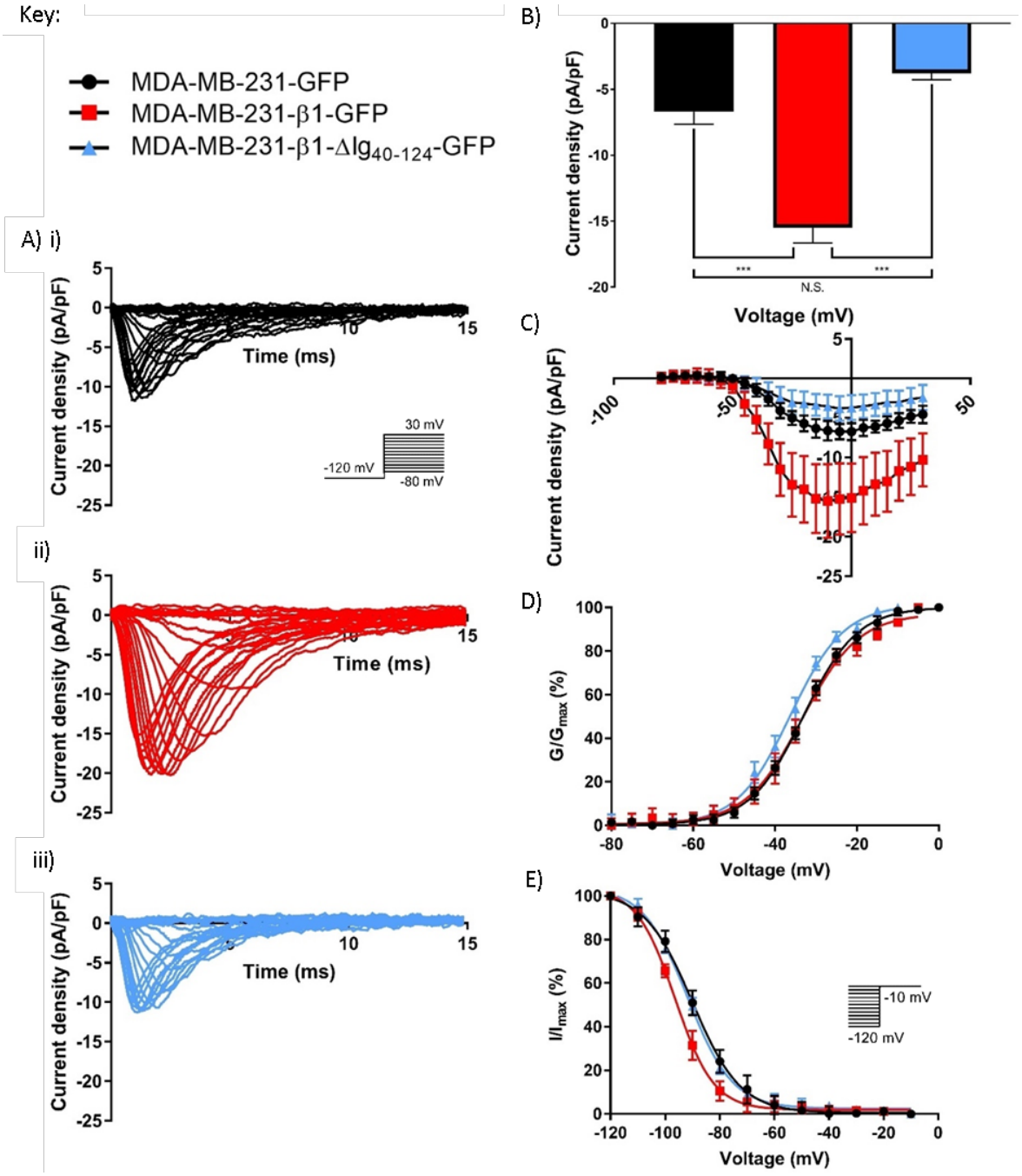

Figure 3.4 Removing the β1 Ig loop significantly affects Na^+ current characteristics in MDA-MB-231 cells

(A) Typical whole-cell Na^+ currents elicited by 50 ms depolarizing pulses between -80 mV and 30 mV applied from a holding potential of -120 mV: (i) a control cell expressing GFP; (ii) a cell overexpressing β1-GFP; (iii) a cell overexpressing β1ΔIg40-124-GFP. (B) Whole-cell peak Na^+ current density for control cells expressing GFP (black), cells overexpressing β1-GFP (red) and cells overexpressing a β1ΔIg40-124-GFP (blue). (C) Current-voltage relationship for control cells expressing GFP, cells expressing β1-GFP (red) and cells expressing β1-GFP lacking the Ig loop. (D) Steady-state activation. Normalised conductance (G/G_{max}), calculated from the current data, plotted as a function of voltage for control cells expressing GFP (black), cells expressing β1-GFP (red) and cells expressing β1 lacking the Ig loop (blue). (E) Steady-state inactivation. Normalised current (I/I_{max}), elicited by 50 ms test pulses at −10 mV following 250 ms conditioning voltage pulses between −120 mV and −10 mV, applied from a holding potential of −120 mV, plotted as a function of the pre-pulse voltage. Data are presented as mean ± SEM. One-way ANOVA with Tukey test was used to test for significance (n ≥ 12/group). ***P < 0.001; N.S., not significant.

Table 3.1 Effect of the β1 Ig loop on Na^+ current characteristics in MDA-MB-231 cells.

Parameter[a]	MDA-MB-231-GFP	MDA-MB-231-β1-GFP	MDA-MB-231-β1-ΔIg_{40-124}-GFP
I_p (pA/pF)	-6.7 ± 0.3	-15.5 ± 2.3 *	-3.8 ± 0.5
V_a (mV)	-40 ± 1.0	-46.6 ± 1.7 *	-44.6 ± 1.2 *
V_p (mV)	-5.0 ± 2.3	-9.1 ± 2.0	-5.00 ± 1.4
Activation $V_{1/2}$ (mV)	-24.1 ± 2.5	-30.0 ± 1.3	-25.3 ± 1.9
Activation k (mV)	7.1 ± 0.5	6.0 ± 0.6	7.6 ± 0.6
Inactivation $V_{1/2}$ (mV)	-91.7 ± 0.9	-95.0 ± 1.5 *	-87.8 ± 2.7
Inactivation k (mV)	-8.3 ± 0.6	-5.8 ± 2.2	-11.2 ± 2.1
T_p (ms)	1.6 ± 0.2	1.7 ± 0.2	1.4 ± 0.2
V_{rev} (mV)	101.3 ± 10.9	111.1 ± 19.9	99.9 ± 21.36

[a] ***Abbreviations:*** I_p, peak current density; V_a, activation voltage; V_p, voltage at current peak; $V_{1/2}$, half (in)activation voltage; *k*, slope factor; T_p, time to peak. Data are expressed as mean ± SEM. Significance: $*P < 0.05$ (significantly different from control), One-way ANOVA with post-hoc Tukey's tests were used to test for significance.

In contrast, there was no significant difference between the voltage at peak current and time to peak between the cell lines, suggesting that β1 does not modulate these properties (Table 3.1). In conclusion, these data suggest that β1 increases Na^+ current in MDA-MB-231 cells and this requires the presence of the Ig loop. Similarly, the hyperpolarising effect of β1 on steady-state inactivation also requires the presence of the Ig loop. On the other hand, the hyperpolarising effect of β1 on the activation voltage appears to be independent of the Ig loop. The average measured V_{rev} for all three cell lines was far removed from the reversal potential of Na^+ based on the internal and external concentrations in the solutions (+86 mV) but did not differ significantly amongst the cell lines.

3.3.4. β1 overexpression increases expression of a TTX sensitive α subunit

As shown in Table 1.1, VGSC α subunits can be separated into TTX-sensitive and TTX-resistant groups. A previous report has shown that β1 upregulates $Na_V1.7$ (TTX-sensitive) VGSCs (Laedermann *et al.*, 2013). In order to establish whether the increased Na^+ current in MDA-MB-231-β1-GFP cells was TTX-resistant or TTX-sensitive, using whole-cell patch clamp, Na^+ currents were recorded following depolarisation to -10 mV. The voltage was recorded at -10 mV as the peak current, or a

substantially large enough Na^+ current was expected to be seen at this voltage based on the above data. Cells were then perfused with 1 μM TTX and the current recorded again. 1 μM TTX was used as this is sufficient to completely block TTX-sensitive α subunits whilst not affecting TTX-resistant α subunits (Tamura *et al.*, 2014). The TTX was washed out and the current recorded once more. Perfusion of the control MDA-MB-231-GFP cells with TTX had no effect on the Na^+ current density (-8.36 pA/pF for PSS and -9.87 pA/pF for TTX; $P > 0.05$; Figure 3.5A). Interestingly, 1μM TTX significantly reduced Na^+ current density in β1-overexpressing cells from -18.52 pA/pF to -11.50 pA/pF ($P < 0.001$) and washing out TTX resulted in recovery of the current to -15.35 pA/pF ($P < 0.001$; Figure 3.5B).

Perfusion of MDA-MB-231-β1$\Delta Ig_{40–124}$-GFP cells with 1 μM TTX did not result in a decrease in current density (-4.25 pA/pF for PSS and –5.20 pA/pF for TTX; Figure 3.5C). In MDA-MB-231-β1-ΔIg_{40-124}-GFP cells, a washout recording was not obtained due to the relatively weak membrane resulting in the loss of the seal with repeated washes. No significant difference was seen between MDA-MB-231-β1-GFP cells perfused with TTX compared to MDA-MB-231-GFP cells perfused with TTX ($P < 0.05$), suggesting that the increased Na^+ current in MDA-MB-231-β1-GFP cells was entirely carried by a TTX-S α subunit. RT-PCR using RNA extracted from all three cell lines revealed that $Na_V1.7$ is expressed in MDA-MB-231-β1-GFP cells but not in MDA-MB-231-GFP or MDA-MB-231-β1-ΔIg_{40-124}-GFP cells (Figure 3.5D). In conclusion, the electrophysiology data suggest that β1 over-expression in MDA-MB-231 cells increases expression of a TTX-sensitive Na^+ current, and the PCR data suggest that the identity of this TTX-sensitive channel may be $Na_V1.7$.

3.3.5. The $Na_V1.7$ blocker PF-04856042 inhibits Na^+ current in MDA-MB-231-β1-GFP cells

PF-04856042 (PF) is a selective $Na_V1.7$ inhibitor which has been shown to have no effect on $Na_V1.5$ (McCormack *et al.*, 2013). Therefore, this compound was used to determine directly whether the TTX-sensitive current in MDA-MB-231-β1-GFP cells was being carried by $Na_V1.7$. MDA-MB-231-GFP

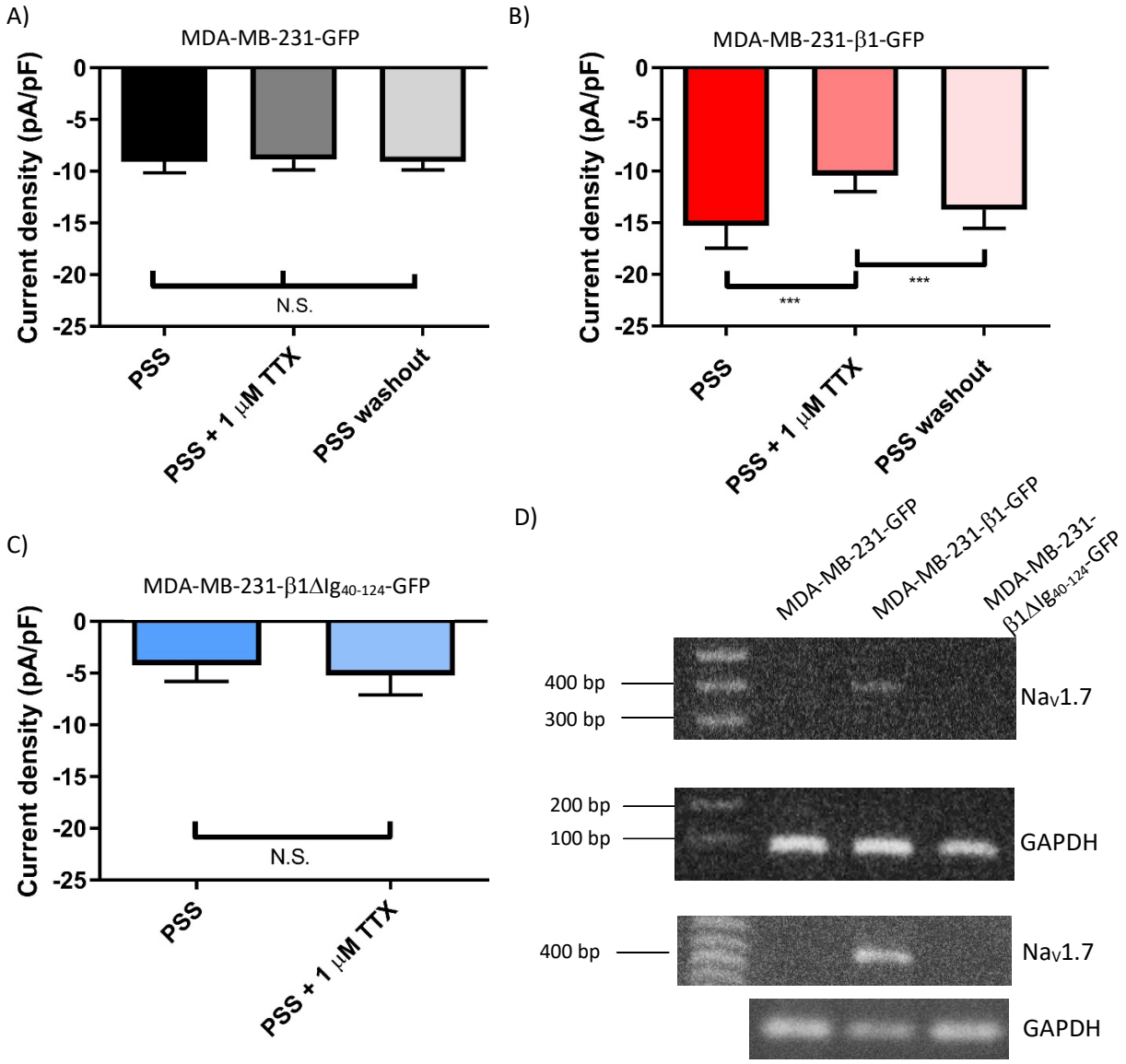

Figure 3.5 β1 increases expression of a TTX-sensitive α subunit in MDA-MB-231 cells.

Cells were clamped at -10 mV in the absence, presence of 1 µM tetrodotoxin (TTX) and following washout. Cells were first recorded in physiological saline solution (PSS) after which the solution was replaced with PSS + 1 µM TTX. This solution was washed out and replaced with PSS and current was recorded once more. (A) Whole-cell Na^+ current density for control MDA-MB-231-GFP cells (n = 12). (B) Whole-cell Na^+ current density for MDA-MB-231-β1-GFP cells (n = 12). (C) Whole-cell Na^+ current density for MDA-MB-231-β1ΔIg$_{40\text{-}124}$-GFP cells (n = 9). It was not possible to obtain washout data due to the relatively weak membrane characteristics of this cell line. (D) PCR of MDA-MB-231-GFP, MDA-MB-231-β1-GFP and MDA-MB-231-β1ΔIg$_{40\text{-}124}$-GFP cells for $Na_V1.7$ with GAPDH as a positive control. Data are presented as mean and SEM. Repeated measures ANOVA (A, B) or paired t-test (C) was used to test for significance; ***P < 0.001; N.S., not significant.

and MDA-MB-231-β1-GFP cells were initially recorded from in PSS and then perfused with PSS + 1 μM PF. Recordings were taken before and after perfusion of PF. Neither the I_P nor the Na^+ current gating characteristics differed significantly between the two treatments in control MDA-MB-231-GFP cells ($p > 0.05$; n = 8; Figure 3.6A-E, Table 3.2) supporting earlier observations that PF has no effect on $Na_V1.5$ (McCormack *et al.*, 2013). When MDA-MB-231-β1-GFP cells were perfused with 1 μM PF, the I_P decreased significantly from -19.2 ± 3.3 pA/pF to -8.2 ± 0.6 ($P < 0.01$; Figure 3.6A-C, Table 3.2).

3.3.6. γ secretase inhibition suppresses the effect of β1 on Na^+ current

Given that β subunits are proteolytically processed by secretases, and cleavage and release of the β2 intracellular domain permits upregulation of α subunit expression at the mRNA level (Kim *et al.*, 2005; Wong *et al.*, 2005), the next set of experiments thus sought to evaluate the possible role of β1 cleavage in the upregulation of TTX-sensitive Na^+ current. To determine whether the intracellular domain of β1 was responsible for the upregulation of TTX-sensitive Na^+ current, 24 h prior to recording, cells were treated with DAPT, an inhibitor of γ-secretase. When MDA-MB-231-GFP cells were treated with DMSO (vehicle control) or DAPT (1 μM), there was no significant difference in the I_P between the two conditions (-8.8 ± 0.6 pA/pF for PSS and -8.9 ± 0.9 pA/pF for DAPT, $P > 0.05$; n = 8; Figure 3.7A,C). However, when MDA-MB-231-β1-GFP cells were treated with 1 μM DAPT, the I_P was significantly smaller than when the same cells were treated with DMSO (-19.7 ± 3.9 for PSS and -10.2 ± 1.3, $P < 0.01$; Figure 3.7A, C). Thus, DAPT-mediated γ-secretase inhibition appears to be blocking the increase in Na^+ current density seen in MDA-MB-231-β1-GFP cells. The activation voltage and voltage corresponding to peak current were both significantly hyperpolarised in MDA-MB-231-β1-GFP cells compared to MDA-MB-231-GFP cells and the DAPT treatment partially reversed this effect in both cases ($P < 0.01$; and $P < 0.05$, respectively; Figure 3.7B; Table 3.3). No significant differences were observed in any of the other Na^+ current parameters (Figure 3.7D, E; Table 3.3). In conclusion, these data suggest that β1-mediated effects on the Na^+ current in MDA-

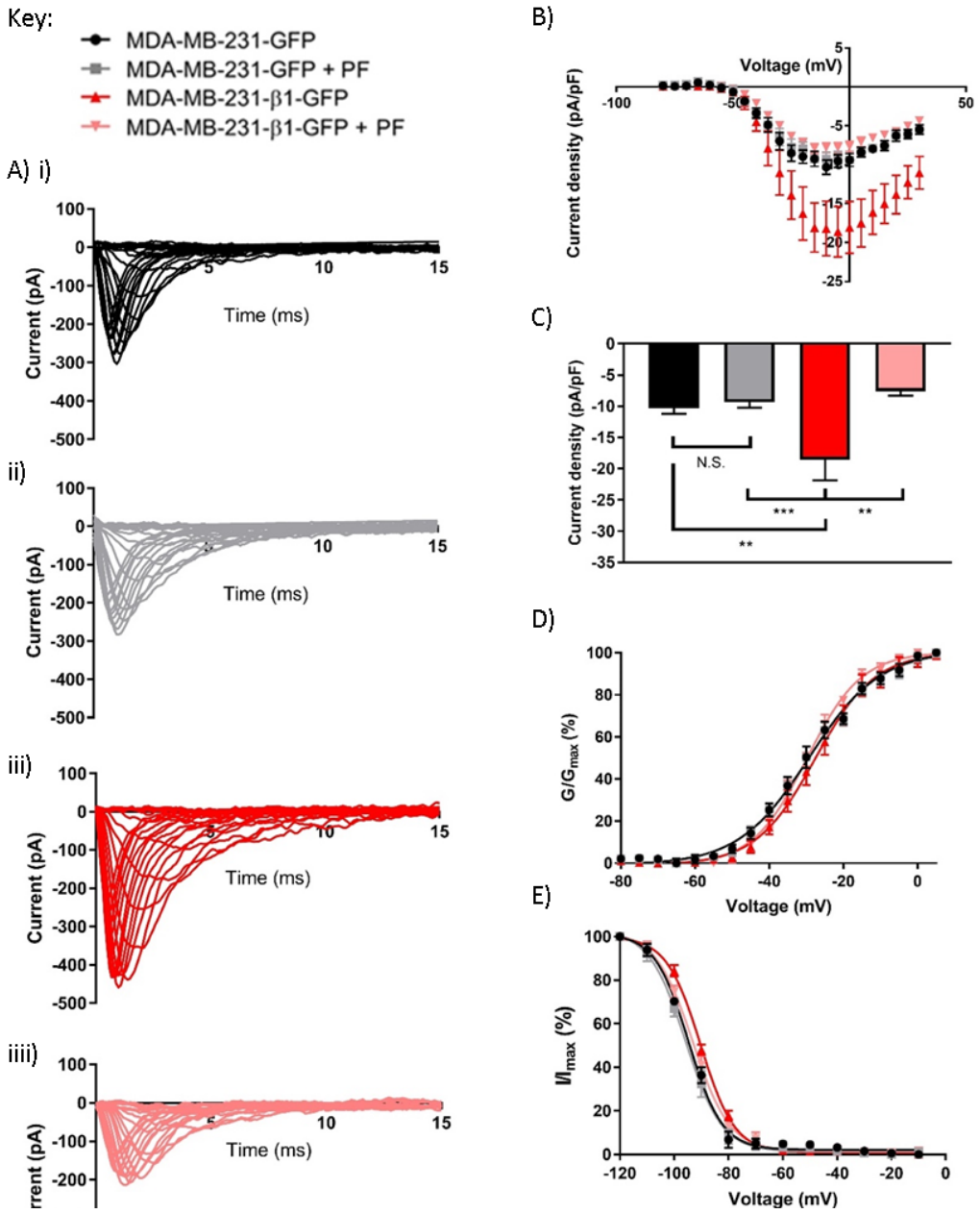

Figure 3.6 Effect of PF-0485642 on Na^+ current in MDA-MB-231-GFP and MDA-MB-231-β1-GFP cells.

(A) Typical whole-cell Na^+ currents elicited by 50 ms depolarizing pulses between -80 mV and 30 mV applied from a holding potential of -120 mV: (i) MDA-MB-231-GFP; (ii) MDA-MB-231-GFP + PF-0485642 (1 µM); (iii) MDA-MB-231-β1-GFP; (iv) MDA-MB-231-β1-GFP + PF-0485642 (1 µM). (B) Current-voltage relationships for MDA-MB-231-GFP and MDA-MB-231-β1-GFP cells before and after perfusion with PF-0485642. (C) Whole-cell peak Na^+ current density for MDA-MB-231-GFP and MDA-MB-231-β1-GFP cells with and without PF-0485642. (D) Steady-state activation. Normalised conductance (G/G_{max}), calculated from the current data, plotted as a function of voltage. (E) Steady-state inactivation. Normalised current (I/I_{max}), elicited by 50 ms test pulses at −10 mV following 250 ms conditioning voltage pulses between −120 mV and −10 mV, applied from a holding potential of −120 mV, plotted as a function of the pre-pulse voltage. Data are presented as mean ± SEM. One-way ANOVA with Tukey test was used to test for significance (n = 8/group). ***P < 0.001; **P < 0.01; N.S., not significant.

Table 3.2 Effect of PF-0485462 treatment on Na^+ current characteristics in MDA-MB-231-GFP and MDA-MB-231-β1-GFP cells.

Parameter[a]	MDA-MB-231-GFP PSS	MDA-MB-231-GFP PSS + 1 μM PF-0485642	MDA-MB-231-β1-GFP PSS	MDA-MB-231-β1-GFP PSS + 1 μM PF-0485642
I_p (pA/pF)	-9.8 ± 0.9	-9.8 ± 0.9	-19.2 ± 3.3 **	-8.2 ± 0.6
V_a (mV)	-45.0 ± 2.0	-44.4 ± 1.2	-46.3 ± 1.3	-45.6 ± 1.2
V_p (mV)	-4.4 ± 2.1	-7.5 ± 2.3	-9.4 ± 1.9	-9.4 ± 2.1
Activation $V_{1/2}$ (mV)	-5.1 ± 0.6	-5.0 ± 0.3	-5.6 ± 0.3	-5.9 ± 0.3
Activation k (mV)	9.0 ± 1.4	9.0 ± 0.4	7.9 ± 0.4	7.3 ± 0.5
Inactivation $V_{1/2}$ (mV)	-95.3 ± 1.5	-95.9 ± 1.5	-91.9 ± 0.7*	-95.8 ± 1.1
Inactivation k (mV)	-6.0 ± 0.6	-4.7 ± 1.6	-7.9 ± 0.7	-4.8 ± 2.2
T_p (ms)	1.6 ± 0.3	1.6 ± 0.3	1.0 ± 0.1	1.1 ± 0.2
V_{rev} (mV)	79.89 ± 8.54	79.52 ± 8.54	86.78 ± 10.92	85.15 ± 10.94

[a] ***Abbreviations:*** I_p, peak current density; V_a, activation voltage; V_p, voltage at current peak; $V_{1/2}$, half (in)activation voltage; *k*, slope factor; T_p, time to peak. Data are expressed as mean ± SEM. Significance: *P<0.05. One-way ANOVA with post-hoc Tukey's tests were used to test for significance.

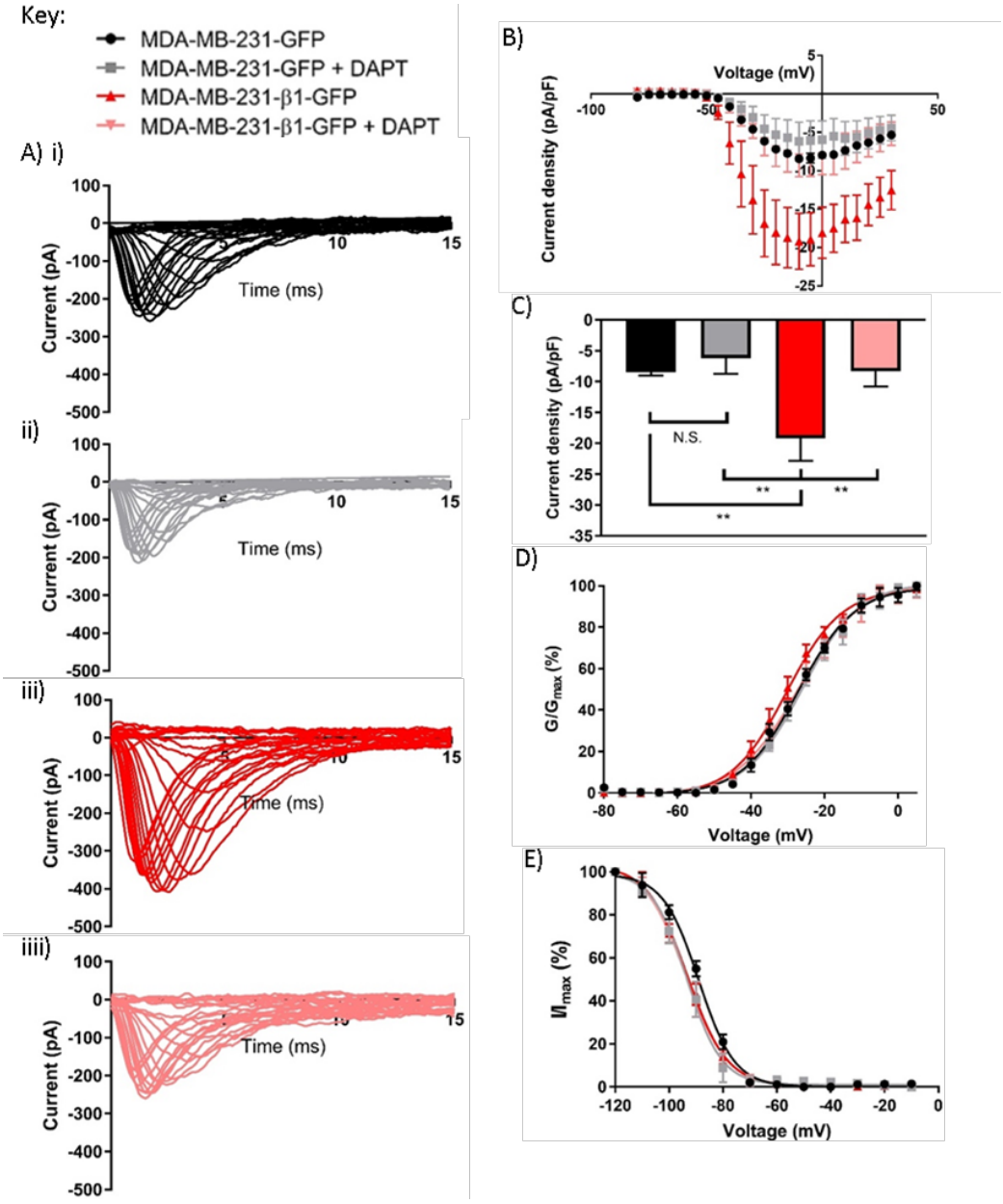

Figure 3.7 Effect of DAPT on Na^+ current in MDA-MB-231-GFP and MDA-MB-231-β1-GFP cells.

(A) Typical whole-cell Na^+ currents elicited by 50 ms depolarizing pulses between -80 mV and 30 mV applied from a holding potential of -120 mV: (i) MDA-MB-231-GFP; (ii) MDA-MB-231-GFP + DAPT (1 µM pre-treatment for 24 h); (iii) MDA-MB-231-β1-GFP; (iv) MDA-MB-231-β1-GFP + DAPT (1 µM pre-treatment for 24 h). (B) Current-voltage relationships for MDA-MB-231-GFP and MDA-MB-231-β1-GFP cells treated with DMSO or DAPT 24 h before recording. (C) Whole-cell peak Na^+ current density for MDA-MB-231-GFP and MDA-MB-231-β1-GFP cells treated with DMSO or DAPT 24 h before recording. (D) Steady-state activation. Normalised conductance (G/G_{max}), calculated from the current data, plotted as a function of voltage. (E) Steady-state inactivation. Normalised current (I/I_{max}), elicited by 50 ms test pulses at −10 mV following 250 ms conditioning voltage pulses between −120 mV and −10 mV, applied from a holding potential of −12 0mV, plotted as a function of the pre-pulse voltage. Data are presented as mean ± SEM. One-way ANOVA with Tukey test was used to test for significance (n = 8/group). **P < 0.01; N.S., not significant.

Table 3.3 Effect of DAPT on Na^+ current characteristics in MDA-MB-231-GFP and MDA-MB-231-β1-GFP cells.

Parameter[a]	MDA-MB-231-GFP	MDA-MB-231-GFP + DAPT	MDA-MB-231-β1-GFP	MDA-MB-231-β1-GFP + DAPT
I_p (pA/pF)	-8.8 ± 0.6	-8.9 ± 0.9	-19.7 ± 3.9 **	-10.2 ± 1.3
V_a (mV)	-40.0 ± 1.0	-41.3 ± 0.9	-46.3 ± 1.3 **	-44.4 ± 1.8
V_p (mV)	-6.9 ± 2.3	-1.3 ± 3.5	-11.9 ± 2.5 *	-8.8 ± 3.8
Activation $V_{1/2}$ (mV)	-5.4 ± 0.2	-4.9 ± 0.3	-5.7 ± 0.5	-5.1 ± 0.3
Activation k (mV)	8.3 ± 0.6	9.6 ± 1.0	7.3 ± 0.5	10.1 ± 1.5
Inactivation $V_{1/2}$ (mV)	-89.4 ± 1.0	-93.0 ± 2.3	-93.2 ± 1.75	-93.0 ± 1.9
Inactivation k (mV)	-6.6 ± 0.2	-6.2 ± 0.4	-7.5 ± 0.5	-5.9 ± 1.7
T_p (ms)	1.1 ± 0.1	1.3 ± 0.2	1.5 ± 0.3	1.2 ± 0.2
V_{rev} (mV)	85.9 ± 8.51	84.77 ± 8.77	86.81 ± 7.11	80.56 ± 4.88

[a] ***Abbreviations:*** I_p, peak current density; V_a, activation voltage; V_p, voltage at current peak; $V_{1/2}$, half (in)activation voltage; *k*, slope factor; T_p, time to peak. Data are expressed as mean ± SEM. Significance: *P<0.05, One-way ANOVA with post-hoc Tukey's tests were used to test for significance.

MB-231 cells depend on γ-secretase activity. Thus, cleavage and release of the β1 intracellular domain may be critical for β1 to increase TTX-sensitive Na^+ current in this cell line.

3.3.7. Effect of β1 overexpression on subthreshold currents

It has been shown previously that cells expressing $Na_V1.7$ display a small inward Na^+ current in response to slow ramp depolarisations at subthreshold voltages, termed a subthreshold current (Cummins *et al.*, 1998). However, previous ramp recordings using parental MDA-MB-231 cells have shown an outward current at subthreshold potentials (Roger *et al.*, 2004), suggesting that $Na_V1.7$ is not present. Given the data in the above sections showing that β1 over-expression in MDA-MB-231 cells results in up-regulation of a TTX-sensitive Na^+ current that can be blocked by the $Na_V1.7$ inhibitor PF, the next set of experiments sought to evaluate whether an inward subthreshold current characteristic of $Na_V1.7$ was also present in response to β1 over-expression. We used a ramping voltage stimulation from -100 mV to -50 mV at a rate of 1 mV/ms to see whether a subthreshold current was present in MDA-MB-231-β1-GFP cells. An outwardly positive (upward) subthreshold current was present in MDA-MB-231-GFP cells and this was unaffected by perfusion with PF (Figure 3.8A,B). This result is consistent with previous recordings in MDA-MB-231 cells (Roger *et al.*, 2004), and suggests that $Na_V1.5$ (the main α subunit in this cell line) does not display a sub-threshold inward current. MDA-MB-231-β1-GFP cells showed an inward (downward) current when these cells were recorded in PSS (Figure 3.8C). When the MDA-MB-231-β1-GFP cells were perfused with PF, the direction of the current reversed, and became outward (Figure 3.8C). The current density at -50 mV (the end of the ramp protocol) was thus significantly different when MDA-MB-231-β1-GFP cells were recorded in PF compared to control (Figure 3.8D). In conclusion, the experiments in this section indicate that, as described previously (Roger *et al.*, 2004), MDA-MB-231 cells normally display an outward subthreshold current (the identity of which is unknown). When β1 is over-expressed in this cell line, there is an up-regulation of functional $Na_V1.7$ expression, which accounts for the increased

I_P, the TTX-sensitive nature of this current, the sensitivity to PF, and the presence of a subthreshold inward current.

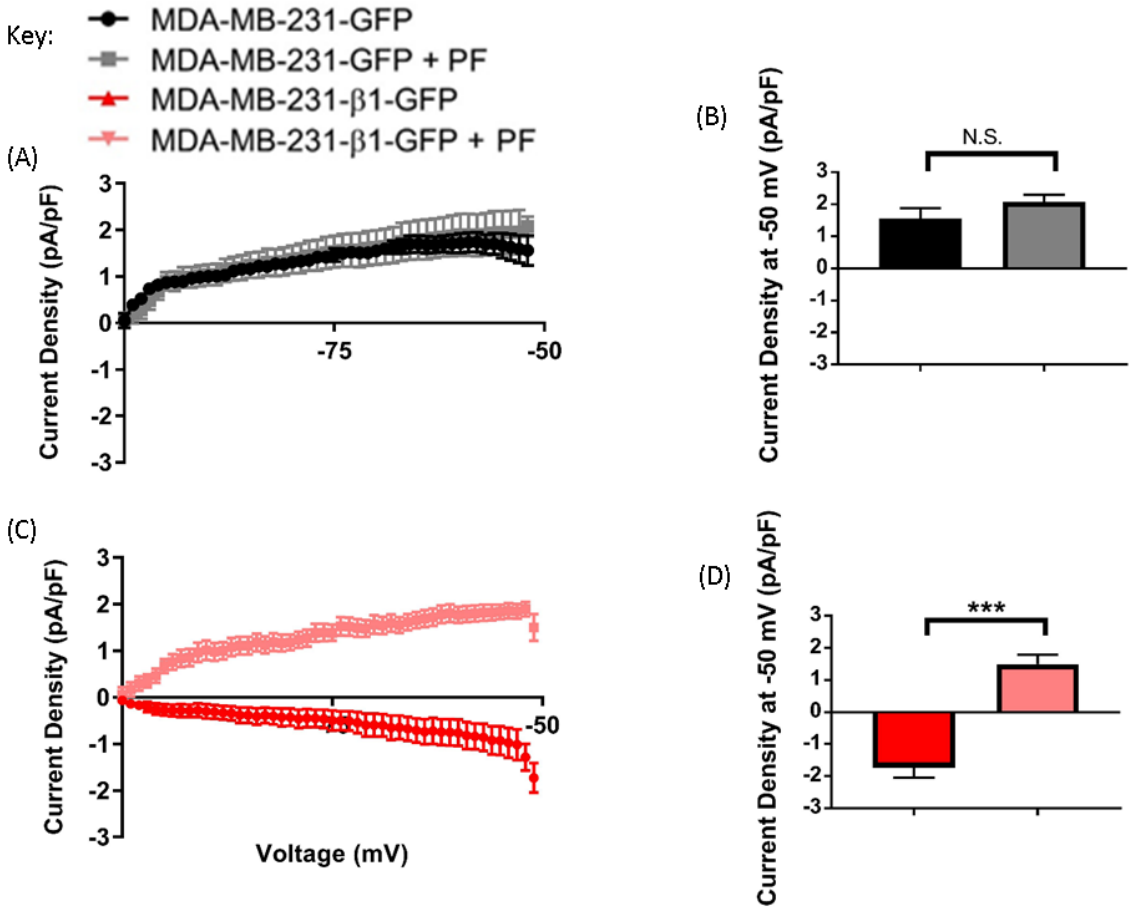

Figure 3.8 Effect of PF-0485642 on subthreshold currents in MDA-MB-231-GFP and MDA-MB-231-β1-GFP cells.

Ramp current density recorded from MDA-MB-231-GFP cells with and without PF-0485642. Cells were depolarised from -100 mV to -50 mV at 1 mV/ms. (B) Current density in MDA-MB-231-GFP cells at -50 mV, the end of the ramp protocol. (C) Ramp current density recorded from MDA-MB-231-β1-GFP cells with and without PF-0485642. (D) Current density at -50 mV in MDA-MB-231-β1-GFP cells before and after application of PF-0485642. Data are presented as mean ± SEM. Student's t test was used to test for significance. ***P < 0.001; N.S., not significant.

3.4. Discussion

3.4.1. The Ig loop is required for β1 to increase adhesion and Na^+ current

It has been shown previously that β1 increases cell-cell adhesion and neurite-like process outgrowth of MDA-MB-231 cells (Chioni *et al.*, 2009; Nelson *et al.*, 2014). Furthermore, creation of a deletion mutant lacking the Ig domain revealed that the Ig loop of β1 is required for it to promote process

outgrowth (Nelson *et al.*, 2014). What has not been shown, however, is whether other regions of β1 play any role in enhancing β1-mediated cell adhesion of MDA-MB-231 cells. The data in this Chapter show that β1 over-expression in MDA-MB-231 cells increased adhesion, consistent with these previous observations (Chioni *et al.*, 2009). This increase in adhesion was not evident in the MDA-MB-231-β1Δ$Ig_{40–124}$-GFP cells, indicating that the Ig loop is required for β1 to promote adhesion in MDA-MB-231 cells, consistent with observations in other cell models (Malhotra *et al.*, 2000). Furthermore, the almost complete abrogation of β1-mediated adhesion in the absence of the Ig domain suggests that only this region of the protein is required to elicit cell-cell adhesion. The addition of an antibody targeting the Ig loop of β1 also decreased adhesion. However, the inhibitory effect of the antibody was considerably smaller than that of the truncation mutant and was only present at one late time point in the assay. This relatively weak effect of the N-terminal antibody could be due to insufficient quantities applied to block all adhesion sites on the cell surface. In addition, the slow kinetics of the effect may be explained by the time required for the antibody to sufficiently bind and prevent adhesion. Further work is required to test these possibilities.

β1 is able to increase cell-cell adhesion through homophilic binding (Malhotra *et al.*, 2000), and interacts heterophilically with several other CAMs and extracellular matrix proteins, including β2, contactin, neurofascin-186, NrCAM and N-cadherin, and tenascin-R (Xiao *et al.*, 1999; Malhotra *et al.*, 2000; Kazarinova-Noyes *et al.*, 2001; Ratcliffe *et al.*, 2001; McEwen & Isom, 2004). Thus, the increase in cell-cell adhesion in MDA-MB-231 cells due to β1 overexpression may be the result of both homophilic and heterophilic interactions. However, whether one mode is predominant cannot be discerned from these experiments. Although *trans*-homophilic adhesion interactions between β1 subunits are well established (Malhotra *et al.*, 2000), interactions between β1 and other binding partners may also play significant functional roles and have diverse downstream consequences. For example, in cardiac myocytes, adhesion-dependent interaction of β1 with $ankyrin_B$ and $ankyrin_G$ results in phosphorylation of Y181 which is required for regulating subcellular distribution of β1

(Malhotra *et al.*, 2002; Malhotra *et al.*, 2004). Similarly, interactions between β1 and contactin increase Na^+ current (Kazarinova-Noyes *et al.*, 2001; McEwen *et al.*, 2004). Further work is required to establish whether the increase in adhesion of MDA-MB-231-β1-GFP cells compared to MDA-MB-231 cells is the result of homophilic adhesion.

Previous data show that, in addition to increasing adhesion, β1 over-expression in MDA-MB-231 cells also increases I_P (Chioni *et al.*, 2009). However, the role of the Ig loop in modulating the Na^+ current in MDA-MB-231 cells is not known. The results presented here show that β1 overexpression increased I_P , in agreement with these previous observations (Chioni *et al.*, 2009). Furthermore, the data in this Chapter show for the first time that the Na^+ current-promoting effect of β1 is dependent on the presence of the Ig loop. These results are important for two main reasons: Firstly, given that Na^+ current carried by VGSCs is critical for promoting cellular invasion and metastasis (Fraser *et al.*, 2005; Nelson *et al.*, 2014; Nelson *et al.*, 2015), it is possible that β1 may function co-operatively with α to potentiate tumour progression. Secondly, the critical dependence on the Ig loop for promoting adhesion and Na^+ current highlights this domain as a potential target for inhibiting VGSC-mediated invasion and metastasis. However, a key issue that remains unresolved is the relative significance of β1-dependent adhesion and increased Na^+ current in the cancer process. Further work is required to separate out these two consequences of β1 function.

3.4.2. γ-secretase activity is required for β1 to increase Na^+ current

The intracellular domains of the β subunits, released by proteolytic processing by α, β and γ secretases, have previously been reported to regulate various β subunit properties, including β4-mediated neurite outgrowth and modulation of the resurgent Na^+ current, and β2-mediated adhesion, migration and upregulation of $Na_V1.1$ expression (Kim *et al.*, 2005; Wong *et al.*, 2005; Kim *et al.*, 2007; Miyazaki *et al.*, 2007). In addition, a mutation in presenilin (which forms the catalytic core of γ-secretase) has been shown to reduce $Na_V1.1$ mRNA level in a neuroblastoma cell line (Kim

et al., 2014). The γ-secretase inhibitor DAPT has previously been shown to abrogate proteolytic release of β subunit intracellular domains (Kim *et al.*, 2005; Wong *et al.*, 2005; Kim *et al.*, 2007). The present data show that DAPT reduced Na^+ current density of MDA-MB-231-β1-GFP cells to a level equivalent to MDA-MB-231-GFP cells, suggesting that γ-secretase-mediated cleavage is required for β1 to increase Na^+ current in MDA-MB-231 cells. Taken together with the available published evidence (Kim *et al.*, 2005; Wong *et al.*, 2005; Kim *et al.*, 2007), this result suggests that the cleaved soluble intracellular domain of β1 may regulate α subunit expression in MDA-MB-231 cells, thus promoting Na^+ current when β1 is over-expressed.

It is important to note in the context of these observations that there was no increase in Na^+ current density in MDA-MB-231-β1$\Delta Ig_{40\text{-}124}$-GFP cells where the intracellular domain is still present. One possible explanation for this is that the Ig loop may be necessary for recruiting the secretase enzymes required for cleavage. Cleavage of β1 is proposed to be sequential, similar to the model identified for amyloid precursor protein, such that the extracellular Ig domain is cleaved by α-secretase or BACE1, after which the intracellular domain is cleaved by γ-secretase (Wong *et al.*, 2005; Gersbacher *et al.*, 2010). Therefore, in MDA-MB-231-$\Delta Ig_{40\text{-}124}$-GFP cells, where the Ig loop is not present, the first secretases may not be recruited, the extracellular region may not be cleaved, and so the intracellular domain may not be released, thus explaining the lack of increased Na^+ current in these cells. Caution should be taken with this interpretation however, because in a murine neuroblastoma cell line, BACE1 increased Na^+ current without cleaving either β1 or β4 (Huth *et al.*, 2009), suggesting the possibility of another BACE1-mediated pathway responsible for increasing Na^+ current. The relationship between secretase enzymes and VGSCs is complicated by the fact that these enzymes have a broad range of target proteins (Carroll & Li, 2016). Together with the fact that the Ig loop has a diverse set of interacting partners, some of which may also modulate Na^+ current, this point makes interpretation of the DAPT treatment data challenging. Further work is required to

evaluate which secretases are involved, the specific cleavage targets, and their precise effect on VGSC activity.

3.4.3. Evidence for up-regulation of $Na_V1.7$

The data in this Chapter show that the increase in Na^+ current in MDA-MB-231-β1-GFP cells is carried by a TTX-sensitive α-subunit. This rules out the possibility that β1 is stabilising or increasing plasma membrane expression of $Na_v1.5$, which is the main α subunit in these cells (Fraser *et al.*, 2005; Brackenbury *et al.*, 2007). However, the fact that γ-secretase-mediated release of the β2 intracellular domain upregulates $Na_v1.1$ expression via a putative transcriptional mechanism (Kim *et al.*, 2007), and that β1 has been shown to increase $Na_V1.7$ expression in lung cancer cells (Laedermann *et al.*, 2013), raises the possibility that β1 may up-regulate $Na_v1.7$ expression in MDA-MB-231 cells. In support of this notion, there was an increase in Nav1.7 mRNA level in MDA-MB-231-β1-GFP cells compared to control MDA-MB-231-GFP cells. In addition, PF, a synthetic peptide blocker, which was recently shown to bind to the inactivated state of $Na_V1.7$ and inhibit Na^+ conductance, and which was also shown to have no effect on $Na_V1.5$ (McCormack *et al.*, 2013), significantly reduced Na^+ current in MDA-MB-231-β1-GFP cells. These results strongly suggest that up-regulated $Na_V1.7$ is responsible for the increased Na^+ current in MDA-MB-231-β1-GFP cells.

$Na_V1.7$ has been shown to display a subthreshold current at hyperpolarised membrane potentials below the action potential threshold (Cummins *et al.*, 1998; Cummins *et al.*, 2004). It has been proposed that this current may make the cells more excitable, and as $Na_V1.7$ is strongly expressed in nociceptive neurons, this current may play a physiological role in making these neurons readily available for excitation, which would be important for nociception (Cummins *et al.*, 2004; Suter *et al.*, 2015). This inward ramp current is also present in transfected HEK293 cells and so far, has been shown to be unique to $Na_V1.7$ (Cummins *et al.*, 1998; Cummins *et al.*, 2009). The data in this Chapter show that an inward subthreshold ramp current was present in MDA-MB-231-β1-GFP cells, which

was sensitive to blockade by PF, consistent with $Na_v1.7$ being up-regulated in this sub-line. There was no inward ramp current in control MDA-MB-231-GFP cells, consistent with a lack of $Na_v1.7$ expression in these cells, although an outward ramp current was present instead. The identity of the outward current is not known but may be due to K^+ channel activity.

In MDA-MB-231-β1-GFP cells, the subthreshold current may not serve a physiological or pathophysiological purpose given that the resting membrane potential and window of Na^+ current availability is far removed from where the subthreshold current is seen (Roger *et al.*, 2003; Fraser *et al.*, 2005; Yang *et al.*, 2012; Yang & Brackenbury, 2013). Nevertheless, the ramp current protocol used here, combined with perfusion of PF, represents a novel and potentially useful method for isolating and verifying $Na_V1.7$ currents in other cell types and may be particularly relevant in the development of therapeutics for paroxysmal extreme pain disorder (PEPD), in which $Na_v1.7$ plays a critical role (Suter *et al.*, 2015). Anecdotally, it was found that subthreshold current in MDA-MB-231-β1-GFP cells was not detected when the room temperature rose above ~26 ^oC, a similar observation to that reported in (Suter *et al.*, 2015). This may be relevant in individuals who suffer from PEPD, where subthreshold currents in nociceptive neurones are larger in lower temperatures, making them more readily excitable, and could possibly explain why joint pain is common in colder climates (Suter *et al.*, 2015). Thus, it was ensured that experiments measuring subthreshold currents were performed below 26 ˚C.

One notable difference between the results here and those reported previously (Cummins *et al.*, 1998; Cummins *et al.*, 2009) is the magnitude of the ramp currents. Generally speaking, Na^+ currents are noticeably larger in both neurons and transfected HEK293T cells compared to MDA-MB-231 cells (Chioni *et al.*, 2009; Laedermann *et al.*, 2013; Suter *et al.*, 2015; Kruger *et al.*, 2016), which may explain the smaller currents reported here compared with other studies. Nonetheless, the combined results in this Chapter strongly suggest that over-expression of β1 in MDA-MB-231 cells results in up-

regulation of $Na_v1.7$ via a mechanism which not only requires the presence of the extracellular Ig domain but is also dependent on γ-secretase-mediated release of the intracellular domain.

3.4.4. Comparing Na^+ current characteristics across experiments

There was considerable variability in baseline current data across the various experiments, such that the I_P recorded in control MDA-MB-231-GFP cells ranged from 6.7 ± 0.3 pA/pF to 9.8 ± 0.9 pA/pF across different experiments. This observation highlights that it is critical to record from control and test cells in the same session, from cells plated at the same time, using the same solutions and pipettes fabricated at the same time, in order to control for experiment to experiment variability, temperature changes in the lab, inconsistencies in cell culture quality, etc. This approach was strictly followed for all experiments and so the large differences in I_P in test samples relative to controls represent valid and properly controlled data, and the conclusions drawn above can be relied upon.

In addition to studying the effect of β1 overexpression, the Ig deletion mutant, DAPT and PF on I_P , the effects on voltage-dependent gating characteristics and activation kinetics were also evaluated in each of these experiments. Although a number of statistically significant effects on various gating properties were seen within various experiments, overall, these appeared to be largely inconsistent when comparing across experiments. For example, compared to control MDA-MB-231-GFP cells, β1-GFP over-expression significantly hyperpolarised the inactivation $V_{1/2}$ in the experiment in Table 3.1, had no significant effect on the inactivation $V_{1/2}$ in the experiment in Table 3.2, and significantly depolarised the inactivation $V_{1/2}$ in the experiment in Table 3.3. Not only were the gating and kinetics data highly variable across experiments, but the effects of β1 on these properties differed in many cases from those reported previously in this cell line and in other studies (Nuss *et al.*, 1995; An *et al.*, 1998; McCormick *et al.*, 1998; Dhar Malhotra *et al.*, 2001; Chioni *et al.*, 2009).

There has been a lot of controversy regarding the exact effect of β1 expression on Na^+ current gating and kinetics in heterologous cells (Brackenbury & Isom, 2011). Relatively large effects on channel inactivation initially reported using two electrode voltage clamping of *Xenopus* oocytes (Isom *et al.*, 1992) have frequently not been replicated when β1 is co-expressed with α subunits in heterologous cells (Nuss *et al.*, 1995; An *et al.*, 1998; McCormick *et al.*, 1998; Dhar Malhotra *et al.*, 2001; McEwen & Isom, 2004; Chioni *et al.*, 2009; McEwen *et al.*, 2009; Yereddi *et al.*, 2013). The reasons for this lack of consistency are not clear. Cell to cell variability and endogenous expression of other β subunits may play a role, and in many early studies, endogenous expression of β subunits in transfected cells was not adequately monitored or controlled for. Whilst cell-to-cell variability, and the possible expression of other endogenous β subunits may, in part, explain some of the inconsistencies in the literature, such an explanation is not plausible for the data presented here, given that the exact same cell line was used throughout. Although recordings may vary in different sessions due to temperature differences, solution batches, etc., other technical issues may also have impacted on the quality of the gating and kinetics data.

The predicted V_{rev} which was calculated using linear regression, was notably higher in Table 3.1 compared with the data in Tables 2 and 3. Predicted V_{rev} should ideally be around ±5 mV of the reversal potential of Na^+, or 86.23 mV and can be used as a measure of the integrity the cell membrane. Thus, it is possible that in the data recorded in Table 3.1, the accuracy of the parameters calculated may not be reliable. One difference is that although series resistance compensation was routinely used throughout the Thesis, it was not applied in the experiment performed to generate the data in Table 3.1. Given that the series resistance was typically >5 MΩ, inadequate compensation may have compromised the voltage control in this particular experiment, which may explain the variability in the results. Additionally, the lack of effect on the slope factor of the Boltzmann fitted curves suggest that the differences observed in the V_a and V_P may not be robust differences, and instead may be the result of other variability in the experiment. In conclusion, the

reason(s) for the variability in gating and kinetics data across experiments are unclear. Given the possibility of experimental and technical issues contributing to this variability, it was decided not to draw further conclusions from these data apart from the peak current density.

3.4.5. Conclusion

It was previously shown that overexpression of β1 in MDA-MB-231 cells increases both adhesion and Na^+ current (Chioni *et al.*, 2009). In this Chapter, it has been shown that the Ig loop is critical for these effects. Further, the VGSC α subunit responsible for the increased Na^+ current has been shown to be likely $Na_v1.7$. Given that both β1 overexpression and Na^+ current increase metastasis *in vivo* (Nelson *et al.*, 2014; Nelson *et al.*, 2015), it is possible that β1-mediated upregulation of $Na_v1.7$ or indeed any α subunit, ultimately increasing the total Na^+ current, may be responsible (at least in part) for potentiating metastasis. Whether β1 directly plays a role in increasing the metastatic phenotype of cancer cells, or if it does so indirectly, e.g. through increasing the intracellular $[Na^+]$ via regulating α subunit expression, remains to be determined.

4. Assessing the effects of the R89C somatic mutation and L1CAM on β1 function

4.1. Introduction

4.1.1. Mutations disrupting the normal function of β1

β1 functions as a CAM through the presence of the extracellular Ig loop (Isom *et al.*, 1992). It also regulates Na^+ current through the pore-forming α subunit (Isom *et al.*, 1992; Isom, 2002). As a result of these dual functions, β1 plays a key role in regulating neuronal morphology, migration, pathfinding and fasciculation during CNS development (Davis *et al.*, 2004; Brackenbury *et al.*, 2008a; Brackenbury *et al.*, 2010). It also plays a critical role in maintaining normal cardiac excitability (Lopez-Santiago *et al.*, 2007). It is perhaps unsurprising, therefore, that mutations in β1 result in defects in normal cellular function, and several mutations have been associated with diseases, including epilepsy (Meadows *et al.*, 2002; Scheffer *et al.*, 2007; Xu *et al.*, 2007; Patino *et al.*, 2009). The Catalogue of Somatic Mutations in Cancer (COSMIC) database (cancer.sanger.ac.uk; accessed 20/08/17) reports the existence of 69 single nucleotide mutations in β1 in cancers. One of these mutations, R89C, detected in a lung tumour sample, is of particular interest because of its proximity to the previously reported R85C and R85H epilepsy mutations (Thomas *et al.*, 2007; Xu *et al.*, 2007) suggesting the possibility that it may cause a similar loss of function. Previously reported mutations of the Ig loop have a range of physiological effects. The C121W mutation is expressed at the cell membrane *in vivo*, but is not glycosylated properly (Kruger *et al.*, 2016), whereas the R85C and R85H mutations lack membrane expression *in vitro* (Scheffer *et al.*, 2007; Xu *et al.*, 2007). We thus sought to evaluate the effect of the cancer mutation R89C on β1 function.

4.1.2. L1CAM

L1CAM is expressed in various cancers, including ovarian cancer, prostate cancer, neuroblastoma, colorectal cancer and breast cancer (Samatov *et al.*, 2016). In the Oncomine database, L1CAM ranks in the top 2 % of genes that are overexpressed in cancers, and advanced cancers have higher L1CAM expression (Li & Galileo, 2010). L1CAM is a substrate for ADAM10-mediated cleavage and the soluble extracellular region was found in serum from patients with ovarian cancer (Gutwein *et al.*, 2000;

Fogel *et al.*, 2003; Finas *et al.*, 2008). Cells which are further advanced along the EMT have a higher level of expression of L1CAM compared to more epithelial-like cells (Kiefel *et al.*, 2012b). L1CAM disrupts E-cadherin interactions at adherens junctions (Gavert *et al.*, 2005; Weidle *et al.*, 2009). L1CAM expression also increases β-catenin levels in MCF-7 cells, increasing motility (Shtutman *et al.*, 2006). Silencing of L1CAM in MCF-7 cells results in a reversion to an epithelial phenotype (Shtutman *et al.*, 2006). In migrating monolayers of uterine and ovarian carcinomas, L1CAM expression was found at increased levels in the leading cells, consistent with other findings showing elevated L1CAM expression in cells at the invasive perimeter of tumours (Fogel *et al.*, 2003; Gavert *et al.*, 2005). Overexpressing L1CAM in MDA-MB-468 breast cancer cells increases adhesion and migration but interestingly does not affect invasion (Li & Galileo, 2010). On the other hand, silencing of L1CAM expression in MDA-MB-231 cells decreases adhesion and migration (Li & Galileo, 2010).

Importantly, whilst the role of L1CAM in regulating adhesion and motility in neurons and breast cancer cells is well established, and neuronal cultures from L1CAM-deficient mice showed reduced Na^+ current density, reduced single cell spiking and overall reduced membrane expression of VGSC expression (Valente *et al.*, 2016), no work has been done to investigate the impact of L1CAM has on Na^+ current in breast cancer cells. Similarly, although the heterophilic interaction between β1 and a number of other CAMs and ECM proteins has been delineated in neurons and cardiomyocytes, including for N-cadherin, contactin, neurofascin-155, neurofascin-186, NrCAM, β2, tenascin-C and tenascin-R (Srinivasan *et al.*, 1998; Kazarinova-Noyes *et al.*, 2001; Malhotra *et al.*, 2004; McEwen & Isom, 2004; McEwen *et al.*, 2004), a possible heterophilic interaction between β1 and L1CAM has not been previously investigated.

4.2. Hypothesis and Aims

The purposes of the set of experiments in this Chapter were twofold: (1) to determine how the cancer-associated somatic mutation R89C affected β1 function, and (2) to investigate the effect of L1CAM on adhesive properties and Na^+ current in MDA-MB-231 cells. The hypotheses were that R89C would result in a loss of function of β1, and that L1CAM would increase adhesion and Na^+ current.

The specific aims were as follows:

1. To express β1R89C in MDA-MB-231 cells.
2. To over-express L1CAM in MDA-MB-231 cells.
3. To assess the effects of β1R89C and L1CAM on cell-cell adhesion and morphology.
4. To evaluate the effects of β1R89C and L1CAM on electrophysiological properties of the Na^+ current.

4.3. Results

4.3.1. Assessing the effects of the R89C somatic mutation in MDA-MB-231 cells

4.3.1.1. *In silico* analysis of the R89C mutation

The predicted structure of the β1R89C mutant was compared to wild type β1 using the online Protein Homology/AnalogY Recognition Engine (Phyre2; http://www.sbg.bio.ic.ac.uk/phyre2)(Kelley *et al.*, 2015). The resolved crystal structure of the related type 1 topology CAM myelin P0 was used as a template (McCormick *et al.*, 1998; Malhotra *et al.*, 2002). In agreement with previous reports (Isom *et al.*, 1992; Malhotra *et al.*, 2002), the wild type sequence has an intact Ig loop containing several connected β-pleated sheets (Figure 4.1A). The R89C mutation results in a break in the protein where it seems the algorithm was unable to predict the structure, together with a slightly shorter β-pleated sheet following the loop (Figure 4.1B). This result suggests that the mutant Ig loop

may be improperly folded when expressed in the cell, thus β1R89C may not be functional, similar to R85C and R85H (Thomas *et al.*, 2007; Xu *et al.*, 2007).

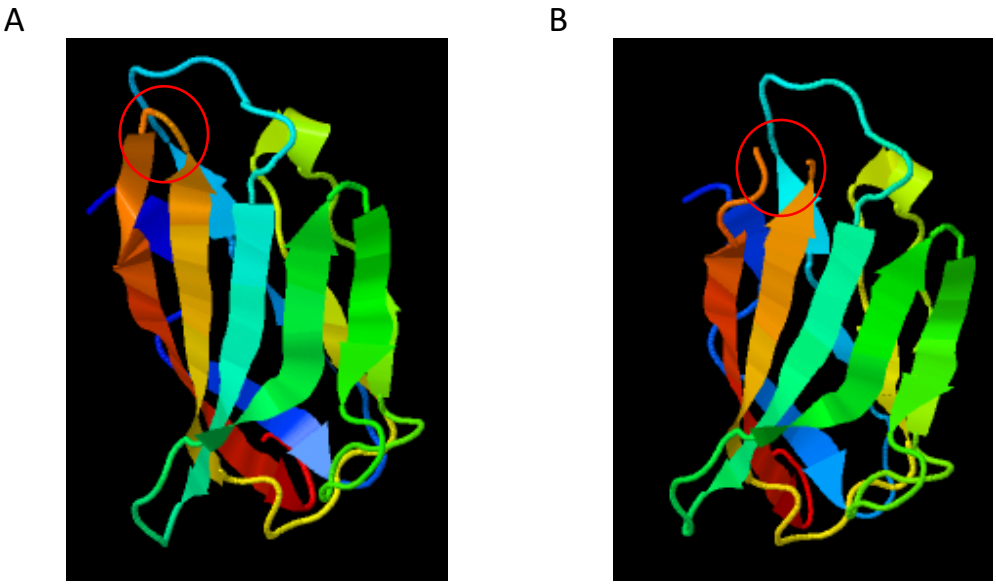

Figure 4.1 Predicted Phyre2 model of β1 and β1-R89C based on myelin P0.

(A) Predicted Phyre2 model of the wild type β1. (B) Predicted Phyre2 Model of β1R89C. The difference between the two models is shown in the red circle in (B): A broken loop and a slightly shorter β-pleated sheet following the break in β1R89C model compared to the WT β1 model. The resolved crystal structure of a type 1 topology CAM, myelin P0, was used as a template for both.

4.3.1.2. Expression of β1R89C-V5 in MDA-MB-231 cells

β1R89C-V5 was generated using site-directed mutagenesis on the wild type human β1-V5 sequence contained in the pcDNA3.1 vector (Section 2.17) (Patino *et al.*, 2011). After ligation, transformation and extraction of DNA from bacteria, samples were sequenced, and the resultant amino acid sequence is shown with the mutated residue highlighted (Figure 4.2). Separate wells of MDA-MB-231 cells were transfected with wildtype β1-V5 and mutant β1R89C-V5, and stable clones were selected (Section 2.6). Expression of protein was evaluated by Western blot using an anti-V5 antibody (Figure 4.3). Interestingly, the mutant construct ran at a lower MW compared to the wild type β1. Clone 2 was used for all subsequent experiments as this had the highest level of expression.

MGTLLALVVGAVLVSSAWGGCVEVDSETEAVYGMTFKILCISCKRRSETTAETFTEWTFR

QKGTEEFVKILRYENEVLQLEEDERFEGCVVWNGSRGTKDLQDLSIFITNVTYNHSGDYE

CHVYRLLFFDNYEHNTSVVKKIHLEVVDKANRDMASIVSEIMMYVLIVVLTIWLVAEMVY

CYKKIAAATEAAAQENASEYLAITSESKENCTGVQVAEGRWLKGNSADIQHSGGRSSLEG

PRFEGKPIPNPLLGLDST

Figure 4.2 Amino acid sequence of β1-R89C.

Pink highlight shows the signal peptide sequence, green highlight shows the Ig loop and the light grey highlighted cysteine shows the mutated residue. Dark grey highlight shows the transmembrane domain. Yellow highlight shows the V5-tag.

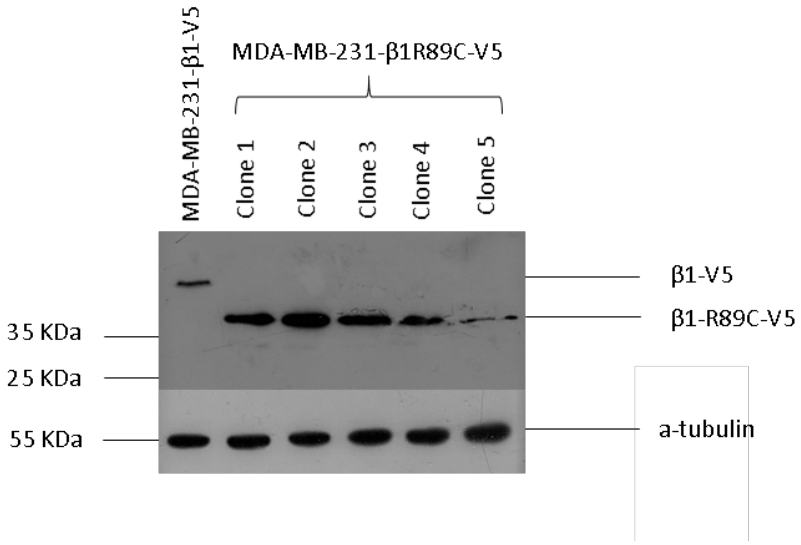

Figure 4.3 Western blot of β1R89C-V5 expression in MDA-MB-231 cells.

(A) β1R89C-V5 expression in 5 clones of MDA-MB-231 cells stably transfected with a β1-R89C-V5 containing vector. Equivalent amounts (50 μg) of whole cell lysate of each sample were loaded. Membrane was probed with an anti-V5 antibody. An MDA-MB-231 cell line stably overexpressing wild type β1-V5 was used as a positive control. (B) Membrane from (A) stripped and reprobed with α-tubulin as a loading control.

To examine whether the reduction in molecular weight of β1R89C compared to wild type β1 was the result of improper glycosylation, whole cell protein extracts were treated with PNGase F to remove N-linked glycosylation (Kruger *et al.*, 2016). A Western blot of control and PNGase F-treated samples showed an equal reduction in the MW of both the wild type β1-V5 and β1R89C-V5 samples (Figure 4.4A). α-tubulin was used as a loading control (Figure 4.4B). The difference between the MW of the deglycosylated β1R89C-V5 and β1-V5 was equal to the difference between the two samples when they were glycosylated (Figure 4.4C). In conclusion, the difference in MW between wildtype β1 and β1R89C is likely not the result of improper N-glycosylation, in contrast to the C121W mutant (Kruger *et al.*, 2016).

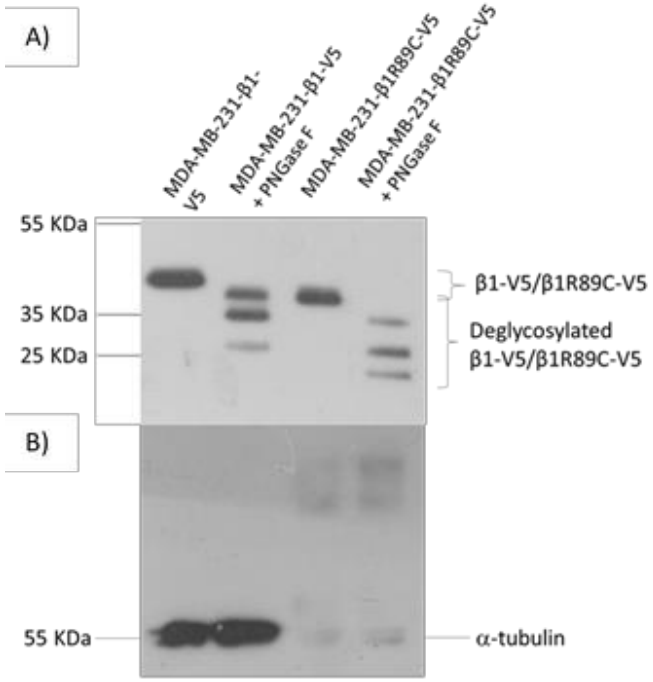

Figure 4.4 Western blot exploring glycosylation of β1R89C-V5.

(A) Whole cell lysate (20 µg) from either MDA-MB-231-β1-V5 or MDA-MB-231-β1R89C-V5 cells treated with or without PNGaseF to remove N glycosylation. The multiple bands observed may be the result of incomplete removal of glycosylation (B) Membrane from (A) stripped and reprobed with α-tubulin as a loading control. α-tubulin bands were not observed in the latter two lanes and it is unclear why.

4.3.1.3. Effect of R89C on Na^+ current

Next, the effect of the R89C mutation on Na^+ current was assessed using whole-cell patch clamp recording. Previously, wild type β1 has been shown to increase Na^+ current in MDA-MB-231 cells (Chioni *et al.*, 2009) and Chapter 3. In agreement with these data, the I_P was significantly larger in MDA-MB-231-β1-V5 cells (-26.4 ± 6.21 pA/pF; n = 6) compared to control MDA-MB-231 cells expressing empty pcDNA3.1 (-10.08 ± 3.67 pA/pF; n = 4; P < 0.001; Figure 4.5A-C). Interestingly, the Na^+ current density in MDA-MB-231-β1R89C-V5 cells was -6.87 ± 2.78 pA/pF; n = 3, which was not significantly different to control MDA-MB-231 cells expressing empty pcDNA3.1 (Figure 4.5A-C). Thus, the R89C mutation prevents the ability of β1 to increase Na^+ current.

Analysis of the voltage-dependence of activation and steady-state inactivation from each cell line revealed several key differences (Figure 4.5D, E and Table 4.1). The voltage at current peak was significantly hyperpolarised in MDA-MB-231-β1-V5 cells compared to MDA-MB-231-pcDNA3.1 (P < 0.05). In addition, the inactivation slope factor for MDA-MB-231-β1-V5 and MDA-MB-231-β1R89C-V5 cells was significantly different compared to MDA-MB-231-pcDNA3.1 (P < 0.01 in both cases). However, the activation voltage, $V_{1/2}$ and slope factor, the inactivation $V_{1/2}$ and the time to peak were not significantly different across all three cell lines. Furthermore, the measured V_{rev} for these cell lines suggest that the integrity of the membranes in this experiment may not be adequate. As discussed in Section 3.4.4, given the general variability in voltage dependence and kinetic data between experiments, it was again decided not to draw further conclusions from these data. In conclusion, the differences in peak current density are consistent with the notion that the R89C mutant is a functional null.

4.3.1.4. Effect of R89C on β1-mediated adhesion

As β1 increases adhesion in MDA-MB-231 cells (Chioni *et al.*, 2009) and this requires the Ig loop (Chapter 3), the effect of the R89C mutant was next tested in a cell-cell adhesion assay. The

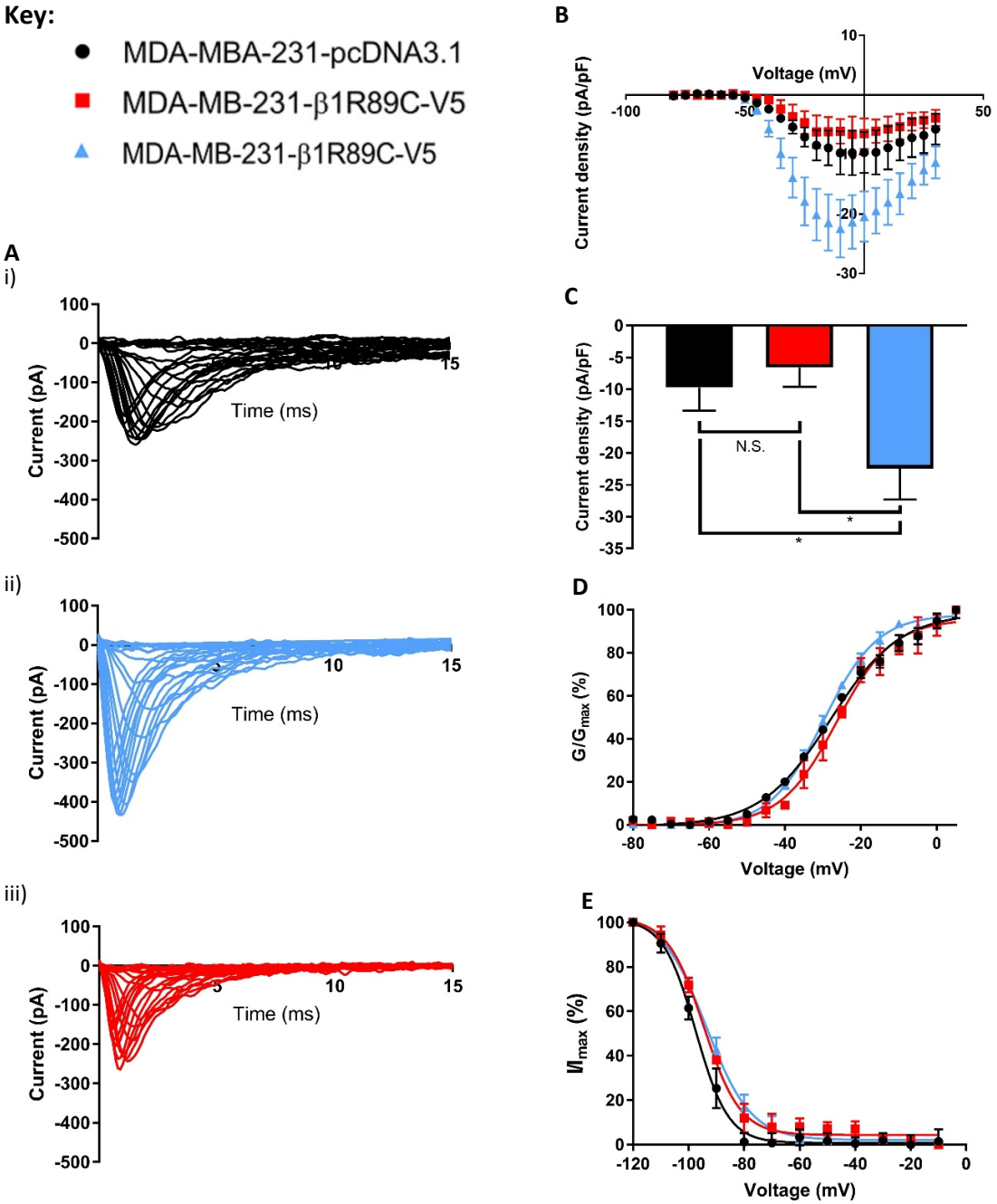

Figure 4.5 Effect of the R89C mutation on Na^+ current in MDA-MB-231 cells.

(A) Typical whole-cell Na^+ currents elicited by 50 ms depolarizing pulses between -80 mV and 30 mV applied from a holding potential of -120mV: (i) control MDA-MB-231-pcDNA3.1 cell; (ii) MDA-MB-231-β1-V5 cell; (iii) MDA-MB-231-β1R89C-V5 cell. (B) Current-voltage relationship for control MDA-MB-231-pcDNA3.1 (n=4), MDA-MB-231-β1R89C-V5 (n=3) and MDA-MB-231-β1-V5 (n=6) cells. (C) Whole-cell peak Na^+ current density for the three cell lines. (D) Steady-state activation. Normalised conductance (G/G_{max}), calculated from the current data, is plotted as a function of voltage. (E) Steady-state inactivation. Normalised current (I/I_{max}), elicited by 50 ms test pulses at −10 mV following 250 ms conditioning voltage pulses between −120 mV and −10 mV, applied from a holding potential of −120 mV, plotted as a function of the pre-pulse voltage. Activation and inactivation data are fitted to Boltzmann functions. Data are presented as mean and SEM. One-way ANOVA with a post-hoc Tukey's test was used to test for significance. *P < 0.05.

Table 4.1 Effect of R89C on VGSC current properties.

Parameter[a]	MDA-MB-231-pcDNA3.1	MDA-MB-231-β1R89C-V5	MDA-MB-231-β1-V5
I_p (pA/pF)	-10.08 ± 3.67	-6.87 ± 2.78 ^{P*}	-26.4 ± 6.21 ^{N*}
V_a (mV)	-45 ± 2.36	-41.67 ± 5.40	-49.2 ± 1.68
V_p (mV)	-2.5 ± 3.73	-5.00 ± 3.54	-10.8 ± 0.91 ^{N*}
Activation $V_{1/2}$ (mV)	-4.97 ± 0.51	-5.79 ± 0.53	-6.0 ± 0.13
Activation k (mV)	9.12 ± 1.32	2.78 ± 0.85	7.36 ± 0.22
Inactivation $V_{1/2}$ (mV)	-97.63 ± 2.15	-93.97 ± 0.72	-97.1 ± 4.73
Inactivation k (mV)	-3.37 ± 3.42	-6.11 ± 0.81 ^{N**}	-7.36 ± 3.67 ^{N**}
T_p (ms)	1.05 ± 0.23	1.23 ± 0.27	1.1 ± 0.037
V_{rev} (mV)	69.99 ± 10.44	80.44 ± 7.21	66.25 ± 2.03

[a] ***Abbreviations:*** I_p, peak current density; V_a, activation voltage; V_p, voltage at current peak; $V_{1/2}$, half (in)activation voltage; *k*, slope factor; T_p, time to peak. Data are expressed as mean ± SEM. Significance: ^{N} - significantly different from the negative control (MDA-MB-231-pcDNA3.1), ^{P} - significantly different from the positive control (MDA-MB-231-β1-V5). **P*<0.05 (significance difference). One-way ANOVA with post-hoc Tukey's tests were used to test for significance.

normalised particle count for MDA-MB-231-β1R89C-V5 cells after 30 minutes (79.4 ± 4.2 %, n = 6; 10 fields of view per n) was significantly higher compared to MDA-MB-231-β1-V5 cells (59.4 ± 4.2 %; n = 3; P < 0.05) and this significant difference persisted at later time points (Figure 4.6). In addition, the normalised particle count for MDA-MB-231-β1R89C-V5 cells was not significantly different from negative control MDA-MB-231-pcDNA3.1 cells after 30 minutes (79.8 ± 3.9 %, n = 3) or at any later time point (Figure 4.6B). Thus, the R89C mutation abrogates β1-mediated cell-cell adhesion such that cells expressing β1R89C-V5 are functionally no different to parental cells not over-expressing β1. These data reflect the observation that deletion of the Ig domain disrupts adhesion function (Chapter 3).

4.3.1.5. Effect of R89C on cell morphology

β1 overexpression increases process outgrowth of MDA-MB-231 cells in monoculture such that they become more elongate (less rounded) (Chioni *et al.*, 2009). Thus, next, the effect of R89C on morphology was investigated. As expected, MDA-MB-231-β1-V5 cells appeared more elongate than

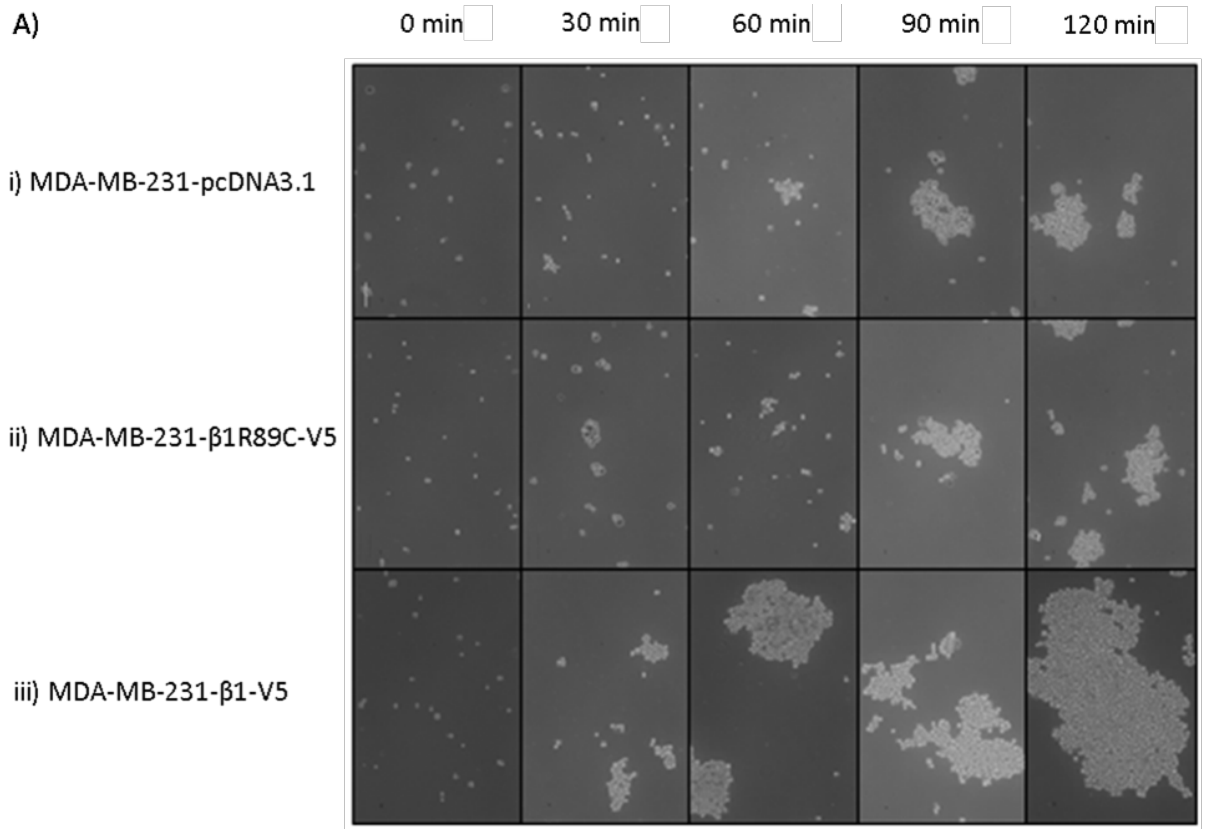

Figure 4.6 Effect of the R89C mutation on β1-mediated adhesion.

(A) Representative images of cells in adhesion assays, taken at 30-minute intervals. i) Negative control MDA-MB-231-pcDNA3.1, ii) experimental MDA-MB-231-β1R89C-V5, iii) positive control MDA-MB-231-β1-V5. Scale bars = 100 µm. B) (Normalized particle counts from control MDA-MB-231-pcDNA3.1, MDA-MB-231-β1R89C-V5 cells and MDA-MB-231-β1-V5 cells. n≥3, 10 fields of view per n. Data are presented as mean and SEM. One-way ANOVA was used to test for significance.

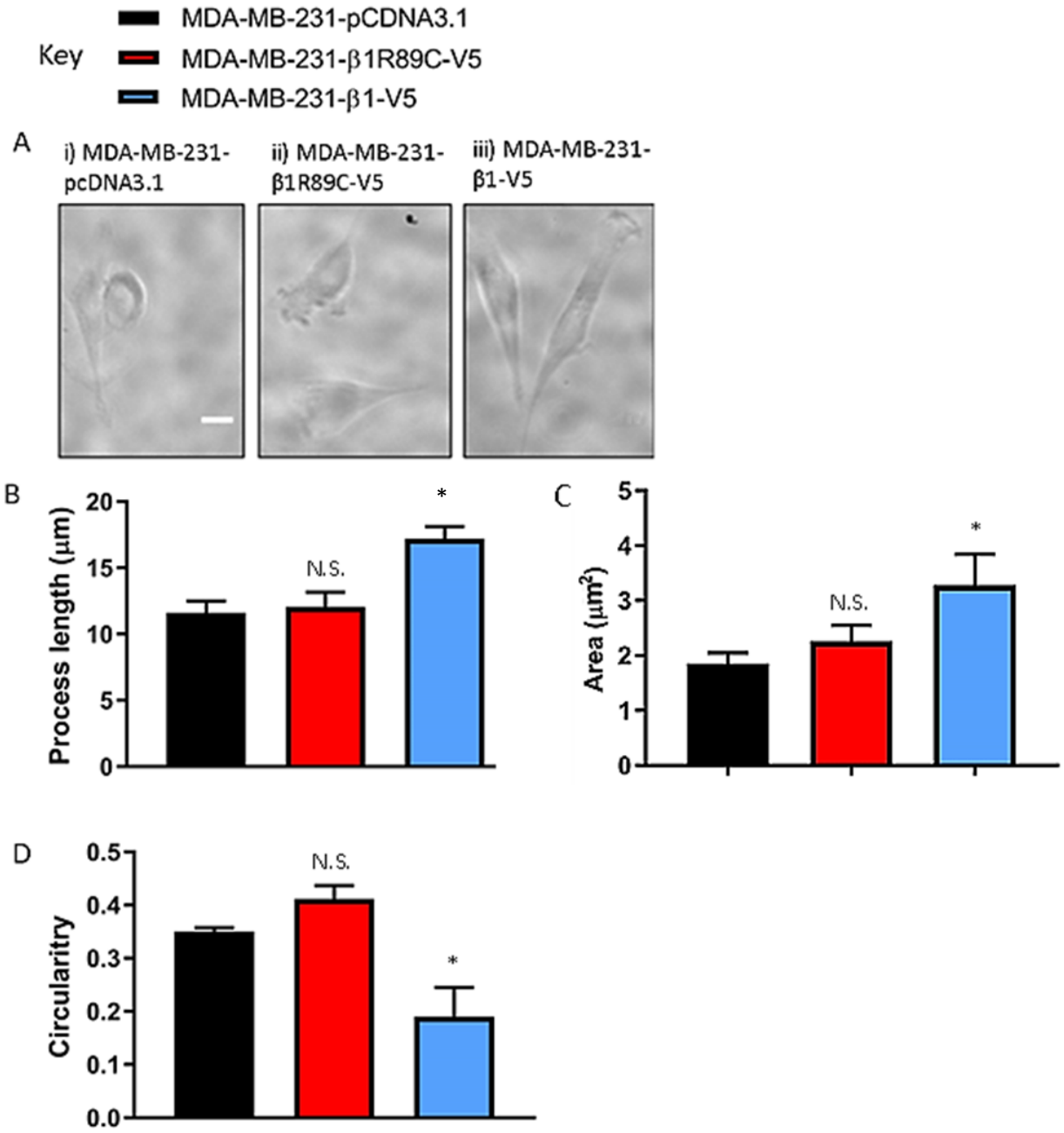

Figure 4.7 Effect of R89C on cell morphology.

(A) Representative bright field images of (i) MDA-MB-231-pcDNA3.1 cells, (ii) MDA-MB-231-β1-R89C-V5 cells and (iii) MDA-MB-231-β1-V5 cells. (B) Process length of MDA-MB-231-pcDNA3.1, MDA-MB-231-β1-V5 and MDA-MB-231-β1-R89C-V5 cells (n = 50). (C) Cell area of MDA-MB-231-pcDNA3.1, MDA-MB-231-β1-V5 and MDA-MB-231-β1-R89C-V5 cells (n = 50). (D) Circularity of MDA-MB-231-pcDNA3.1, MDA-MB-231-β1-V5 and MDA-MB-231-β1-R89C-V5 cells (n = 50). Scale bar = 10 μm. One-way ANOVA was with a post-hoc Tukey's test used to test for significance. *P < 0.05. N.S., not significant.

the negative control MDA-MB-231-pcDNA3.1 cells (Nelson *et al.*, 2014). In contrast, MDA-MB-231-β1R89C-V5 cells appeared similar in morphology to the negative control cells (Figure 4.7A). This observation was borne out in the quantification: β1-V5 significantly increased process length compared to control cells ($P < 0.05$; $n = 50$), whereas β1R89C had no effect (Figure 4.7B). Similarly, β1-V5 significantly increased cell area compared to control cells ($P < 0.05$; $n = 50$), whereas β1R89C-V5 had no effect (Figure 4.7C). In addition, β1-V5 significantly reduced circularity compared to control and β1R89C-V5-expressing cells ($P < 0.05$; $n = 50$; Figure 4.7D). When MDA-MB-231 cells are co-cultured on top of a monolayer of CHL fibroblasts, β1 has been shown to increase outgrowth of neurite-like processes as a result of *trans*-homophilic adhesion (Nelson *et al.*, 2014). MDA-MB-231-β1-V5 and MDA-MB-231-β1R89C-V5 cells were therefore grown on top of monolayers of CHL cells for 24 h, fixed, stained with an anti-CD44 antibody which specifically labels the cancer cells and not the CHL cells (Nelson *et al.*, 2014), and visualised using fluorescence microscopy (Figure 4.8A). The mean process length of MDA-MB-231-β1-V5 cells grown on a monolayer of CHL cells was 52.8 ± 5.9 μm ($n = 50$), which was significantly larger than MDA-MB-231-β1R89C-V5 cells, which had a mean process length of 29.4 ± 3.1 μm ($n = 50$; $P < 0.001$, Figure 4.8B). In conclusion, these data suggest that the R89C mutation disrupts the ability of β1 to regulate morphology in MDA-MB-231 cells, both in monoculture, and when co-cultured with fibroblasts.

4.3.1.6. Effect of R89C on subcellular localisation of β1

The R85C and R85H epilepsy mutations result in a loss of membrane expression (Xu *et al.*, 2007). Therefore, the effect of the R89C mutation on distribution of β1 in MDA-MB-231 cells was investigated using confocal microscopy (Figure 4.9). In agreement with previous reports (Yang *et al.*, 2012; Nelson *et al.*, 2014), β1-V5 was highly expressed at the cell membrane, colocalising with the plasma membrane marker, wheatgerm agglutinin (Figure 4.9B). However, presence of β1R89C-V5 at the membrane was weaker, and there was no colocalization with wheatgerm agglutinin at the plasma membrane (Figure 4.9C). These results suggest that although the R89C mutant is expressed

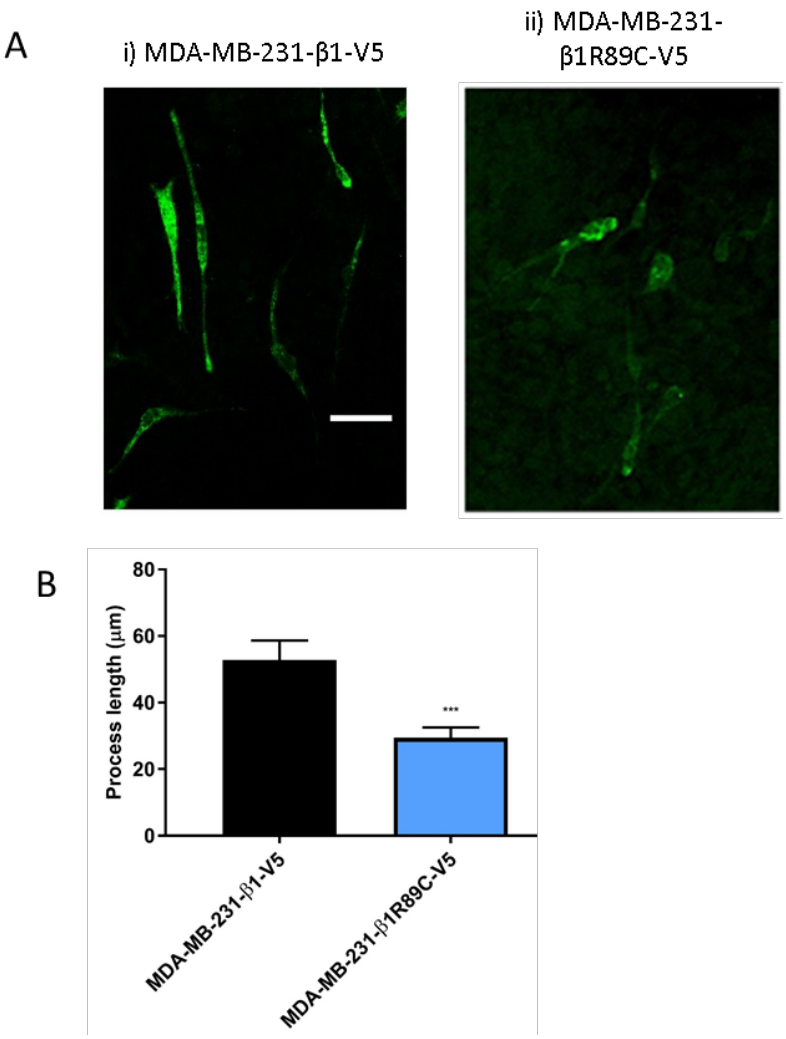

Figure 4.8 Effect of the R89C mutation on process outgrowth of MDA-MB-231 cells grown on a monolayer of fibroblasts.

(A) Fluorescent images of (i) MDA-MB-231-β1-V5 and (ii) MDA-MB-231-β1R89C-V5 cells grown on a monolayer of Chinese hamster lung (CHL) cells. Cells were labelled with an anti-CD44 antibody. Scale bar = 50 μm. (B) Process length of MDA-MB-231-β1-V5 or MDA-MB-231-β1R89C-V5 cells (n = 50, ***P < 0.001). A two-sample t-test was used to test for significance.

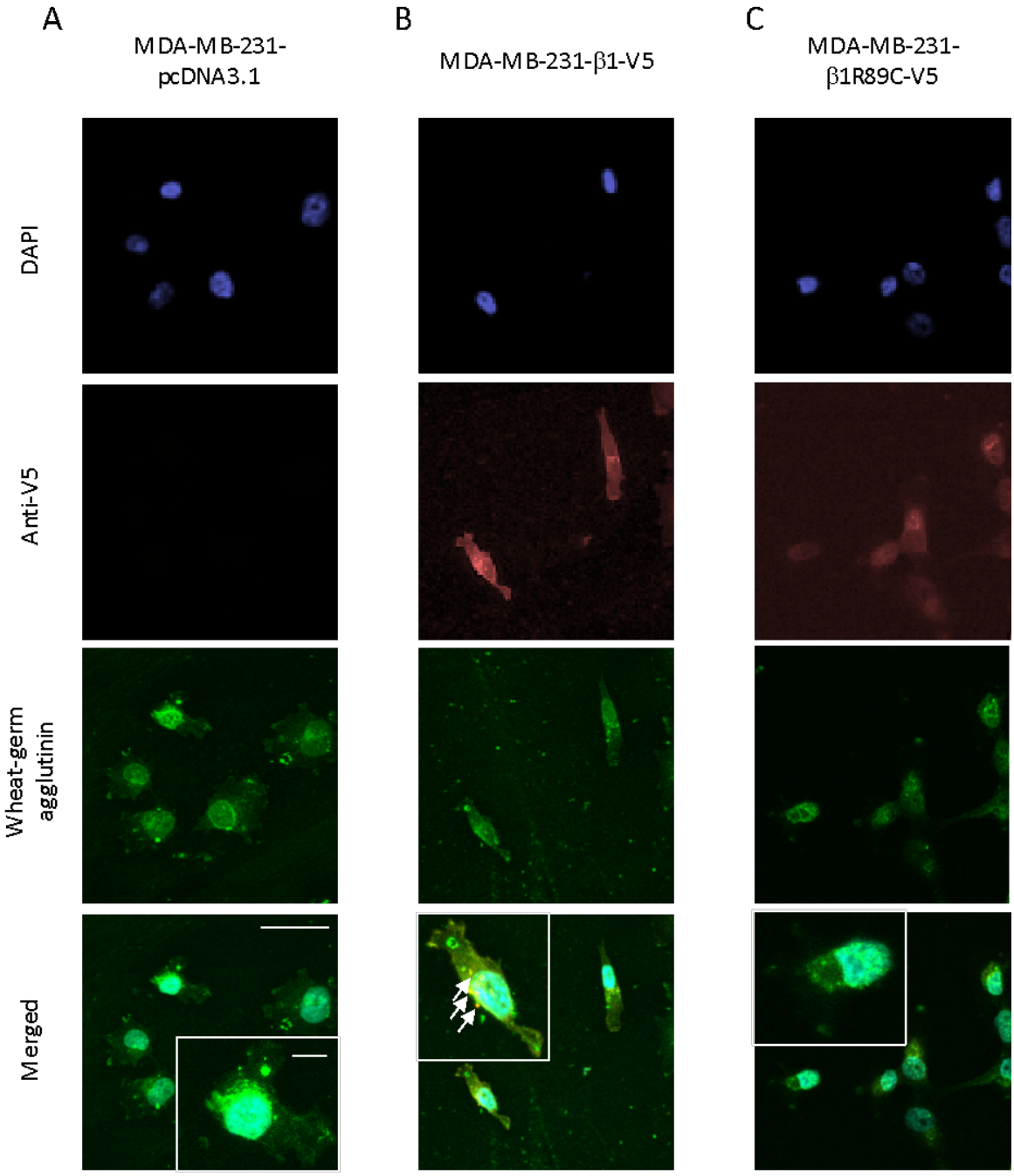

Figure 4.9 Expression of β1-V5 and β1R89C-V5 at the plasma membrane.

Confocal maximum intensity projections of z-stacked images of (A) MDA-MB-231-pcDNA3.1 cells, (B) MDA-MB-231-β1-V5 cells, and (C) MDA-MB-231-β1R89C-V5 cells. Cells were stained with DAPI (blue), anti-V5 with a secondary Alexa-fluor 568 (red) and wheat germ agglutinin conjugated to Alexa-fluor 488 (green). Arrows highlight yellow areas where β1-V5 expression colocalised with the plasma membrane marker wheat germ agglutinin. Scale bar = 20 μm on main image and 5 μm on inset. Images were taken at 63x magnification with a resolution of 1024 x 1024 pixels.

at the protein level, it does not correctly localise to the plasma membrane. In conclusion, the data presented here suggest that the R89C mutation renders the β1 subunit a functional null: the mutation inhibits both the channel current-modulating and cell adhesive properties of β1.

4.3.2. Assessing the effects of L1CAM upregulation in MDA-MB-231 cells

In this second part of Chapter 4, the effect of L1CAM on adhesion and Na^+ current was evaluated in order to test the possibility that, like β1, L1CAM could fulfil both channel and adhesion-modulating functions.

4.3.2.1. L1CAM expression in MDA-MB-231 cells

MDA-MB-231 cells were transfected with L1CAM in the pcDNA3.1 vector, and a stable clone was selected for further analysis. Expression of L1CAM protein was evaluated by Western blot (Figure 4.10A, B). Rat brain was used as a positive control. The Western blot revealed that L1CAM was expressed endogenously at a low level in MDA-MB-231 cells. The line stably transfected with L1CAM had an increased level of total L1CAM expression, and interestingly, L1CAM expression was also elevated in MDA-MB-231-β1-GFP cells. The higher weight band observed in both the β1-GFP and L1CAM overexpressing cells was likely the NOVA-2 variant of L1CAM. Next, a Western blot was carried out using a β1 antibody on whole cell lysate from MDA-MB-231-GFP, MDA-MB-231-β1-GFP and MDA-MB-231-L1CAM cells. β1 expression was higher in MDA-MB-231-L1CAM cells compared to MDA-MB-231-GFP, MDA-MB-231-β1-GFP cells (Figure 4.11A, B). Thus, expression of β1 and L1CAM may be co-operatively regulated, such that L1CAM increases β1 expression, and *vice versa*.

4.3.2.2. Effect of L1CAM on adhesion

L1CAM has been shown in MDA-MB-468 cells to increase adhesion to wells coated with fibronectin, laminin and Matrigel (Li & Galileo, 2010). However, its effect on breast cancer cell-cell adhesion is unknown. Thus, the effect of L1CAM on MDA-MB-231 cell-cell adhesion was investigated (Figure

4.12). The normalised particle count for MDA-MB-231-L1CAM cells was 49.5 ± 7.9 % after 30 min, compared to 82.4 ± 4.1 % for control MDA-MB-231 pcDNA3.1 empty vector cells ($P < 0.05$; n = 3; 10 fields of view per n; Figure 4.12B). This significant difference in adhesion was maintained at the 60 and 90 min time points, but was diminished at 120 min. In summary, L1CAM increases MDA-MB-231 cell-cell adhesion.

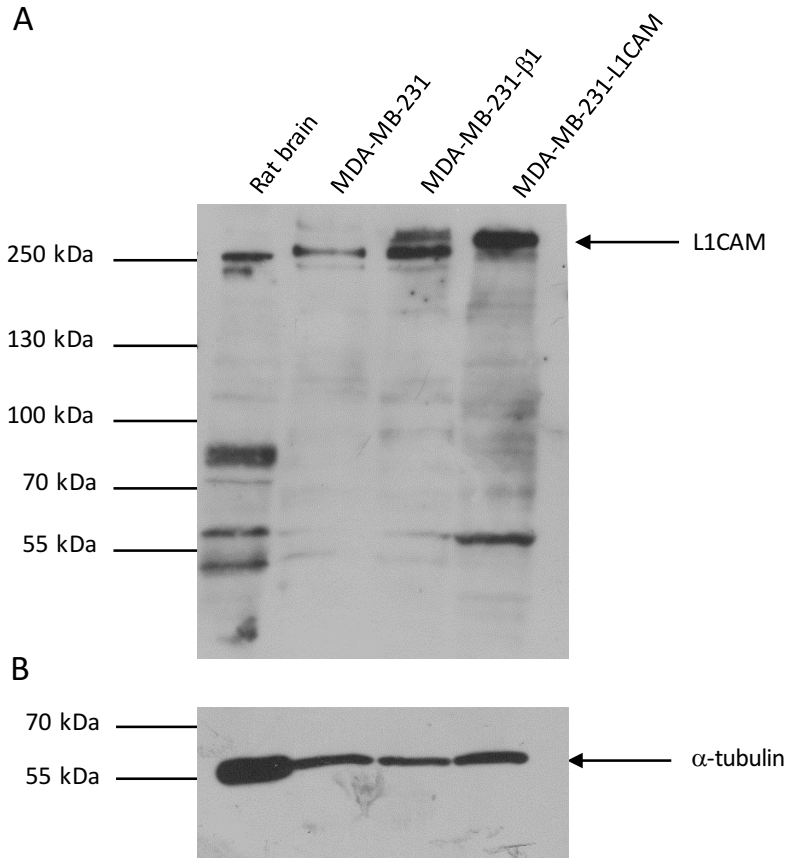

Figure 4.10 Western blot of L1CAM expression in MDA-MB-231 cells.

(A) Comparison of L1CAM expression in MDA-MB-231 cells, MDA-MB-231-β1-GFP cells, and MDA-MB-231 cells transiently transfected with a L1CAM containing vector. Equivalent amounts (50 µg) of whole cell lysate of each sample were loaded. Membrane was probed with an L1CAM antibody which recognises both human and rat L1CAM. Rat brain lysate was used as a positive control. Bands present at 60 and 80 kDa are degradation products recognised by the L1CAM antibody (Li and Galileo, 2010). (B) Membrane from (A) stripped and reprobed with α-tubulin as a loading control.

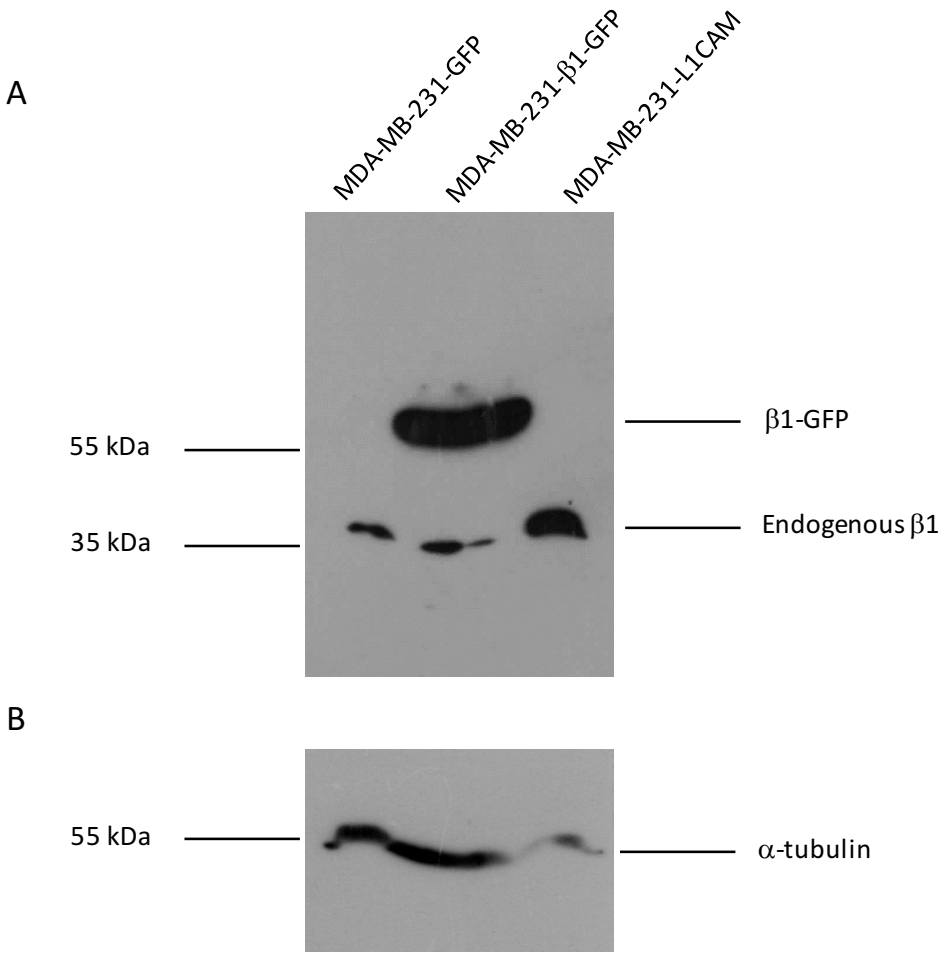

Figure 4.11 Western blot of β1 expression in MDA-MB-231-L1CAM cells.

(A) Comparison of β1 expression in MDA-MB-231-GFP cells, MDA-MB-231-β1-GFP cells, and MDA-MB-231 cells stably transfected with a L1CAM containing vector. Equivalent amounts (50 µg) of whole cell lysate of each sample were loaded. Membrane was probed with an anti-β1 antibody. MDA-MB-231-GFP cell was used as a negative control and MDA-MB-231-β1-GFP used as a positive control. (B) Membrane from (A) stripped and reprobed with α-tubulin as a loading control.

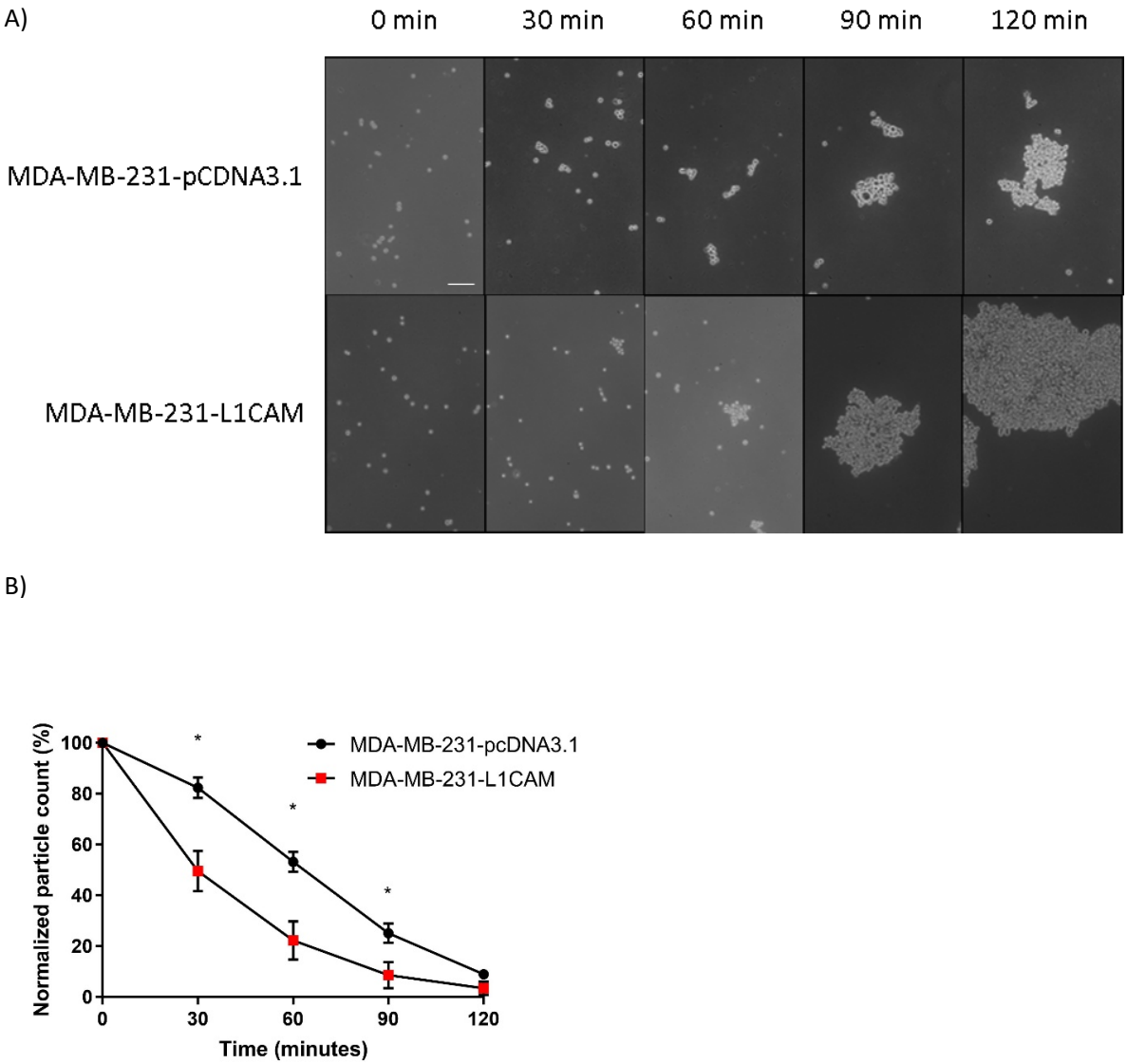

Figure 4.12 Effect of L1CAM on cell-cell adhesion of MDA-MB-231 cells.

(A) Representative images of cells in adhesion assays, taken at 30-minute intervals. i) Negative control MDA-MB-231-pcDNA3.1 and ii) experimental MDA-MB-231-L1CAM cells. Scale bar = 100 µm. (B) Normalized particle counts from control MDA-MB-231-pcDNA3.1 and MDA-MB-231-L1CAM cells. Particles were counted on an Axiovert 135 microscope at 10X zoom. Data are presented as mean and SEM. One-way ANOVA was used to test for significance. *P<0.05 (n = 3).

4.3.2.3. Effect of L1CAM on cell morphology

Given that L1CAM, like β1, results in an increase in adhesion and migration (Li & Galileo, 2010), and that β1 overexpression results in process outgrowth in MDA-MB-231 cells (Chioni *et al.*, 2009;

Nelson *et al.*, 2014), it was possible that L1CAM may also alter cell morphology. This was next tested in a morphology assay. MDA-MB-231-L1CAM cells appeared more elongate than control MDA-MB-231 cells expressing empty vector (Figure 4.13A). The mean process length on MDA-MB-231-L1CAM cells was 16.6 ± 0.9 μm, which was significantly larger than for MDA-MB-231 cells expressing empty vector (11.4 ± 0.7 μm; $P < 0.001$; n = 50; Figure 4.13B). The area of MDA-MB-231-L1CAM cells was also significantly larger compared to MDA-MB-231-pcDNA3.1 cells (3.5 ± 0.4 μm vs. 2.1 ± 0.5 μm respectively; $P < 0.05$; n = 50; Figure 4.13C). In addition, the circularity of MDA-MB-231-L1CAM cells was significantly reduced compared to MDA-MB-231-pcDNA3.1 cells (0.6 ± 0.1 μm vs. 0.2 ± 0.1 μm respectively, $P < 0.05$; n = 50; Figure 4.13D). In conclusion, L1CAM, like β1, promotes an elongate, mesencyhmal phenotype in MDA-MB-231 cells.

4.3.2.4. Effect of L1CAM on Na^+ current

It has been previously shown that L1CAM-deficient neurons have reduced Na^+ current density and that these neurons also have reduced VGSC expression at the protein level (Valente *et al.*, 2016). However, no work has been done to investigate the effect of L1CAM on Na^+ current in cancer cells. Therefore, next, whole cell patch clamp recording was used to measure the Na^+ currents from MDA-MB-231-pcDNA3.1 cells and MDA-MB-231-L1CAM cells. The mean I_P of MDA-MB-231-L1CAM cells was -11.4 ± 0.8 pA/pF which did not differ significantly from the I_P of control cells (-9.4 ± 0.1 pA/pF; n = 3; Figure 4.14A, B, C). In addition, there was no difference in the I-V relationship between control and L1CAM-expressing cells, and none of the Na^+ current kinetics differed significantly between the two cell lines suggesting that channel gating was unaffected (Figure 4.14B, C, D, E and Table 4.2). Na^+ current in MDA-MB-231 cells is carried by $Na_V1.5$, which is a TTX-resistant channel. To determine whether the Na^+ current in MDA-MB-231-L1CAM cells was also TTX-resistant, the effect of 1 μM TTX, which is sufficient to inhibit all the TTX-sensitive VGSCs without having any effect on $Na_V1.5$, was investigated. The I_P in control empty vector-expressing MDA-MB-231 cells was unaffected by perfusion with 1 μM TTX (-8.5 ± 0.7 pA/pF in PSS and -7.0 ± 1.8 pA/pF in 1 μM TTX; $P > 0.05$; n = 6;

Figure 4.15A). Similarly, the I_P in MDA-MB-231-L1CAM cells was unaffected by 1 μM TTX (-8.8 ± 0.5 pA/pF in PSS vs. -9.2 ± 1.2 pA/pF in 1 μM TTX; P > 0.05; n = 6; Figure 4.15B). Thus, L1CAM overexpression in MDA-MB-231 cells does not affect Na^+ current properties or TTX sensitivity, in contrast to the effects of β1 demonstrated in Chapter 3. In conclusion, L1CAM promotes β1 expression, adhesion, and morphological changes, but does not affect Na^+ current in MDA-MB-231 cells.

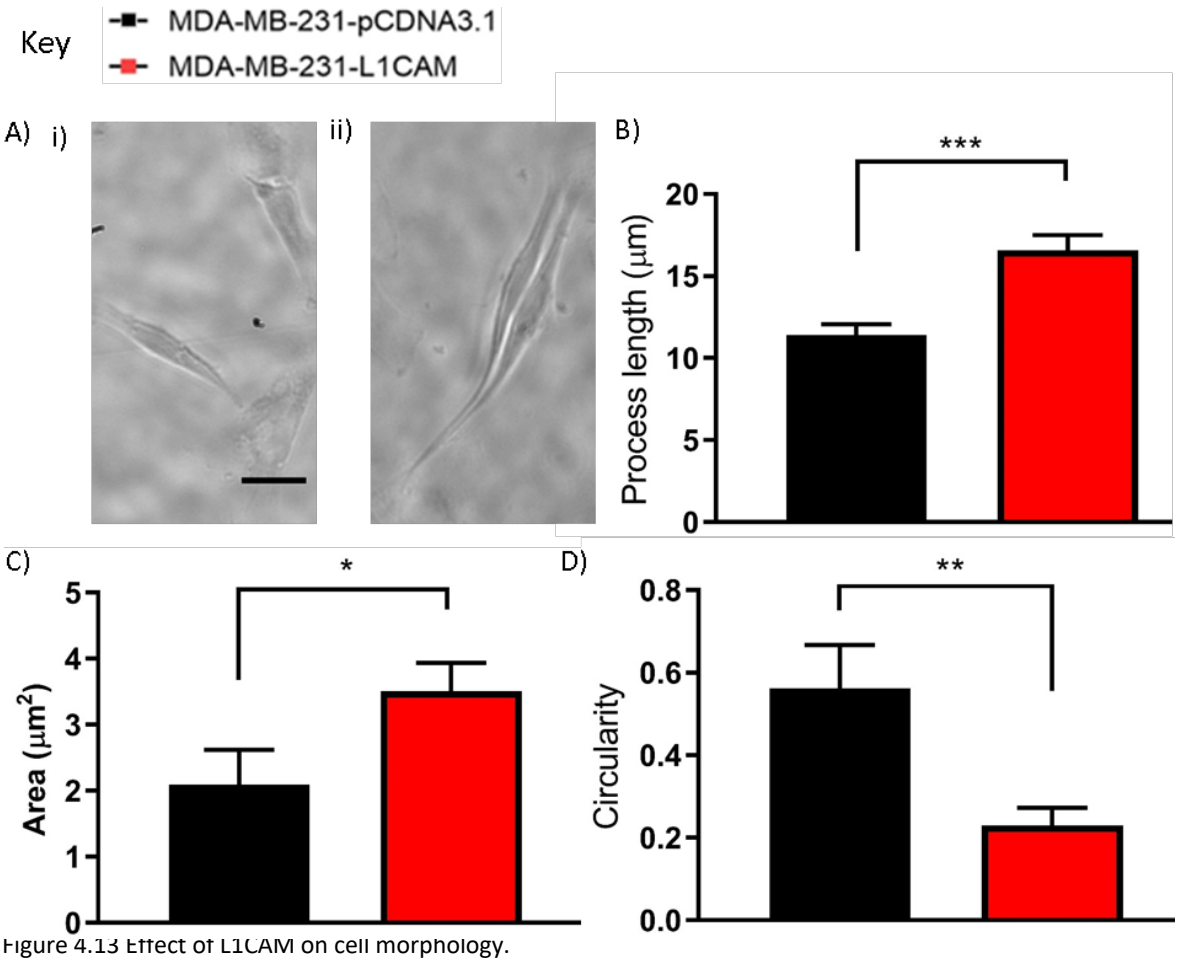

Figure 4.13 Effect of L1CAM on cell morphology.

(A) Representative bright field images of (i) MDA-MB-231-pcDNA3.1 cells and (ii) MDA-MB-231-L1CAM cells. (B) Process length of MDA-MB-231-pcDNA3.1 and MDA-MB-231-β1-L1CAM cells (n = 50). (C) Cell area of MDA-MB-231-pcDNA3.1 and MDA-MB-231-β1-L1CAM cells (n = 50). (D) Circularity of MDA-MB-231-pcDNA3.1 and MDA-MB-231-β1-L1CAM cells (n = 50). Scale bar = 10 μm. A two-sample t test was used to test for significance. *P < 0.05. **P < 0.01. ** P < 0.001.

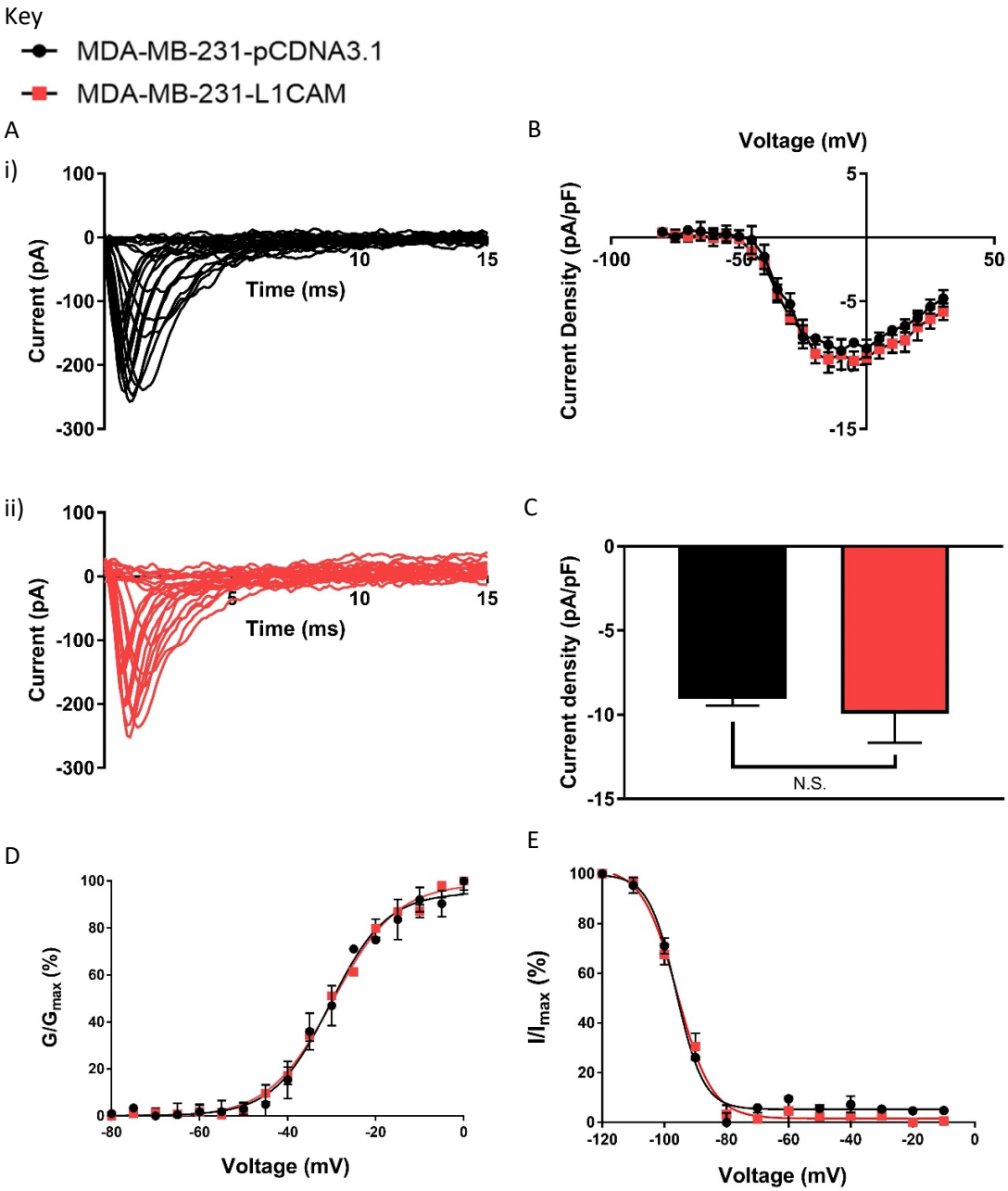

Figure 4.14 Effect of L1CAM on the Na^+ current in MDA-MB-231 cells.

(A) Typical whole-cell Na^+ currents elicited by 50 ms depolarizing pulses between -80 mV and 30 mV applied from a holding potential of -120 mV: (i) control MDA-MB-231-pcDNA3.1 cell (ii) MDA-MB-231-L1CAM cell. (B) Current-voltage relationship for control MDA-MB-231-pcDNA3.1 (n = 3) and MDA-MB-231-L1CAM (n = 3). (C) Whole-cell peak I_P for the two cell lines. (D) Activation. Normalised conductance (G/G_{max}), calculated from the current data, plotted as a function of voltage. (E) Steady-state inactivation. Normalised current (I/I_{max}), elicited by 50 ms test pulses at −10mV following 250 ms conditioning voltage pulses between −120 mV and −10 mV, applied from a holding potential of −120mV, plotted as a function of the pre-pulse voltage. Data are presented as mean and SEM. One-way ANOVA with a post-hoc Tukey's test was used to test for significance. NS, not significant.

Table 4.2 Effect of L1CAM on VGSC current properties.

Parameter[a]	MDA-MB-231-pcDNA3.1	MDA-MB-231-L1CAM
I_p (pA/pF)	-9.37 ± 0.1	-11.4 ± 0.76
V_a (mV)	-41.67 ± 2.04	-46.67 ± 2.89
V_p (mV)	-8.33 ± 5.40	-6.67 ± 3.40
Activation $V_{1/2}$ (mV)	-6.46 ± 0.61	-5.98 ± 0.45
Activation k (mV)	6.73 ± 0.83	7.61 ± 0.93
Inactivation $V_{1/2}$ (mV)	-98.49 ± 2.94	-95.60 ± 1.65
Inactivation k (mV)	-4.43 ± 0.24	-5.31 ± 0.53
T_p (ms)	1.03 ± 0.04	1.27 ± 0.22
V_{rev} (mV)	89.50 ± 14.71	73.3 ± 1.90

[a] ***Abbreviations:*** I_p, peak current density; V_a, activation voltage; V_p, voltage at current peak; $V_{1/2}$, half (in)activation voltage; *k*, slope factor; T_p, time to peak. Data are expressed as mean ± SEM. There were no significant differences from the negative control (MDA-MB-231-pcDNA3.1). Student's t tests were used to test for significance.

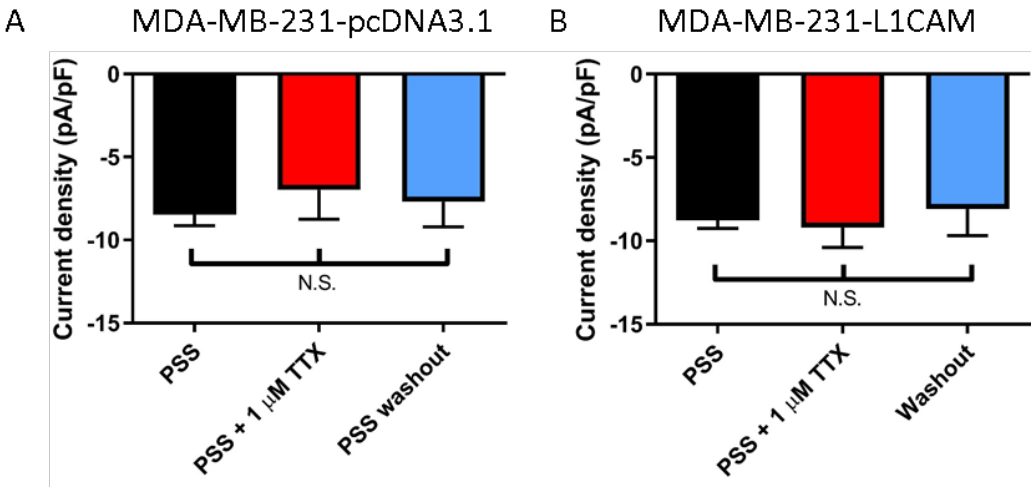

Figure 4.15 Effect of L1CAM on TTX sensitivity.

(A) Na^+ current density of MDA-MB-231-pcDNA3.1 cells depolarised to -10 mV in the absence, presence and following washout of 1 μM TTX (n = 10). (B) Na^+ current density of MDA-MB-231-L1CAM depolarised to -10 mV in the absence, presence and following washout of 1 μM TTX (n = 10). Data are presented as mean ± SEM. Repeated measures ANOVA was used to test for significance (P > 0.05).

4.4. Discussion

4.4.1. Summary of results

The data presented in this chapter show that mutation of the 89th arginine to cysteine prevents proper function of β1 as both a channel auxiliary subunit and as a CAM. β1R89C was expressed at a lower MW than for the wild type β1 subunit. The R89C mutation abrogated the effect of β1 on electrophysiological, adhesive and morphological properties of MDA-MB-231 cells. β1R89C-V5, unlike β1-V5, was not expressed at the plasma membrane. In addition, L1CAM over-expression in MDA-MB-231 cells increased β1 expression, cell-cell adhesion and process outgrowth, but did not affect Na^+ current properties.

4.4.2. The R89C mutation disrupts β1 function as a CAM

Modelling the predicted structure of β1R89C using the Phyre II server revealed a gap in the Ig loop, likely the result of an inability of the server to predict how the protein folds following the introduction of the mutation or the presence of an actual break resulting from the introduction of an extra cysteine into the Ig loop. A break in the protein at this location is unlikely, as it would predict the existence of a small N-terminal fragment attached to the signal peptide and lacking a transmembrane domain. Although the β1R89C mutant ran at a slightly lower MW than wild type β1 on SDS PAGE, this difference in size could not be explained by a break in the protein at position 89. An alternative possibility is that introduction of the mutation disrupts the glycosylation of β1, and this in turn could explain the reduction in MW. Indeed, the related β1C121W mutation results in a reduction of N-glycosylation, thus reducing the MW of β1 when expressed in HEK293T cells (Kruger *et al.*, 2016). However, use of PNGase F to deglycosylate the protein extract from MDA-MB-231 cells resulted in an equal reduction in MW for both wild type β1 and β1R89C. One possible explanation for this disagreement with Kruger et al., (2016) is that post-translational modification of β1 may be cell type specific and could differ between MDA-MB-231 and HEK293T cells (Croset *et al.*, 2012). It is also likely that the reduction in MW in the mutant is the result of altered stability leading to

cleavage, truncation and/or aberrant folding (Lee *et al.*, 2010; Brookes *et al.*, 2015). Improperly folded proteins in which there is an increased exposure of hydrophobic regions to the cytosol are often targeted for degradation by E3 ligases (Cromm & Crews, 2017). Also, disulphide bond formation is important for protein stability and reduces entropy of the native state (Betz, 1993). The introduction of the extra cysteine in this study may have resulted in the formation of a less stable disulphide bond (Chen *et al.*, 2015). A less favourable disulphide bond may result in improper folding and the exposure of hydrophobic regions (Chen *et al.*, 2015). Therefore, it is possible that the folding of the protein may be energetically unfavourable and part of it is being degraded. Such a possibility is supported by the Western blot data showing that the R89C mutant is expressed but runs at a lower MW. Thus, only part of the protein may be being degraded, with the remaining protein being the retained portion (Katz, 1989). The introduction of the cysteine in the R89C mutant did not introduce any known cleavage peptides, therefore binding of ubiquitin to exposed hydrophobic regions remains the most plausible explanation for degradation of the protein.

The role of β1 as a CAM is well documented and has been studied extensively (Malhotra *et al.*, 2000; McEwen & Isom, 2004). As discussed in Chapter 1, a role for β subunits as CAMs in cancer has also been described, including for β1 in breast cancer (Chioni *et al.*, 2009; Nelson *et al.*, 2014) and non-small cell lung cancer (Campbell *et al.*, 2013). In breast cancer cells, it has been shown than β1 increases cell-cell adhesion and process outgrowth and this is mediated by the Ig loop (Chioni *et al.*, 2009; Nelson *et al.*, 2014) (Chapter 3). β1 is able to increase adhesion through homophilic binding (Malhotra *et al.*, 2000), and also interacts heterophilically with several other CAMs (Xiao *et al.*, 1999; Brackenbury & Isom, 2011). The R89C mutation inhibited the ability of β1 to enhance cell-cell adhesion of MDA-MB-231 cells. Thus, R89C critically disrupts the adhesion capability of β1, and this is likely through lack of localisation of β1 to the cell membrane. The effect of the related R85C and R85H epilepsy mutations on cell adhesion has not been investigated (Xu *et al.*, 2007). However, the C121W epilepsy mutation also reduces β1-mediated adhesive capability, likely as a result of a

disrupted disulphide bridge (Meadows *et al.*, 2002). Therefore, it is possible that introduction of a 5th cysteine into the Ig loop of β1 by the R89C mutation may result in improper disulphide bridge formation and thus incorrect folding of the adhesion domain. However, further work is required to separate this from alternative possibilities, including partial cleavage/degradation, lack of proper post-translational modifications, and improper localisation to the membrane.

4.4.3. β1R89C does not regulate cell morphology

β1 increases processes outgrowth on MDA-MB-231 cells (Chioni *et al.*, 2009; Nelson *et al.*, 2014). This agrees with other data showing that β1 expression promotes process outgrowth in neurons (Brackenbury *et al.*, 2010). However, β1R89C did not increase process length compared to negative control MDA-MB-231-pcDNA3.1 cells. Similarly, βR89C was incapable of altering cell area or circularity. Thus, the R89C mutation abrogates the ability of β1 to change morphology and increase process outgrowth. It is possible that *cis* interactions of the Ig loops are required to increase process length on breast cancer cells (Chioni *et al.*, 2009). Another possibility is that β1 increases process length indirectly through the α subunit via altering Na^+ influx (Chioni *et al.*, 2009; Gillet *et al.*, 2009; Brackenbury *et al.*, 2010; Brisson *et al.*, 2011). Interestingly, the mechanism by which β1 increases process outgrowth in MDA-MB-231 cells is proposed to be the same mechanism by which β1 increases process outgrowth in neurons (Brackenbury *et al.*, 2010; Nelson *et al.*, 2014). In both the above possibilities, β1 localisation to the plasma membrane, and direct interaction with α subunits, is critical. Given that β1R89C was not expressed at the membrane, regulation of Na^+ influx through α subunits and/or β1-mediated *cis* adhesion interactions were presumably not possible. It has been shown that growing MDA-MB-231-β1-GFP cells on a monolayer of CHL cells resulted in an increased neurite-like process outgrowth (Nelson *et al.*, 2014). As with the monoculture, the R89C mutation disrupted the ability of β1 to regulate neurite-like process outgrowth when MDA-MB-231 cells were co-cultured with fibroblasts. As β1 is not expressed in CHL cells (Isom *et al.*, 1992), the interactions between β1 on the MDA-MB-231-β1-V5 cells and the CHL cells are likely to be heterophilic, although

the partner CAM(s) are unknown. There may also be other β1-independent adhesion interactions taking place between other CAMs on both cell types, which would explain why MDA-MB-231-pcDNA3.1 cells were notably more elongate when grown on CHL cells compared to when they were grown in monoculture. Further work is required to establish the molecular partners involved in these heterophilic interactions.

4.4.4. Mechanism for functional disruption by R89C

The role of $Na_v1.5$ in promoting a metastatic phenotype in MDA-MB-231 cells has been well described (Brackenbury, 2012). $Na_v1.5$ activity is proposed to permit Na^+ influx, which then allosterically promotes H^+ efflux via NHE1, and local extracellular acidification, which in turn allows pH-dependent proteases to enhance invasion (Fraser *et al.*, 2005; Yang *et al.*, 2012; Brisson *et al.*, 2013). Thus, $Na_v1.5$ promotes migration, invasion and metastasis *in vivo* (Nelson *et al.*, 2015). In MDA-MB-231 cells overexpressing β1, an increased Na^+ current density was observed (Chapter 3) (Chioni *et al.*, 2009). Furthermore, β1 overexpression in MDA-MB-231 cells increases invasion, tumour growth and metastasis *in vivo* (Nelson *et al.*, 2014). On the other hand, in A549 non-small-cell lung cancer cells, transfection with siRNA targeting *SCN1B* decreased adhesion and increased invasion, whereas overexpressing β1-GFP reduced the invasion of H460 non-small cell lung cancer cells (Campbell *et al.*, 2013). Thus, β1 appears to play contrasting roles in regulating invasion in different tumour and/or cell lines. In MDA-MB-231 cells, the increased Na^+ current caused by β1 was abolished by the R89C mutation. This means that β1, in addition to increasing the invasive capacity of breast cancer cells directly through regulating adhesion and process outgrowth (Nelson *et al.*, 2014), may also increase their invasive capability indirectly through promoting Na^+ influx. The disruption of plasma membrane expression of β1 by the R89C mutation suggests that improper folding and/or post-translational processing of β1R89C prevented correct localisation of the subunit to the membrane, thus disrupting its interaction with the α subunit and consequently blocking its effect on Na^+ currents and abrogating its ability to function as a CAM. This finding is also consistent

with the previously reported epilepsy R85C mutation, which was not normally located to the plasma membrane and displayed a decreased Na^+ current density compared to wild type β1 in transfected HEK293T cells (Thomas *et al.*, 2007). In relation to the data in Chapter 3, a further possibility is that the β1ΔIg-GFP truncation mutant, which lacks the Ig loop, may also not be normally localised to the membrane. Further work is required to investigate this possibility.

In summary, these data highlight the importance of an intact Ig loop for the proper function of β1. Interestingly, the R89C mutation may in fact be protective, given the pro-invasive function of β1 in breast cancer (Nelson *et al.*, 2014). However, the situation may be more complex, and cancer- and/or cell-type dependent. Given that in non-small cell lung cancer cells, β1 appears to have a protective role inhibiting invasion (Campbell *et al.*, 2013), it is possible that the R89C somatic mutation, which was originally reported in lung cancer, may potentiate tumour progression in that cancer type. Clearly, the relationship between β1 and cancer progression is complex and may be dependent on other modifiers, which, in turn, could be dependent on cancer type or local microenvironment. Although the results in this Chapter demonstrate that the R89C mutant subunit is a functional null, further work would be required to evaluate the consequences of this loss of β1 function on tumour progression.

4.4.5. L1CAM interacts with β1 and regulates adhesion of MDA-MB-231 cells

L1CAM, in addition to its canonical function as a CAM, has been shown to modulate Na^+ current in neuronal cultures (Valente *et al.*, 2016). Given that β1 interacts heterophilically with a number of other CAMs in neurons and cardiomyocytes, we were therefore interested in the potential interaction between L1CAM and β1 in breast cancer cells. L1CAM has been shown to increase breast cancer cell proliferation and tumour growth through a Munc-18-1 interacting protein 3 (Mint3)-mediated pathway involving fibroblasts (Nakaoka *et al.*, 2017). L1CAM expression is also increased in migrating cells and at the invasive edges of tumours (Fogel *et al.*, 2003; Gavert *et al.*, 2005). L1CAM

expression is elevated in MDA-MB-231 cells over-expressing β1, and β1 is elevated in MDA-MB-231 cells over-expressing L1CAM, implying that a reciprocal signalling pathway is involved in regulation of these proteins. However, the nature of this pathway remains to be determined. Reciprocity in expression and/or function may be a more general phenomenon relating to VGSC biology. For example, β1-mediated neurite outgrowth requires Na^+ current carried by $Na_V1.6$, and proper localisation of $Na_V1.6$ and subsequent high frequency action potential firing in cerebellar granule neurons requires β1 (Brackenbury *et al.*, 2010). However, caution should be taken with the results presented here: as both cell lines were clonal populations grown from a single transfected colony, the reciprocal expression pattern could be an artefact of the clones selected. Further analysis of additional clones is required to exclude this possibility. In both the MDA-MB-231-β1-GFP cells and the MDA-MB-231-L1CAM cells, a higher weight band was present for L1CAM, which suggests the presence of the NOVA-2 variant (Shtutman *et al.*, 2006). The implications of the expression of the NOVA-2 variant of L1CAM are discussed further in Chapter 6.

L1CAM over-expression increased the adhesion of MDA-MB-231 cells. Whilst this increase in adhesion is most likely the result of overexpressing L1CAM, it is also possible that the elevated β1 expression in L1CAM-overexpressing cells may, in part, be responsible. The reverse may also be true: the increase in adhesion seen in MDA-MB-231-β1-GFP cells (Chapter 3) and (Chioni *et al.*, 2009) may be due in part to increased expression of L1CAM in these cells. Although the data here point to an interaction between β1 and L1CAM that may regulate expression (e.g. at mRNA and protein level) and/or protein stabilisation (e.g. in an adhesion complex), the exact nature of the interaction, and how this leads to a promotion of adhesion remains to be determined. One possibility is that β1 and L1CAM interact as CAMs in *cis* and/or *trans*, thus promoting adhesion. This has been shown for β1 heterophilic interactions with other CAMs and ECM proteins, including N-cadherin, contactin, neurofascin-155, neurofascin-186, NrCAM, β2, tenascin-C and tenascin-R (Srinivasan *et al.*, 1998; Kazarinova-Noyes *et al.*, 2001; Malhotra *et al.*, 2004; McEwen & Isom, 2004; McEwen *et al.*, 2004).

Interestingly, the interaction between L1CAM and β1 may be limited to adhesion, rather than additionally impacting on Na^+ current. Whole-cell patch clamp recording revealed no difference in the Na^+ current properties or TTX sensitivity when L1CAM was overexpressed compared to control. This suggests that the Na^+ current in MDA-MB-231-L1CAM cells is not functionally different from that in the control cells. Given that L1CAM increases Na^+ current in hippocampal neurons (Valente *et al.*, 2016), interaction between L1CAM, β1, and Na^+ current may be cell type-dependent. For example, neurons typically express $Na_v1.1$, $Na_v1.2$ and $Na_v1.6$, whereas MDA-MB-231 cells express $Na_v1.5$ (Catterall, 2000; Fraser *et al.*, 2005). Thus, α subunit subtype expression in different cell types may be important for L1CAM-dependent modulation of Na^+ current. In addition, the contrast between Valente *et al.,* (2016) and the data in this Chapter may be explained by the possibility that not all α subunits can be modulated by L1CAM, e.g. perhaps neuronal VGSCs ($Na_v1.1$, $Na_v1.2$, $Na_v1.6$) are L1CAM-sensitive, whereas $Na_v1.5$ is not. A further difference between these results and those of Valente *et al*., (2016) is that they silenced endogenous L1CAM expression by RNAi, whereas the present study overexpressed L1CAM. Thus, any L1CAM-dependent effect on Na^+ current may be saturated in our system. In the future, it would therefore be important to investigate the effect of silencing L1CAM in MDA-MB-231 cells.

4.5. Conclusion

The results in this Chapter add further insight to the conclusions made in Chapter 3. Together, the results from both Chapters now clearly indicate that disruption of the Ig domain (through its deletion, or the R89C mutation) abrogates β1-mediated adhesive capability and modulation of Na^+ current density. However, complex differences between β1 function between non-small cell lung cancer and breast cancer cells (Campbell *et al.*, 2013; Nelson *et al.*, 2014) raise the interesting possibility that somatic mutations disrupting the Ig domain may have opposing effects in different cancer types. The second part of this Chapter focused on L1CAM as a potential functional partner for

β1 signalling. However, whilst L1CAM has a role in changing the morphology of the cells to a more elongate phenotype and increases adhesion in line with its role as a CAM, it has no effect on the Na^+ current. Furthermore, it is still not clear whether or not β1 interacts directly with L1CAM. L1CAM in breast cancer cells may exclusively increase cell invasiveness through cell adhesion and downstream signalling, rather than through an ion conduction-dependent mechanism. In addition to its hypothesized role in triggering EMT, the ability of L1CAM to alter the cells to a more invasive morphology, combined with its adhesive properties, make it a relevant therapeutic target worthy of continued investigation (Shtutman *et al.*, 2006). However, further work is required to establish whether L1CAM is a functional modulator of VGSC activity in tumour cells.

5. Production of aptamers targeting the β1 subunit extracellular domain

5.1. Introduction

Given that overexpressing β1 in MDA-MB-231 cells results in a more invasive phenotype and that β1 expression is increased in breast cancer samples compared to control breast tissue (Nelson *et al.*, 2014), it is possible that specific targeting of β1 may abrogate its ability to interact with other cell surface molecules. This could result in a loss of adhesion, process outgrowth, invasion and other cellular functions which depend on β1 mediated binding (Brackenbury *et al.*, 2008a; Chioni *et al.*, 2009; Brackenbury *et al.*, 2010; Nelson *et al.*, 2014; Patel & Brackenbury, 2015). One potential approach that could be used to inhibit β1 function is to use aptamers targeting the extracellular Ig domain. Aptamers have been successfully developed to distinguish cancer cells and to act as delivery agents for both imaging probes or targeted therapeutics (Cerchia & de Franciscis, 2010). Furthermore, aptamers have been used previously to target CAMs and other plasma membrane proteins on cancer cells, including EpCAM, CD133 and CEA (Shigdar *et al.*, 2011; Orava *et al.*, 2013; Shigdar *et al.*, 2013). In the case of CEA, blocking its adhesive function using aptamers inhibited peritoneal tumour nodule formation *in vivo* (Orava *et al.*, 2013). Given these observations, we therefore proposed to generate aptamers to inhibit β1 function in breast cancer cells.

Aptamer production using the SELEX approach requires approximately 5 mg of purified target protein (Blackwell & Weintraub, 1990; Charlton *et al.*, 1997; Manley, 2013). Attempting to purify β1, which is a type 1 transmembrane protein, from cell lysates runs the risk of potential changes in conformation and post-translational modifications given the stringent conditions required to purify transmembrane proteins. An alternative approach would be to utilise β1B, the soluble secreted splice variant of β1 (Patino *et al.*, 2011). During alternative splicing of *SCN1B,* β1B is produced by transcribing an extended exon 3 (exon 3A) which includes a premature stop codon (Qin *et al.*, 2003). Thus, β1B shares an identical N-terminal region with β1, including the Ig loop, but the C-terminal

region only shares 33 % homology with β1 (Qin *et al.*, 2003). To be effective against β1, the aptamers selected using β1B would need to bind to the extracellular domain.

Secreted β1B has been successfully isolated from conditioned medium using Ni^{2+} bead-based His-tag purification (Patino *et al.*, 2011). Patino *et al*. (2011) stably expressed β1B in CHL cells. However, as post-translational modifications may vary between species cell type, and our goal was to purify aptamers against a target on human cancer cells, we chose HEK293T cells as the expression system (Pham *et al.*, 2003). Given the substantial amounts of purified protein required to perform SELEX, it was also necessary to increase production and/or capture of β1B in order to maximise yield. One way to increase expression/yield is through the addition of specific tags. For example, the F_C tag, from the constant domain of IgG, has been shown to increase protein secretion (Dalton & Barton, 2014).

One issue with the selection of aptamers against protein purified protein is that post-translational modifications can differ between cell lines, which may affect target specificity (Croset *et al.*, 2012). It is therefore desirable to select aptamers against the protein of interest in a close to a native environment as possible. Thus, cell-SELEX using MCF-7 breast cancer cells was planned for later selection rounds given the abundance of endogenous β1 expression in this cell line relative to other breast cancer cell lines (Cooper, 1999; Hicke *et al.*, 2001; Chioni *et al.*, 2009; Nelson *et al.*, 2014; Darmostuk *et al.*, 2015). The efficiency of cell-SELEX can be improved through the addition of a subtractive step in which non-specific aptamers are removed through binding to a negative counter selection cell line which does not express the protein of interest (Shangguan *et al.*, 2006). For negative selection, we planned to generate an MCF-7 line in which β1 expression was knocked-out using CRISPR/*cas9*.

Efficiency of cell-SELEX can be further improved through the use of FACS combined with fluorescent aptamers (Mayer *et al.*, 2010). FACS affords a far greater partitioning efficiency for cells with bound aptamers, reducing the number of non-specific aptamers carried over and therefore theoretically reducing the number of cycles required (Zhang *et al.*, 2010). FACS also presents the opportunity to remove dead cells which may act as non-specific sinks taking up the fluorescent aptamers and therefore acting as false positives. Commonly, dead cells are removed in FACS studies based on cellular granularity and size (Mayer *et al.*, 2010). However, the use of vital dyes could afford a more effective means of partitioning and removing dead and apoptotic cells, thus reducing the number of rounds of selection required. Removal of apoptotic cells by FACS during cell-SELEX has not been attempted before.

5.2. Hypothesis and Aims

The purpose of the set of experiments in this Chapter was to select aptamers targeting the extracellular Ig domain of β1 that could then be used for experimental and potentially diagnostic and therapeutic purposes. The hypothesis of this Chapter was that aptamer-mediated binding to β1 would result in an abrogation of its adhesion function.

The overall goal was to select aptamers specific to β1 and determine how these aptamers affect β1 function. The specific aims were as follows:

1. To purify β1 from HEK293T cells for SELEX.
2. To generate a negative selection tool for cell-SELEX by knocking out β1 in MCF-7 cells using CRISPR/*cas9*.
3. To select aptamers using FACS-based cell-SELEX.
4. To determine the effect of aptamers on β1-mediated adhesion.

5.3. Results

5.3.1. Optimisation of transfection for maximum expression

In order to generate sufficient quantities of β1B for purification and subsequent aptamer selection, the first step was to express β1B in HEK293T cells. Agilent Xl10 ultracompetent cells were transformed with an *SCN1B* construct and a V5/His-tag subcloned into pcDNA3.1. DNA was extracted from successfully transformed colonies and the *SCN1B* construct was amplified by PCR. The PCR products were run on a 0.5 % agarose gel. Eight colonies were successfully transformed (Figure 5.1A). Samples were sequenced and the resultant amino acid sequence from the sample showing greatest homology to the rat β1B reference sequence is shown in Figure 5.1B. DNA from this clone was used for subsequent transfections. HEK293T cells were next transfected with the pcDNA3.1 plasmid containing β1BV5 using Fugene 6. To verify successful transfection and determine the optimum time for harvesting after transfection, transiently transfected cells were harvested after 24 h, 48 h, 72 h, or 96 h and a Western blot was carried out (Figure 5.2A). α-tubulin was used as a loading control (Figure 5.2B). The presence of β1 protein (~37 kDa) confirmed that the transfection was successful. The expression was strongest in cells harvested 96 h after transfection. To keep costs down, polyethylimine (PEI) was planned to be used for larger-scale transfections (~50,000,000 cells), instead of Fugene 6. Thus, next the optimum DNA:PEI ratio had to be determined. Cells transfected with Fugene 6 were used as a positive control, and cells treated with PEI but no DNA were used as a negative control. A HEK293T cell line stably expressing β1BV5 was also generated to save time and avoid repeated transfections going forward (Figure 5.3A, B), but expression was notably lower than for transiently transfected cells. The optimal DNA:PEI ratio for maximum β1B-V5 expression was 1:3 (Figure 5.3A, B), yielding a level close to that seen when cells were transfected with Fugene 6. In conclusion, this set of experiments generated a set of optimum conditions for transfecting β1B into HEK293T cells using PEI.

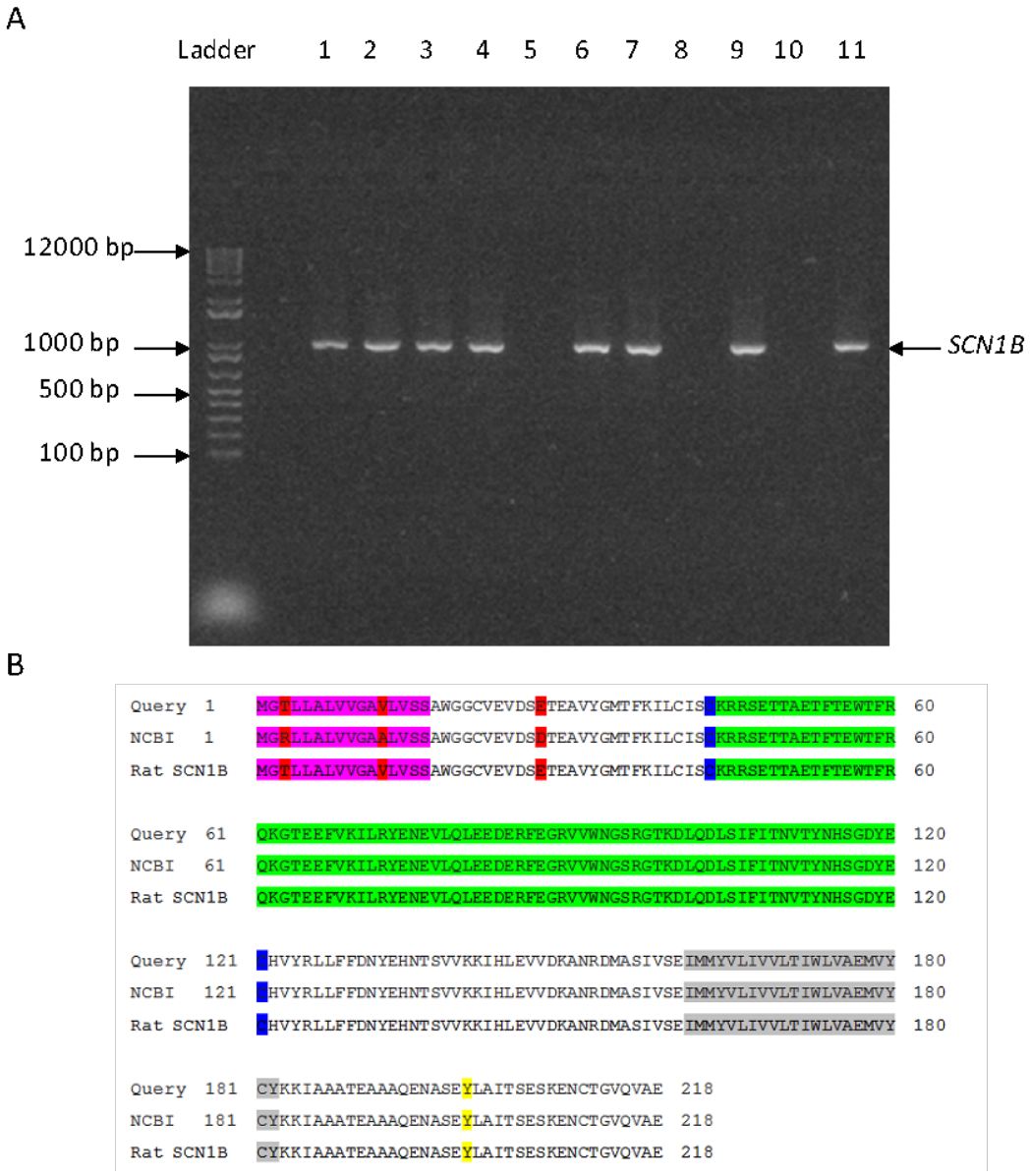

Figure 5.1 PCR products and sequences from clones transformed with a pcDNA3.1 plasmid containing *SCN1B*.

(A) PCR amplification and gel electrophoresis from bacterial colonies transformed with a pcDNA3.1 plasmid containing *SCN1B* (lanes 1-4, 6, 7, 9, 11). All lanes showed a band at the expected weight of ~1100 bp. Lanes 5, 8, 10 were intentionally left empty. (B) Comparison of the cloned product query sequence against NCBI reference sequences for human ("NCBI") and Rat *SCN1B*. Red highlights mismatches in amino acid sequence. Green highlights the Ig region. Purple highlights the signal peptide. Grey highlights the transmembrane domain. Yellow highlights tyrosine 181. Blue highlights the cysteines involved in making the disulphide bridge.

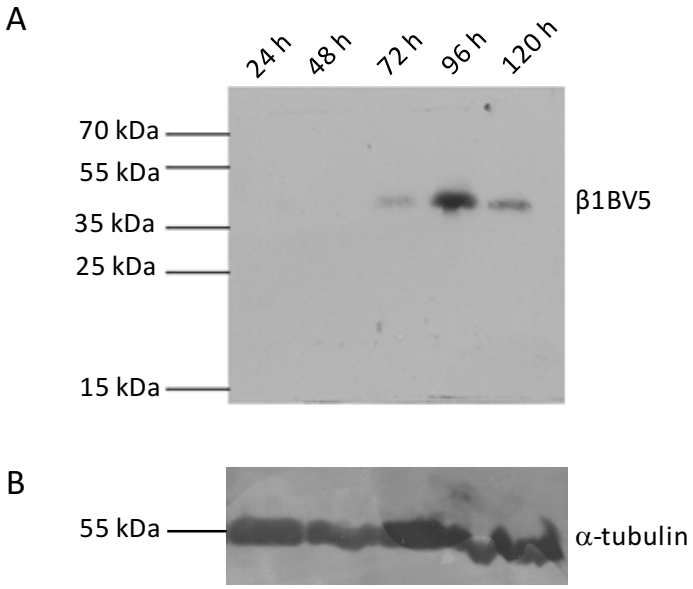

Figure 5.2 Western blot showing β1BV5 expression in HEK293T cells at various time points after transient transfection.

(A) Western blot of β1BV5 expression (38 kDa) in HEK293T cells at indicated times after transfection, probed with anti-V5 antibody. (B) Membrane was stripped and re-probed with α-tubulin as a loading control.

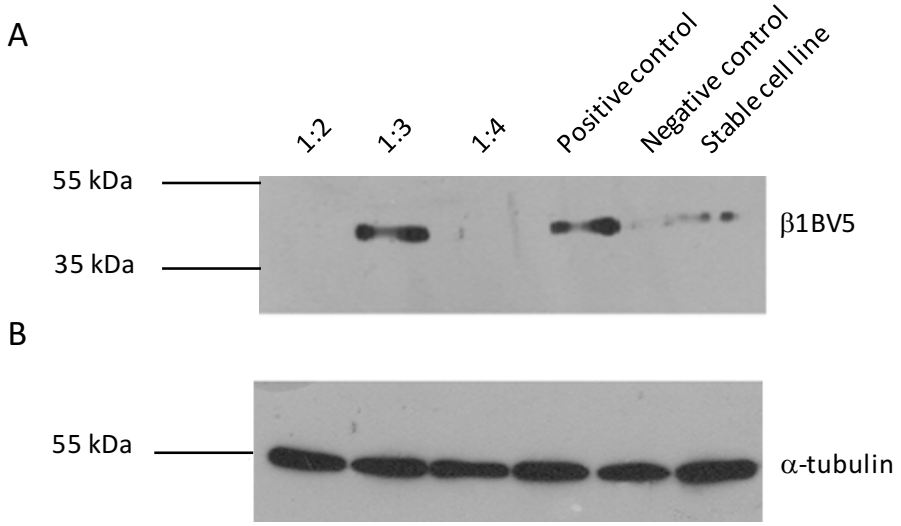

Figure 5.3 Western blot showing the optimum DNA:PEI ratio for transient transfection.

(A) Western blot showing the levels β1BV5 expression in HEK293T cells transfected with different ratios of DNA:PEI, cells transfected with Fugene-6 as a positive control, a negative control where no DNA was added to the PEI, and a cell line stably expressing β1BV5. (B) Blot was stripped and reprobed with α-tubulin as a loading control. Experiment was repeated twice with the same results.

5.3.2. β1B is present in the soluble fraction

To design an appropriate purification protocol, it was first necessary to establish whether β1B was expressed predominantly in the soluble cytosolic or insoluble membrane fractions of the cell. Cells were transfected with β1BV5/His, protein harvested after 96 h, and cytosolic and insoluble fractions separated using centrifugation. Both fractions were split into three equal aliquots and then run on an SDS-PAGE gel. GAPDH and the transferrin receptor, CD71, were used as controls for the soluble and insoluble fractions, respectively (Brackenbury *et al.*, 2008a). β1BV5/His was largely, but not exclusively, present in the soluble fraction with GAPDH (Figure 5.4A, B). When separating the two fractions it was not possible to remove all the supernatant (soluble fraction) from the pellet (insoluble fraction) without disturbing the pellet. Therefore, some of the β1BV5/His and GAPDH seen in the insoluble fraction may be contamination from the soluble fraction. CD71 was exclusively present in the insoluble fraction as expected (Figure 5.4C). The addition of Triton X100 to solubilise proteins in the insoluble fraction slightly increased the CD71 yield (Figure 5.4C). In conclusion, β1B was mainly present in the soluble fraction of transfected cells and this was therefore used for purification.

5.3.3. Optimization of the purification protocol

It was planned to use Ni^{2+} beads for His-tag purification. It was first necessary to establish whether this method could be used to purify the His-tagged protein and also determine at what concentration of imidazole β1BV5/His would uncouple from the beads. Protein was extracted from cells and purified using a Ni^{2+} column before being subjected to elution washes with increasing concentrations of imidazole. β1BV5/His was present in the sample applied to the beads and uncoupled in 500 mM and 1 M imidazole; no detectable β1BV5/His remained coupled to the Ni^{2+} beads (Figure 5.5A). However, staining an SDS-PAGE gel of the same samples with Fairbanks Coomassie solution showed a considerable number of additional proteins were also present at similar levels in all the eluates (Figure 5.5B). This process was attempted eight times, increasing the

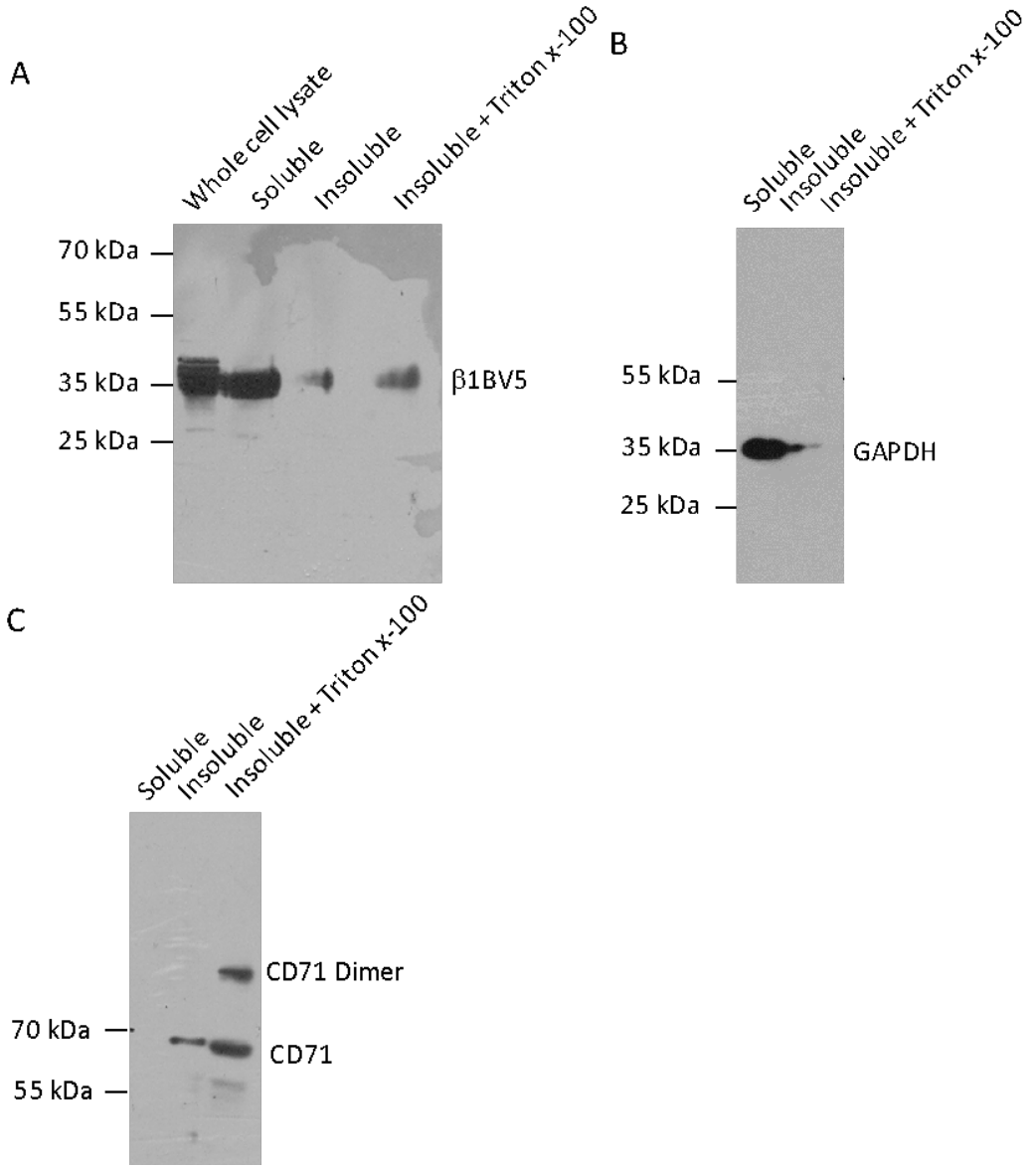

Figure 5.4 Comparison of β1BV5 expression in the soluble and insoluble fractions of transfected HEK293T cells.

(A) Equivalent amounts of the whole cell lysate, soluble fraction, insoluble fraction, and insoluble fraction treated with 1 % Triton X-100 and probed with a mouse anti-V5 primary antibody. (B) Membrane was stripped and re-probed with a mouse anti-GAPDH antibody as a control for the soluble fraction. (C) The membrane was stripped and re-probed with a mouse anti-CD71 antibody as a control for the insoluble fraction.

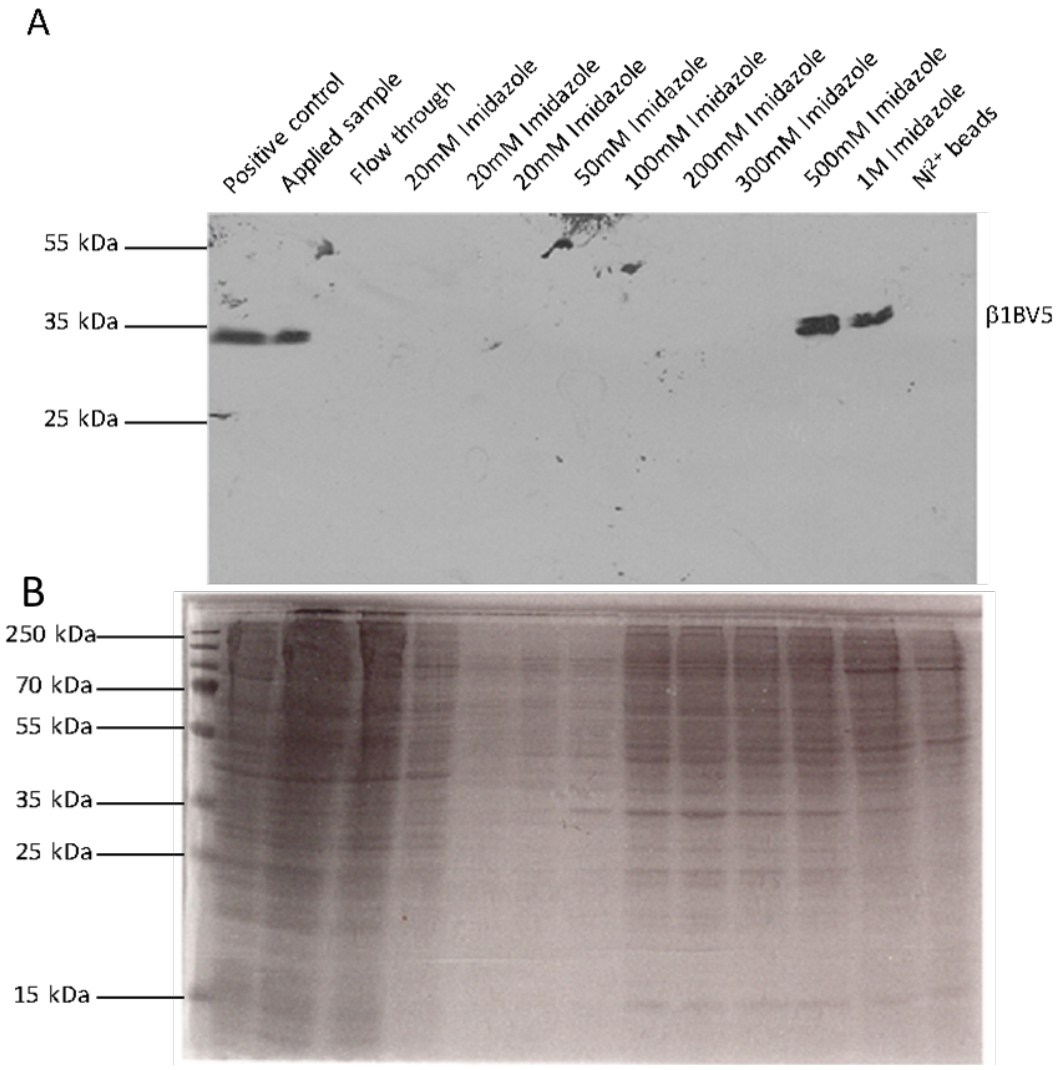

Figure 5.5 Binding and uncoupling of the soluble fraction of lysates of HEK293T cells transfected with β1BV5.

Equivalent volumes (50 µl) of applied sample, flow through after initial coupling to beads, washes in increasing concentrations of imidazole in the range 20 mM – 1 M, and Ni^{2+} beads, were loaded onto a 12 % SDS-PAGE gel. (A) Gel was transferred to a nitrocellulose membrane and probed with a mouse anti-V5 antibody. (B) Gel stained with Fairbanks Coomassie to show all the proteins present at each stage during the protocol. The soluble fraction of transfected HEK293T cells confirmed for β1BV5 expression previously was used as a positive control.

number of different imidazole concentrations in an attempt to uncouple His-rich proteins from the Ni^{2+} beads at the lowest concentration possible. The gels in Figure 5.5 show the final attempt at purification with the highest number of washes and intermediate imidazole concentrations. Previous attempts often resulted in either absent protein or poorly defined bands. In conclusion, this Ni^{2+}

purification protocol was considered not to be appropriate for purifying β1BV5/His protein from HEK293T cells.

5.3.4. Creation of pOPINTGneo vectors

As Ni^{2+} affinity-based purification was found not to be an appropriate approach, three new vectors were created with human β1B, followed by either a His-tag, a CD4-tag followed by a His-tag, or an F_C-tag followed by a His tag. The tags were chosen as they could possibly increase secretion to enable purification from conditioned culture medium (Dalton & Barton, 2014). As controls to test for expression, cells were transfected with three vectors, one containing a gene for a protein which is secreted in lesser amounts (9816), another which is secreted in large quantities (6218), and eGFP. The vectors were transfected into HEK293T cells to test whether they promoted secretion of β1B to the medium. Unfortunately, although the three positive controls were present in the medium to varying extents, β1B was not detectable (Figure 5.6). Therefore, neither of these new vectors were suitable for expression/purification of β1B from the medium. This work was carried out as a single attempt during a visit to the MRC Oxford Protein Production Facility (OPPF), with the assistance of Dr Joanne Nettleship. Finally, a protein production company (National Research Council Canada) was hired to purify β1B. Unfortunately, they were also unable to purify β1BV5 from cell lysate or conditioned medium. It was therefore decided to change approach and instead use cell-SELEX for aptamer selection.

5.3.5. Knocking out β1 expression in MCF-7 cells

Given that target purification had been unsuccessful, the revised plan was to use the cell-SELEX approach on wild type MCF-7 cells (positive selection) and MCF-7 cells in which β1 had been knocked out (negative selection). The CRISPR*/cas9* system (Ran *et al.*, 2013) was chosen over other established permanent silencing methods such as zinc-finger nucleases (ZFNs) and transcription activator-like effector nucleases (TALENs) (Gaj *et al.*, 2013). At the time, commercially-available

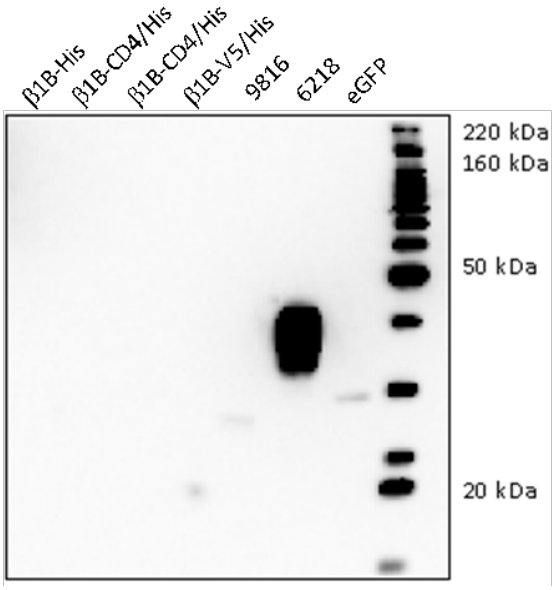

Figure 5.6 Western blot of medium from cultured HEK293T cells transfected with the pOPINTTGneo β1B constructs.

The Western protocol used at the MRC OPPF differed from that described in Methods. Briefly, 20 µl of medium was collected and 20 µl of sample buffer. Sample was boiled and 20 µl loaded onto a 12 % acrylamide gel. Membrane was probed with a mouse anti-His antibody in 5 % non-fat dry milk PBST for one hour. After washing, the membrane was then probed with a goat anti-mouse secondary antibody overnight. The membrane was imaged with a chemi-imager with a 30 ms exposure time. β1B-His, β1B-CD4 and β1B-Fc were the experimental constructs. 9816, 6218 and the eGFP containing plasmids were positive controls. The identities of 9816 and 6218 were not disclosed by the OPPF. This western blot was carried out with the help of Dr Joanne Nettleship at the OPPF.

CRISPR guide RNAs were available for β1 (Section 2.18), whereas no such constructs were readily available for ZFNs or TALENs. The vectors containing the guide RNAs did not allow for selection of successfully transfected cells with an antibiotic but did contain GFP, so FACS was used to select successfully transfected cells (Section 2.19). Control (non-transfected and mock transfected) cells were compared against cells transfected with the GFP-guide RNA construct. Gates were set using the controls, and the number of transfected cells appeared shifted to the right on the FITC log scale compared to the controls, with no difference on the phycoerythrin channel (PE log) (Figure 5.7 and Figure 5.8). In total, ~10^4 GFP-expressing MCF-7 cells were sorted and these were grown in a 35 mm dish and 12 colonies grown from picked single cells. The colonies were then grown up for downstream analysis (next section).

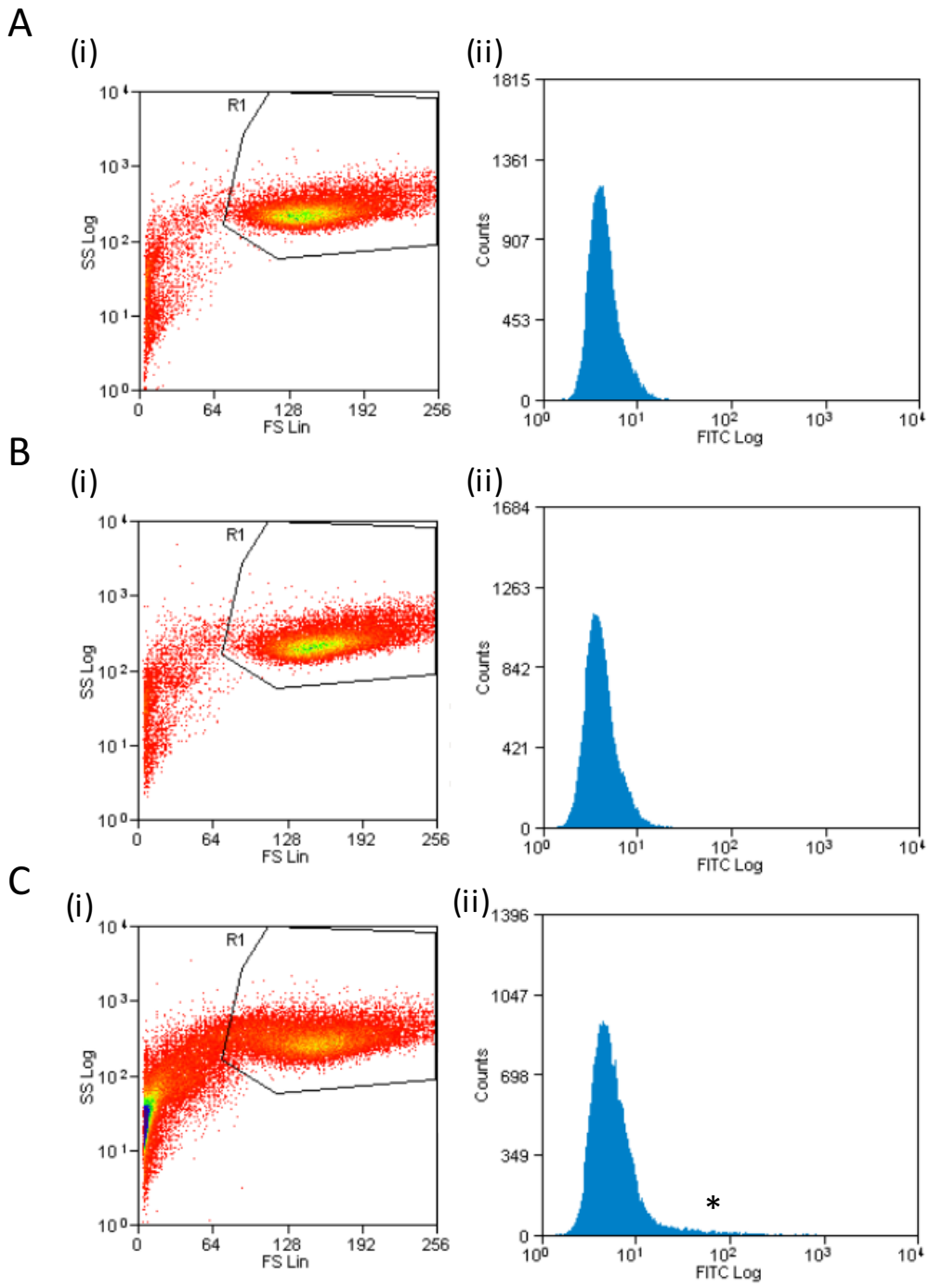

Figure 5.7 Fluorescence-activated cell sorting of MCF-7 cells transfected with GFP-expressing CRISPR vector.

(A) Cell count of non-transfected MCF-7 cells. (B) Cell count from mock-transfected MCF-7 cells (no DNA). (C) Cell count from MCF-7 cells transfected with GFP-expressing CRISPR vector. Left-hand panels (i): Side scatter on log scale (SS Log) vs. forward scatter on linear scale (FS Lin). Selected area R1 encompasses the live cells of expected size and granularity. Right-hand panels (ii): Histograms of cell counts along FITC log scale. Asterisk in (Cii) indicates the GFP-expressing cells.

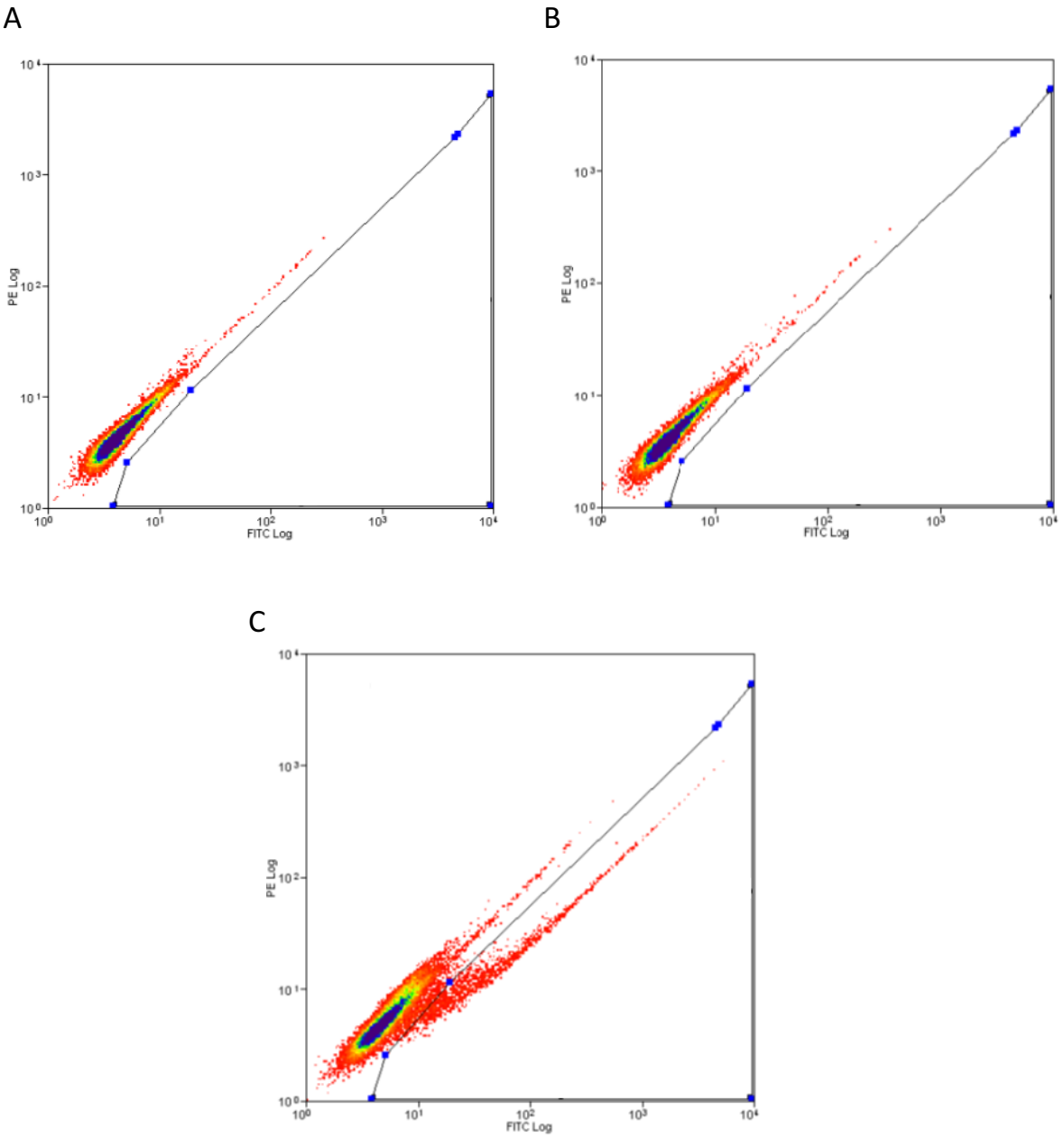

Figure 5.8 Total cell count of CRISPR cells sorted by GFP fluorescence.

PE log plotted vs. FITC channel (FITC log) for non-transfected MCF-7 cells (A), mock-transfected MCF-7 cells (B), and MCF-7 cells transfected with GFP-expressing CRISPR vector (C). The non-transfected and mock transfected cells were used to set the gates outside of GFP expression. PE, the next detector channel along, was used to help detect potentially weakly expressing proteins more cleanly than using FITC/GFP detector alone. Cells expressing GFP show a rightward shift on the FITC scale.

5.3.6. Selecting MCF-7 clones deficient for β1

One of the complications with performing a CRISPR/Cas9-mediated deletion of a gene in MCF-7 cells is that this cell line is potentially tetraploid and has been shown to have unstable chromosomes (Kleensang *et al.*, 2016). A surveyor mutation assay (Section 2.20; a method by which DNA mutations and polymorphisms can be detected) was used to determine which of the selected 12 colonies had all copies of *SCN1B* gene successfully mutated (Vouillot *et al.*, 2015). Briefly, the surveyor assay requires mixing the genomic DNA of control cells with those of cells which have been potentially mutated, and the DNA allowed to bind after melting. It is assumed, in this method, that ~25 % of the DNA binding will be from a mix of both the control and mutated DNA. Therefore, this binding should result in a mismatch. The surveyor nuclease should be able to detect the mismatch and cleave the DNA, which can then be visualized on an agarose gel (Ran *et al.*, 2013). Initially, the standard method of the surveyor mutation assay with mixed genomic DNA was carried out. This was to determine whether at least one copy of the *SCN1B* gene had been mutated. To determine whether all four copies have been mutated, a variant of this method was used in which the DNA was not mixed. By not mixing the genomic DNA of clones which have at least one copy of *SCN1B* mutated, if no cleavage products are seen, then these clones should have had all copies of the *SCN1B* gene mutated. The genomic DNA was extracted from each clone and the surveyor mutation assay carried out first on mixed genomic DNA (Figure 5.9A, B). As cleavage products were seen in MCF-7-Δβ1 clones 1, 2, 4, 6, 7, 8, 9, and 10, these clones were used for the next surveyor mutation assay. The genomic DNA of pure unmixed mutant clones was not mixed, and the surveyor mutation assay revealed that only clones 4, 9 and 10 were not cleaved (Figure 5.10). This result showed that these are the only three clones where all four copies of *SCN1B* have been mutated. A qPCR and Western blot were then carried out on clones 4 and 9, confirming knock-out of β1 mRNA and protein expression (Figure 5.11A, B). Clone 4 was used for all subsequent experiments, and the resultant cell line named MCF-7-Δβ1. In conclusion, this set of experiments successfully generated a β1 knock-out MCF-7 cell line that could be used for a negative selection step in cell-SELEX.

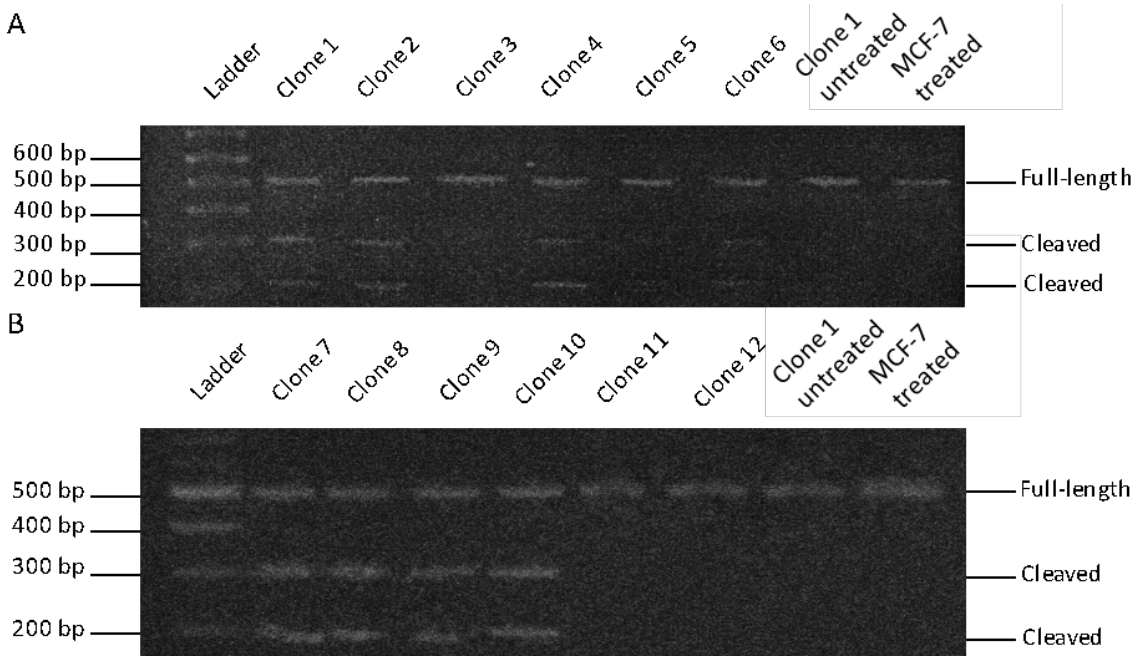

Figure 5.9 Surveyor mutation assay for MCF-7 clones successfully transfected with CRISPR/Cas9 plasmid targeting *SCN1B*.

(A) Cleavage products for Clones 1-6. (B) Cleavage products for Clones 7-12. The assay was carried out using a heterogenous mixture of wild type and potentially mutant clone gDNA from MCF-7 cells transfected with a CRSIPR/*cas9* plasmid. Clones 1, 2, 4, 6, 7, 8, 9, and 10 showed cleavage by the surveyor nuclease, indicating that these clones contained at least one copy of the *SCN1B* gene mutated.

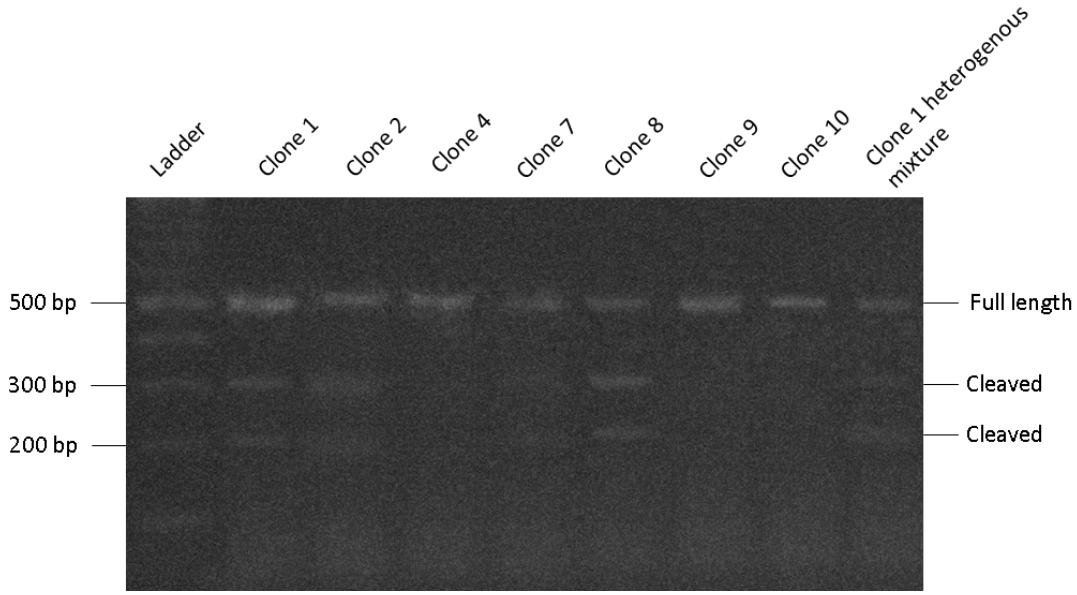

Figure 5.10 Second Surveyor mutation assay for MCF-7 clones which had at least one mutated copy of *SCN1B*.

Gel shows results of a second Surveyor assay in which homogenous gDNA was used from each clone (without mixing with wild type DNA). Clones 4, 9, and 10 had no cleavage products, indicating that these clones had all copies of the *SCN1B* gene mutated.

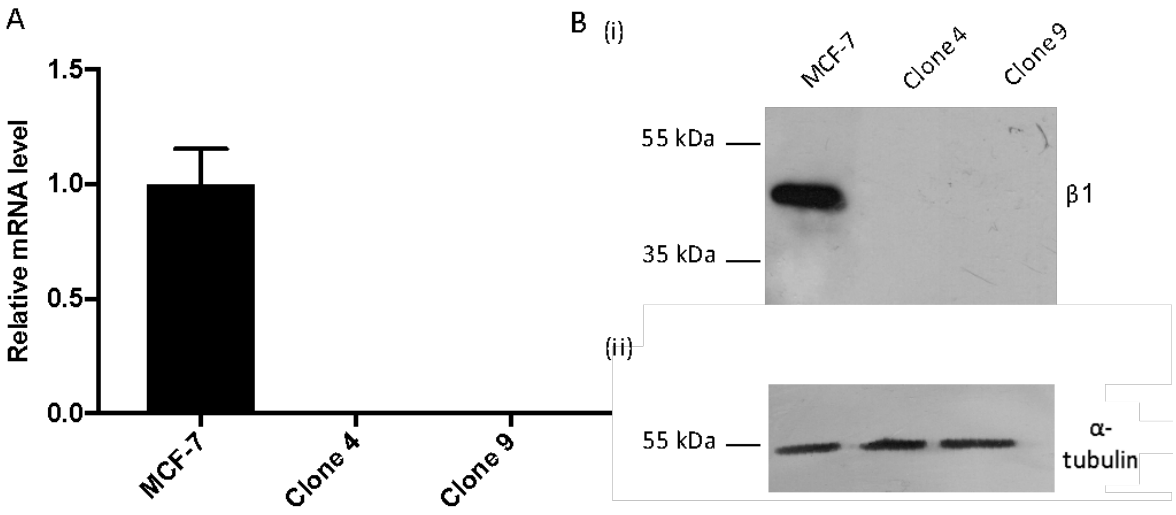

Figure 5.11 Evaluating lack of β1 expression in MCF-7-Δβ1 clones 4 and 9.

(A) QPCR showing *SCN1B* mRNA level in MCF-7 and MCF-7-Δβ1 clones 4 and 9 (n=3). (B) (i) Western blot showing β1 expression (38 kDa) in MCF-7 and MCF-7-Δβ1 clones 4 and 9, probed with anti-β1 N-terminus antibody. (ii) Membrane was stripped and re-probed with α-tubulin as a loading control.

5.3.7. FACS-based aptamer selection using live cells

Cell SELEX, using MCF-7 cells, was next undertaken for aptamer selection. The MCF-7 cells were used for positive selection of aptamers, whilst the MCF-7-Δβ1 cells were used for negative selection. A novel approach was employed, using FACS-based aptamer selection in which apoptotic and dead cells, which could act as false positives, were identified and removed using dyes. DRAQ-7 was used to remove dead cells whilst TMRE was used to isolate non-apoptotic cells (Section 2.19). Using these dyes, FACS gating was used to isolate only live cells (Figure 5.12). As TMRE only stains cells which are not apoptotic, a positive shift was seen in the PE-Texas Red log scale for healthy cells (Figure 5.12). DRAQ-7 stains dead cells and this is seen as a positive shift in the allophycocyanin (APC)-Cy7 log scale (Figure 5.12). Combining this live cell selection with the use of FITC-modified aptamers, it was possible to isolate live, healthy, strongly fluorescing cells, with FITC-modified aptamers bound to them in the 488-526 log scale, in the same sort.

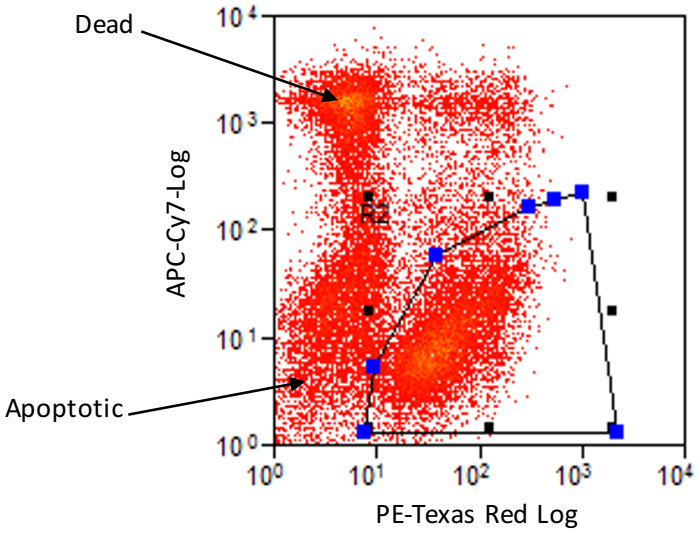

Figure 5.12 Dot plot of healthy, apoptotic and dead cells in flow cytometry.

TMRE (PE-Texas red log scale) was used to distinguish apoptotic vs. non-apoptotic cells and DRAQ-7 (APC-Cy7 Log scale) was used to distinguish live from dead cells. TMRE uptake, seen as a rightward shift on x-axis, signified live and healthy cells. DRAQ-7 uptake, seen as an upward shift on y-axis, signified dead cells. Cells were gated on the region labelled R2 for live and healthy cells for all subsequent sorts.

Aptamer selection proceeded as follows: a pool of commercially available synthesised FITC-modified DNA aptamers was allowed to bind to the target cells in suspension (Section 2.24). Next, unbound aptamers were removed by spinning the cells down and removing the supernatant, after which the cells with bound aptamers in DMEM underwent FACS. For the first three rounds, parental MCF-7 cells were used for positive selection of aptamers binding to the surface. In the fourth round, a negative selection step was added by pre-incubating the aptamers with MCF-7-$\Delta\beta$1 cells and using the unbound aptamers (supernatant) for subsequent positive selection. The histogram after the first sorting is shown in Figure 5.13. The histogram shows which cells were selected for (pink and green regions – only the top 40 % of live fluorescing cells) and shows the false positive of dead cells fluorescing strongly in the 488-526 nm range. As the rounds progressed, a noticeable shift in the 488-526 nm scale was visible suggesting that with each round, the aptamers were becoming more specific to MCF-7 cells (Figure 5.14). Only after round four, where the negative selection step was

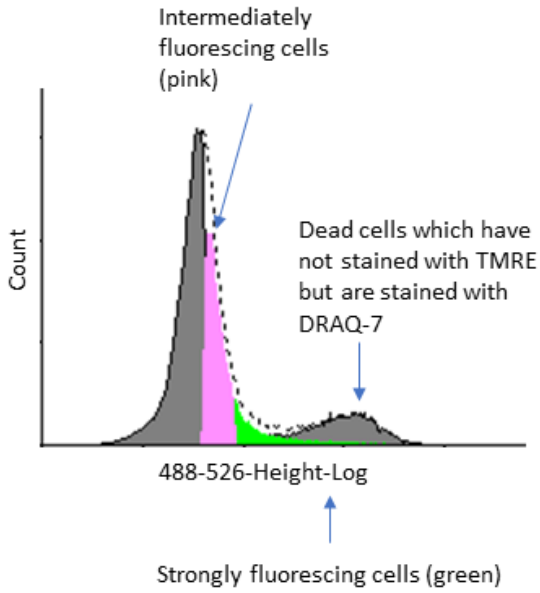

Figure 5.13 Histogram from the first round of cell-SELEX.

Apoptotic cells (white area under dotted line) have been removed. Dead cells, which have likely internalised significant amounts of aptamers, are strongly fluorescing (grey right-hand peak). For each round of selection, the top 40 % of live fluorescing cells were taken. These were sub-divided into intermediate and strongly fluorescing live cells, shown as the pink and green regions.

introduced, was a leftward shift seen. The leftward shift was likely due to the removal of a large number of different sequences which were not binding to β1 being in the negative selection step. Therefore, the number of remaining sequences was likely comparatively smaller than for round 3, explaining the shift. In round six, a strong rightward shift was seen compared to the previous round, thus it was decided that this would be the final round because the majority of the aptamers were binding strongly to the cells, yielding a strong fluorescence reading. In conclusion, a novel variant of the cell-SELEX approach was adopted to select aptamers targeting β1. By using FACS to exclude both dead and apoptotic cells, in combination with a negative selection step using MCF-7-Δβ1 cells, it was possible to generate an aptamer pool in only six rounds of selection.

5.3.8. Amplification and preparation of aptamers

Within each round of selection, it was necessary to amplify and prepare aptamers for the subsequent round. Once cells with bound aptamers had been sorted by FACS after each round of

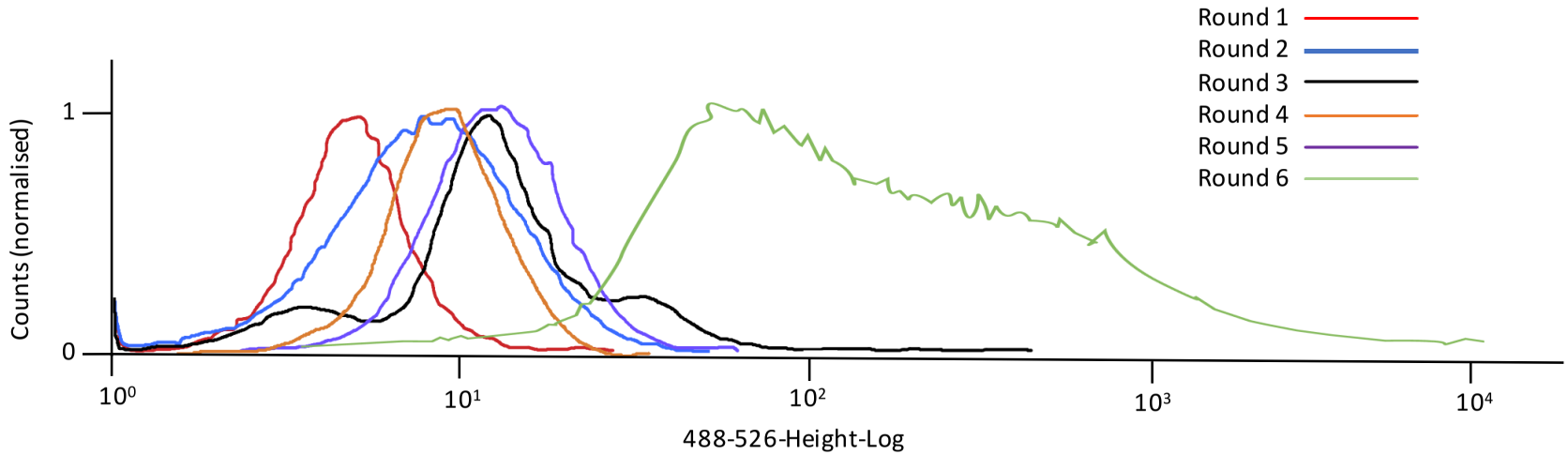

Figure 5.14 Histogram of cellular fluorescence excited in the 488-526 channel from each round of selection.

Histogram of fluorescence from each round of selection with live and healthy FITC-modified aptamer-bound cells. Counts for each individual histogram are normalised to the peak count for that round. Excitation measured in the 488-526 channel represents fluorescence from the FITC modified aptamers. In round 4, a negative selection was added.

selection, aptamers were separated from the cells by heating to 95 ˚C, and then amplified using a symmetric PCR, after which a semi-quantitative PCR was used to determine ideal number of cycles for clean double stranded material with no artefacts from over cycling PCR contents. An aliquot of PCR product at each cycle was run on a gel to determine the number of cycles required to amplify aptamers without forming artefacts (Figure 5.15A). Aliquots of the product were then amplified again initially using a semi-asymmetric PCR to amplify the forward strand in abundance with FITC-modified primers to determine the ideal number of cycles for the maximum intensity band of single stranded material, followed by a semi-asymmetric PCR to amplify the aptamers to form the next pool for selection (Figure 5.15B). The unwanted double-stranded PCR products were removed by digestion using lambda nuclease. It was necessary to ensure only single stranded DNA was used for selection because double stranded DNA may result in off target hybridisation between aptamers leading to abnormal folding. Specifically, the primers used in the asymmetric amplification contained a PO_4 modification which allowed the lambda digest to begin digestion of that strand. This also ensured that the correct strand of the two was digested. Exonuclease-1 was used to treat a small sample of product to confirm presence of single-stranded DNA aptamers (Figure 5.15C). Following each amplification and the digestion step, aptamers were bead purified and eluted in water (Section 2.26). Aptamers were then ready to commence the next round of selection.

5.3.9. Confirmation of binding

Following the six rounds of selection, it was necessary to next characterise the ability of the aptamers to bind to β1 in situ. Confocal microscopy was used to confirm binding of aptamers after the final selection and amplification using fluorescently modified primers (Section 2.23). Aptamers bound much more strongly to MCF-7 cells than MCF-7-Δβ1 cells, evidenced by stronger FITC signal in the wild type cells (Figure 5.16A-C). The aptamers were likely binding to β1 and/or another protein which may have been upregulated following the knocking-out of β1. Interestingly, a small amount of

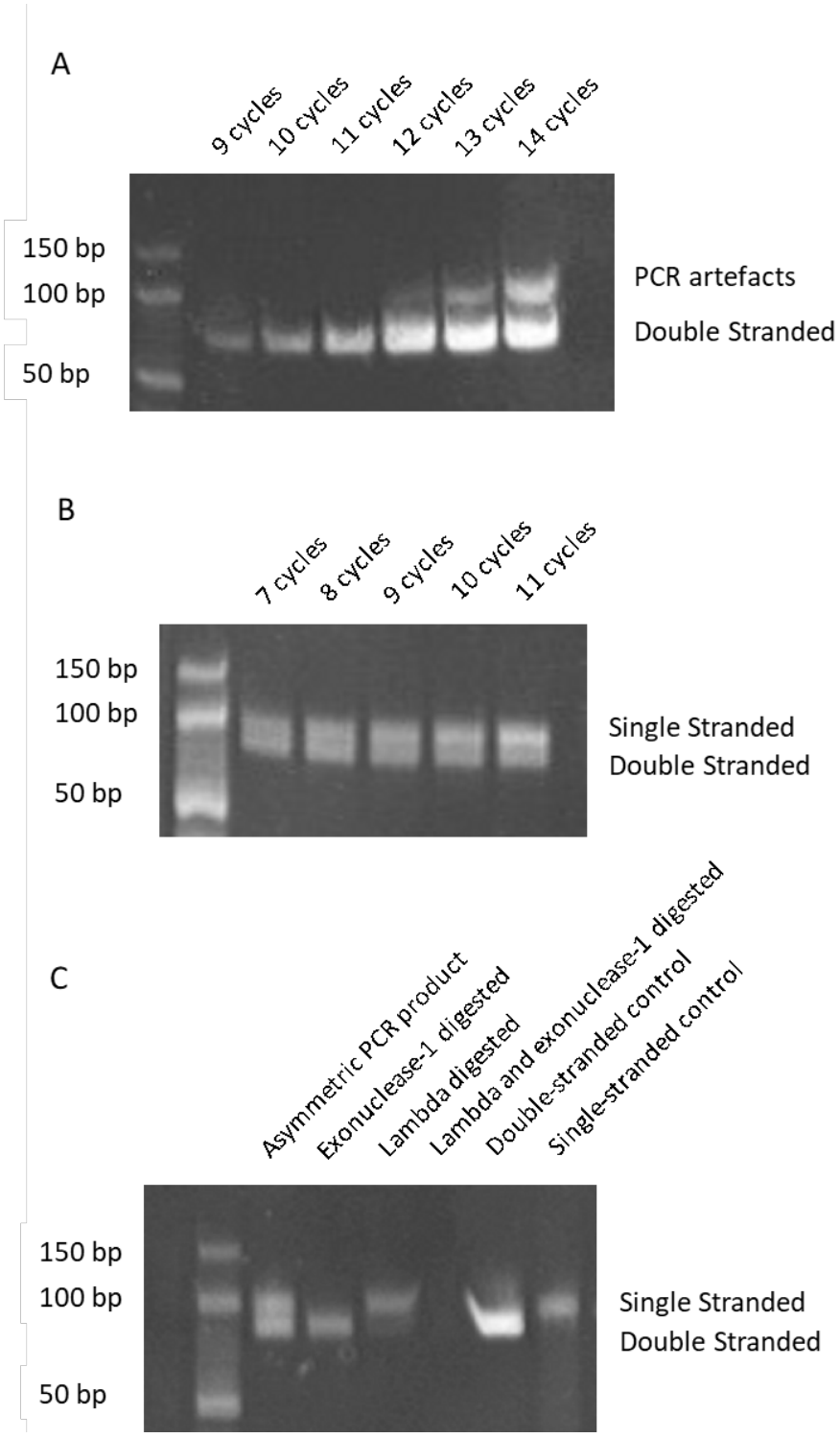

Figure 5.15 Amplification of aptamers.

(A) Representative symmetric cycle course PCR determining the optimum number of cycles required to amplify double stranded DNA aptamers without PCR artefacts. For this round, 11 cycles was determined to be the optimum. (B) Asymmetric PCR with a FITC-modified forward primer used to amplify aptamer sequences. The FITC-modified forward primer was in excess of reverse primer. (C) Products of asymmetric PCR digested with either Exonuclease-1 or Lambda nuclease to remove single- or double-stranded DNA, respectively. Double-stranded DNA runs at an apparent lower weight than single-stranded DNA due to coiling and supercoiling.

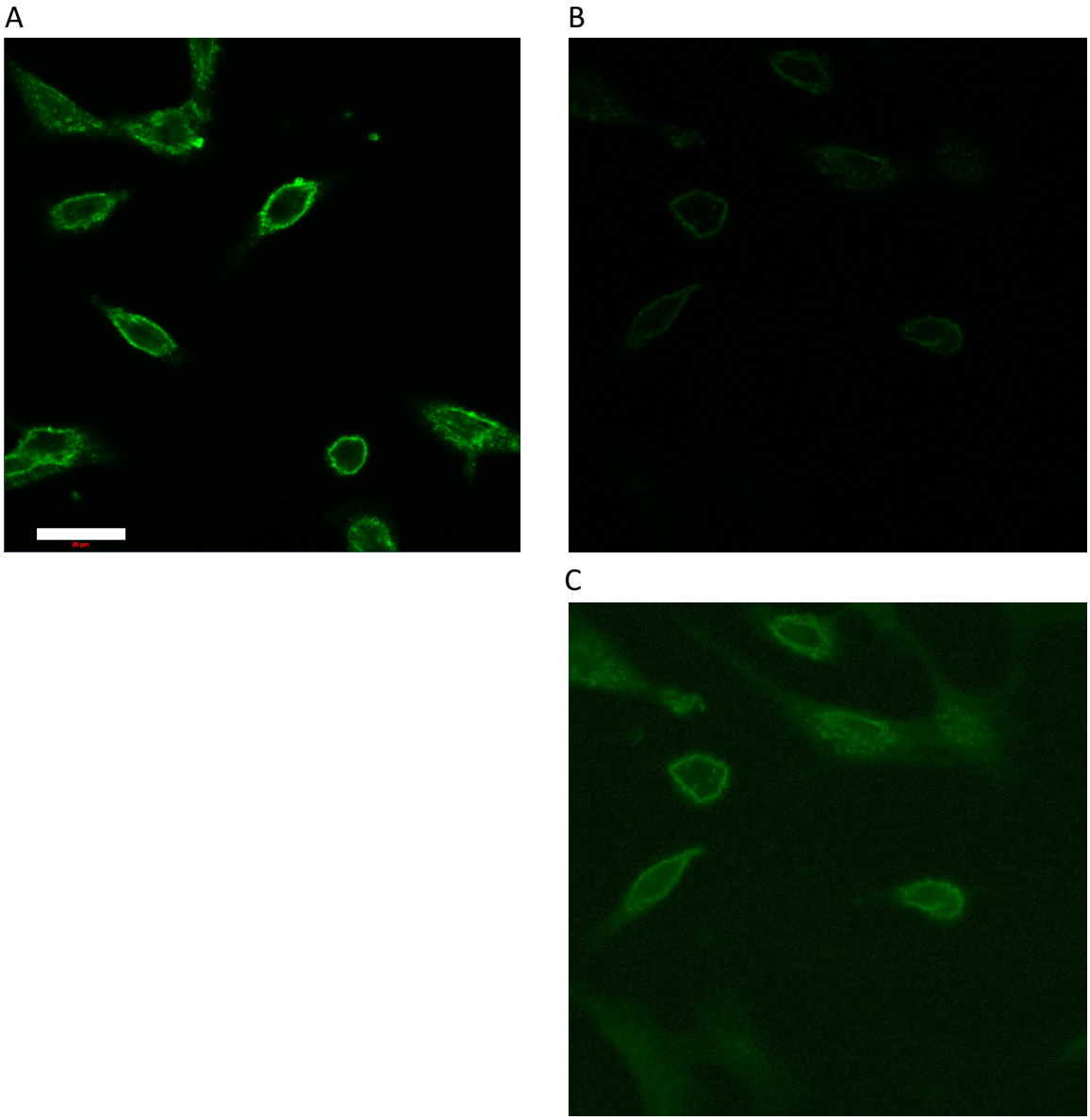

Figure 5.16 Confocal micrographs of MCF-7 cells treated with aptamers.

(A) MCF-7 cells fixed on coverslips and incubated with FITC- modified aptamers (40 pmol per coverslip) following the final round of cell-SELEX. (B) MCF-7-Δβ1 cells incubated with the same set of fluorescent aptamers showing much weaker binding. (C) Image from (B) with contrast enhanced to indicate presence of cells and very weak signal. Scale bar = 20 µm.

signal is visible from within the cells. This could be due to aptamers entering the cells or signal from the plasma membrane dipping into the focal plane from above and/or below. In conclusion, the confocal microscopy data suggest that the aptamers specifically bind to β1 on MCF-7 cells.

5.3.10. Aptamer binding to β1 inhibits adhesion

Given that the aptamers appeared to bind specifically to MCF-7 and not MCF-7-Δβ1 cells, we next evaluated the effect of the aptamers on blocking β1 function. Given the critical role of β1 in regulating cell-cell adhesion, it was decided to study the effect of the aptamers in an adhesion assay. First, the effect of knocking-out β1 on adhesion of MCF-7 cells was determined (Figure 5.17A). Knock-out of β1 significantly increased the normalised particle count in MCF-7-Δβ1 cells after 30 min (0.75 ± 0.09) compared to MCF-7 cells (0.51 ± 0.05; $P < 0.05$; n = 3, 10 fields of view per n; Figure 5.17B), consistent with a reduction in adhesion in the absence of β1. The next step was to determine whether the aptamers could inhibit β1-mediated adhesion in wild type MCF-7 cells. An adhesion assay using MCF-7 cells was performed in the presence vs. absence of aptamers. (Figure 5.18A). Salmon sperm DNA was used a negative control. The normalised particle count of MCF-7 cells with aptamers added (0.80 ± 0.06) was significantly higher after 30 min than for the control cells (0.61 ± 0.04; $P < 0.05$; n=3, 10 fields of view per n; Figure 5.18B), consistent with a reduction in adhesion in the presence of aptamers.

Although the aptamers inhibited adhesion in MCF-7 cells, this did not necessarily mean that they were doing so by inhibiting β1 function. To specifically test this, the same adhesion assay was next carried out using MCF-7-Δβ1 cells (Figure 5.19A). There was no significant difference in the normalised particle count between the MCF-7-Δβ1 cells with salmon sperm DNA compared to aptamers (Figure 5.19B). In conclusion, the data from these adhesion assays suggest that the aptamers inhibited the adhesion of MCF-7 cells by specifically binding to, and abrogating the function of, the extracellular β1 Ig domain.

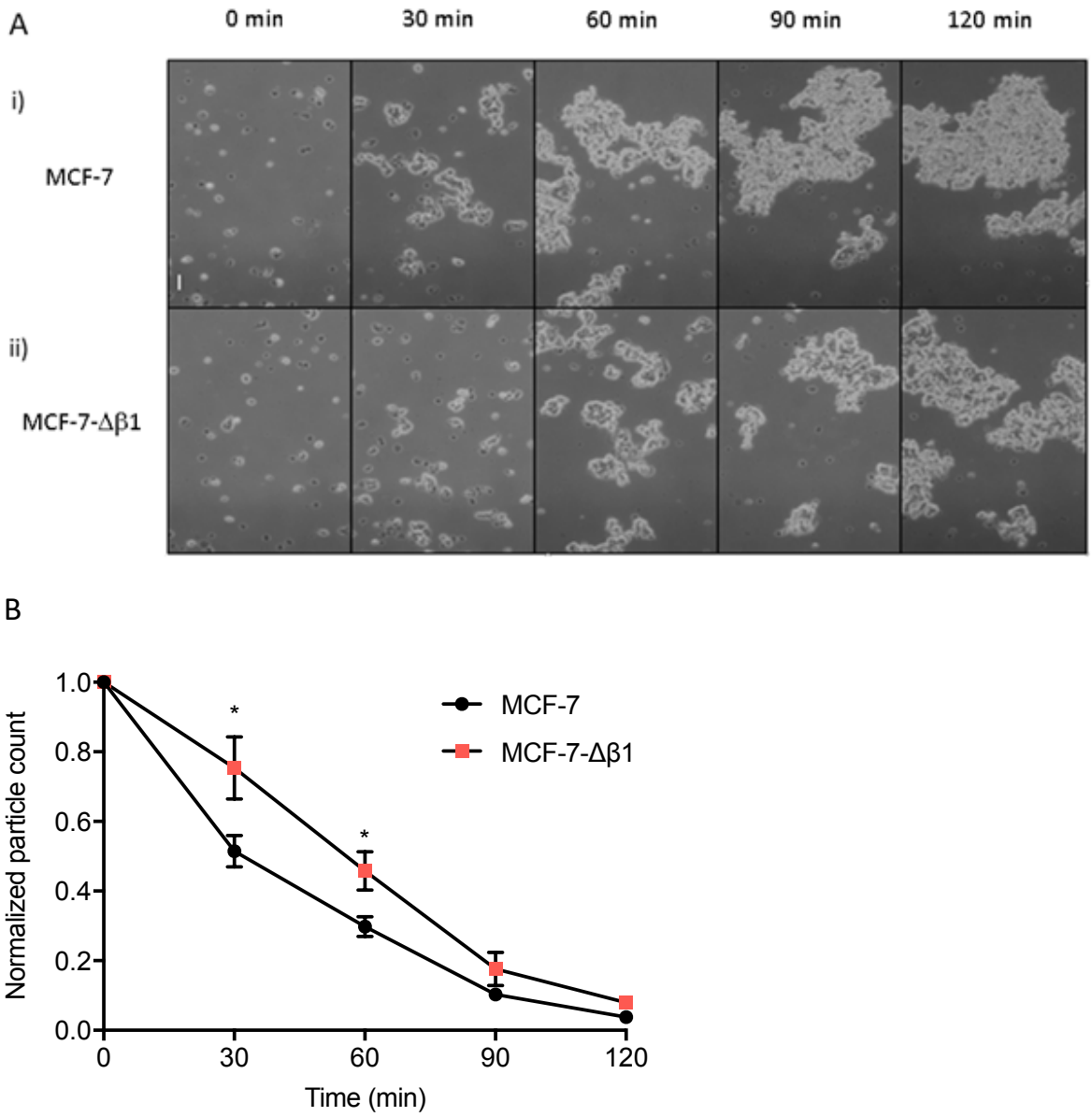

Figure 5.17 Effect of knocking-out β1 on adhesion of MCF-7 cells.

(A) Representative images of MCF-7 cells in an adhesion assay. (i) Bright field images of parental MCF-7 cells. (ii) Bright field images of MCF-7-Δβ1 cells. Scale bar = 50 µm. (B) Normalised particle count from control MCF-7 cells and experimental MCF-7-Δβ1 cells. A two-sample t-test was used to test for significance at each time point (*P < 0.05).

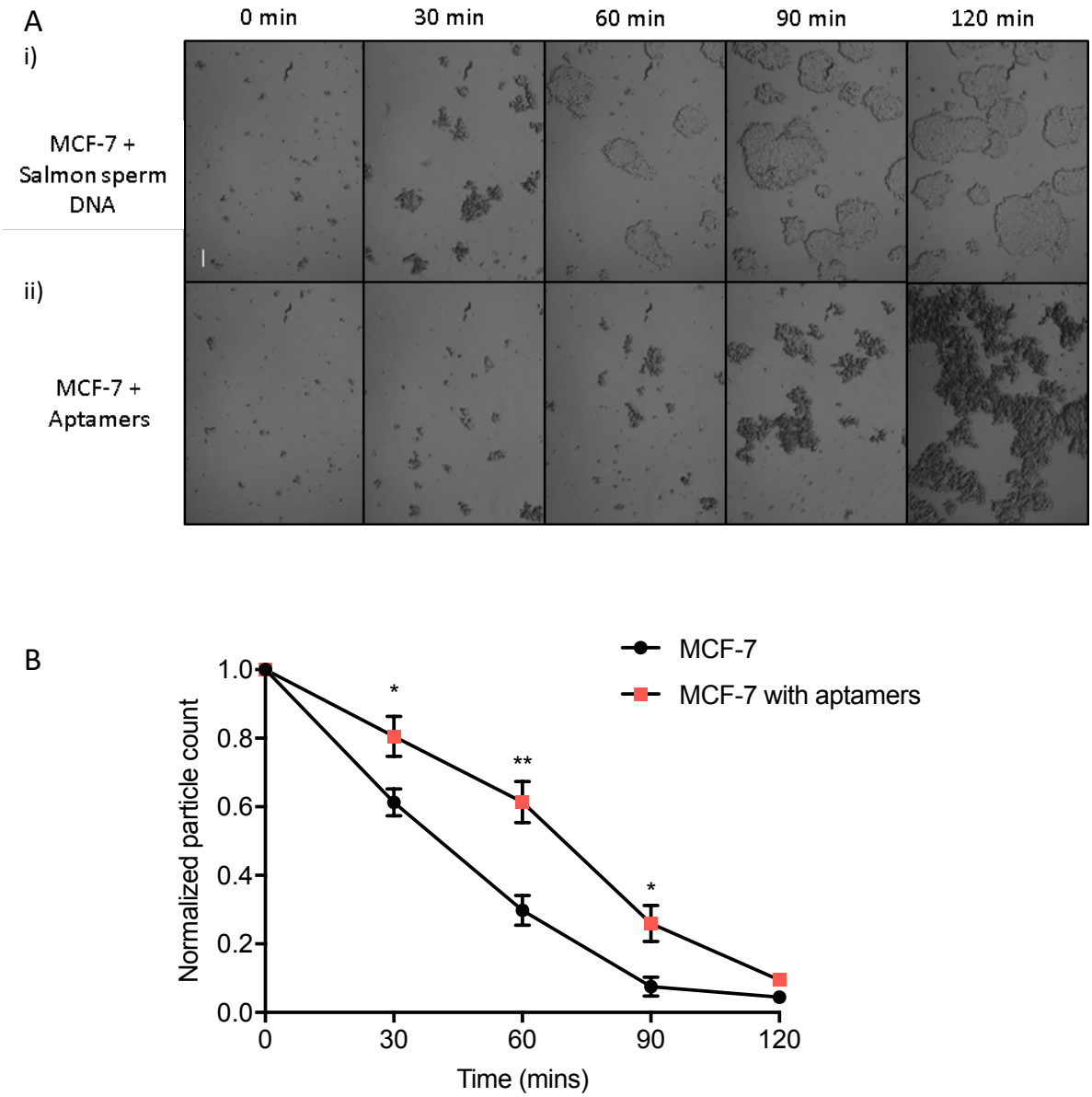

Figure 5.18 Effect of aptamers selected against β1 on adhesion of MCF-7 cells.

(A) Representative images of MCF-7 cells in an adhesion assay with aptamers. (i) Bright field images of control MCF-7 cells treated with salmon sperm DNA. (ii) Bright field images of MCF-7 cells treated with aptamers. Scale bar = 50 µm. (B) Normalised particle count from control MCF-7 cells treated with salmon sperm DNA and MCF-7 cells treated with aptamers selected against β1. A two-sample t-test was used to test for significance at each time point (**P < 0.01; *P< 0.05).

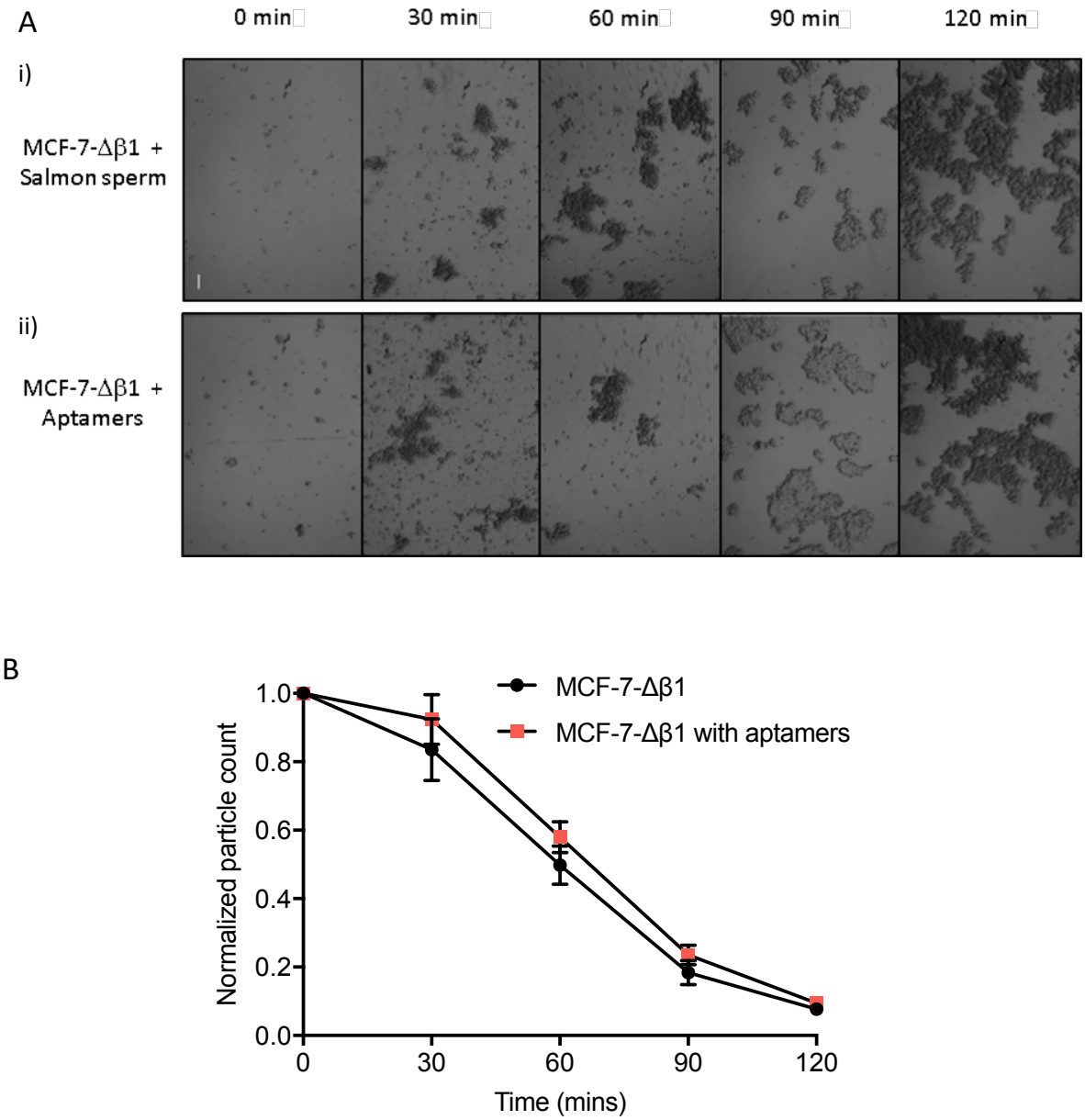

Figure 5.19 Effect of aptamers selected against β1 on adhesion of MCF-7-Δβ1 cells.

(A) Representative images of MCF-7-Δβ1 cells in an adhesion assay with aptamers. (i) Bright field images of control MCF-7-Δβ1 cells treated with salmon sperm DNA. (ii) Bright field images of MCF-7-Δβ1 cells treated with aptamers. Scale bar = 50 µm. (B) Normalised particle count from control MCF-7-Δβ1 cells treated with salmon sperm DNA and MCF-7-Δβ1 cells treated with aptamers. A two-sample t-test was used to test for significance at each time point ($P > 0.05$).

5.4. Discussion

It has been shown previously that β1 is up-regulated in breast cancer cells compared to normal breast tissue (Nelson *et al.*, 2014). In addition, over-expression of β1 increases mammary tumour growth and metastasis in mice (Nelson *et al.*, 2014). It has been proposed that β1 promotes tumour progression and metastasis via an adhesion-dependent mechanism, which increases mesenchymal-like neurite formation, promoting local invasion (Nelson *et al.*, 2014). The data in the preceding Chapters add to this body of evidence, showing that the Ig domain of β1 is critical for its adhesion function. Furthermore, the β1 Ig domain positively regulates Na^+ current in breast cancer cells. Given the critical role of VGSC-mediated Na^+ current in promoting tumour growth, invasion and metastasis (Nelson *et al.*, 2015), these data collectively suggest that the β1 Ig domain may be a useful target for inhibiting adhesion, process outgrowth, Na^+ current, and invasion. Therefore, there may be considerable therapeutic potential for compounds that could be produced to inhibit function of the β1 Ig domain, particularly to reduce tumour progression and metastasis. To address this possibility, the overarching goal of the experiments in this Chapter was to develop aptamers that could be used to inhibit β1 function.

The initial approach was to use the SELEX method, for which purified target protein is required (Blackwell & Weintraub, 1990; Charlton *et al.*, 1997; Manley, 2013). Several attempts were made to express and purify the soluble β1B splice variant from HEK293T cells, without success. Although β1BV5 was robustly expressed in the soluble fraction of cell lysates, many other His-rich proteins were also present when analysed by Coomassie stain, and it was not possible to isolate β1B by Ni^{2+} affinity purification. It has been shown previously that HEK293T cells contain a considerable number of His-rich proteins (Ohana *et al.*, 2011). However, the Ohana *et al.,* study should be interpreted with caution, as this study is promoting the Halo-tag purification method, a commercially available means of purifying proteins from cells. An alternative attempt, adding C-terminal His, CD4-His or F_C-His

fusion tags to increase secretion and then purifying secreted β1B from cell medium, was also unsuccessful. The addition of an F_c tag to constructs has previously been shown to result in secretion of the protein by solubilizing hydrophobic regions of proteins (Lo *et al.*, 1998; Czajkowsky *et al.*, 2012), however, in our case, secreted β1B was still below detectable levels. One explanation for this is a possible lack of expression of β1B. Whole cell expression was not tested with these constructs, so it was not possible to determine whether the cells were successfully transfected. Another explanation for the lack of detectable secreted protein, assuming that the constructs were being expressed, is that the protein was being overexpressed to such an extent that it became aggregated within the cells. This explanation is plausible given that β1 can adhere homophilically (Malhotra *et al.*, 2000), however, the possibility was not examined due to time constraints. Interestingly, another group was able to successfully express β1BV5 in CHL cells and purify it from conditioned medium using a Ni^{2+} column (Patino *et al.*, 2011). It is not clear why this attempt worked whereas ours did not. One possible explanation may lie with the different cell lines used. CHL cells, successfully used by Patino *et al.,* (2011) were not used for this project as the aim was to purify the protein from a human cell line, given that post-translational modifications may vary between cell line species, and that aptamers recognise target shape rather than protein sequence (Croset *et al.*, 2012). Given that purification of soluble β1B for SELEX was not feasible, despite considerable troubleshooting, it was decided to employ the cell-SELEX aptamer production approach instead.

5.4.1. Aptamer production using the cell-SELEX approach

Cell-SELEX, in which aptamers are selected using a cell line expressing the target protein of interest, can be improved through the addition of a negative selection step in which non-specific aptamers are removed using the same cell line lacking the protein of interest (Shangguan *et al.*, 2006). We used MCF-7 cells for cell-SELEX, given that this cell line expresses robust levels of β1 (Chioni *et al.*, 2009; Nelson *et al.*, 2014). However, it was also necessary to generate a β1-null MCF-7 cell line for

negative selection. The CRISPR/Cas9 system (Ran *et al.*, 2013) was used to mutate *SCN1B* in MCF-7 cells and a complete knock-out cell line was generated.

Cell-SELEX has been used in conjunction with fluorescent aptamers and FACS previously to eliminate dead cells during the selection process (Mayer *et al.*, 2010; Ohuchi, 2012). Removing dead cells results in the elimination of a considerable number of false positives, which reduces the number of cycles required (Mayer *et al.*, 2010). However, apoptotic cells may also act as a sink for aptamers, similar to dead cells, therefore also resulting in additional false positives. Thus, in our FACS approach, not only did we remove dead cells, but we also removed apoptotic cells based on TMRE uptake. A considerable number of apoptotic cells were present in the sorting steps, and if they were acting as sinks, binding aptamers non-specifically, they could have significantly reduced the specificity of selection of aptamers, dramatically reducing the efficiency of the cell-SELEX process. In the Mayer *et al.,* (2010) study, it is possible that at least some of the apoptotic cells were removed where the granularity was high. However, in our approach, the use of TMRE revealed that a large population of apoptotic cells remained after gating for abnormally large or granular cells. Also, surprisingly, the use of DRAQ-7 revealed that a relatively large population of dead cells remained after gating for size and granularity. Therefore, our data suggest that gating for size and granularity may not be a sufficient means to removing dead cells in FACS, and the addition of DRAQ-7 and TMRE dyes provide a refinement to this approach.

A thorough search of PubMed resulted in no papers reporting removal of apoptotic cells using a combination of dyes and FACS during cell-SELEX, suggesting that this approach is completely novel. Through the generation of the MCF-$\Delta\beta$1 cell line it was also possible to use subtractive cell-SELEX to enrich aptamers against β1. Combining the previous methods (Shangguan *et al.*, 2006; Mayer *et al.*, 2010) with the novel approach of removing apoptotic cells with the use of TMRE, and being more conservative by sorting only the top ~40% of the brightest healthy cells, resulted in a reduction in

the number of rounds typically required for aptamer selection from 10 rounds to 6, a significant improvement considering the time and costs required for aptamer selection (Mayer *et al.*, 2010). However, it is not possible to conclude whether it was the removal of the apoptotic cells or the more conservative selection of only the brightest cells, or both, which resulted in a decrease of the number of rounds.

The specificity of the aptamers amplified from the final round was tested using confocal microscopy. The aptamers bound to a much greater extent to MCF-7 cells than to MCF-7-$\Delta\beta1$ cells, consistent with specificity for $\beta1$. Further, the FITC signal from the aptamers was almost wholly present at the membrane, suggesting the aptamers were binding to surface proteins only. This distribution is consistent with previous studies showing high $\beta1$ expression at the plasma membrane (Brackenbury *et al.*, 2008a; Chioni *et al.*, 2009; Brackenbury *et al.*, 2010; Nelson *et al.*, 2014; Patel & Brackenbury, 2015). Very weak fluorescence in MCF-7-$\Delta\beta1$ cells suggests that there may have been some limited binding of some aptamers to other proteins. It is also possible that some aptamers were also binding to proteins which may have been upregulated in MCF-7-$\Delta\beta1$ cells following the knock-out of $\beta1$. For example, it has previously been shown that RNAi-mediated knock down of $\beta1$ expression in MCF-7 cells results in up-regulation of $Na_v1.5$ mRNA and protein (Chioni *et al.*, 2009). However, it is also possible that the signal present in micrographs of MCF-7-$\Delta\beta1$ cells was autofluorescence from those cells as opposed to FITC-modified aptamers, or indeed a combination of both. To select a sequence which binds specifically to $\beta1$, the next step will be to transform bacteria with individual sequences and then a small selection of these sequences will be amplified and tested individually for target specificity. This part of the project will be continued by another member of the lab.

5.4.2. A role for β1 regulating adhesion of MCF-7 cells

Knock-down of $\beta1$ significantly reduced the adhesion of MCF-7 cells. Similarly, the mixed population of $\beta1$-targeting aptamers amplified from the final round significantly reduced the adhesion of MCF-7

cells. These results suggest that (1) β1 promotes adhesion of MCF-7 cells, consistent with previous reports (Chioni *et al.*, 2009), and (2) the aptamers are binding to β1 to inhibit adhesion. Furthermore, it is highly likely that the aptamers are specific to β1 as they had no effect on MCF-7-Δβ1 cells. These findings are consistent with the data in Chapters 3 and 4 showing that the Ig loop of β1 regulates adhesion of MDA-MB-231 cells. The fact that β1 plays a similar role in two different breast cancer cell lines suggests that its functional contribution to adhesion may be a general phenomenon of breast tumours, rather than a cell-specific feature. It is also consistent with the fact that β1 is generally upregulated in clinical breast tumour specimens compared to normal tissue (Nelson *et al.*, 2014).

MDA-MB-231 cells are further along the EMT compared to MCF-7 cells, which are more epithelial-like (Shtutman *et al.*, 2006). The profile of CAMs changes as cells progress through EMT. Notably, E-cadherin expression is decreased, whereas L1CAM is increased (Shtutman *et al.*, 2006). N-cadherin expression is also increased as cells progress through EMT, and cadherin-11 was found to only be expressed in MDA-MB-231 cells (Nieman *et al.*, 1999). Thus, the heterophilic binding partners of β1 may change as cells go through EMT. Therefore, the significant decrease in adhesion of MCF-7-Δβ1 cells compared to MCF-7 cells may be due to either homophilic β1-β1 interactions, or heterophilic interactions between β1 and another CAM present in these cells, e.g. E-cadherin. Whether such an interaction exists remains to be determined and could be tested by screening fibroblast cell lines expressing possible binding partners using adhesion assays (McEwen & Isom, 2004; McEwen *et al.*, 2009). It is likely that both heterophilic and homophilic interactions are responsible for β1-dependent adhesion in breast tumours *in vivo*. Heterophilic interactions may occur between β1 and other CAMs, including integrin-β1, hepaCAM, and NCAM, which have also been shown to be expressed in MCF-7 cells (Takahashi, 2001; Moh *et al.*, 2008). An additional possibility is that β1 knock-out in MCF-7 cells may result in an altered expression profile of CAMs, which in turn could also explain the decreased adhesion. Such a scenario would be consistent with the data in Chapter 4

showing that β1 overexpression in MDA-MB-231 cells increased L1CAM expression, and β1 expression increased in MDA-MB-231 cells overexpressing L1CAM. An intriguing possibility is that knocking-out β1 expression in MCF-7 may concurrently silence L1CAM expression. Further work is required to evaluate these potential interactions across different breast cancer cell lines.

5.4.3. Conclusion

The production of aptamers targeting β1 in this Chapter has important implications. Firstly, they may prove to be a more specific alternative to currently available β1-targeting antibodies, many of which are polyclonal and of variable quality. An improved tool to label and visualise β1 in tissue may be useful for deepening understanding of β1 expression in breast tumours and in studies of epilepsy linked to abnormal or mutant β1 expression (Chioni *et al.*, 2009; Nelson *et al.*, 2014; Kruger *et al.*, 2016). Secondly, since the aptamers appear to disrupt adhesion, and as β1 increases breast cancer metastasis via an adhesion-dependent mechanism (Chioni *et al.*, 2009; Nelson *et al.*, 2014), these aptamers may also have therapeutic value. Thirdly, given that some of the β1 aptamers appeared to be internalised in MCF-7 cells, they may also have value for delivery of small molecule therapeutics to the intracellular space. The next step would be to test this possibility in a mouse model. Finally, the refinements made to the cell-SELEX approach should be of interest to others working in this field: the addition of vital dyes to remove both dead and apoptotic cells after gating for abnormal size or granularity, alongside stricter gating parameters, results in a more efficient, quicker selection process that may yield considerable cost savings during aptamer production.

6. Discussion

6.1. The knowledge gap

The overarching aim of this project was to understand the role of the Ig loop in both the channel modulating and cell adhesion functions of the VGSC β1 subunit and to select a set of aptamers which would inhibit these β1-mediated functions. Developing new strategies to target β1 function is relevant because VGSC α and β subunits are known to potentiate metastatic behaviours, such as migration and invasion, in a range of cancers (Roger *et al.*, 2003; Brackenbury *et al.*, 2007; Roger *et al.*, 2007; Chioni *et al.*, 2009; House *et al.*, 2010; Campbell *et al.*, 2013; Nelson *et al.*, 2014; Nelson *et al.*, 2015; Roger *et al.*, 2015).

In a range of models focusing primarily on excitable cells, e.g. neurons, β subunits have specifically been shown to regulate α subunit gating and kinetics (Isom *et al.*, 1992), mRNA levels (Kim *et al.*, 2007), and trafficking (Thomas *et al.*, 2007), as well as cell adhesion (Malhotra *et al.*, 2000), neurite outgrowth and pathfinding (Davis *et al.*, 2004; Brackenbury *et al.*, 2008a). More recently, a growing body of evidence indicates that β subunits also play similar roles in cancer cells (Adachi *et al.*, 2004; Diss *et al.*, 2008; Chioni *et al.*, 2009; Hernandez-Plata *et al.*, 2012; Nelson *et al.*, 2014; Bon *et al.*, 2016). However, whilst recent work shows that β1 expression in breast cancer cells facilitates the development of a metastatic phenotype (Nelson *et al.*, 2014), it remains unclear what specific role the Ig loop plays in this process. If the Ig loop is instrumental in β1-mediated cancer progression, it may serve as a valuable therapeutic target in inhibiting invasion or metastasis.

6.2. The Ig loop is critical for β1 function

Ever since the initial discovery of β1 (Isom *et al.*, 1992), the Ig loop was assumed to be central to its function. Indeed, studies in heterologous cells have shown that the extracellular domain is critical both for mediating adhesion and regulating Na^+ current (Isom & Catterall, 1996; McCormick *et al.*,

1998; Malhotra *et al.*, 2000; Meadows *et al.*, 2002; McEwen *et al.*, 2004). Furthermore, although studies have shown that residues outside of the Ig loop are also involved in regulating the α subunit, they still require the presence of the Ig loop for correct orientation and function (McCormick *et al.*, 1998). The data presented in this Thesis broadly agree with these observations. Overexpressing β1-GFP or β1-V5 increased both Na^+ current density and adhesion in MDA-MB-231 cells, consistent with previous findings in this cell line (Chioni *et al.*, 2009). Deletion of the Ig domain blocked the adhesion and Na^+ current-promoting properties of β1 in MDA-MB-231 cells, which is, again, consistent with previous observations in heterologous cells (McCormick *et al.*, 1998; Malhotra *et al.*, 2000; Malhotra *et al.*, 2002; Malhotra *et al.*, 2004). Together, these data indicate that in MDA-MB-231 cells, as in other cell models, the β1 Ig domain is critical to sustain the function of β1 as a CAM and as a potentiator of Na^+ current.

As the Ig loop contains at least one disulphide bridge, it is possible that a change in the number of cysteines present in the Ig loop may impact on the structure and therefore affect proper β1 function. Indeed, the inherited mutations C121W, and R85C are associated with epilepsy (Meadows *et al.*, 2002; Scheffer *et al.*, 2007; Thomas *et al.*, 2007; Wimmer *et al.*, 2010; Kruger *et al.*, 2016). It is likely that these mutations result in improper folding of the Ig domain, and as a result, cause impaired channel modulation (Meadows *et al.*, 2002; Scheffer *et al.*, 2007; Thomas *et al.*, 2007; Wimmer *et al.*, 2010; Kruger *et al.*, 2016). Additionally, the R85C and R85H mutations impair trafficking of β1 to the plasma membrane (Thomas *et al.*, 2007; Xu *et al.*, 2007). This Thesis investigated the effect of the R89C somatic mutation identified in a lung tumour. Similar to the above heritable epileptogenic mutations, R89C resulted in a null phenotype in MDA-MB-231 cells, showing similar electrophysiological and adhesive profiles to negative control MDA-MB-231 cells not overexpressing β1. Although the structural impact of this mutation is not known, *In silico* analysis predicted a potentially incorrectly folded Ig loop, and western blot analysis demonstrated that the mutant β1 subunit had a reduced MW. The phenotypic similarities between the β1 Ig domain deletion mutant

and the R89C mutant highlight the importance of a correctly folded Ig loop for normal β1 function. The results also suggest that if R89C were present in neurons, this mutation would give rise to an epileptogenic phenotype.

The R89C mutation abrogated the adhesive function of β1 in MDA-MB-231 cells, inhibited β1 localisation to the plasma membrane, and also inhibited β1-mediated process outgrowth. These data thus support the notion that the mutation disrupts proper folding of the Ig domain, rendering it non-functional. These results are broadly similar to those described for the epileptogenic C121W mutation, which disrupts adhesion function (Meadows *et al.*, 2002; Wimmer *et al.*, 2010; Kruger *et al.*, 2016). However, one interesting difference is that The C121W mutant is expressed at the plasma membrane (Wimmer *et al.*, 2015; Kruger *et al.*, 2016). On the other hand, the R85C and R85H mutants are not expressed at the plasma membrane (Xu *et al.*, 2007). Given that the R89C-mutated β1 was not present at the membrane in MDA-MB-231 cells it is possible that the β1 mutant lacking the Ig domain was also not expressed at the plasma membrane, although this was not tested directly. Together, these results suggest that although C121 is critical for proper adhesion and channel modulating properties of β1, R85 and R89 play an additional role in regulating β1 externalisation and/or stabilisation at the plasma membrane. Correct plasma membrane expression and/or localisation is, in turn, required for β1-mediated regulation of the α subunit and adhesion. Further work is required to establish the mechanistic basis of this plasma membrane expression.

Over-expression of β1 constructs and mutants, together with the use of various pharmacological tools, elicited diverse effects on channel gating and kinetics, described in detail in the Results Chapters. In general, there was very little consistency between these effects. This lack of consistency reflects considerable contradictions in the field with respect to the effect of β1 on VGSC gating (Brackenbury & Isom, 2011). As regards the inconsistent gating and kinetic data presented in this Thesis, technical issues, e.g. inadequate series resistance compensation in some experiments, may

have played a role. In addition, there may have been compensatory up or down-regulation of other β subunits in MDA-MB-231 cells in response to overexpression of wild-type and mutant β1 subunits and/or pharmacological perturbations. A shortcoming of the studies presented here is that the expression of the other β subunits was not monitored. Further work is required to evaluate whether changes in endogenous β subunit expression could explain some of the variation in the gating and kinetics data.

6.3. Cleavage-dependent upregulation of $Na_V1.7$ and the possible role of L1CAM

It is likely that the presence of a properly folded Ig loop extends its influence on other regions of the β1 subunit. Indeed, the Ig loop has been shown to be required for correct orientation and function (McCormick *et al.*, 1998). In support of this, γ-secretase inhibition decreased Na^+ current when the Ig loop was present but had no effect on cells expressing the β1 mutant lacking the Ig domain. The cleavage site for γ-secretase on β1 is present intracellularly and therefore in a physically separate compartment to the Ig loop (Wong *et al.*, 2005). The prevailing model for secretase-mediated processing of β subunits involves sequential cleavage, firstly of the Ig domain by α secretase/BACE1, followed by cleavage of the intracellular domain by γ secretase (Kim *et al.*, 2005; Kim *et al.*, 2007). Thus, this result suggests that absence of the Ig domain would disrupt the sequential cleavage process by secretase enzymes. Given that the C121W, R85C/H and R89C mutations inhibit the β1-mediated increase in Na^+ current density, an interesting possibility is that some or all of these mutations might disrupt secretase cleavage. The pharmacological data presented in this Thesis are consistent with β1 over-expression in turn promoting plasma membrane levels of $Na_v1.7$. Furthermore, treatment with DAPT suggests that γ-secretase-mediated cleavage of β1 is required for the increase in Na^+ current. Taken together with previous reports (Kim *et al.*, 2005; Wong *et al.*, 2005; Kim *et al.*, 2007), these findings suggest that proteolytic release of the β1 intracellular domain may be required to regulate functional $Na_v1.7$ expression at the plasma membrane.

Given that the β2 intracellular domain has been shown to accumulate in the nucleus and regulate $Na_v1.1$ mRNA levels (Kim *et al.*, 2007), this raises the possibility that the β1 intracellular domain may function in a similar fashion to regulate $Na_v1.7$ expression (Figure 6.1). Interestingly, other studies have shown that β1 can also regulate the mRNA level of $Na_v1.5$ (Lopez-Santiago *et al.*, 2007; Chioni *et al.*, 2009). However, it is still not known how β subunit intracellular domains are transported to the nucleus, or whether they have any intrinsic transcription-regulating function. Indeed, the absence of any putative nucleus localisation sequence in β subunit intracellular domains suggests that if they are indeed transported to the nucleus to interact with transcription machinery this must be as part of a larger complex.

While it is tempting to assume that a similar mechanism to that observed by (Kim *et al.*, 2007) is taking place in the MDA-MB-231-β1-GFP cells, caution should be taken with this interpretation. γ-secretase is likely to have multiple cleavage targets within breast cancer cells, and so its inhibition may affect the function and fate of a number of different proteins. It is possible that one or more of these other proteins or pathways may contribute to $Na_V1.7$ regulation. In this regard, L1CAM is an interesting target. L1CAM is a substrate for γ-secretase cleavage (Kiefel *et al.*, 2012a). In addition,

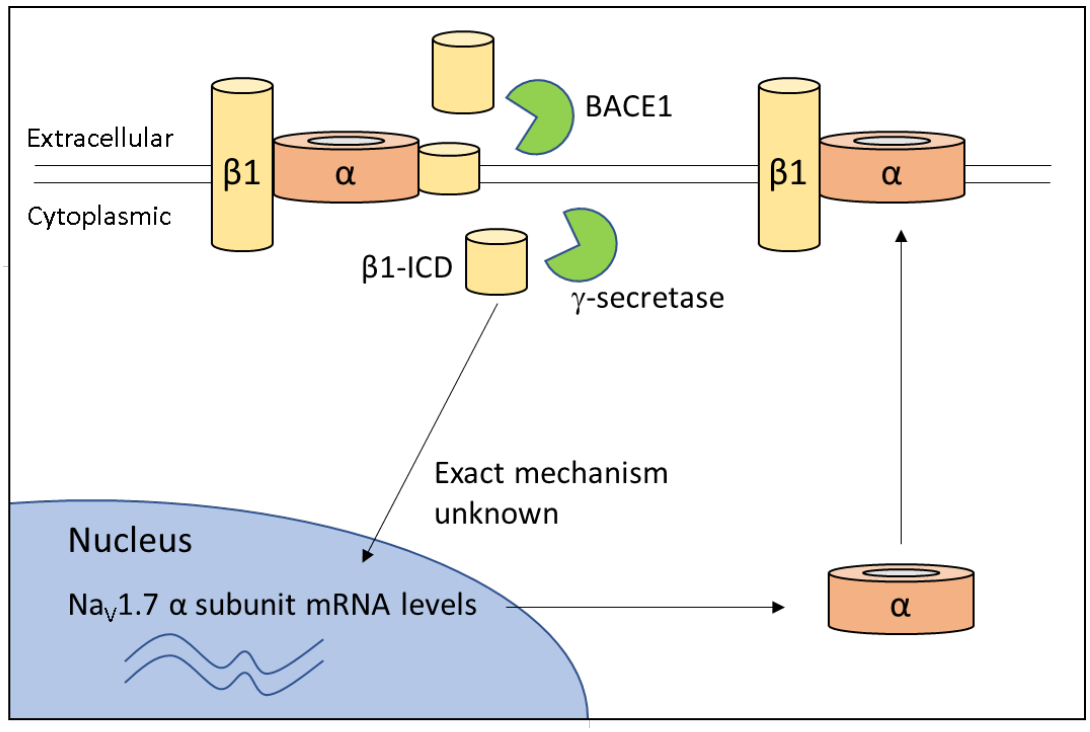

Figure 6.1 Possible mechanism for β1-mediated increase in Na$_V$1.7 expression in MDA-MB-231 cells.

BACE1 and then γ-secretase sequentially cleave the extracellular and intracellular domains of β1. The intracellular domain (ICD) then translocates to the nucleus and increases mRNA level of Na$_V$1.7 via an unidentified transcriptional mechanism. This then results in elevated Na$_V$1.7 expression at the plasma membrane and therefore an increased Na^+ current. Figure adapted from Kim *et al*. (2007).

the NOVA-2-regulated full-length splice variant of L1CAM, which is expressed in breast cancer cells (Shtutman *et al.*, 2006), is increased following β1 over-expression. L1CAM can bind and activate EGFR in HEK293 cells (Donier *et al.*, 2012) and a separate study has shown that activation of the ERK1/2 pathway by EGFR increases Na$_V$1.7 expression in H460 non-small cell lung cancer cells (Campbell *et al.*, 2013), thus providing a potential mechanistic link between L1CAM, EGFR activation and Na$_V$1.7 regulation. L1CAM has also been shown to increase Na^+ current in cultured hippocampal neurons, supporting such a hypothesis (Valente *et al.*, 2016). However, overexpression of L1CAM in MDA-MB-231 cells did not alter the Na^+ current. This result may suggest that L1CAM is not involved in Na$_V$1.7 regulation in MDA-MB-231 cells. Alternatively, the situation may be more complex and dependent on other factors, e.g. endogenous expression of functionally distinct L1CAM splice variants (Shtutman *et al.*, 2006; Mikulak *et al.*, 2012).

The presence of a higher weight L1CAM band in MDA-MB-231-β1-GFP cells suggests that the NOVA-2 variant of L1CAM is being expressed in these cells. If the NOVA-2 splice variant of L1CAM is present in MDA-MB-231-β1-GFP cells, this may explain the results observed. For example, γ-secretase-mediated cleavage of the NOVA-2 variant of L1CAM may be responsible for the increase in $Na_V1.7$ expression in MDA-MB-231-β1-GFP cells, via binding of L1CAM to EGFR (Figure 6.2) (Donier *et al.*, 2012). It is unclear which variant of L1CAM was silenced in the Valente *et al.,* (2016) study, leading to a decrease in Na^+ current. However, it is probable that the NOVA-2 variant was silenced as primary cultures of hippocampal and cortical neurones were used, and this variant is highly expressed in CNS neurones (Mikulak *et al.*, 2012). Although this is not the first study to hypothesize a link between EGFR activation and $Na_V1.7$ expression (Campbell *et al.*, 2013), in the model proposed here, the NOVA-2 variant of L1CAM is responsible for the activation of EGFR.

Interestingly, β1 expression was increased when L1CAM was overexpressed, and reciprocally, L1CAM expression was increased when β1 was overexpressed. This bidirectional co-dependence of β1/L1CAM expression raises an important question over the interpretation of the β1-mediated adhesion experiments. In line with previous studies (Malhotra *et al.*, 2000; Davis *et al.*, 2004), it has been assumed that the increase in cell-cell adhesion in MDA-MB-231 cells overexpressing β1 is due to β1-mediated *trans*-homophilic adhesion interactions (Chioni *et al.*, 2009; Nelson *et al.*, 2014). However, given that L1CAM expression was also elevated, an alternative possibility is that L1CAM itself may have been, at least in part, responsible for the observed increase in cell-cell adhesion. Furthermore, L1CAM-mediated increase in adhesion could occur either homophilically or heterophilically through direct interaction with β1. Further work is required to establish whether L1CAM and β1 interact with each other heterophilically through their Ig loops to increase adhesion. Whichever mode of interaction is responsible, it can be concluded that the Ig loop of β1 is required for adhesion, either directly, indirectly through upregulation of other CAMs, or both.

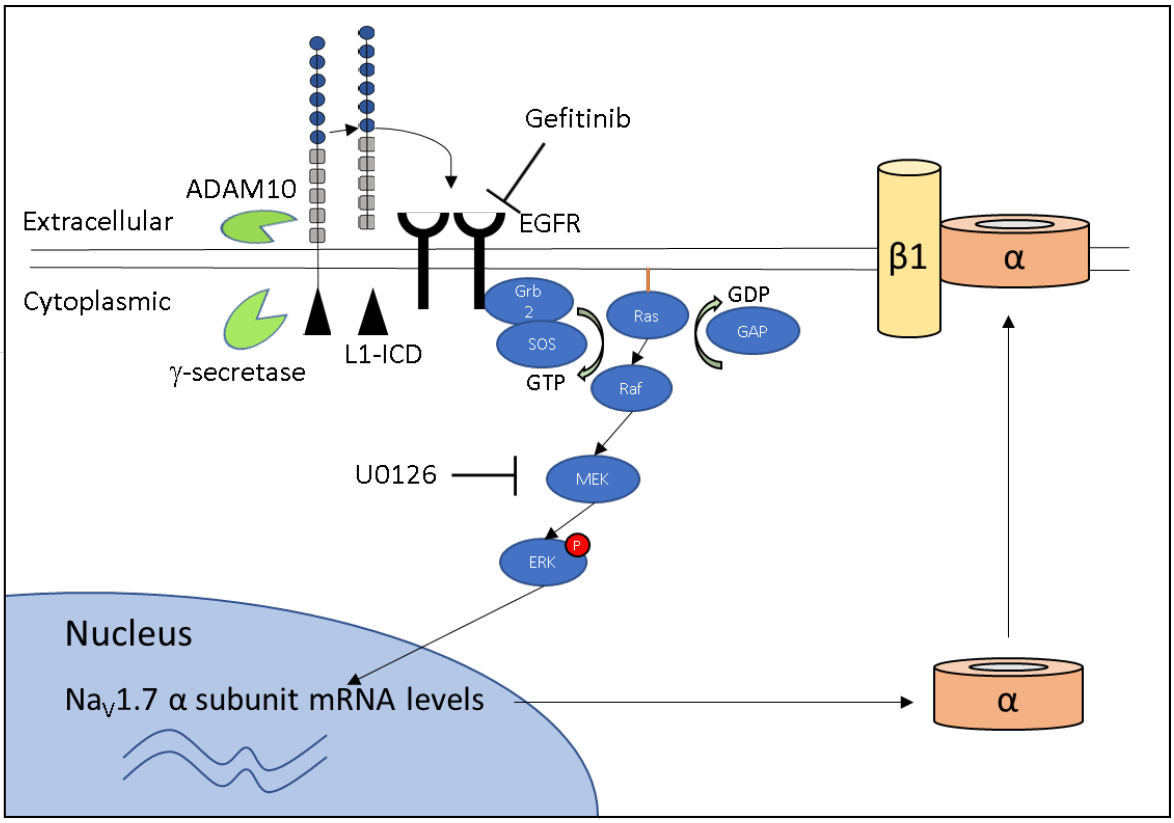

Figure 6.2 Possible mechanism of L1CAM-mediated increase in $Na_V1.7$ in MDA-MB-231 cells.

γ-secretase cleaves the intracellular domain of L1CAM and ADAM10 cleaves the extracellular domain. The extracellular soluble domain of L1CAM binds and activates the EGFR. EGFR activation results in an increase in $Na_V1.7$ mRNA levels through the ERK1/2 pathway which results in $Na_V1.7$ expression at the membrane and therefore an increased Na^+ current.

It is generally assumed that VGSC activity increases intracellular Na^+ in breast cancer cells, which in turn promotes invasion through activation of NHE1 (Brisson *et al.*, 2013). However, it is unclear whether the increased invasion and metastasis observed *in vivo* as a result of overexpression of β1 (Nelson *et al.*, 2014) is through β1 increasing Na^+ current, adhesion, or a combination of both. Although the experiments presented in this Thesis do not resolve this issue, they do provide potential insight into how β1 may function *in vivo*. Importantly, the results suggest that the Ig domain may play a critical role in β1-mediated promotion of metastasis and thus somatic mutations in this region may provide value as prognostic markers for recurrence and disease-free survival. In

addition, given that β1 and L1CAM both promote angiogenesis (Friedli *et al.*, 2009; Nelson *et al.*, 2014), improved understanding of the expression and reciprocal function of both proteins may uncover new biomarkers or therapeutic targets.

6.4. Therapeutic value of targeting β1 function with aptamers

The data in Chapter 3 demonstrating that the Ig loop is required for increasing adhesion, $Na_V1.7$ expression and Na^+ current density, which may, in turn promote a more metastatic phenotype (Gillet *et al.*, 2009; Brisson *et al.*, 2013; Nelson *et al.*, 2014; Nelson *et al.*, 2015), highlight the potential therapeutic value of aptamers targeting β1. Aptamers are proving to be a valuable new tool in the arsenal of therapeutics for a range of diseases (Orava *et al.*, 2013) in addition to their role as diagnostic tools (Santosh & Yadava, 2014). Indeed, aptamers are being selected against a various targets in cancer cells and can be used to distinguish between the same proteins expressed in cancer and non-cancer cells based on differences in post-translational modifications and folding (Sett *et al.*, 2017). They are desirable tools given the inexpensive production process and the fact that no specialised equipment is required for development post selection (Lakhin *et al.*, 2013). In Chapter 5, *in vitro* cell-SELEX was employed to produce aptamers targeting β1, and this presented the opportunity of introducing additional steps with the aim of improving the efficiency of selection and thereby reducing the number of selection rounds required. The use of FACS to remove dead and apoptotic cells, in addition to stricter gating criteria, permitted a decrease in the number of cycles from a typical ten rounds to only six. This approach has not been attempted before and is completely novel.

The results in Chapter 3 characterised the Ig loop as a potential unutilised anti-metastatic target. Antibodies targeting the Ig loop of β1 slightly but significantly reduced β1-mediated cell-cell adhesion. The β1-targeting aptamers selected in Chapter 5 were far more potent and significantly

reduced adhesion in MCF-7 cells. This suggests that the aptamers may display a greater inhibitory effect and may play a suitable role in therapeutics or as a diagnostic tool. In addition to their potential value in the oncology setting, aptamers targeting the β1 Ig loop may prove useful in limiting pathology in other conditions where aberrant β1/β1B expression may be involved. Further work is required to test these possibilities.

One potential issue with the cell-SELEX aptamer production approach used here relates to the observation discussed above that β1 and L1CAM expression were both increased when the other protein was overexpressed. Thus, it is possible that silencing β1 expression in MCF-7 cells may have resulted in a change in expression of another CAM or membrane protein, e.g. L1CAM. If such a scenario occurred as a result of silencing of β1 in MCF-7 cells, this may be problematic because some of the aptamers selected may be targeting this up-regulated membrane protein. Clearly, this possibility needs to be tested as a priority when these aptamers are further characterised.

6.5. Future work

The work presented in this Thesis highlights the Ig loop of β1 as a possible therapeutic target in breast cancer. At the same time, it raises new questions about previous studies. Avenues for future work based on this Thesis are as follows:

- A large part of the work demonstrates, unequivocally, that β1 overexpression in MDA-MB-231 cells increases $Na_V1.7$ expression and this requires both the Ig loop and γ-secretase-mediated cleavage. However, the exact downstream mechanism and whether it is cleavage of β1 or another protein that results in $Na_V1.7$ expression remains unknown. If the ICD of β1 is involved in $Na_V1.7$ upregulation as suggested in Figure 6.1, then overexpression of this region alone should show a similar increase in $Na_V1.7$ expression. If EGFR is involved in $Na_V1.7$ upregulation as suggested in Figure 6.2, then inhibition of EGFR with gefitinib

followed by inhibition of specific downstream components of EGFR-mediated signalling pathways would provide a more robust picture of the signalling mechanism.

- Given that L1CAM has been shown to increase invasion (Cavallaro & Christofori, 2004), it is reasonable to hypothesize that it may interact with β1 in breast cancer cells to co-operatively regulate adhesion, process outgrowth and invasion. Stable knock-down of L1CAM ± β1 can be used to evaluate effects on adhesion, cellular morphology and invasion (Chioni *et al.*, 2009). It has been shown that L1CAM is not expressed in COS-7 cells (Colombo *et al.*, 2014) but the data in this Thesis show that it is expressed in MDA-MB-231 cells. Therefore, COS-7 cells can be stably transfected to overexpress L1CAM, and it could be silenced in MDA-MB-231 cells using shRNA. Using these cell lines, it would then be possible to assess whether growing breast cancer cells on COS-7 cells expressing L1CAM or β1 increases process outgrowth.
- The potential co-operative roles of β1 and L1CAM in regulating tumour growth and metastasis can be investigated *in vivo* using murine xenografts (Nelson *et al.*, 2014). The increased L1CAM expression in MDA-MB-231-β1-GFP cells allows for new interpretation of previous results (Nelson *et al.*, 2014). Increased invasion and metastasis and decreased apoptosis, previously attributed to β1, may instead be explained by L1CAM or interaction between both CAMs.
- With respect to the aptamers produced, the next step will be to sequence possible candidates from the current mixed population and determine the best binding sequence through cell-based process outgrowth and adhesion assays. Following these *in vitro* experiments, the aptamers should be tested for anti-metastatic efficacy *in vivo.* A suitable model would be the β1-overexpressing MDA-MB-231 xenograft model used previously (Nelson *et al.*, 2014). It will first be necessary to determine a suitable delivery method for the aptamers, e.g. intraperitoneal injection and a suitable tolerable, non-toxic dosage regimen using dose escalation studies (Rosenberg *et al.*, 2014). As cells are able to

internalise aptamers relatively quickly (McNamara *et al.*, 2006), sustained local administration may be a more viable method.

6.6. Conclusion

The role of VGSCs in the development of metastatic breast cancer is well documented and functions for both the pore-forming α subunit and the auxiliary β1 subunit have been established previously. However, the tumour-promoting role of the Ig loop of β1 has not been studied. This Thesis has shown that the Ig loop possesses dual functions, increasing adhesion and Na^+ influx via $Na_V1.7$ in breast cancer cells *in vitro*. In both cases, the downstream consequences of these functions have been shown by others to facilitate an increase in metastatic potential. Therefore, the Ig loop of β1 represents an interesting target for possible therapeutic intervention to inhibit invasion and metastasis. The aptamers selected in this project may therefore have therapeutic value. Further, it may be possible to use aptamers targeting β1 as a diagnostic or experimental tool in a manner akin to antibodies.

Abbreviations

ADAM-10: A distintegrase and metalloproteinase

AmpR: Ampicillin resistance

ANOVA: Analysis of variance

APC: Allophycocyanin

BACE1 – β-secretase

BCa: Breast cancer

BSA: Bovine serum albumin

CAM: Cell adhesion molecule

CAF: Cancer associated fibroblast

CCD: Charge-coupled device

CD(XX): Cluster of differentiation

CEA: Carcinoembryonic antigen

CGN: cerebellar granule neurones

CHL: Chinese hamster lungs

CMV: Cytomegalovirus

CNS: Central nervous system

COSMIC: Catalogue of somatic mutations in cancer

CRISPR: Clustered Regularly Interspaced Short Palindromic Repeats

CSC: Cancer stem cell

DAPT: N-[N-(3,5-Difluorophenacetyl)- L -alanyl]-S-phenylglycine t-butyl Ester

DI:S3: Domain I segment 3

DMEM: Dulbecco's modified eagle medium

DMSO: Dimethyl sulfoxide

ECM: Extracellular matrix

EDTA Ethylenediaminetetraacetic acid

EGF: Epidermal growth factor

EGFR: Epidermal growth factor receptor

(e)GFP: Enhanced green fluorescent protein

EGTA: ethylene glycol-bis(β-aminoethyl ether)

EMT: Epithelial to mesenchymal transition

ENC: Extracellular negatively-charged cluster

EpCAM: Epithelial cell adhesion molecule

ER: Estrogen receptor

ERK: Extracellular signal-regulated kinase

FACS: Fluorescent activated cell sorting

FGFR1: Fibroblast growth factor receptor 1

FITC: Fluorescein isothiocyanate

FN: Fibronectin

GAPDH: Glyceraldehyde 3-phosphate dehydrogenase

GEFS+: Genetic epilepsy with febrile seizures plus

gRNA: Guide RNA

HCS: Hydrophobic constriction site

HEK: Human embryonic kidney

HEPES: 4-(2-hydroxyethyl)-1-piperazineethanesulfonic acid

HER-2: Herceptin epidermal growth factor receptor /Receptor tyrosine-protein kinase erbB2

HygR: Hygromycin resistance

ICD: Intracellular domain

Ig immunoglobulin

INC: Intracellular negatively-charged cluster

I_p: Peak current density

IPTG: Isopropyl β-D-1-thiogalactopyranoside

IPS: Intracellular pipette solution

IV: Current-voltage

k: slope factor

MCF: Michigan cancer foundation

MEF: Mouse embryo fibroblast

MINT3: Munc-18-1 interacting protein

MW: Molecular weight

NeoR: Neomycin resistance

NGF: Nerve growth factor

NHE: Na^+/H^+ exchanger

NIH: National Institutes of Health

NOVA-2: Neurooncological ventral antigen 2

OPPF: Oxford protein production facility

PB: Phosphate buffer

PBS: Phosphate buffered saline

PE: Phycoerythrin

PEI: Polyethylimine

PF: PF-04856042 – Selective $Na_V1.7$ blocker

PFA: Paraformaldehyde

PKA: Protein kinase A

PNGase F: Peptide-N-Glycosidase F

PR:P Progesterone receptor

PSS: Physiological saline solution

QPCR: Quantitative PCR

REST: Repressor element-1 silencing transcription factor

RPTPβ: Receptor tyrosine phosphatase β

SDS: Sodium dodecyl sulphate

SELEX: Systematic evolution of ligands by exponential enrichment

SSI: Steady state inactivation

SV40: Simian virus 40

TALEN: Transcription activator-like effector nucleases

TBST: Tris-buffered saline with tween

TEMED: Tetramethylethylenediamine

TLE: Temporal lobe epilepsy

TM: Transmembrane

TMRE: Tetraethylrhodamine ethyl ester

TNBC: Triple negative breast cancer

T_p: time to peak

TTX: Tetrodotoxin

$V_{1/2}$: half (in)activation voltage

V_a: activation voltage

VEGF: Vascular endothelial growth factor

VGSC: Voltage-gates sodium channel

V_m: Membrane potential

V_p: voltage at current peak

$V_{rev+:}$ Reversal potential

VSD: Voltage sensing domain

WGA: Wheat germ agglutinin

ZFN: Zinc-finger nucleases

References

Abdul M & Hoosein N. (2001). Inhibition by anticonvulsants of prostate-specific antigen and interleukin-6 secretion by human prostate cancer cells. *Anticancer Res* **21,** 2045-2048.

Abdul M & Hoosein N. (2002). Voltage-gated sodium ion channels in prostate cancer: expression and activity. *Anticancer Res* **22,** 1727-1730.

Adachi K, Toyota M, Sasaki Y, Yamashita T, Ishida S, Ohe-Toyota M, Maruyama R, Hinoda Y, Saito T, Imai K, Kudo R & Tokino T. (2004). Identification of SCN3B as a novel p53-inducible proapoptotic gene. *Oncogene* **23,** 7791-7798.

Ahern CA. (2013). What activates inactivation? *The Journal of general physiology* **142,** 97-100.

Aman TK, Grieco-Calub TM, Chen C, Rusconi R, Slat EA, Isom LL & Raman IM. (2009). Regulation of persistent Na current by interactions between beta subunits of voltage-gated Na channels. *J Neurosci* **29,** 2027-2042.

An RH, Wang XL, Kerem B, Benhorin J, Medina A, Goldmit M & Kass RS. (1998). Novel LQT-3 mutation affects Na+ channel activity through interactions between alpha- and beta1-subunits. *Circ Res* **83,** 141-146.

Bagal SK, Marron BE, Owen RM, Storer RI & Swain NA. (2015). Voltage gated sodium channels as drug discovery targets. *Channels (Austin, Tex)* **9,** 360-366.

Baird RD & Caldas C. (2013). Genetic heterogeneity in breast cancer: the road to personalized medicine? *BMC medicine* **11,** 151.

Beckh S, Noda M, Lubbert H & Numa S. (1989). Differential regulation of three sodium channel messenger RNAs in the rat central nervous system during development. *EMBO J* **8,** 3611-3616.

Bennett ES, Smith BA & Harper JM. (2004). Voltage-gated Na+ channels confer invasive properties on human prostate cancer cells. *Pflugers Arch* **447,** 908-914.

Betz SF. (1993). Disulfide bonds and the stability of globular proteins. *Protein science : a publication of the Protein Society* **2,** 1551-1558.

Black JA, Dib-Hajj S, Baker D, Newcombe J, Cuzner ML & Waxman SG. (2000). Sensory neuron-specific sodium channel SNS is abnormally expressed in the brains of mice with experimental allergic encephalomyelitis and humans with multiple sclerosis. *Proc Natl Acad Sci U S A* **97,** 11598-11602.

Blackwell TK & Weintraub H. (1990). Differences and similarities in DNA-binding preferences of MyoD and E2A protein complexes revealed by binding site selection. *Science* **250,** 1104-1110.

Bodding M. (2007). TRP proteins and cancer. *Cellular signalling* **19,** 617-624.

Boiko T, Rasband MN, Levinson SR, Caldwell JH, Mandel G, Trimmer JS & Matthews G. (2001). Compact myelin dictates the differential targeting of two sodium channel isoforms in the same axon. *Neuron* **30,** 91-104.

Boiko T, Van Wart A, Caldwell JH, Levinson SR, Trimmer JS & Matthews G. (2003). Functional specialization of the axon initial segment by isoform-specific sodium channel targeting. *J Neurosci* **23,** 2306-2313.

Bon E, Driffort V, Gradek F, Martinez-Caceres C, Anchelin M, Pelegrin P, Cayuela ML, Marionneau-Lambot S, Oullier T, Guibon R, Fromont G, Gutierrez-Pajares JL, Domingo I, Piver E, Moreau A, Burlaud-Gaillard J, Frank PG, Chevalier S, Besson P & Roger S. (2016). SCN4B acts as a metastasis-suppressor gene preventing hyperactivation of cell migration in breast cancer. *Nat Commun* **7,** 13648.

Brackenbury WJ. (2012). Voltage-gated sodium channels and metastatic disease. *Channels (Austin)* **6,** 352-361.

Brackenbury WJ, Calhoun JD, Chen C, Miyazaki H, Nukina N, Oyama F, Ranscht B & Isom LL. (2010). Functional reciprocity between Na+ channel Nav1.6 and β1 subunits in the coordinated regulation of excitability and neurite outgrowth. *Proc Natl Acad Sci U S A* **107,** 2283-2288.

Brackenbury WJ, Chioni AM, Diss JK & Djamgoz MB. (2007). The neonatal splice variant of Nav1.5 potentiates in vitro invasive behaviour of MDA-MB-231 human breast cancer cells. *Breast Cancer Res Treat* **101,** 149-160.

Brackenbury WJ, Davis TH, Chen C, Slat EA, Detrow MJ, Dickendesher TL, Ranscht B & Isom LL. (2008a). Voltage-gated Na+ channel β1 subunit-mediated neurite outgrowth requires fyn kinase and contributes to central nervous system development in vivo. *J Neurosci* **28,** 3246-3256.

Brackenbury WJ & Djamgoz MB. (2006). Activity-dependent regulation of voltage-gated Na+ channel expression in Mat-LyLu rat prostate cancer cell line. *J Physiol* **573,** 343-356.

Brackenbury WJ & Djamgoz MB. (2007). Nerve growth factor enhances voltage-gated Na+ channel activity and Transwell migration in Mat-LyLu rat prostate cancer cell line. *J Cell Physiol* **210,** 602-608.

Brackenbury WJ, Djamgoz MB & Isom LL. (2008b). An emerging role for voltage-gated Na+ channels in cellular migration: regulation of central nervous system development and potentiation of invasive cancers. *Neuroscientist* **14,** 571-583.

Brackenbury WJ & Isom LL. (2008). Voltage-gated Na+ channels: potential for beta subunits as therapeutic targets. *Expert Opin Ther Targets* **12,** 1191-1203.

Brackenbury WJ & Isom LL. (2011). Na Channel beta Subunits: Overachievers of the Ion Channel Family. *Front Pharmacol* **2,** 53.

Brackenbury WJ, Yuan Y, O'Malley HA, Parent JM & Isom LL. (2013). Abnormal neuronal patterning occurs during early postnatal brain development of Scn1b-null mice and precedes hyperexcitability. *Proc Natl Acad Sci U S A* **110,** 1089-1094.

Brisson L, Driffort V, Benoist L, Poet M, Counillon L, Antelmi E, Rubino R, Besson P, Labbal F, Chevalier S, Reshkin SJ, Gore J & Roger S. (2013). NaV1.5 Na(+) channels allosterically regulate the NHE-1 exchanger and promote the activity of breast cancer cell invadopodia. *J Cell Sci* **126,** 4835-4842.

Brisson L, Gillet L, Calaghan S, Besson P, Le Guennec JY, Roger S & Gore J. (2011). Na(V)1.5 enhances breast cancer cell invasiveness by increasing NHE1-dependent H(+) efflux in caveolae. *Oncogene* **30,** 2070-2076.

Brodie MJ. (2017). Sodium Channel Blockers in the Treatment of Epilepsy. *CNS drugs* **31,** 527-534.

Brookes E, Laurent B, Ounap K, Carroll R, Moeschler JB, Field M, Schwartz CE, Gecz J & Shi Y. (2015). Mutations in the intellectual disability gene KDM5C reduce protein stability and demethylase activity. *Hum Mol Genet* **24,** 2861-2872.

Buchanan PJ & McCloskey KD. (2016). CaV channels and cancer: canonical functions indicate benefits of repurposed drugs as cancer therapeutics. *European biophysics journal : EBJ* **45,** 621-633.

Campbell TM, Main MJ & Fitzgerald EM. (2013). Functional expression of the voltage-gated Na(+)-channel Nav1.7 is necessary for EGF-mediated invasion in human non-small cell lung cancer cells. *J Cell Sci* **126,** 4939-4949.

Cardone RA, Bagorda A, Bellizzi A, Busco G, Guerra L, Paradiso A, Casavola V, Zaccolo M & Reshkin SJ. (2005). Protein kinase A gating of a pseudopodial-located RhoA/ROCK/p38/NHE1 signal module regulates invasion in breast cancer cell lines. *Molecular biology of the cell* **16,** 3117-3127.

Carrithers MD, Chatterjee G, Carrithers LM, Offoha R, Iheagwara U, Rahner C, Graham M & Waxman SG. (2009). Regulation of podosome formation in macrophages by a novel splice variant of the sodium channel SCN8A. *J Biol Chem* **284,** 8114-8126.

Carroll CM & Li YM. (2016). Physiological and pathological roles of the gamma-secretase complex. *Brain research bulletin* **126,** 199-206.

Casagrande VA & Condo GJ. (1988). The effect of altered neuronal activity on the development of layers in the lateral geniculate nucleus. *J Neurosci* **8,** 395-416.

Catterall WA. (2000). From ionic currents to molecular mechanisms: the structure and function of voltage-gated sodium channels. *Neuron* **26,** 13-25.

Catterall WA. (2012). Voltage-gated sodium channels at 60: structure, function and pathophysiology. *J Physiol* **590,** 2577-2589.

Catterall WA, Goldin AL & Waxman SG. (2005). International Union of Pharmacology. XLVII. Nomenclature and structure-function relationships of voltage-gated sodium channels. *Pharmacol Rev* **57**.

Catterall WA & Zheng N. (2015). Deciphering voltage-gated Na(+) and Ca(2+) channels by studying prokaryotic ancestors. *Trends in biochemical sciences* **40,** 526-534.

Cavallaro U & Christofori G. (2004). Multitasking in tumor progression: signaling functions of cell adhesion molecules. *Annals of the New York Academy of Sciences* **1014,** 58-66.

Cerchia L & de Franciscis V. (2010). Targeting cancer cells with nucleic acid aptamers. *Trends Biotechnol* **28,** 517-525.

Cetin I & Topcul M. (2014). Triple negative breast cancer. *Asian Pacific journal of cancer prevention : APJCP* **15,** 2427-2431.

Charlton J, Kirschenheuter GP & Smith D. (1997). Highly potent irreversible inhibitors of neutrophil elastase generated by selection from a randomized DNA-valine phosphonate library. *Biochemistry* **36,** 3018-3026.

Chen C, Bharucha V, Chen Y, Westenbroek RE, Brown A, Malhotra JD, Jones D, Avery C, Gillespie PJ, 3rd, Kazen-Gillespie KA, Kazarinova-Noyes K, Shrager P, Saunders TL, Macdonald RL, Ransom BR, Scheuer T, Catterall WA & Isom LL. (2002). Reduced sodium channel density, altered voltage dependence of inactivation, and increased susceptibility to seizures in mice lacking sodium channel beta 2-subunits. *Proc Natl Acad Sci U S A* **99,** 17072-17077.

Chen C, Westenbroek RE, Xu X, Edwards CA, Sorenson DR, Chen Y, McEwen DP, O'Malley HA, Bharucha V, Meadows LS, Knudsen GA, Vilaythong A, Noebels JL, Saunders TL, Scheuer T, Shrager P, Catterall WA & Isom LL. (2004). Mice lacking sodium channel beta1 subunits display defects in neuronal excitability, sodium channel expression, and nodal architecture. *J Neurosci* **24,** 4030-4042.

Chen Y, Yang C, Li T, Zhang M, Liu Y, Gauthier MA, Zhao Y & Wu C. (2015). The Interplay of Disulfide Bonds, alpha-Helicity, and Hydrophobic Interactions Leads to Ultrahigh Proteolytic Stability of Peptides. *Biomacromolecules* **16,** 2347-2355.

Chioni AM, Brackenbury WJ, Calhoun JD, Isom LL & Djamgoz MB. (2009). A novel adhesion molecule in human breast cancer cells: voltage-gated Na+ channel beta1 subunit. *Int J Biochem Cell Biol* **41,** 1216-1227.

Chioni AM, Shao D, Grose R & Djamgoz MB. (2010). Protein kinase A and regulation of neonatal Nav1.5 expression in human breast cancer cells: activity-dependent positive feedback and cellular migration. *Int J Biochem Cell Biol* **42,** 346-358.

Chopra SS, Stroud DM, Watanabe H, Bennett JS, Burns CG, Wells KS, Yang T, Zhong TP & Roden DM. (2010). Voltage-gated sodium channels are required for heart development in zebrafish. *Circ Res* **106,** 1342-1350.

Colombo F, Racchetti G & Meldolesi J. (2014). Neurite outgrowth induced by NGF or L1CAM via activation of the TrkA receptor is sustained also by the exocytosis of enlargeosomes. *Proc Natl Acad Sci U S A* **111,** 16943-16948.

Cooper TA. (1999). In vivo SELEX in vertebrate cells. *Methods Mol Biol* **118,** 405-417.

Craner MJ, Newcombe J, Black JA, Hartle C, Cuzner ML & Waxman SG. (2004). Molecular changes in neurons in multiple sclerosis: altered axonal expression of Nav1.2 and Nav1.6 sodium channels and Na^+/Ca^{2+} exchanger. *Proc Natl Acad Sci U S A* **101,** 8168-8173.

Cromm PM & Crews CM. (2017). Targeted Protein Degradation: from Chemical Biology to Drug Discovery. *Cell chemical biology* **24,** 1181-1190.

Croset A, Delafosse L, Gaudry JP, Arod C, Glez L, Losberger C, Begue D, Krstanovic A, Robert F, Vilbois F, Chevalet L & Antonsson B. (2012). Differences in the glycosylation of recombinant proteins expressed in HEK and CHO cells. *J Biotechnol* **161,** 336-348.

Cummins TR, Dib-Hajj SD & Waxman SG. (2004). Electrophysiological properties of mutant Nav1.7 sodium channels in a painful inherited neuropathy. *J Neurosci* **24,** 8232-8236.

Cummins TR, Howe JR & Waxman SG. (1998). Slow closed-state inactivation: a novel mechanism underlying ramp currents in cells expressing the hNE/PN1 sodium channel. *J Neurosci* **18,** 9607-9619.

Cummins TR, Rush AM, Estacion M, Dib-Hajj SD & Waxman SG. (2009). Voltage-clamp and current-clamp recordings from mammalian DRG neurons. *Nat Protoc* **4,** 1103-1112.

Cusdin FS, Nietlispach D, Maman J, Dale TJ, Powell AJ, Clare JJ & Jackson AP. (2010). The sodium channel {beta}3-subunit induces multiphasic gating in NaV1.3 and affects fast inactivation via distinct intracellular regions. *J Biol Chem* **285,** 33404-33412.

Czajkowsky DM, Hu J, Shao Z & Pleass RJ. (2012). Fc-fusion proteins: new developments and future perspectives. *EMBO Mol Med* **4,** 1015-1028.

Dalton AC & Barton WA. (2014). Over-expression of secreted proteins from mammalian cell lines. *Protein Sci* **23,** 517-525.

Darmostuk M, Rimpelova S, Gbelcova H & Ruml T. (2015). Current approaches in SELEX: An update to aptamer selection technology. *Biotechnol Adv* **33,** 1141-1161.

Dastjerdi K, Tabar GH, Dehghani H & Haghparast A. (2011). Generation of an enriched pool of DNA aptamers for an HER2-overexpressing cell line selected by Cell SELEX. *Biotechnol Appl Biochem* **58,** 226-230.

Davis TH, Chen C & Isom LL. (2004). Sodium channel beta1 subunits promote neurite outgrowth in cerebellar granule neurons. *J Biol Chem* **279,** 51424-51432.

Debiec H, Christensen EI & Ronco PM. (1998). The cell adhesion molecule L1 is developmentally regulated in the renal epithelium and is involved in kidney branching morphogenesis. *J Cell Biol* **143,** 2067-2079.

Deschenes I, Armoundas AA, Jones SP & Tomaselli GF. (2008). Post-transcriptional gene silencing of KChIP2 and Navbeta1 in neonatal rat cardiac myocytes reveals a functional association between Na and Ito currents. *J Mol Cell Cardiol* **45,** 336-346.

Deschenes I & Tomaselli GF. (2002). Modulation of Kv4.3 current by accessory subunits. *FEBS Lett* **528,** 183-188.

Dhar Malhotra J, Chen C, Rivolta I, Abriel H, Malhotra R, Mattei LN, Brosius FC, Kass RS & Isom LL. (2001). Characterization of sodium channel alpha- and beta-subunits in rat and mouse cardiac myocytes. *Circulation* **103,** 1303-1310.

Ding Y, Brackenbury WJ, Onganer PU, Montano X, Porter LM, Bates LF & Djamgoz MB. (2008). Epidermal growth factor upregulates motility of Mat-LyLu rat prostate cancer cells partially via voltage-gated Na^+ channel activity. *J Cell Physiol* **215,** 77-81.

Diss JK, Fraser SP & Djamgoz MB. (2004). Voltage-gated Na^+ channels: multiplicity of expression, plasticity, functional implications and pathophysiological aspects. *Eur Biophys J* **33,** 180-193.

Diss JK, Fraser SP, Walker MM, Patel A, Latchman DS & Djamgoz MB. (2008). Beta-subunits of voltage-gated sodium channels in human prostate cancer: quantitative in vitro and in vivo analyses of mRNA expression. *Prostate Cancer Prostatic Dis* **11,** 325-333.

Djamgoz MBA, Mycielska M, Madeja Z, Fraser SP & Korohoda W. (2001). Directional movement of rat prostate cancer cells in direct-current electric field: involvement of voltage gated Na^+ channel activity. *J Cell Sci* **114,** 2697-2705.

Doberstein K, Harter PN, Haberkorn U, Bretz NP, Arnold B, Carretero R, Moldenhauer G, Mittelbronn M & Altevogt P. (2015). Antibody therapy to human L1CAM in a transgenic mouse model blocks local tumor growth but induces EMT. *Int J Cancer* **136,** E326-339.

Donier E, Gomez-Sanchez JA, Grijota-Martinez C, Lakoma J, Baars S, Garcia-Alonso L & Cabedo H. (2012). L1CAM binds ErbB receptors through Ig-like domains coupling cell adhesion and neuregulin signalling. *PLoS One* **7,** e40674.

Dou X, Menkari CE, Shanmugasundararaj S, Miller KW & Charness ME. (2011). Two alcohol binding residues interact across a domain interface of the L1 neural cell adhesion molecule and regulate cell adhesion. *J Biol Chem* **286,** 16131-16139.

Driffort V, Gillet L, Bon E, Marionneau-Lambot S, Oullier T, Joulin V, Collin C, Pages JC, Jourdan ML, Chevalier S, Bougnoux P, Le Guennec JY, Besson P & Roger S. (2014). Ranolazine inhibits NaV1.5-mediated breast cancer cell invasiveness and lung colonization. *Molecular cancer* **13,** 264.

Eccles SA, Aboagye EO, Ali S, Anderson AS, Armes J, Berditchevski F, Blaydes JP, Brennan K, Brown NJ, Bryant HE, Bundred NJ, Burchell JM, Campbell AM, Carroll JS, Clarke RB, Coles CE, Cook GJ, Cox A, Curtin NJ, Dekker LV, Silva Idos S, Duffy SW, Easton DF, Eccles DM, Edwards DR, Edwards J, Evans D, Fenlon DF, Flanagan JM, Foster C, Gallagher WM, Garcia-Closas M, Gee JM, Gescher AJ, Goh V, Groves AM, Harvey AJ, Harvie M, Hennessy BT, Hiscox S, Holen I, Howell SJ, Howell A, Hubbard G, Hulbert-Williams N, Hunter MS, Jasani B, Jones LJ, Key TJ, Kirwan CC, Kong A, Kunkler IH, Langdon SP, Leach MO, Mann DJ, Marshall JF, Martin L, Martin SG, Macdougall JE, Miles DW, Miller WR, Morris JR, Moss SM, Mullan P, Natrajan R, O'Connor JP, O'Connor R, Palmieri C, Pharoah PD, Rakha EA, Reed E, Robinson SP, Sahai E, Saxton JM, Schmid P, Smalley MJ, Speirs V, Stein R, Stingl J, Streuli CH, Tutt AN, Velikova G, Walker RA, Watson CJ, Williams KJ, Young LS & Thompson AM. (2013). Critical research gaps and translational priorities for the successful prevention and treatment of breast cancer. *Breast Cancer Res* **15,** R92.

Elliott AA & Elliott JR. (1993). Characterization of TTX-sensitive and TTX-resistant sodium currents in small cells from adult rat dorsal root ganglia. *The Journal of physiology* **463,** 39-56.

Escayg A & Goldin AL. (2010). Sodium channel SCN1A and epilepsy: mutations and mechanisms. *Epilepsia* **51,** 1650-1658.

Estacion M, Gasser A, Dib-Hajj SD & Waxman SG. (2010). A sodium channel mutation linked to epilepsy increases ramp and persistent current of Nav1.3 and induces hyperexcitability in hippocampal neurons. *Exp Neurol* **224,** 362-368.

Eyetech Study G. (2002). Preclinical and phase 1A clinical evaluation of an anti-VEGF pegylated aptamer (EYE001) for the treatment of exudative age-related macular degeneration. *Retina* **22,** 143-152.

Fairbanks G, Steck TL & Wallach DF. (1971). Electrophoretic analysis of the major polypeptides of the human erythrocyte membrane. *Biochemistry* **10,** 2606-2617.

Fairhurst C, Watt I, Martin F, Bland M & Brackenbury WJ. (2015). Sodium channel-inhibiting drugs and survival of breast, colon and prostate cancer: a population-based study. *Sci Rep* **5,** 16758.

Farmer C, Cox JJ, Fletcher EV, Woods CG, Wood JN & Schorge S. (2012). Splice variants of Na(V)1.7 sodium channels have distinct beta subunit-dependent biophysical properties. *PloS one* **7,** e41750.

Fidler IJ. (2003). Timeline: The pathogenesis of cancer metastasis: the 'seed and soil' hypothesis revisited. *Nat Rev Cancer* **3,** 453-458.

Finas D, Huszar M, Agic A, Dogan S, Kiefel H, Riedle S, Gast D, Marcovich R, Noack F, Altevogt P, Fogel M & Hornung D. (2008). L1 cell adhesion molecule (L1CAM) as a pathogenetic factor in endometriosis. *Hum Reprod* **23,** 1053-1062.

Fischer E, Grunberg J, Cohrs S, Hohn A, Waldner-Knogler K, Jeger S, Zimmermann K, Novak-Hofer I & Schibli R. (2012). L1-CAM-targeted antibody therapy and (177)Lu-radioimmunotherapy of disseminated ovarian cancer. *International journal of cancer* **130,** 2715-2721.

Fogel M, Gutwein P, Mechtersheimer S, Riedle S, Stoeck A, Smirnov A, Edler L, Ben-Arie A, Huszar M & Altevogt P. (2003). L1 expression as a predictor of progression and survival in patients with uterine and ovarian carcinomas. *Lancet* **362,** 869-875.

Fraser SP, Ding Y, Liu A, Foster CS & Djamgoz MB. (1999). Tetrodotoxin suppresses morphological enhancement of the metastatic MAT-LyLu rat prostate cancer cell line. *Cell Tissue Res* **295,** 505-512.

Fraser SP, Diss JK, Chioni AM, Mycielska M, Pan H, Yamaci RF, Pani F, Siwy Z, Krasowska M, Grzywna Z, Brackenbury WJ, Theodorou D, Koyuturk M, Kaya H, Battaloglu E, Tamburo De Bella M, Slade MJ, Tolhurst R, Palmieri C, Jiang J, Latchman DS, Coombes RC & Djamgoz MB. (2005). Voltage-gated sodium channel expression and potentiation of human breast cancer metastasis. *Clin Cancer Res* **11,** 5381-5389.

Fraser SP, Grimes JA & Djamgoz MB. (2000). Effects of voltage-gated ion channel modulators on rat prostatic cancer cell proliferation: comparison of strongly and weakly metastatic cell lines. *Prostate* **44,** 61-76.

Fraser SP, Ozerlat-Gunduz I, Brackenbury WJ, Fitzgerald EM, Campbell TM, Coombes RC & Djamgoz MB. (2014). Regulation of voltage-gated sodium channel expression in cancer: hormones, growth factors and auto-regulation. *Philos Trans R Soc Lond B Biol Sci* **369,** 20130105.

Fraser SP, Ozerlat-Gunduz I, Onkal R, Diss JK, Latchman DS & Djamgoz MB. (2010). Estrogen and non-genomic upregulation of voltage-gated Na(+) channel activity in MDA-MB-231 human breast cancer cells: role in adhesion. *J Cell Physiol* **224,** 527-539.

Fraser SP, Salvador V, Manning EA, Mizal J, Altun S, Raza M, Berridge RJ & Djamgoz MB. (2003). Contribution of functional voltage-gated Na^+ channel expression to cell behaviors involved in the metastatic cascade in rat prostate cancer: I. lateral motility. *J Cell Physiol* **195,** 479-487.

Friedli A, Fischer E, Novak-Hofer I, Cohrs S, Ballmer-Hofer K, Schubiger PA, Schibli R & Grunberg J. (2009). The soluble form of the cancer-associated L1 cell adhesion molecule is a pro-angiogenic factor. *Int J Biochem Cell Biol* **41,** 1572-1580.

Gaj T, Gersbach CA & Barbas CF, 3rd. (2013). ZFN, TALEN, and CRISPR/Cas-based methods for genome engineering. *Trends Biotechnol* **31,** 397-405.

Gao R, Shen Y, Cai J, Lei M & Wang Z. (2010). Expression of voltage-gated sodium channel alpha subunit in human ovarian cancer. *Oncol Rep* **23,** 1293-1299.

Gavert N, Conacci-Sorrell M, Gast D, Schneider A, Altevogt P, Brabletz T & Ben-Ze'ev A. (2005). L1, a novel target of beta-catenin signaling, transforms cells and is expressed at the invasive front of colon cancers. *J Cell Biol* **168,** 633-642.

Gentile S. (2016). hERG1 potassium channel in cancer cells: a tool to reprogram immortality. *European biophysics journal : EBJ* **45,** 649-655.

Gersbacher MT, Kim DY, Bhattacharyya R & Kovacs DM. (2010). Identification of BACE1 cleavage sites in human voltage-gated sodium channel beta 2 subunit. *Mol Neurodegener* **5,** 61.

Ghovanloo MR, Aimar K, Ghadiry-Tavi R, Yu A & Ruben PC. (2016). Physiology and Pathophysiology of Sodium Channel Inactivation. *Current topics in membranes* **78,** 479-509.

Gilchrist J, Das S, Van Petegem F & Bosmans F. (2013). Crystallographic insights into sodium-channel modulation by the beta4 subunit. *Proc Natl Acad Sci U S A*.

Gillet L, Roger S, Besson P, Lecaille F, Gore J, Bougnoux P, Lalmanach G & Le Guennec JY. (2009). Voltage-gated Sodium Channel Activity Promotes Cysteine Cathepsin-dependent Invasiveness and Colony Growth of Human Cancer Cells. *J Biol Chem* **284,** 8680-8691.

Goldin AL, Barchi RL, Caldwell JH, Hofmann F, Howe JR, Hunter JC, Kallen RG, Mandel G, Meisler MH, Netter YB, Noda M, Tamkun MM, Waxman SG, Wood JN & Catterall WA. (2000). Nomenclature of voltage-gated sodium channels. In *Neuron*, pp. 365-368. United States.

Gouveia RM, Gomes CM, Sousa M, Alves PM & Costa J. (2008). Kinetic analysis of L1 homophilic interaction: role of the first four immunoglobulin domains and implications on binding mechanism. *J Biol Chem* **283,** 28038-28047.

Grieco TM, Malhotra JD, Chen C, Isom LL & Raman IM. (2005). Open-channel block by the cytoplasmic tail of sodium channel beta4 as a mechanism for resurgent sodium current. *Neuron* **45,** 233-244.

Grimes JA, Fraser SP, Stephens GJ, Downing JE, Laniado ME, Foster CS, Abel PD & Djamgoz MB. (1995). Differential expression of voltage-activated Na^+ currents in two prostatic tumour cell lines: contribution to invasiveness in vitro. *FEBS Lett* **369,** 290-294.

Gutwein P, Oleszewski M, Mechtersheimer S, Agmon-Levin N, Krauss K & Altevogt P. (2000). Role of Src kinases in the ADAM-mediated release of L1 adhesion molecule from human tumor cells. *J Biol Chem* **275,** 15490-15497.

Hakim P, Gurung IS, Pedersen TH, Thresher R, Brice N, Lawrence J, Grace AA & Huang CL. (2008). Scn3b knockout mice exhibit abnormal ventricular electrophysiological properties. *Prog Biophys Mol Biol* **98,** 251-266.

Hanahan D & Weinberg RA. (2011). Hallmarks of cancer: the next generation. *Cell* **144,** 646-674.

Harris JB & Pollard SL. (1986). Neuromuscular transmission in the murine mutants "motor end-plate disease" and "jolting". *J Neurol Sci* **76,** 239-253.

Hernandez-Plata E, Ortiz CS, Marquina-Castillo B, Medina-Martinez I, Alfaro A, Berumen J, Rivera M & Gomora JC. (2012). Overexpression of NaV 1.6 channels is associated with the invasion capacity of human cervical cancer. *Int J Cancer* **130,** 2013-2023.

Hicke BJ, Marion C, Chang YF, Gould T, Lynott CK, Parma D, Schmidt PG & Warren S. (2001). Tenascin-C aptamers are generated using tumor cells and purified protein. *J Biol Chem* **276,** 48644-48654.

Hille B. (1992). *Ionic channels of excitable membranes*. Sinauer Associates Inc., Sunderland (Massachusetts).

Hoshino D, Branch KM & Weaver AM. (2013). Signaling inputs to invadopodia and podosomes. *Journal of cell science* **126,** 2979-2989.

House CD, Vaske CJ, Schwartz A, Obias V, Frank B, Luu T, Sarvazyan N, Irby RB, Strausberg RL, Hales T, Stuart J & Lee NH. (2010). Voltage-gated Na+ channel SCN5A is a key regulator of a gene transcriptional network that controls colon cancer invasion. *Cancer Res* **70,** 6957-6967.

Huth T, Schmidt-Neuenfeldt K, Rittger A, Saftig P, Reiss K & Alzheimer C. (2009). Non-proteolytic effect of beta-site APP-cleaving enzyme 1 (BACE1) on sodium channel function. *Neurobiol Dis* **33,** 282-289.

Ishikawa T, Takahashi N, Ohno S, Sakurada H, Nakamura K, On YK, Park JE, Makiyama T, Horie M, Arimura T, Makita N & Kimura A. (2013). Novel SCN3B mutation associated with brugada syndrome affects intracellular trafficking and function of Nav1.5. *Circ J* **77,** 959-967.

Isom LL. (2001). Sodium channel beta subunits: anything but auxiliary. *Neuroscientist* **7,** 42-54.

Isom LL. (2002). The role of sodium channels in cell adhesion. *Front Biosci* **7,** 12-23.

Isom LL & Catterall WA. (1996). Na+ channel subunits and Ig domains. *Nature* **383,** 307-308.

Isom LL, De Jongh KS, Patton DE, Reber BF, Offord J, Charbonneau H, Walsh K, Goldin AL & Catterall WA. (1992). Primary structure and functional expression of the beta 1 subunit of the rat brain sodium channel. *Science* **256,** 839-842.

Isom LL, Ragsdale DS, De Jongh KS, Westenbroek RE, Reber BF, Scheuer T & Catterall WA. (1995). Structure and function of the beta 2 subunit of brain sodium channels, a transmembrane glycoprotein with a CAM motif. *Cell* **83,** 433-442.

Israel MR, Tay B, Deuis JR & Vetter I. (2017). Sodium Channels and Venom Peptide Pharmacology. *Advances in pharmacology (San Diego, Calif)* **79,** 67-116.

Jansson KH, Castillo DG, Morris JW, Boggs ME, Czymmek KJ, Adams EL, Schramm LP & Sikes RA. (2014). Identification of beta-2 as a key cell adhesion molecule in PCa cell neurotropic behavior: a novel ex vivo and biophysical approach. *PLoS One* **9,** e98408.

Jansson KH, Lynch JE, Lepori-Bui N, Czymmek KJ, Duncan RL & Sikes RA. (2012). Overexpression of the VSSC-associated CAM, beta-2, enhances LNCaP cell metastasis associated behavior. *Prostate* **72,** 1080-1092.

Jemal A, Bray F, Center MM, Ferlay J, Ward E & Forman D. (2011). Global cancer statistics. *CA Cancer J Clin* **61,** 69-90.

Kaback HR. (1974). Transport studies in bacterial membrane vesicles. *Science (New York, NY)* **186,** 882-892.

Kang HS, Huh YM, Kim S & Lee D. (2009). Isolation of RNA Aptamers Targeting HER-2-overexpressing Breast Cancer Cells Using Cell-SELEX. *Bulletin of the Korean Chemical Society* **30,** 1827-1831.

Kannicht C, Ramstrom M, Kohla G, Tiemeyer M, Casademunt E, Walter O & Sandberg H. (2013). Characterisation of the post-translational modifications of a novel, human cell line-derived recombinant human factor VIII. *Thrombosis research* **131,** 78-88.

Kaplan MR, Cho MH, Ullian EM, Isom LL, Levinson SR & Barres BA. (2001). Differential control of clustering of the sodium channels Na(v)1.2 and Na(v)1.6 at developing CNS nodes of Ranvier. *Neuron* **30,** 105-119.

Katz ML. (1989). Incomplete proteolysis may contribute to lipofuscin accumulation in the retinal pigment epithelium. *Advances in experimental medicine and biology* **266,** 109-116; discussion 116-108.

Kazarinova-Noyes K, Malhotra JD, McEwen DP, Mattei LN, Berglund EO, Ranscht B, Levinson SR, Schachner M, Shrager P, Isom LL & Xiao Z-C. (2001). Contactin associates with Na^+ channels and increases their functional expression. *J Neurosci* **21,** 7517-7525.

Kazen-Gillespie KA, Ragsdale DS, D'Andrea MR, Mattei LN, Rogers KE & Isom LL. (2000). Cloning, localization, and functional expression of sodium channel b1A subunits. *J Biol Chem* **275,** 1079-1088.

Kelley LA, Mezulis S, Yates CM, Wass MN & Sternberg MJE. (2015). The Phyre2 web portal for protein modeling, prediction and analysis. *Nat Protocols* **10,** 845-858.

Kiefel H, Bondong S, Hazin J, Ridinger J, Schirmer U, Riedle S & Altevogt P. (2012a). L1CAM: a major driver for tumor cell invasion and motility. *Cell adhesion & migration* **6,** 374-384.

Kiefel H, Bondong S, Pfeifer M, Schirmer U, Erbe-Hoffmann N, Schafer H, Sebens S & Altevogt P. (2012b). EMT-associated up-regulation of L1CAM provides insights into L1CAM-mediated integrin signalling and NF-kappaB activation. *Carcinogenesis* **33,** 1919-1929.

Kim DY, Carey BW, Wang H, Ingano LA, Binshtok AM, Wertz MH, Pettingell WH, He P, Lee VM, Woolf CJ & Kovacs DM. (2007). BACE1 regulates voltage-gated sodium channels and neuronal activity. *Nat Cell Biol* **9,** 755-764.

Kim DY, Ingano LA, Carey BW, Pettingell WH & Kovacs DM. (2005). Presenilin/gamma-secretase-mediated cleavage of the voltage-gated sodium channel beta2-subunit regulates cell adhesion and migration. *J Biol Chem* **280,** 23251-23261.

Kim DY, Wertz MH, Gautam V, D'Avanzo C, Bhattacharyya R & Kovacs DM. (2014). The E280A presenilin mutation reduces voltage-gated sodium channel levels in neuronal cells. *Neuro-degenerative diseases* **13,** 64-68.

Kim YJ, Lee HS, Jung DE, Kim JM & Song SY. (2017). The DNA aptamer binds stemness-enriched cancer cells in pancreatic cancer. *J Mol Recognit* **30**.

Kleensang A, Vantangoli MM, Odwin-DaCosta S, Andersen ME, Boekelheide K, Bouhifd M, Fornace AJ, Jr., Li HH, Livi CB, Madnick S, Maertens A, Rosenberg M, Yager JD, Zhaog L & Hartung T. (2016). Genetic variability in a frozen batch of MCF-7 cells invisible in routine authentication affecting cell function. *Sci Rep* **6,** 28994.

Klemke RL. (2012). Trespassing cancer cells: 'fingerprinting' invasive protrusions reveals metastatic culprits. *Current opinion in cell biology* **24,** 662-669.

Klugbauer N, Marais E & Hofmann F. (2003). Calcium channel alpha2delta subunits: differential expression, function, and drug binding. *J Bioenerg Biomembr* **35,** 639-647.

Kowey PR. (1998). Pharmacological effects of antiarrhythmic drugs. Review and update. *Archives of internal medicine* **158,** 325-332.

Kruger LC, O'Malley HA, Hull JM, Kleeman A, Patino GA & Isom LL. (2016). beta1-C121W Is Down But Not Out: Epilepsy-Associated Scn1b-C121W Results in a Deleterious Gain-of-Function. *J Neurosci* **36,** 6213-6224.

Kulahin N, Li S, Hinsby A, Kiselyov V, Berezin V & Bock E. (2008). Fibronectin type III (FN3) modules of the neuronal cell adhesion molecule L1 interact directly with the fibroblast growth factor (FGF) receptor. *Mol Cell Neurosci* **37,** 528-536.

Laedermann CJ, Syam N, Pertin M, Decosterd I & Abriel H. (2013). beta1- and beta3- voltage-gated sodium channel subunits modulate cell surface expression and glycosylation of Nav1.7 in HEK293 cells. *Front Cell Neurosci* **7,** 137.

Lakhin AV, Tarantul VZ & Gening LV. (2013). Aptamers: problems, solutions and prospects. *Acta naturae* **5,** 34-43.

Lee WC, Kang D, Causevic E, Herdt AR, Eckman EA & Eckman CB. (2010). Molecular characterization of mutations that cause globoid cell leukodystrophy and pharmacological rescue using small molecule chemical chaperones. *J Neurosci* **30,** 5489-5497.

Li WM, Zhou LL, Zheng M & Fang J. (2018). Selection of Metastatic Breast Cancer Cell-Specific Aptamers for the Capture of CTCs with a Metastatic Phenotype by Cell-SELEX. *Molecular therapy Nucleic acids* **12,** 707-717.

Li Y & Galileo DS. (2010). Soluble L1CAM promotes breast cancer cell adhesion and migration in vitro, but not invasion. *Cancer Cell Int* **10,** 34.

Lin X, O'Malley H, Chen C, Auerbach D, Foster M, Shekhar A, Zhang M, Coetzee W, Jalife J, Fishman GI, Isom L & Delmar M. (2015). Scn1b deletion leads to increased tetrodotoxin-sensitive sodium current, altered intracellular calcium homeostasis and arrhythmias in murine hearts. *J Physiol* **593,** 1389-1407.

Livak KJ & Schmittgen TD. (2001). Analysis of relative gene expression data using real-time quantitative PCR and the 2(-Delta Delta C(T)) Method. *Methods* **25,** 402-408.

Lo KM, Sudo Y, Chen J, Li Y, Lan Y, Kong SM, Chen L, An Q & Gillies SD. (1998). High level expression and secretion of Fc-X fusion proteins in mammalian cells. *Protein Eng* **11,** 495-500.

Lopez-Santiago LF, Meadows LS, Ernst SJ, Chen C, Malhotra JD, McEwen DP, Speelman A, Noebels JL, Maier SK, Lopatin AN & Isom LL. (2007). Sodium channel Scn1b null mice exhibit prolonged QT and RR intervals. *J Mol Cell Cardiol* **43,** 636-647.

Lopez-Santiago LF, Pertin M, Morisod X, Chen C, Hong S, Wiley J, Decosterd I & Isom LL. (2006). Sodium channel beta2 subunits regulate tetrodotoxin-sensitive sodium channels in small dorsal root ganglion neurons and modulate the response to pain. *J Neurosci* **26,** 7984-7994.

Lu F, Chen H, Zhou C, Liu S, Guo M, Chen P, Zhuang H, Xie D & Wu S. (2008). T-type Ca2+ channel expression in human esophageal carcinomas: a functional role in proliferation. *Cell Calcium* **43,** 49-58.

Malhotra JD, Kazen-Gillespie K, Hortsch M & Isom LL. (2000). Sodium channel beta subunits mediate homophilic cell adhesion and recruit ankyrin to points of cell-cell contact. *J Biol Chem* **275,** 11383-11388.

Malhotra JD, Koopmann MC, Kazen-Gillespie KA, Fettman N, Hortsch M & Isom LL. (2002). Structural requirements for interaction of sodium channel b1 subunits with ankyrin. *J Biol Chem* **277,** 26681-26688.

Malhotra JD, Thyagarajan V, Chen C & Isom LL. (2004). Tyrosine-phosphorylated and nonphosphorylated sodium channel beta1 subunits are differentially localized in cardiac myocytes. *J Biol Chem* **279,** 40748-40754.

Manley JL. (2013). SELEX to Identify Protein-Binding Sites on RNA. *Cold Spring Harbor Protocols* **2013,** pdb.prot072934.

Marionneau C, Carrasquillo Y, Norris AJ, Townsend RR, Isom LL, Link AJ & Nerbonne JM. (2012). The sodium channel accessory subunit Navbeta1 regulates neuronal excitability through modulation of repolarizing voltage-gated K(+) channels. *J Neurosci* **32,** 5716-5727.

Mayer G, Ahmed MS, Dolf A, Endl E, Knolle PA & Famulok M. (2010). Fluorescence-activated cell sorting for aptamer SELEX with cell mixtures. *Nat Protoc* **5,** 1993-2004.

McCarthy JB, El-Ashry D & Turley EA. (2018). Hyaluronan, Cancer-Associated Fibroblasts and the Tumor Microenvironment in Malignant Progression. *Frontiers in cell and developmental biology* **6,** 48.

McCormack K, Santos S, Chapman ML, Krafte DS, Marron BE, West CW, Krambis MJ, Antonio BM, Zellmer SG, Printzenhoff D, Padilla KM, Lin Z, Wagoner PK, Swain NA, Stupple PA, de Groot M, Butt RP & Castle NA. (2013). Voltage sensor interaction site for selective small molecule inhibitors of voltage-gated sodium channels. *Proc Natl Acad Sci U S A* **110,** E2724-2732.

McCormick KA, Isom LL, Ragsdale D, Smith D, Scheuer T & Catterall WA. (1998). Molecular determinants of Na+ channel function in the extracellular domain of the beta1 subunit. *J Biol Chem* **273,** 3954-3962.

McCusker EC, Bagneris C, Naylor CE, Cole AR, D'Avanzo N, Nichols CG & Wallace BA. (2012). Structure of a bacterial voltage-gated sodium channel pore reveals mechanisms of opening and closing. *Nature communications* **3,** 1102.

McEwen DP, Chen C, Meadows LS, Lopez-Santiago L & Isom LL. (2009). The voltage-gated Na+ channel beta3 subunit does not mediate trans homophilic cell adhesion or associate with the cell adhesion molecule contactin. *Neurosci Lett* **462,** 272-275.

McEwen DP & Isom LL. (2004). Heterophilic interactions of sodium channel beta1 subunits with axonal and glial cell adhesion molecules. *J Biol Chem* **279,** 52744-52752.

McEwen DP, Meadows LS, Chen C, Thyagarajan V & Isom LL. (2004). Sodium channel beta1 subunit-mediated modulation of Nav1.2 currents and cell surface density is dependent on interactions with contactin and ankyrin. *J Biol Chem* **279,** 16044-16049.

McNamara JO, 2nd, Andrechek ER, Wang Y, Viles KD, Rempel RE, Gilboa E, Sullenger BA & Giangrande PH. (2006). Cell type-specific delivery of siRNAs with aptamer-siRNA chimeras. *Nature biotechnology* **24,** 1005-1015.

Meadows LS & Isom LL. (2005). Sodium channels as macromolecular complexes: implications for inherited arrhythmia syndromes. *Cardiovasc Res* **67,** 448-458.

Meadows LS, Malhotra J, Loukas A, Thyagarajan V, Kazen-Gillespie KA, Koopman MC, Kriegler S, Isom LL & Ragsdale DS. (2002). Functional and biochemical analysis of a sodium channel beta1

subunit mutation responsible for generalized epilepsy with febrile seizures plus type 1. *J Neurosci* **22,** 10699-10709.

Mikulak J, Negrini S, Klajn A, D'Alessandro R, Mavilio D & Meldolesi J. (2012). Dual REST-dependence of L1CAM: from gene expression to alternative splicing governed by Nova2 in neural cells. *J Neurochem* **120,** 699-709.

Miyazaki H, Oyama F, Wong HK, Kaneko K, Sakurai T, Tamaoka A & Nukina N. (2007). BACE1 modulates filopodia-like protrusions induced by sodium channel beta4 subunit. *Biochem Biophys Res Commun* **361,** 43-48.

Moh MC, Zhang T, Lee LH & Shen S. (2008). Expression of hepaCAM is downregulated in cancers and induces senescence-like growth arrest via a p53/p21-dependent pathway in human breast cancer cells. *Carcinogenesis* **29,** 2298-2305.

Moran O, Conti F & Tammaro P. (2003). Sodium channel heterologous expression in mammalian cells and the role of the endogenous beta1-subunits. *Neurosci Lett* **336,** 175-179.

Morgan K, Stevens EB, Shah B, Cox PJ, Dixon AK, Lee K, Pinnock RD, Hughes J, Richardson PJ, Mizuguchi K & Jackson AP. (2000). beta 3: an additional auxiliary subunit of the voltage-sensitive sodium channel that modulates channel gating with distinct kinetics. *Proc Natl Acad Sci U S A* **97,** 2308-2313.

Mualla R, Nagaraj K & Hortsch M. (2013). A phylogenetic analysis of the L1 family of neural cell adhesion molecules. *Neurochem Res* **38,** 1196-1207.

Munasinghe NR & Christie MJ. (2015). Conotoxins That Could Provide Analgesia through Voltage Gated Sodium Channel Inhibition. *Toxins* **7,** 5386-5407.

Mycielska ME, Fraser SP, Szatkowski M & Djamgoz MB. (2003). Contribution of functional voltage-gated Na^+ channel expression to cell behaviors involved in the metastatic cascade in rat prostate cancer: II. Secretory membrane activity. *J Cell Physiol* **195,** 461-469.

Mycielska ME, Palmer CP, Brackenbury WJ & Djamgoz MB. (2005). Expression of Na^+-dependent citrate transport in a strongly metastatic human prostate cancer PC-3M cell line: regulation by voltage-gated Na^+ channel activity. *J Physiol* **563,** 393-408.

Nakajima T, Kubota N, Tsutsumi T, Oguri A, Imuta H, Jo T, Oonuma H, Soma M, Meguro K, Takano H, Nagase T & Nagata T. (2009). Eicosapentaenoic acid inhibits voltage-gated sodium channels and invasiveness in prostate cancer cells. *Br J Pharmacol* **156,** 420-431.

Nakaoka HJ, Tanei Z, Hara T, Weng JS, Kanamori A, Hayashi T, Sato H, Orimo A, Otsuji K, Tada K, Morikawa T, Sasaki T, Fukayama M, Seiki M, Murakami Y & Sakamoto T. (2017). Mint3-mediated L1CAM expression in fibroblasts promotes cancer cell proliferation via integrin alpha5beta1 and tumour growth. *Oncogenesis* **6,** e334.

Namadurai S, Balasuriya D, Rajappa R, Wiemhofer M, Stott K, Klingauf J, Edwardson JM, Chirgadze DY & Jackson AP. (2014). Crystal Structure and Molecular Imaging of the Nav Channel beta3 Subunit Indicates a Trimeric Assembly. *J Biol Chem* **289,** 10797-10811.

Nelson M, Millican-Slater R, Forrest LC & Brackenbury WJ. (2014). The sodium channel beta1 subunit mediates outgrowth of neurite-like processes on breast cancer cells and promotes tumour growth and metastasis. *Int J Cancer* **135,** 2338-2351.

Nelson M, Yang M, Dowle AA, Thomas JR & Brackenbury WJ. (2015). The sodium channel-blocking antiepileptic drug phenytoin inhibits breast tumour growth and metastasis. *Mol Cancer* **14,** 13.

Nguyen HM, Miyazaki H, Hoshi N, Smith BJ, Nukina N, Goldin AL & Chandy KG. (2012). Modulation of voltage-gated K+ channels by the sodium channel beta1 subunit. *Proc Natl Acad Sci U S A* **109,** 18577-18582.

Nieman MT, Prudoff RS, Johnson KR & Wheelock MJ. (1999). N-cadherin promotes motility in human breast cancer cells regardless of their E-cadherin expression. *J Cell Biol* **147,** 631-644.

Nuss HB, Chiamvimonvat N, Perez-Garcia MT, Tomaselli GF & Marban E. (1995). Functional association of the beta 1 subunit with human cardiac (hH1) and rat skeletal muscle (mu 1) sodium channel alpha subunits expressed in Xenopus oocytes. *J Gen Physiol* **106,** 1171-1191.

O'Malley HA, Shreiner AB, Chen G-H, Huffnagle GB & Isom LL. (2009). Loss of Na^+ channel 2 subunits is neuroprotective in a mouse model of multiple sclerosis. *Mol Cell Neurosci* **40,** 143-155.

Ohana RF, Hurst R, Vidugiriene J, Slater MR, Wood KV & Urh M. (2011). HaloTag-based purification of functional human kinases from mammalian cells. *Protein expression and purification* **76,** 154-164.

Ohuchi S. (2012). Cell-SELEX Technology. *Biores Open Access* **1,** 265-272.

Orava EW, Abdul-Wahid A, Huang EH, Mallick AI & Gariepy J. (2013). Blocking the attachment of cancer cells in vivo with DNA aptamers displaying anti-adhesive properties against the carcinoembryonic antigen. *Mol Oncol* **7,** 799-811.

Oyama F, Miyazaki H, Sakamoto N, Becquet C, Machida Y, Kaneko K, Uchikawa C, Suzuki T, Kurosawa M, Ikeda T, Tamaoka A, Sakurai T & Nukina N. (2006). Sodium channel beta4 subunit: down-regulation and possible involvement in neuritic degeneration in Huntington's disease transgenic mice. *J Neurochem* **98,** 518-529.

Patel F & Brackenbury WJ. (2015). Dual roles of voltage-gated sodium channels in development and cancer. *Int J Dev Biol* **59,** 357-366.

Patino GA, Brackenbury WJ, Bao Y, Lopez-Santiago LF, O'Malley HA, Chen C, Calhoun JD, Lafreniere RG, Cossette P, Rouleau GA & Isom LL. (2011). Voltage-gated Na+ channel beta1B: a secreted cell adhesion molecule involved in human epilepsy. *J Neurosci* **31,** 14577-14591.

Patino GA, Claes LR, Lopez-Santiago LF, Slat EA, Dondeti RS, Chen C, O'Malley HA, Gray CB, Miyazaki H, Nukina N, Oyama F, De Jonghe P & Isom LL. (2009). A functional null mutation of SCN1B in a patient with Dravet syndrome. *J Neurosci* **29,** 10764-10778.

Patino GA & Isom LL. (2010). Electrophysiology and beyond: multiple roles of Na+ channel beta subunits in development and disease. *Neurosci Lett* **486,** 53-59.

Payandeh J, Scheuer T, Zheng N & Catterall WA. (2011). The crystal structure of a voltage-gated sodium channel. In *Nature*, pp. 353-358. England.

Peng SP, Schachner M, Boddeke E & Copray S. (2016). Effect of Cell Adhesion Molecules on the Neurite Outgrowth of Induced Pluripotent Stem Cell-Derived Dopaminergic Neurons. *Cell Reprogram* **18,** 55-66.

Perkins KL. (2006). Cell-attached voltage-clamp and current-clamp recording and stimulation techniques in brain slices. *Journal of neuroscience methods* **154,** 1-18.

Pham PL, Perret S, Doan HC, Cass B, St-Laurent G, Kamen A & Durocher Y. (2003). Large-scale transient transfection of serum-free suspension-growing HEK293 EBNA1 cells: peptone additives improve cell growth and transfection efficiency. *Biotechnology and bioengineering* **84,** 332-342.

Planells-Cases R, Caprini M, Zhang J, Rockenstein EM, Rivera RR, Murre C, Masliah E & Montal M. (2000). Neuronal death and perinatal lethality in voltage-gated sodium channel alpha(II)-deficient mice. *Biophys J* **78,** 2878-2891.

Prevarskaya N, Skryma R & Shuba Y. (2010). Ion channels and the hallmarks of cancer. *Trends Mol Med* **16,** 107-121.

Prevarskaya N, Skryma R & Shuba Y. (2018). Ion Channels in Cancer: Are Cancer Hallmarks Oncochannelopathies? *Physiol Rev* **98,** 559-621.

Qin N, D'Andrea MR, Lubin ML, Shafaee N, Codd EE & Correa AM. (2003). Molecular cloning and functional expression of the human sodium channel beta1B subunit, a novel splicing variant of the beta1 subunit. *Eur J Biochem* **270,** 4762-4770.

Qu Y, Curtis R, Lawson D, Gilbride K, Ge P, DiStefano PS, Silos-Santiago I, Catterall WA & Scheuer T. (2001). Differential modulation of sodium channel gating and persistent sodium currents by the beta1, beta2, and beta3 subunits. *Mol Cell Neurosci* **18,** 570-580.

Radom F, Jurek PM, Mazurek MP, Otlewski J & Jelen F. (2013). Aptamers: Molecules of great potential. *Biotechnol Adv* **31,** 1260-1274.

Ran FA, Hsu PD, Wright J, Agarwala V, Scott DA & Zhang F. (2013). Genome engineering using the CRISPR-Cas9 system. *Nat Protocols* **8,** 2281-2308.

Ratcliffe CF, Westenbroek RE, Curtis R & Catterall WA. (2001). Sodium channel beta1 and beta3 subunits associate with neurofascin through their extracellular immunoglobulin-like domain. *J Cell Biol* **154,** 427-434.

Riccio RV & Matthews MA. (1985). Effects of intraocular tetrodotoxin on dendritic spines in the developing rat visual cortex: a Golgi analysis. *Brain Res* **351,** 173-182.

Richmond JE, Featherstone DE, Hartmann HA & Ruben PC. (1998). Slow inactivation in human cardiac sodium channels. *Biophysical journal* **74,** 2945-2952.

Roger S, Besson P & Le Guennec JY. (2003). Involvement of a novel fast inward sodium current in the invasion capacity of a breast cancer cell line. *Biochim Biophys Acta* **1616,** 107-111.

Roger S, Gillet L, Le Guennec JY & Besson P. (2015). Voltage-gated sodium channels and cancer: is excitability their primary role? *Front Pharmacol* **6,** 152.

Roger S, Potier M, Vandier C, Le Guennec JY & Besson P. (2004). Description and role in proliferation of iberiotoxin-sensitive currents in different human mammary epithelial normal and cancerous cells. *Biochim Biophys Acta* **1667,** 190-199.

Roger S, Rollin J, Barascu A, Besson P, Raynal PI, Iochmann S, Lei M, Bougnoux P, Gruel Y & Le Guennec JY. (2007). Voltage-gated sodium channels potentiate the invasive capacities of human non-small-cell lung cancer cell lines. *Int J Biochem Cell Biol* **39,** 774-786.

Rosenberg JE, Bambury RM, Van Allen EM, Drabkin HA, Lara PN, Jr., Harzstark AL, Wagle N, Figlin RA, Smith GW, Garraway LA, Choueiri T, Erlandsson F & Laber DA. (2014). A phase II trial of AS1411 (a novel nucleolin-targeted DNA aptamer) in metastatic renal cell carcinoma. *Investigational new drugs* **32,** 178-187.

Samatov TR, Wicklein D & Tonevitsky AG. (2016). L1CAM: Cell adhesion and more. *Prog Histochem Cytochem* **51,** 25-32.

Santosh B & Yadava PK. (2014). Nucleic acid aptamers: research tools in disease diagnostics and therapeutics. *Biomed Res Int* **2014,** 540451.

Schaller KL & Caldwell JH. (2000). Developmental and regional expression of sodium channel isoform NaCh6 in the rat central nervous system. *J Comp Neurol* **420,** 84-97.

Scheffer IE, Harkin LA, Grinton BE, Dibbens LM, Turner SJ, Zielinski MA, Xu R, Jackson G, Adams J, Connellan M, Petrou S, Wellard RM, Briellmann RS, Wallace RH, Mulley JC & Berkovic SF. (2007). Temporal lobe epilepsy and GEFS+ phenotypes associated with SCN1B mutations. *Brain* **130,** 100-109.

Sett A, Borthakur BB & Bora U. (2017). Selection of DNA aptamers for extra cellular domain of human epidermal growth factor receptor 2 to detect HER2 positive carcinomas. *Clin Transl Oncol*.

Shangguan D, Li Y, Tang Z, Cao ZC, Chen HW, Mallikaratchy P, Sefah K, Yang CJ & Tan W. (2006). Aptamers evolved from live cells as effective molecular probes for cancer study. *Proc Natl Acad Sci U S A* **103,** 11838-11843.

Shigdar S, Lin J, Yu Y, Pastuovic M, Wei M & Duan W. (2011). RNA aptamer against a cancer stem cell marker epithelial cell adhesion molecule. *Cancer Sci* **102,** 991-998.

Shigdar S, Qiao L, Zhou SF, Xiang D, Wang T, Li Y, Lim LY, Kong L, Li L & Duan W. (2013). RNA aptamers targeting cancer stem cell marker CD133. *Cancer Lett* **330,** 84-95.

Shtutman M, Levina E, Ohouo P, Baig M & Roninson IB. (2006). Cell adhesion molecule L1 disrupts E-cadherin-containing adherens junctions and increases scattering and motility of MCF7 breast carcinoma cells. *Cancer Res* **66,** 11370-11380.

Song KM, Lee S & Ban C. (2012). Aptamers and their biological applications. *Sensors (Basel)* **12,** 612-631.

Srinivasan J, Schachner M & Catterall WA. (1998). Interaction of voltage-gated sodium channels with the extracellular matrix molecules tenascin-C and tenascin-R. *Proc Natl Acad Sci U S A* **95,** 15753-15757.

Suter MR, Bhuiyan ZA, Laedermann CJ, Kuntzer T, Schaller M, Stauffacher MW, Roulet E, Abriel H, Decosterd I & Wider C. (2015). p.L1612P, a novel voltage-gated sodium channel Nav1.7 mutation inducing a cold sensitive paroxysmal extreme pain disorder. *Anesthesiology* **122,** 414-423.

Takahashi K. (2001). The linkage between beta1 integrin and the actin cytoskeleton is differentially regulated by tyrosine and serine/threonine phosphorylation of beta1 integrin in normal and cancerous human breast cells. *BMC Cell Biol* **2,** 23.

Tamura R, Nemoto T, Maruta T, Onizuka S, Yanagita T, Wada A, Murakami M & Tsuneyoshi I. (2014). Up-regulation of NaV1.7 sodium channels expression by tumor necrosis factor-alpha in cultured bovine adrenal chromaffin cells and rat dorsal root ganglion neurons. *Anesth Analg* **118,** 318-324.

Thomas EA, Xu R & Petrou S. (2007). Computational analysis of the R85C and R85H epilepsy mutations in Na+ channel beta1 subunits. *Neuroscience* **147,** 1034-1046.

Tom R, Bisson L & Durocher Y. (2008). Transfection of HEK293-EBNA1 Cells in Suspension with Linear PEI for Production of Recombinant Proteins. *CSH Protoc* **2008,** pdb.prot4977.

Tuerk C, MacDougal S & Gold L. (1992). RNA pseudoknots that inhibit human immunodeficiency virus type 1 reverse transcriptase. *Proceedings of the National Academy of Sciences of the United States of America* **89,** 6988-6992.

Turner KL & Sontheimer H. (2014). Cl- and K+ channels and their role in primary brain tumour biology. *Philosophical transactions of the Royal Society of London Series B, Biological sciences* **369,** 20130095.

Valente P, Lignani G, Medrihan L, Bosco F, Contestabile A, Lippiello P, Ferrea E, Schachner M, Benfenati F, Giovedi S & Baldelli P. (2016). Cell adhesion molecule L1 contributes to neuronal excitability regulating the function of voltage-gated Na+ channels. *J Cell Sci* **129,** 1878-1891.

van Zijl F, Krupitza G & Mikulits W. (2011). Initial steps of metastasis: cell invasion and endothelial transmigration. *Mutation research* **728,** 23-34.

Vouillot L, Thelie A & Pollet N. (2015). Comparison of T7E1 and surveyor mismatch cleavage assays to detect mutations triggered by engineered nucleases. *G3 (Bethesda)* **5,** 407-415.

Wei CH & Ryu SE. (2012). Homophilic interaction of the L1 family of cell adhesion molecules. *Exp Mol Med* **44,** 413-423.

Weidle UH, Eggle D & Klostermann S. (2009). L1-CAM as a target for treatment of cancer with monoclonal antibodies. *Anticancer Res* **29,** 4919-4931.

Wimmer VC, Harty RC, Richards KL, Phillips AM, Miyazaki H, Nukina N & Petrou S. (2015). Sodium channel beta1 subunit localizes to axon initial segments of excitatory and inhibitory neurons and shows regional heterogeneity in mouse brain. *J Comp Neurol* **523,** 814-830.

Wimmer VC, Reid CA, Mitchell S, Richards KL, Scaf BB, Leaw BT, Hill EL, Royeck M, Horstmann MT, Cromer BA, Davies PJ, Xu R, Lerche H, Berkovic SF, Beck H & Petrou S. (2010). Axon initial segment dysfunction in a mouse model of genetic epilepsy with febrile seizures plus. *J Clin Invest* **120,** 2661-2671.

Wolterink S, Moldenhauer G, Fogel M, Kiefel H, Pfeifer M, Luttgau S, Gouveia R, Costa J, Endell J, Moebius U & Altevogt P. (2010). Therapeutic antibodies to human L1CAM: functional characterization and application in a mouse model for ovarian carcinoma. *Cancer research* **70,** 2504-2515.

Wong HK, Sakurai T, Oyama F, Kaneko K, Wada K, Miyazaki H, Kurosawa M, De Strooper B, Saftig P & Nukina N. (2005). beta Subunits of voltage-gated sodium channels are novel substrates of beta-site amyloid precursor protein-cleaving enzyme (BACE1) and gamma-secretase. *J Biol Chem* **280,** 23009-23017.

Xiao ZC, Ragsdale DS, Malhotra JD, Mattei LN, Braun PE, Schachner M & Isom LL. (1999). Tenascin-R is a functional modulator of sodium channel beta subunits. *J Biol Chem* **274,** 26511-26517.

Xu R, Thomas EA, Gazina EV, Richards KL, Quick M, Wallace RH, Harkin LA, Heron SE, Berkovic SF, Scheffer IE, Mulley JC & Petrou S. (2007). Generalized epilepsy with febrile seizures plus-associated sodium channel beta1 subunit mutations severely reduce beta subunit-mediated modulation of sodium channel function. *Neuroscience* **148,** 164-174.

Yang L & Lin PC. (2017). Mechanisms that drive inflammatory tumor microenvironment, tumor heterogeneity, and metastatic progression. *Seminars in cancer biology* **47,** 185-195.

Yang M & Brackenbury WJ. (2013). Membrane potential and cancer progression. *Front Physiol* **4,** 185.

Yang M, Kozminski DJ, Wold LA, Modak R, Calhoun JD, Isom LL & Brackenbury WJ. (2012). Therapeutic potential for phenytoin: targeting Na(v)1.5 sodium channels to reduce migration and invasion in metastatic breast cancer. *Breast Cancer Res Treat* **134,** 603-615.

Yereddi NR, Cusdin FS, Namadurai S, Packman LC, Monie TP, Slavny P, Clare JJ, Powell AJ & Jackson AP. (2013). The immunoglobulin domain of the sodium channel beta3 subunit contains a surface-localized disulfide bond that is required for homophilic binding. *FASEB J* **27,** 568-580.

Yip PM, Zhao X, Montgomery AM & Siu CH. (1998). The Arg-Gly-Asp motif in the cell adhesion molecule L1 promotes neurite outgrowth via interaction with the alphavbeta3 integrin. *Mol Biol Cell* **9,** 277-290.

Yu FH, Mantegazza M, Westenbroek RE, Robbins CA, Kalume F, Burton KA, Spain WJ, McKnight GS, Scheuer T & Catterall WA. (2006). Reduced sodium current in GABAergic interneurons in a mouse model of severe myoclonic epilepsy in infancy. *Nat Neurosci* **9,** 1142-1149.

Yu FH, Westenbroek RE, Silos-Santiago I, McCormick KA, Lawson D, Ge P, Ferriera H, Lilly J, DiStefano PS, Catterall WA, Scheuer T & Curtis R. (2003). Sodium channel beta4, a new disulfide-linked auxiliary subunit with similarity to beta2. *J Neurosci* **23,** 7577-7585.

Zhang Y, Chen Y, Han D, Ocsoy I & Tan W. (2010). Aptamers selected by cell-SELEX for application in cancer studies. *Bioanalysis* **2,** 907-918.

Zhao Y, Scheuer T & Catterall WA. (2004). Reversed voltage-dependent gating of a bacterial sodium channel with proline substitutions in the S6 transmembrane segment. *Proceedings of the National Academy of Sciences of the United States of America* **101,** 17873-17878.

Zhu G, Ye M, Donovan MJ, Song E, Zhao Z & Tan W. (2012). Nucleic acid aptamers: an emerging frontier in cancer therapy. *Chem Commun (Camb)* **48,** 10472-10480.

Zimmer T, Biskup C, Bollensdorff C & Benndorf K. (2002). The beta1 subunit but not the beta2 subunit colocalizes with the human heart Na^+ channel (hH1) already within the endoplasmic reticulum. *J Membr Biol* **186,** 13-21.

Zubeda S, Kaipa PR, Shaik NA, Mohiuddin MK, Vaidya S, Pavani B, Srinivasulu M, Latha MM & Hasan Q. (2013). Her-2/neu status: a neglected marker of prognostication and management of breast cancer patients in India. *Asian Pacific journal of cancer prevention : APJCP* **14,** 2231-2235.